

DENDROCHEMICAL RESPONSES TO THE ERUPTION OF MOUNT SAINT
HELENS, WASHINGTON

By Colleen S. Donegan

A Thesis
Submitted in Partial Fulfillment
Of the Requirements for the Degree of
Master of Science
In Geology

Northern Arizona University

May 2011

Approved:

Michael Ort, Ph.D., Chair

James Sample, Ph.D.

Kirk Anderson, Ph.D.

ABSTRACT

DENDROCHEMICAL RESPONSES TO THE ERUPTION OF MOUNT SAINT HELENS, WASHINGTON

Colleen S. Donegan

Laser-ablation inductively coupled mass-spectroscopic (LA-ICP-MS) analysis of individual tree rings is a potential means of attributing abnormalities in growth or chemistry of xylem tissue to volcanic eruptions. Previous studies in Gifford Pinchot National Forest, Washington, have identified thin annual growth rings in Douglas firs that coincide temporally with the 1980 and 1800 volcanic eruptions of Mount Saint Helens. Data from LA-ICP-MS analysis of 52 tree cores taken from eight locations north, east, and south of the AD 1980 crater of Mount Saint Helens are presented in this study. Laser-ablation analyses isolate individual growth rings corresponding to the eleven-year period centered at AD 1980 and the ten-year period centered at AD 1800 and do not indicate a chemical response to these eruptions that is consistent among the sample set. However, at least five of the analyzed tree cores show similar changes in the concentrations of two or more elements (Al, Ca, Zn, K, Na) that may indicate a response to one or both eruptions.

Douglas firs growing at altitudes greater than 1000 m in dacitic tephra deposits greater than 10 cm thick comprise the majority of cored trees. Elemental concentrations in isolated annual-growth rings are reported for B, Na, Al, K, S, P, Ca, Ti, Mn, Zn, Cu, Rb, Sr, Ba, Cd, La, and Pb. Acid-digestion ICP-MS of a subset of seven tree cores and carbon isotopic analysis of a subset of five tree cores are also reported. Comparison of data obtained by three independent micro-analytical techniques is used to evaluate the

quality of LA-ICP-MS analysis of xylem tissue, as a protocol for this type of analysis is not yet an established for analysis of natural wood.

ACKNOWLEDGEMENTS

My sincere thanks to Richard Sink for countless hours spent in the ICP-MS lab. This research would have been impossible without you. I have benefited greatly from your knowledge of chemistry, willingness to teach, and friendship. NAU is lucky to have you.

Thank you to Michael Ort and the NAU geology department for the opportunity to pursue this degree. My passion for geology is owed to the instruction, encouragement, and wisdom that you have shared with me.

Several people helped me along the way by providing expert opinions, abilities, and company when I needed it most. Thanks to Don Normandin for your assistance in the forestry lab and wood shop. I greatly appreciate your guidance and second opinion regarding the dendrochronology of my sample set and would not have been able to build the block plane track without you. Many thanks to Nathan Baier for sharing your talent of design in ArcMap that brought the figures in appendix 1.0 to life. Thanks also to Kurt Eisle and to John and James Merrick for your help in the field. You and my fellow grad students at NAU made it seem a little less like work.

I would also like to thank my friends and family for their support throughout this process. Special thanks go to my parents for always encouraging and enabling the pursuit of education.

This research was funded by the Kleinman Grant for Volcano Research, the Geological Society of America, the Tom and Rose Bedwell Earth Physics Award, Pioneer Natural Resources, BP, and the Friday Lunch Clubbe. Without the support of

these organizations, research in the field and the laboratory would have been impossible to achieve. My thanks and gratitude to everyone involved.

TABLE OF CONTENTS

Chapter 1: Introduction	
1.1 Project Summary.....	pg 1
1.2 Significance.....	pg 2
1.3 Geologic Setting.....	pg 3
1.4 Eruptive History.....	pg 7
1.5 Principles of Dendrochronology.....	pg 15
1.6 Principles of Dendrochemistry.....	pg 19
1.7 Isotopes in Tree Rings	pg 21
1.8 Previous Work.....	pg 23
1.9 Project Outline.....	pg 33
Chapter 2: Methods	
2.1 Field Methods	pg 36
2.2 Sample Sites	pg 40
2.3 Lab Methods	pg 48
2.4 Dendrochronology	pg 50
2.5 Laser Ablation of Natural Wood.....	pg 59
2.6 Calibration Standards.....	pg 62
2.7 Instrumentation	pg 64
2.8 Data Reduction.....	pg 64
2.9 Acid Digestion.....	pg 68
2.10 Carbon Isotope Analysis.....	pg 71
2.11 Statistical Analysis.....	pg 72
Chapter 3: Results.....	pg 74
3.1 LA-ICP-MS Calibration.....	pg 75
3.2 Elemental Abundances.....	pg 81
3.3 Elemental Concentrations Measured on 12/14.....	pg 103
3.4 Statistical Analysis of LA-ICP-MS Data.....	pg 110

3.5 Solution ICP-MS.....	pg 129
3.6 Isotopes.....	pg 133
Chapter 4: Discussion.....	pg 134
4.1 LA-ICP-MS Analysis- Limitations.....	pg 136
4.2 Comparison of Two Configurations- Data Reliability.....	pg 146
4.3 Evaluation of Site and Species Selection.....	pg 149
4.4 Dendrochemical Evidence for Volcanic Eruption of Mount Saint Helens	pg 154
Chapter 5: Summary.....	pg 159
5.1 Sample Collection	pg 160
5.2 Sample Preparation.....	pg 162
5.3 Data Analysis.....	pg 163
5.4 Carbon Isotope Analysis.....	pg 165
5.5 Evidence for Volcanic Eruption at Mount Saint Helens.....	pg 166
References.....	pg 167
Appendix 1.0: Maps of Sampled Localities.....	pg 174

LIST OF TABLES

Appendix 3.1 (compact disc)

Table 2.4	CPI International Standardized Solution Chemistry
Table 3.7	Elements LA-ICP-MS Configurations
Table 3.8	Concentrations of Boron in all Samples (1980)
Table 3.9	Concentrations of Sodium in all Samples (1980)
Table 3.10	Concentrations of Aluminum in all Samples (1980)
Table 3.11	Concentrations of Potassium in all Samples (1980)
Table 3.12	Concentrations of Calcium in all Samples (1980)
Table 3.13	Concentrations of Titanium in all Samples (1980)
Table 3.14	Concentrations of Manganese in all Samples (1980)
Table 3.15	Concentrations of Iron in all Samples (1980)
Table 3.16	Concentrations of Nickel in all Samples (1980)
Table 3.17	Concentrations of Copper in all Samples (1980)
Table 3.18	Concentrations of Zinc in all Samples (1980)
Table 3.19	Concentrations of Rubidium in all Samples (1980)
Table 3.20	Concentrations of Strontium in all Samples (1980)
Table 3.21	Concentrations of Cadmium in all Samples (1980)
Table 3.22	Concentrations of Barium in all Samples (1980)
Table 3.23	Concentrations of Lanthanum in all Samples (1980)
Table 3.24	Concentrations of Lead in all Samples (1980)
Table 3.25	Concentrations of Phosphorus in all Samples (1980)
Table 3.26	Concentrations of Sulfur in all Samples (1980)

Appendix 3.2 (compact disc)

Table 3. 28	Elemental Concentrations at Jefferson Creek (1980)
Table 3.29	Elemental Concentrations at Forest Road 77 (1980)
Table 3.30	Elemental Concentrations at Forest Road 7506 (1980)
Table 3.31	Elemental Concentrations at Bear Meadow (1980)
Table 3.32	Elemental Concentrations at Straight Creek (1980)

Table 3.33	Elemental Concentrations at Control Sites (1980)
Table 3.44	Elemental Concentrations for Five-Element Configuration(1980) (Excludes P and S data)
Table 3.45	Comparison of Elemental Concentrations Measured by Five and Eighteen-Element Configurations (1980)

Appendix 3.3 (compact disc)

Table 2.3	Solution ICP-MS Sample Weights
Table 4.1	Statistical Outliers- Aluminum (1980)
Table 4.2	Statistical Outliers- Aluminum (1800)
Table 4.3	Statistical Outliers- Barium (1980)
Table 4.4	Statistical Outliers- Barium (1800)
Table 4.5	Statistical Outliers- Boron (1980)
Table 4.6	Statistical Outliers- Boron (1800)
Table 4.7	Statistical Outliers- Cadmium (1980)
Table 4.8	Statistical Outliers- Cadmium (1800)
Table 4.9	Statistical Outliers- Calcium (1980)
Table 4.10	Statistical Outliers- Calcium (1800)
Table 4.11	Statistical Outliers- Copper (1980)
Table 4.12	Statistical Outliers- Copper (1800)
Table 4.13	Statistical Outliers- Iron (1980)
Table 4.14	Statistical Outliers- Iron (1800)
Table 4.15	Statistical Outliers- Lanthanum (1980)
Table 4.16	Statistical Outliers- Lanthanum (1800)
Table 4.17	Statistical Outliers- Lead (1980)
Table 4.18	Statistical Outliers- Lead (1800)
Table 4.19	Statistical Outliers- Manganese (1980)
Table 4.20	Statistical Outliers- Manganese (1800)
Table 4.21	Statistical Outliers- Nickel (1980)
Table 4.22	Statistical Outliers- Nickel (1800)
Table 4.23	Statistical Outliers- Phosphorus (1980)

Table 4.24	Statistical Outliers- Phosphorus (1800)
Table 4.25	Statistical Outliers- Potassium (1980)
Table 4.26	Statistical Outliers- Potassium (1800)
Table 4.27	Statistical Outliers- Rubidium (1980)
Table 4.28	Statistical Outliers- Rubidium (1800)
Table 4.29	Statistical Outliers- Sodium (1980)
Table 4.30	Statistical Outliers- Sodium (1800)
Table 4.31	Statistical Outliers- Strontium (1980)
Table 4.32	Statistical Outliers- Strontium (1800)
Table 4.33	Statistical Outliers- Sulfur (1980)
Table 4.34	Statistical Outliers- Sulfur (1800)
Table 4.35	Statistical Outliers- Titanium (1980)
Table 4.36	Statistical Outliers- Titanium (1800)
Table 4.37	Statistical Outliers- Zinc (1980)
Table 4.38	Statistical Outliers- Zinc (1800)
Table 5.1	Statistical Outliers at Jefferson Creek (sheet 2)
Table 5.2	Statistical Outliers at Forest Road 77 (sheet 2)
Table 5.3	Statistical Outliers at Forest Road 7506 (sheet 2)
Table 5.4	Statistical Outliers at Bear Meadow (sheet 2)
Table 5.5	Statistical Outliers at Straight Creek(sheet 2)
Table 5.6	Statistical Outliers at Control Sites (sheet 2)

Appendix 3.5 (compact disc)

Table 2.5	Samples Submitted for Carbon Isotopic Analysis
-----------	--

LIST OF FIGURES
(In text)

1.0*	Location map of Mount Saint Helens.....	4
1.1	Location map Gifford Pinchot National Forest	6
1.2	Layer We, Wn, T 20 cm Isopach.....	9
1.3	Stratigraphic section of MSH eruptions.....	11
1.4	Path of ash cloud from May, 1980 eruption.....	14
1.5	Cross section of a Tree.....	17
1.6	Photo showing earlywood/latewood transition.....	18
1.7	Chemistry of tree rings at Volcán Paricutín.....	27
1.8	Photo showing thin growth rings at Volcán Paricutín.. ..	27
2.0*	Map showing locations of cored trees at MSH.....	37
2.1*	Map showing locations of cored trees E of Salem, OR.....	38
2.3*	Map showing locations of cored trees at Jefferson Creek.....	41
2.4*	Map showing locations of cored trees at Bear Meadow.....	43
2.5*	Map showing locations of cored trees at forest road 77.....	44
2.6*	Map showing locations of cored trees at forest road 7506....	45
2.7*	Map showing locations of cored trees at Marble Mountain Snow Park.....	47
2.8	Sketch- custom block plane tracks.....	49
2.9*	Location map of ITRDB master chronologies.....	52
2.10	Photo micrograph of JFCK 4A.....	55
2.11	Example of False Rings.....	56
2.12	Photo showing dot notation on a core segment.....	57
2.13	Example of calibration curve plots.....	67
3.25T	Example of inadequate calibration curve. Taken from figure 3.25 in appendix 3.1.....	76
3.27T	Plots showing instrument drift. Taken from figure 3.27 in in appendix 3.1.....	79
3.27T_2	Plots showing instrument drift. Taken from figure 3.27 in appendix 3.1.....	80
3.38T	Potassium and Calcium concentrations in several core segments from Jefferson Creek. Taken from figure 3.38 in appendix 3.2.....	84
3.38T_2	Examples of spikes in elemental concentrations in four elements at Jefferson Creek. Taken from figure 3.38 in appendix 3.2.....	87
3.29T	Plots showing concentrations of four elements in core segments from forest road 77. Taken from figure 3.29 in appendix 3.2.....	91
3.40T	Plots showing concentrations of four elements in core segments from forest road 7506. Taken from figures 3.30 and 3.40 in appendix 3.2.....	93

3.30T	Plots showing concentrations of four elements in core segments from forest road 7506. Taken from figure 3.30 in appendix 3.2.....	94
3.41T	Plots showing concentrations of four elements in core segments from Bear Meadow. Taken from figure 3.41 in appendix 3.2.....	96
3.31T	Plots showing concentrations of two elements in core segments from Bear Meadow. Taken from figure 3.31 in appendix 3.2.....	97
3.32T	Plots showing concentrations of two elements in core segments from Straight Creek. Taken from figure 3.32 in appendix 3.2.....	100
3.33T	Plots showing concentrations of four elements in core segments from forest road 225 and Marble Mountain Snow Park. Taken from figure 3.33 in appendix 3.2.....	102
3.45T	Plots comparing the concentrations of tree elements measured by two configurations for LA-ICP-MS. Taken from figure 3.45 in appendix 3.2.....	108
4.1**	Plots showing the elemental concentrations in standard wafers as measured by solution ICP-MS.....	139
5.2a	Calibration curve demonstrating sulfur contamination in the quadrupole. Taken from figure 5.2 in appendix 3.4.....	145

* These figures are also available in Appendix 1.0 (printed and on compact disc)

** These figures are also available in Appendix 3.4 (compact disc)

LIST OF FIGURES
(In appendices)

Appendix 1.0 (printed)

Figure captions pages 174-177

Figures pages 178-211

Appendix 2.0 (compact disc)

Field notes An example of notes taken in the field at the site of each cored tree. Data are shown for Bear Meadow (BM_Oct_2008) and Jefferson Creek (JFCK_Oct_2008).

Photos Photographs of each cored tree. Numbered photos in three files correspond to a labeled tree, as documented in field notes. These photos were archived so that physical and chemical characteristics of trees in this data set can be cross-checked as needed for future studies.

Appendix 3.1 (compact disc)

Figures 3.1-3.6

Calibration curves for all elements by date. Plots are shown on sheet 3 and source data for plots are on sheet 1. Column A on sheet 1 indicates the date of the analysis of a standard wafer. Column B indicates the concentration (0, 0.5, 1.0, 2.0) of the standard wafer. Columns C through V indicate the element, and all values are in counts per sweep. Each value is derived from the average number of counts for three sweeps. The title of each plot on sheet 3 indicates the date and the element that it represents. Plots that do not have a line of best fit indicate unsuccessful calibration. Equations shown were used to convert counts per sweep to concentration in ppm (section 2.8).

Figure 3.1 Calibration curves for May 19, 2009 and May 20, 2009

Figure 3.2 Calibration curves for May 21, 2009 and May 23, 2009

Figure 3.3 Calibration curves for July 4, 2009 and July 5, 2009

Figure 3.4 Calibration curves for June 13, 2009 and August 29, 2009

Figure 3.5 Calibration curves for December 10, 2009

Figure 3.6 Calibration curves for December 14, 2009 (five-element configuration)

Figures 3.8-3.26

Calibration curves for all dates by element. These plots have the same format as figures 3.1-3.6.

Figure 3.8 Boron

Figure 3.9 Sodium

Figure 3.10 Aluminum

Figure 3.11 Potassium

Figure 3.12 Calcium
Figure 3.13 Titanium
Figure 3.14 Manganese
Figure 3.15 Iron
Figure 3.16 Nickel
Figure 3.17 Copper
Figure 3.18 Zinc
Figure 3.19 Rubidium
Figure 3.20 Strontium
Figure 3.21 Cadmium
Figure 3.22 Barium
Figure 3.23 Lanthanum
Figure 3.24 Lead
Figure 3.25 Phosphorus
Figure 3.26 Sulfur

Figure 3.27 Calibration curves for all elements showing instrument drift. Each “run” (see figure 2.13 in text) indicates an analysis conducted at a different time of day. The drift (section 3.1) in instrument sensitivity is apparent when all four points in one run are higher or lower than all four points in another run.

Appendix 3.2 (compact disc)

Figures 3.28-3.33

Concentrations in ppm (y-axis) for all elements by location. The element is indicated in the plot title (sheet 2). Each point represents the elemental concentration measured in a single growth ring for a given year (x-axis). Source data for these plots are available on sheet 1.

Figure 3.28 Jefferson Creek
Figure 3.29 Forest road 77
Figure 3.30 Forest road 7506
Figure 3.31 Bear Meadow
Figure 3.32 Straight Creek
Figure 3.33 Control trees from Marble Mountain Snow Park and forest road 225, east of Salem, OR

Figures 3.38-3.43

Highlight of cores from figures 3.28-3.33 that exhibit a robust variation in elemental concentration over the ten-year period of growth analyzed. Plots are aligned in the same way as in figures 3.28-3.33. Plots from the above group that did not show any samples with robust variation in elemental concentration are not present in these figures. Spaces between plots were left blank to emphasize the lack of robust variation.

- Figure 3.38 Jefferson Creek
- Figure 3.39 Forest road 77
- Figure 3.40 Forest road 7506
- Figure 3.41 Bear Meadow
- Figure 3.42 Straight Creek
- Figure 3.43 Control trees from Marble Mountain Snow Park and forest road 225, east of Salem, OR
- Figure 3.45 Comparison of the five-element and eighteen-element experiments discussed in section 3.3. Sheet 2 shows plots for core-segments from AD 1975-1986 and sheet 3 shows data for core segments from AD 1795-1805. Source data for these plots is on sheet 1. Y-axis values are elemental concentrations in ppm and years are plotted on the x-axis. The plot title indicates the element represented in the plot. The five- and eighteen-element configurations are indicated by different data-point symbols. Where a plot is absent (void space) element concentrations are below detection.
- Figure 3.46 Concentrations for all samples analyzed by the five-element configuration on December 14th. Plots are formatted the same as in figure 3.45.

Appendix 3.3 (compact disc)

Contains tables 2.3, 4.1-4.38, and 5.1-5.6

Appendix 3.4 (compact disc)

- Figure 4.1 Plots showing the concentrations of all elements in standard wafers as analyzed by solution ICP-MS. X axis indicates concentration (ppm) of elements indicated. Y axis indicates the concentration of standard solution in each wafer (section 2.6 of the text). Figure caption on page 139.
- Figure 5.1 Calibration curves for all elements in samples analyzed by solution ICP-MS on April 27, 2010 (sheet 3). Plots follow the same format as for figures 3.1-3.6. Source data are available on sheet 1.
- Figure 5.2 Calibration curves for all elements in samples analyzed by solution ICP-MS on May 4, 2010 (sheet 3). Plots follow the same format as for figures 3.1-3.6. Source data are available on sheet 1.

Figures 6.1-6.3

Comparison plots for the concentrations of calcium and zinc in PSF MMSP 1B, FR77 2C, FR7506 5B, JFCK 2B, and BM 1A. Concentrations (ppm) are plotted on the y-axis and years are plotted on the x-axis. Each tree is designated by the symbol shown at the bottom of the plot. Figures 6.1 and 6.2 show the same data, collected by the eighteen-element

configuration), plotted on two different scales. Figure 6.3 shows data collected by the five-element configuration.

Appendix 3.5 (compact disc)

Figure 4.0 Carbon isotopic data for five trees. Plot format is discussed in section 3.6. Source data for these plots are on sheet 1, also shown in table 2.5.

Appendix 3.6 (compact disc)

Contains the raw data for all LA-ICP-MS analyses. Counts for each of three sweeps, rather than an average, are reported in these spreadsheets. Also contains a basic flow chart for future studies involving LA-ICP-MS analysis of tree rings.

Appendix 4.1 (compact disc)

Contains the COFECHA output files for the ITRDB master chronologies used in this study along with a .pdf document of the master chronology used by Dr. Yamaguchi in his 1985 study.

Appendix 4.2 (compact disc)

Contains word documents explaining sample preparation procedures for solution ICP-MS and samples submitted for carbon isotopic analysis.

CHAPTER 1: INTRODUCTION

1.1 Project Summary

Dendrochronological studies previously conducted at Mount St. Helens and elsewhere related narrow annual growth rings in dated sequences with known historical volcanic eruptions (Brantley et al., 1986; Sheppard et al., 2008; Sheppard et al., 2009; Yamaguchi, 1983; Yamaguchi 1985; Yamaguchi and Hoblitt, 1986; Yamaguchi et al., 1990; Yamaguchi and Lawrence, 1993). Additionally, several unrelated studies correlated enrichment of ^{13}C in tree rings with documented instances of site-specific industrial pollution (Savard et al., 2004). The variation in elemental abundance (dendrochemical expression) associated with volcanic eruption remains largely unexplored. Some changes in the elemental abundance of phosphorus, sulfur, calcium, strontium, and several rare earth elements have been observed in dated tree rings that were produced in years coincident and subsequent to the eruption of nearby volcanoes (Hall et al., 1990; Pearson et al., 2005; Sheppard et al., 2008; Sheppard et al., 2009). These data and other previous work will be discussed further in section 1.7. The goal of this study is to investigate whether chemical signatures in tree rings can be correlated with volcanic eruptions at Mount Saint Helens. In order to quantify chemical changes between annual growth rings, a combination of laser-ablation inductively-coupled plasma mass spectrometry (LA-ICP-MS) and acid-digestion ICP-MS were applied to dated tree rings that survived fallout from the AD 1980 and AD 1800 eruptions of Mount Saint Helens. Variations in elemental abundance on or after the date of eruption in these tree rings may serve as an indication of one or many volcanically induced changes to the microclimate of the tree. Deposition of volcanic material may cause changes in soil pH

that affect the mobility of certain elements. Acid rain may also contribute to the alteration of soil pH, or to the weathering and transport of material from ash and pumice.

Additionally, tree chemistry may be influenced by biological processes that arise within a stressed tree or the environment from which it draws sustenance. Any observed change in elemental abundance may be attributed to one or many of these and other processes.

Carbon isotope analyses of the same tree rings were performed to test specifically for ^{13}C enrichment. Previous studies have shown that sulfur dioxide aerosols can induce closure of stomata in exposed trees, resulting in a temporary reduction of photosynthetic activity that leads to an enrichment of ^{13}C in wood cellulose, as explained in section 1.6. While changes in elemental abundance are likely to be influenced by the uptake of nutrients available in the root system, ^{13}C enrichment is likely a product of reduced photosynthesis. Therefore, variations in elemental abundance within tree rings and the enrichment of ^{13}C could serve as two independent chemical indications of the same volcanic eruption. Inhibited radial growth, indicated by the presence of thin annual rings, is a third indicator of eruption that is independent of the other two.

1.2 Significance

The connection between volcanic eruption and tree-ring composition is agriculturally, ecologically and geologically significant. The consequences of large-scale eruptions have the potential to affect the hundreds of millions of people worldwide that live and farm in areas proximal to volcanoes. An enhanced knowledge of the effects of volcanism on area plant life may enable better anticipation of volcanically induced famine and productivity. Additionally, application of chemical studies in conjunction

with dendrochronological work may aid in the development of more precise (to-the-year) dating techniques for eruptions of the past few hundred to thousand years. The frequent and recent volcanic activity at Mount St. Helens elucidates the need for a thorough reconstruction of the eruptive history. A more precise comprehension of past activity may instill greater confidence and ability to predict future activity, and its consequences.

1.3 Geologic Setting

Mount St. Helens is located in the Cascade volcanic arc of southeastern Washington, 150 kilometers south of Seattle and 85 kilometers northeast of Portland, Oregon (fig 1.0). The 1980 eruption of Mount Saint Helens resulted in the creation of a 2 by 2.5 km wide, U-shaped crater (Doukas, 1990). This crater is now partially filled with a recently developed lava dome. The U-shaped crater opens to the north, where a slope failure initiated the famous lateral blast that removed a significant amount of the pre-1980 cone. The current summit of Mount Saint Helens is at 2,550 m elevation, down 400 m from the 2,950 m summit prior to 1980.

Mount Saint Helens is surrounded by dense coniferous forest that is sustained by a substantial amount of annual precipitation (from 1,140 mm/year near the Columbia River to 3,200 mm/year on the upper slopes of the volcano). Nearly 75% of the total precipitation for the area falls between October and March and snowpack stays consistent during these months above an elevation of approximately 1000 m (Iverson and Martinson, 1986). Douglas fir and western hemlock are considered dominant species below 1200 m elevation (Iverson and Martinson, 1986). Trees were cored for this study

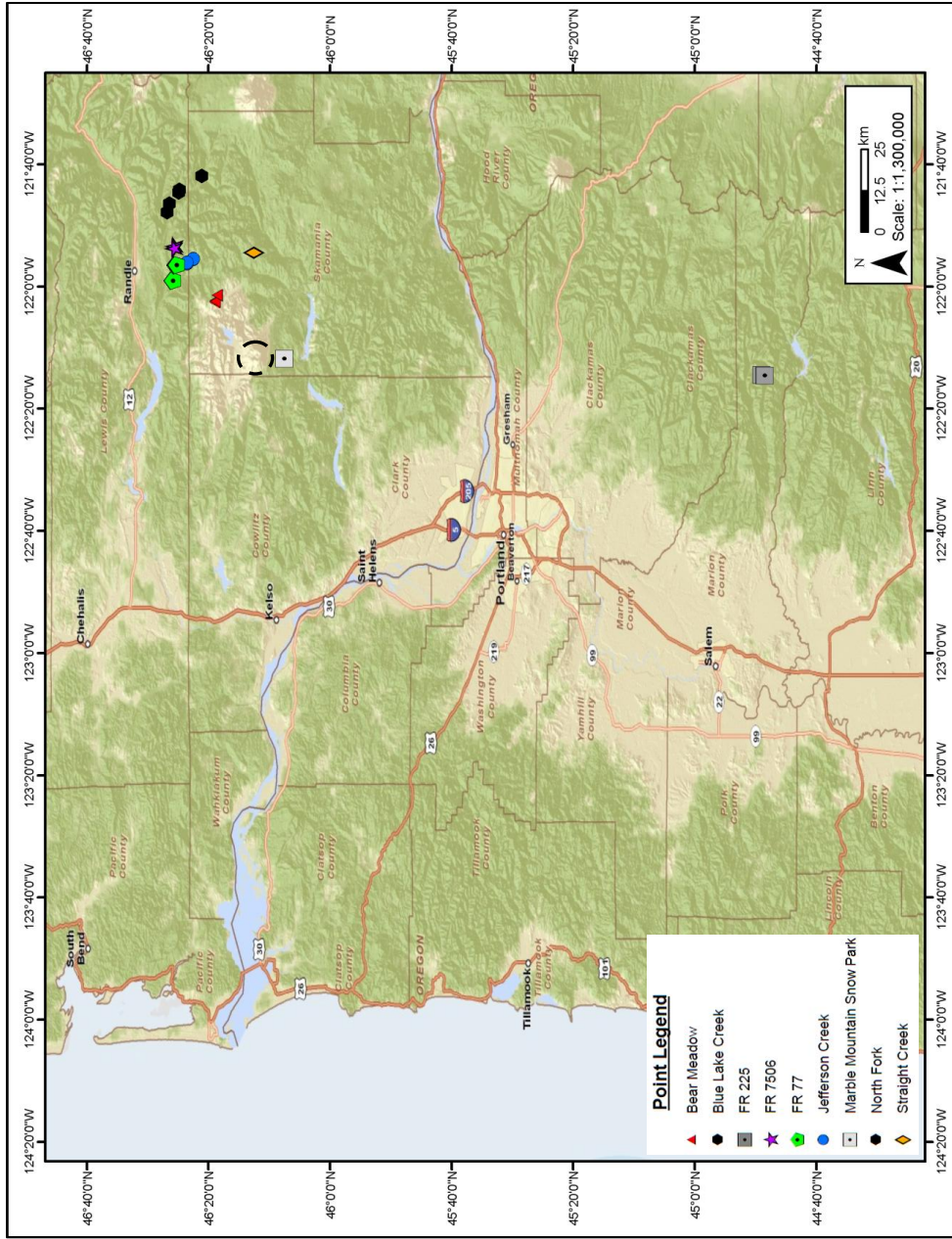


Figure 1.0*
 Location Map showing location of Mount Saint Helens (dashed circle) in southeastern Washington. Symbols indicate the locations of cored trees. FR225 is located east of Salem, Oregon.
 *Also available in appendix 1.0

from several field sites located almost exclusively within Gifford Pinchot National Forest. Only one of eight field sites, chosen as a control site, lies beyond the boundaries of this forest to the south.

Gifford Pinchot National Forest includes nearly 566,600 hectares of natural forest in southwestern Washington (figure 1.1). Approximately 44,500 hectares that define the area of Mount Saint Helens National Volcanic Monument constitute the western-most section of the forest. Mount Rainier National Park abuts the forest in the north, and the Columbia River Gorge marks the border to the south. Precipitation near the Columbia River Gorge averages over 100 cm per year, compared to 320 cm per year on the upper slopes of the volcano (Iverson and Martinson, 1986).

The forests of the Pacific Northwest are home to approximately 25 species of native trees, the majority of which are green firs and cedars. Common species in Gifford Pinchot National Forest thrive in environments of abundant precipitation and include Douglas fir (*pseudotsuga menziesii*), western red cedar (*Thuja plicata*), western hemlock (*tsuga heterophylla*) and Pacific silver fir (*Abies amabilis*). Ponderosa pines in Washington are only present in arid climates, east of the Cascade Range. Douglas firs constitute the largest population of old-growth trees in the area surrounding Mount Saint Helens, and the majority of trees sampled in this study. Annual rainfall averaged between 200 and 300 cm between AD 1961 and AD 1990 within the area of Mount Saint Helens National Volcanic Monument (nationalatlas.gov).

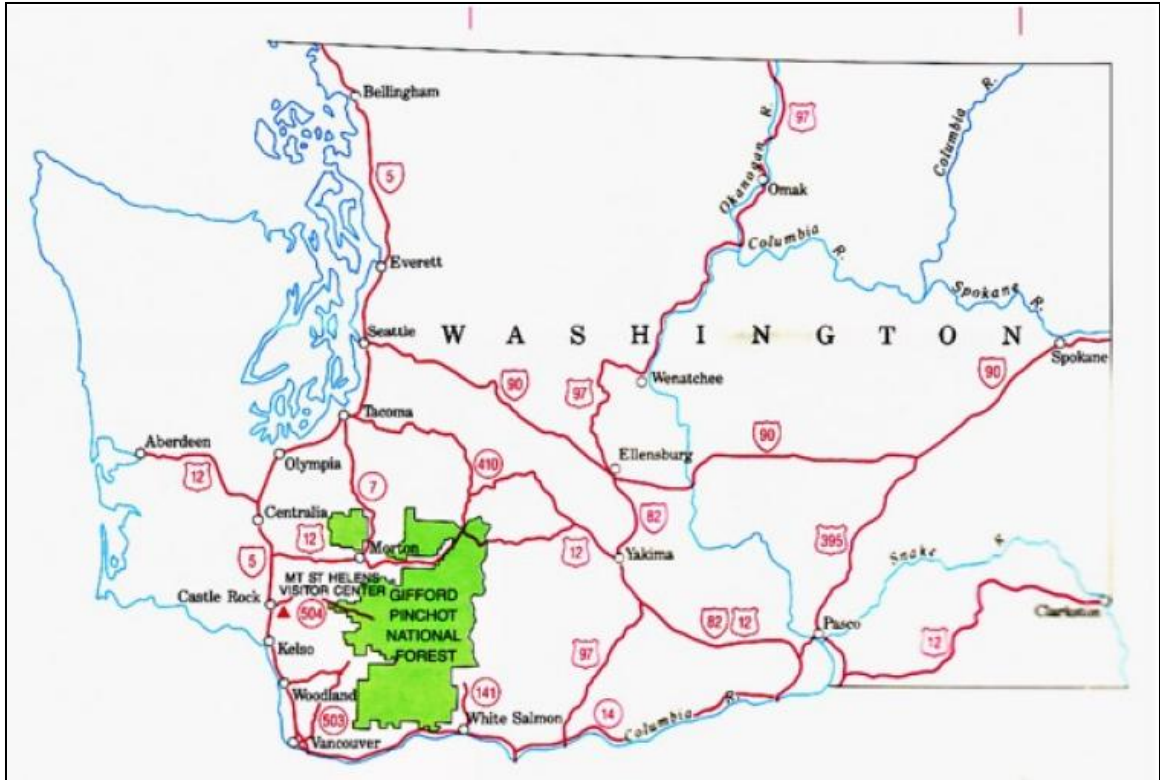


Figure 1.1

USDA Forest Service map displaying the location of Gifford Pinchot National Forest in southern Washington. The location of Mount Saint Helens Visitor Center is also shown.

Created May 2008 by USDA Forest Service
From fs.fed.us

1.4 Eruptive History

Mount Saint Helens has been the most active of Cascade Range volcanoes during the Holocene epoch. Since its birth approximately 40,000 years ago, eruptions produced more than 100 tephra deposits that can be identified in stratigraphic section (Mullineaux, 1996). The eruptive history of Mount Saint Helens has been divided into four eruptive stages (Crandell, 1987). The Ape Canyon eruptive stage (40,000-35,000 years b.p.) delineates the onset of volcanism at Mount Saint Helens, followed by the Cougar eruptive stage (20,000 years b.p.) and the Swift Creek eruptive stage (13,000 years b.p.). The fourth and most recent eruptive stage is the Spirit Lake eruptive stage, initiated approximately 4,000 years b.p. This eruptive stage was further divided into six eruptive periods, the most recent of which produced tephra deposits that are of interest to this study (Crandell, 1987). The Swift Creek, Pine Creek, Castle Creek, and Sugar Bowl eruptive periods produced pumiceous and lithic pyroclastic flows, lahars, and lava flows intermittently between 4,000 years b.p. and 1,150 years b.p. (Crandell, 1987). Eruptive material was compositionally limited to dacite and silicic andesite for the largest part of the volcanic history. The Castle Creek eruptive period (2,200 years b.p.) marks a change in eruptive behavior and the first appearance of mafic lava (Mullineaux and Crandell, 1981; Crandell, 1987). The final two eruptive periods of the Spirit Lake eruptive stage are the Kalama (CE 1480) and Goat Rocks (CE 1800) eruptive periods. Four major eruptions and several minor eruptions since the onset of the Kalama eruptive period 530 years ago deposited tephra in what is now Gifford Pinchot National Forest (Wolfe and Pierson, 1995). Trees amenable to dendrochronology (those that produce annual growth rings at the time of eruption) that were covered by deposits of some or all of the four eruptions still survive. The oldest trees in the area approach 700 years of age. Trees cored for this

study were sought in areas where tephra deposits from Kalama and Goat Rocks eruptive periods underlie deposition from the AD 1980 eruption of Mount Saint Helens. Units in the field were identified with the aid of published descriptions and isopach maps, and observed in stratigraphic section wherever possible.

The Kalama eruptive period began in AD 1480 with an explosive eruption of dacitic tephra (layer Wn) (Mullineaux and Crandell, 1981; Crandell, 1987). Layer Wn tephra was deposited northeast of the cone, across Washington and into Canada (Smith et al., 1977). The thickest deposits of this unit (>20 cm) occur northeast of the volcano, disappearing just beyond the Cowlitz river (figure 1.2) (Yamaguchi, 1985). A second major eruption followed approximately two years later, and deposited a large volume of dacitic tephra (layer We) east of Mount Saint Helens (Yamaguchi, 1985). Pyroclastic flow deposits associated with this eruptive period have been identified on the southwest flanks of the volcano (Mullineaux and Crandell, 1981).

Identification of tephra in the field was completed using the descriptions put forth in US Geological Survey Professional Paper 1563 (Mullineaux, 1996). Those descriptions are summarized here. Layers Wn and We are the thickest depositional units of tephra set W. At least three thinner layers are part of the same set, and because each unit extends in a different lateral direction from the cone, the layers generally do not all appear together in stratigraphic sequence. Wn and We are composed of mostly vesicular pumice with 5-20% lithic fragments. Hypersthene constitutes the vast majority of ferromagnesian minerals in all units of set W. In the field, set W is distinguished as a

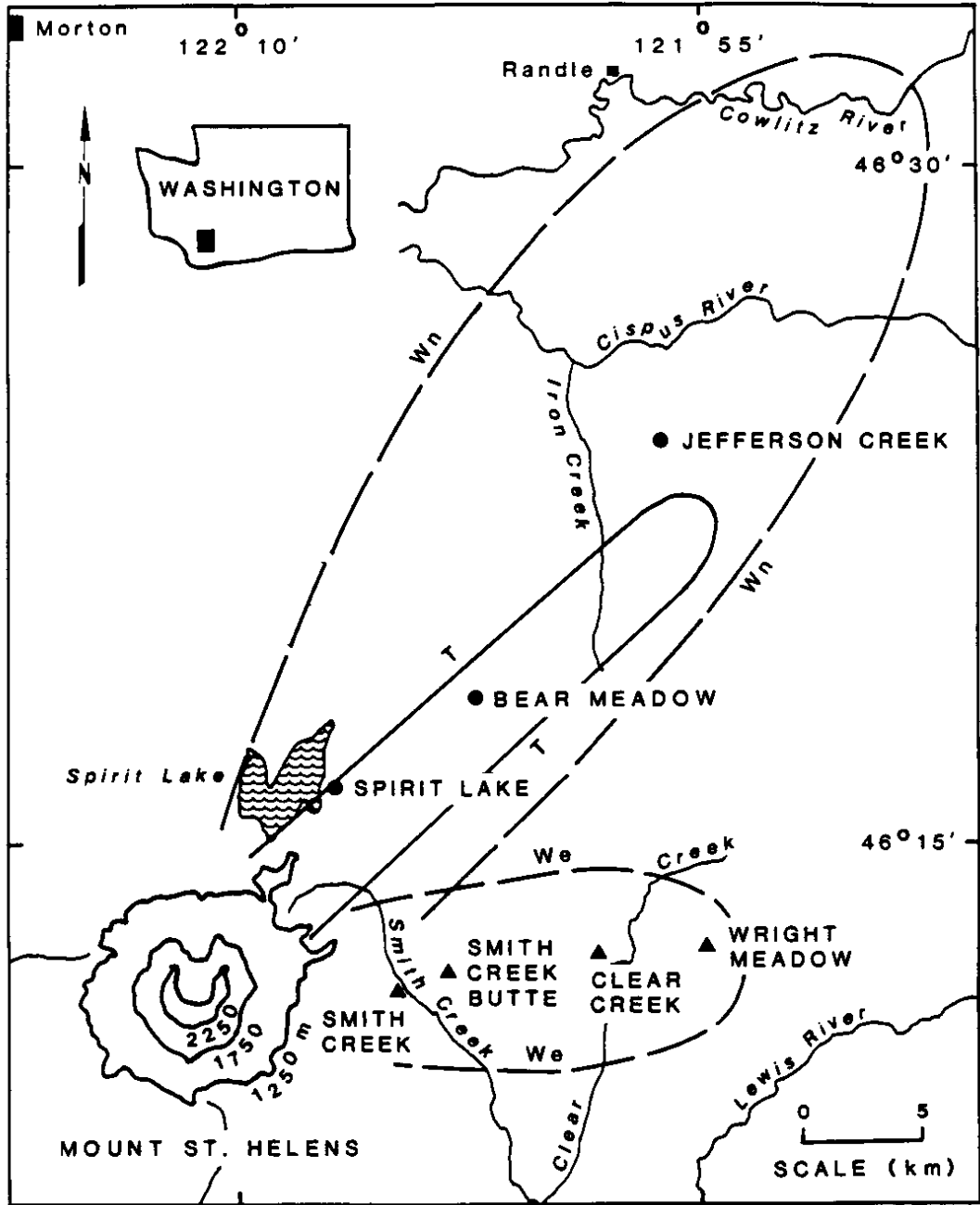


Figure 1.2

Location of sampled forest stands and the 20 cm isopach for the We, Wn, and T tephra layers (Yamaguchi, 1983 and 1985). Triangles indicate Yamaguchi's 1985 sites and circles indicate his 1983 sites.

thick, coarse, nearly unweathered white pumice layer. It is similar in appearance to tephra T (CE 1800) but with a different ferromagnesian composition.

In stratigraphic section, set W lies below layer X, a deposit associated with minor eruptions of the Kalama eruptive period (figure 1.3). Layer X is composed of a thin, dark, fine-grained andesite to basaltic andesite tephra bed.

Tephra Wn is the basal unit of set W. It is composed of coarse and highly vesicular pumice with some lithic fragments (<20%). No grading or stratification is apparent, and the yellowish-white color of the pumice in Wn sets it apart from all other units except the T tephra. As mentioned earlier, the hypersthene crystals in Wn and T are of distinct compositions and can be distinguished in thin section. In the field, layer Wn is generally a thicker deposit than tephra T, and the two can be distinguished by stratigraphic position (Mullineaux, 1996).

The Goat Rocks eruptive period (1800-1857) was initiated by an explosive eruption that produced the dacitic pumice of tephra layer T (Lawrence, 1939, 1954; Yamaguchi, 1983). This eruption was followed several decades later by multiple eruptions, which were recorded by local newspapers between 1835 and 1857 (Crandell, 1987). At least six eye-witness accounts verify that smoke and ash emission occurred from the north flank of Mount Saint Helens between November and December of 1842 (Holmes, 1955; Majors, 1980). Approximately 1.25 cm of lithic ash associated with these eruptions was deposited at least 100 km southeast of the volcano in the Dalles, Oregon (Holmes, 1955; Hoblitt et al., 1980).

T tephra from the initial explosive phase of the Goat Rocks period was deposited along a narrow belt trending northeast from the volcano across Washington, Idaho and

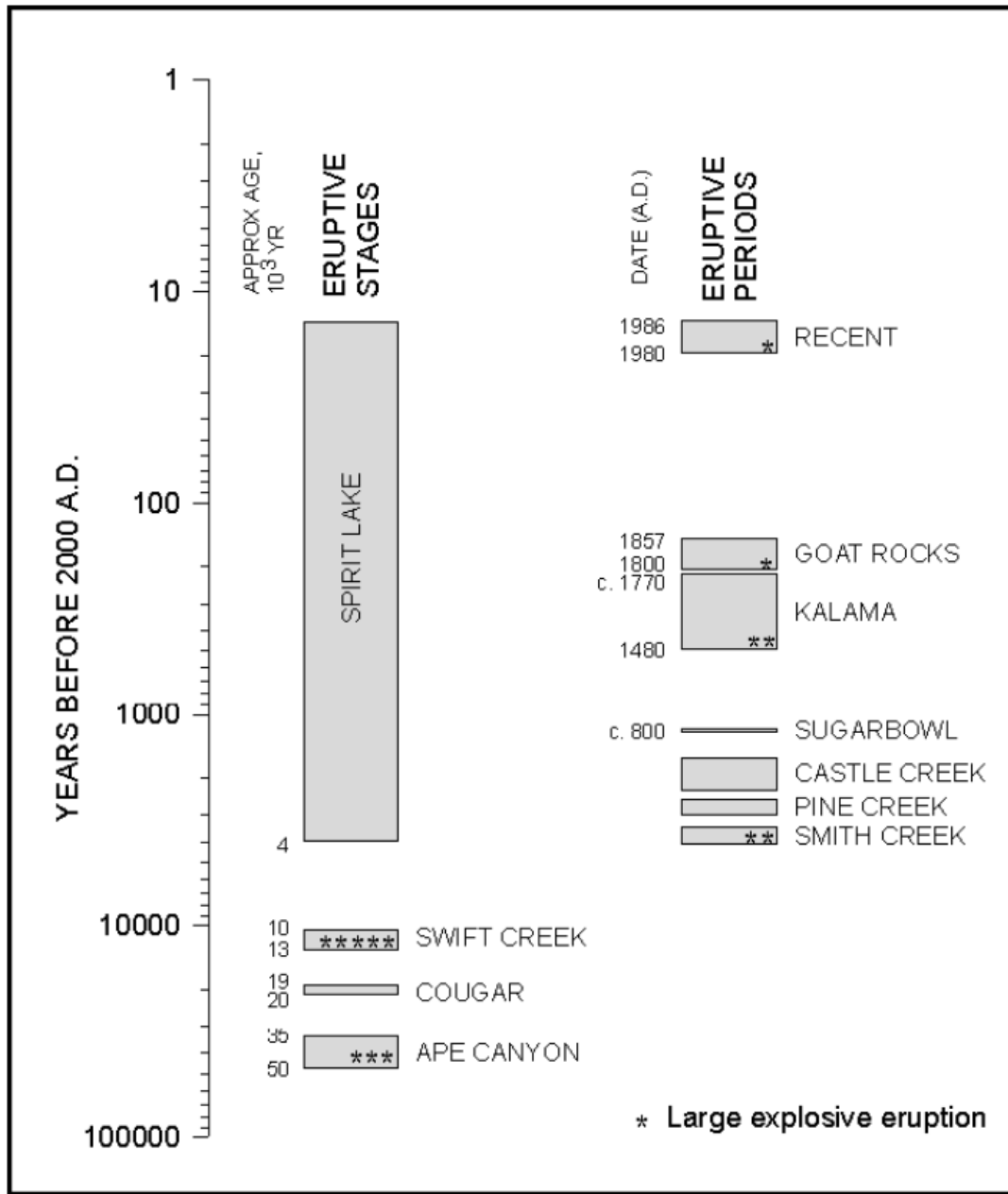


Figure 1.3

Eruptive history of Mount St. Helens shown on a logarithmic time scale (expands with decreasing age). Eruptive periods (at right) are subdivisions of the Spirit Lake eruptive stage. Large explosive eruptions are those that deposited at least 25 cm of tephra at distances of 8 to 10 km downwind of Mount St. Helens. Modified from Pallister and others (1992). Additional data from Mullineaux (1996), and Yamaguchi and Hoblitt (1990).

From Edward W. Wolfe and Thomas C. Pierson, 1995, Volcanic-Hazard Zonation for Mount St. Helens, Washington, 1995: U.S. Geological Survey Open-File Report 95-497.

part of Montana (Okazaki et al., 1972). The thickest deposits of this unit (>20 cm) stop outside of Jefferson Creek (Yamaguchi, 1985) (figure 1.2). Several features, such as the Goat Rocks dome, the Floating Island Lava Flow, and multiple debris flows on the northern flanks of the volcano, are attributed to this eruptive period, but were destroyed by the AD 1980 eruption (Crandell, 1987; Hoblitt et al., 1980; Yamaguchi et al., 1990).

In the field, tephra layer T can be identified as a thick deposit of well sorted, coarse grained, light gray pumice with subspherical vesicles, deposited exclusively northeast of the cone (Mullineaux, 1996). Minor amounts of oxidation are visible in the uppermost section of the unit. Hypersthene, hornblende and lesser amounts of augite compose the ferromagnesian minerals. Tephra T sits stratigraphically above set X and set W deposits, and is coarser and thicker than overlying deposits associated with the AD 1980 eruption.

Mount Saint Helens erupted catastrophically on May 18, 1980, when a magnitude 5.1 earthquake centered approximately 1600 m below the base of the volcano caused a massive slope failure on the northern flank (Voight et al., 1983; Voight et al., 1981). The previously conical summit was reduced to a 2 by 2.5 km wide crater (Doukas, 1990). Debris avalanches were deposited over 60 square kilometers of surrounding land, terminating almost 26 km west of the volcano (Doukas, 1990). Deposits from the lateral blast reached up to 27 km north of the cone and a subsequent pyroclastic surge fanned outward from the crater to the north, killing most trees and wildlife within an area of 550 square kilometers (Moore and Sisson, 1981). The eruptive column reached a height of 24 km in fewer than 15 minutes, and prevailing westerly winds transported ash more than

480 km from the source (Lipman and Mullineaux, 1981) (figure 1.4). The AD 1980 eruption of Mount Saint Helens is the most economically destructive in the history of the United States, resulting in the destruction of several hundred homes, more than 40 bridges, and large expanses of railroad and highway. Smaller eruptions that led to the formation of a lava dome in the crater of the 1980 eruption persisted until October 1986. From October 2004 until January 2008, Mount Saint Helens produced a dome-building eruption that added to the lava dome in the 1980 crater (Sherrod et al., 2008). Dome growth ceased completely in January of 2008, and the volcano remains inactive at the present time. No tree rings produced after AD 1986 were analyzed in this study, and effects of the most recent activity at Mount Saint Helens are not considered.

The AD 1980 eruption of Mount Saint Helens produced tephra that is dacitic in composition (Swanson et al., 1989). The chemical content of this deposit varies significantly with fragment size (Hoffer and Hoffer, 1986) and contains more lithic and crystalline material than earlier depositional units (Zobel and Antos, 1991). It can be easily distinguished by stratigraphic position, as the uppermost layer of volcanic ash and pumice in every field site of this study (figure 1.3).

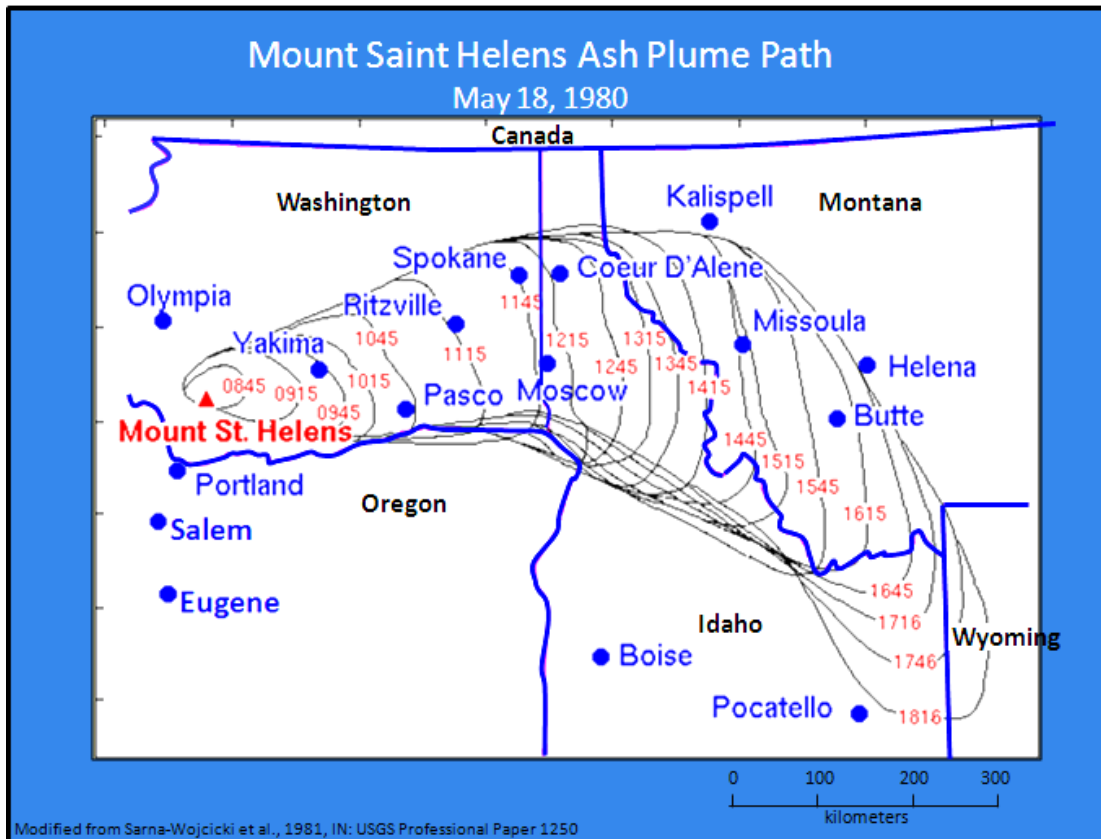


Figure 1.4

Isochron map showing maximum downwind extent of ash from ash plume erupted from Mount Saint Helens on May 18, 1980, and carried by fastest moving wind layer, as observed on satellite photos. Map is compiled from NOAA satellite photos (sectors KB7 and SA40) taken at 30 minute intervals between 0845 and 1816 PDT. Plot of plume position relative to ground was visually corrected for zenith angle. Error in position of plume boundaries is +/- 10 km in the N-S direction and +/- 5 km in the E-W direction.

Modified from Topinka, USGSICVO, 1999

1.5 Principles of Dendrochronology

Dendrochronology is the study of chronological sequences of tree rings. It is based on the principle that annual growth rings exhibit characteristic patterns that reflect the growth environment in which they were produced. Four conditions must be met in order for a sequence of tree rings to be assigned dates (Stokes and Smiley, 1968). First, only trees that produce annual growth rings may be considered. Second, a group of trees sampled for the purpose of establishing a chronology must have one locally dominant cause for restricted growth. The third condition is that the growth-limiting factor must not be consistent in strength over time. Annual fluctuations in intensity make it possible for ring-width variations to form recognizable patterns in sequence. Finally, the growth-limiting factor must also be prominent over a geographical area that is large enough to establish a chronology based on common macroclimatic conditions. Trees cored in this study meet all of the above requirements. Douglas firs produce annual growth rings, and are limited by the same annually fluctuating growth-limiting factor over a large geographic expanse. In the region that trees from this study were sampled, precipitation is the dominant growth-limiting factor for Douglas firs (Littell, 2008). Douglas-fir chronologies that date back several centuries have been established and made available through the International Tree Ring Data Bank (noaa.gov).

A main objective of this study is to measure the variation of elemental abundance in wood cellulose from annual growth rings produced coincident and subsequent to volcanic eruption at Mount Saint Helens. In order to isolate core segments for chemical analysis, calendar dates had to first be assigned to a sequence of growth rings. Restricted growth on and after eruption years in previous studies suggest that the growth-limiting factor for these years is attributable to volcanic eruption rather than some other

environmental factor. It was hypothesized that chemical analysis of the wood cellulose in these rings might show evidence to support such an idea.

A tree increases in height (apical growth) through the formation of tissue in the apical meristem (Stokes and Smiley, 1968). The radial growth of a tree is attributed to secondary tissue development by the vascular cambium that is derived from the lateral meristem (Stokes and Smiley, 1968). Cells formed on the inside of the cambium make up the woody xylem in the form of annual growth rings. Cells formed to the outside of the cambium make up the phloem, along which nutrients are transported (figure 1.5). The pith, located in the center of the stem, represents the earliest growth interval in the history of the tree. Protective bark is constantly shed and reproduced, and does not have any measurable correlation to a particular block of time.

The boundaries of an annual growth ring are defined by two successive transitions from latewood to earlywood. Latewood can be identified as thick-walled cell growth that is generally darker than thin-walled earlywood cells. The transition from earlywood to latewood is gradual, while that of latewood to earlywood is prominent and sudden (figure 1.6). The addition of one layer of earlywood that transitions to latewood is representative of a period of seasonal growth that corresponds to one calendar year. Younger trees generally produce thick annual rings. As the stem becomes larger, progressively thinner rings are generated (Stokes and Smiley, 1968). This effect must be taken into account when comparing ring widths over long growth intervals. Some features, such as false or double rings, micro rings, and absent rings, may complicate the development of a chronology. These complications are addressed in chapter 2.

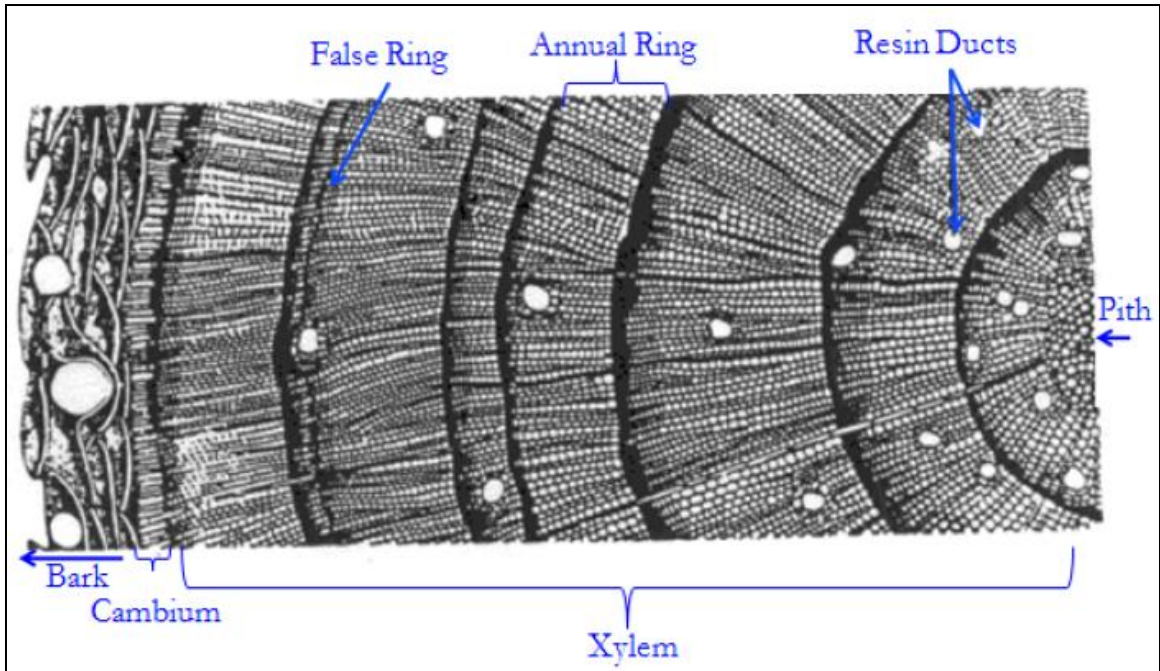


Figure 1.5

Cross-sectional view of a tree showing features that may be used in dendrochronology.
Modified from Fritts, 1979.

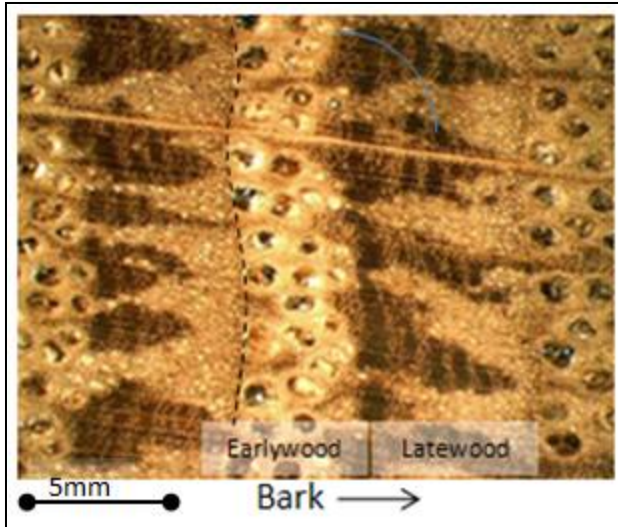


Figure 1.6

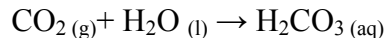
Thin section of oak showing the contrast in size and cell-wall thickness of earlywood and latewood. The sharp contact between latewood and earlywood (dotted line) indicates that growth is outward to the right. Scale is approximate. Modified from McCarrol and Loader, 2004.

1.6 Principles of Dendrochemistry

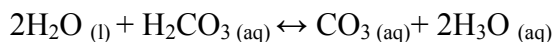
Dendrochemistry is the study of chemical changes in a dated sequence of tree rings, and is founded on the principle that trees that produce annual growth rings have the potential to retain chemical information about the local environment in which growth occurred (Savard et al., 2004; Pearson et al., 2005). In order for chemical evidence of a volcanic eruption to be recorded in the growth ring of a tree, the eruption must chemically alter the air, water or soils that sustain the tree. For example, if water in the soil is chemically altered and taken into the tree via the root system, then a record of the chemical alteration may be retained in the wood cellulose of the subsequently produced growth ring.

It is reasonable to presume that a volcanic eruption will produce significant chemical alteration of the surrounding ecosystem. The generation and release of sulfur dioxide gas associated with large-scale eruptions is enough to reduce solar radiation and lower global surface temperatures (Pearson et al., 2005). Acid rain, a common byproduct of volcanic eruption, can significantly affect the pH of soils and groundwater, thereby increasing the mobility of elements such as phosphorus that are not otherwise transportable (Pritchett and Fisher, 1981).

Acid rain refers to the wet or dry deposition of acidic species from the atmosphere on the surface of the earth. Volcanic emissions that are primarily responsible for the production of acid rain include sulfur dioxide (SO_2), nitric oxides, (NO_x) and carbon dioxide (CO_2). Normal, non-polluted rain has a slightly acidic pH due to a natural reaction between water and atmospheric CO_2 that produces carbonic acid via the following reaction (Virtual ChemBook):

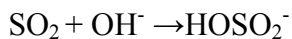


Carbonic acid may then ionize in water to form hydronium and carbonate ions:

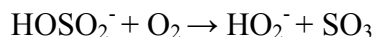


Hydronium in soils can affect plant life by mobilizing toxins and leaching away minerals that are nutritionally significant (Driscoll et al., 2001). Volcanic emissions of carbon dioxide may lead to an increased production of carbonic acid and contribute to higher than normal acidity in rain water.

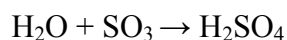
Sulfur dioxide (SO_2) reacts with hydroxyl and water vapor in the atmosphere to produce sulfuric trioxide (SO_3) and ultimately sulfuric acid (H_2SO_4) through the following series of reactions:



Then



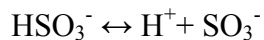
And



In the presence of water, as in cloud droplets, sulfur dioxide gas may produce sulfuric dioxide through hydrolysis:



And



Nitric oxides contribute to the post-eruptive production of acid rain when, for example, nitrogen dioxide reacts with atmospheric OH to form nitric acid:



The production of acid rain may occur either in the presence of atmospheric H₂O, as in cloud droplets, or at the surface of the earth when water interacts with particles and gasses that are present on the surfaces of tephra fragments, plant matter, or soil. Consequent changes in water, air, soil, flora, or fauna may upset the local bionetwork, enhancing the productivity of some organisms and reducing that of others (Krug and Frink, 1983). The productivity of micro-organisms, such as sulfate-reducing bacteria, can also significantly affect soil chemistry. Trees that sustain growth during and after volcanic eruption may therefore retain some chemical record of the event in successively produced wood cellulose. Multiple recent eruptions of Mount Saint Helens in the proximity of a national forest contribute greatly to the likelihood that such a chemical record will be preserved.

1.7 Isotopes in Tree Rings

The three main chemical constituents in wood are carbon, oxygen and hydrogen, all of which have more than one stable isotope in nature. Photosynthesis is a metabolic pathway that converts light energy to chemical energy. In photosynthesis, the energy absorbed by chlorophyll transforms carbon dioxide and water into carbohydrates and oxygen via the reaction $\text{CO}_2 + \text{H}_2\text{O} \rightarrow (\text{CH}_2\text{O}) + \text{O}_2$ (where chlorophyll donates an electron to facilitate the reduction of CO₂ by water). Through the process of photosynthesis, isotopic fractionation of carbon occurs at two stages (McCarroll and Loader, 2004). The first point of fractionation is at the interface between air and stomata (pores on leaves and needles of trees). The relative abundance of ¹²C and ¹³C at this interface is affected primarily by the abundance of each isotopologue in the atmosphere

(Barbour et al., 2002). The second point of fractionation occurs when CO₂ is used to produce carbohydrates, as in the above reaction (McCarrol and Loader, 2003). Both instances of fractionation lead to a depletion of ¹³C relative to ¹²C in the tree. The ratio of ¹³C to ¹²C is written in delta (δ) notation, and expresses a value in parts per thousand (‰) that is relative to some standard with a known isotopic ratio. The chosen standard for carbon is known as VPDB (Coplen, 1995), and δ¹³C is calculated by the equation:

$$\delta^{13}\text{C} = (\text{R}_{\text{sample}}/\text{R}_{\text{standard}} - 1)1000$$

where R = the ¹³C/¹²C ratio of the sample or the standard, as noted

A depletion of ¹³C relative to ¹²C will result in a negative δ¹³C value (McCarroll and Loader, 2004). δ¹³C values are even lower in wood cellulose, as further fractionation occurs during the production of various constituents of the tree, and biological processes almost always preferentially incorporate the lighter isotope.

If some external influence were to suddenly limit the amount of CO₂ taken into a tree, then the amount of internal CO₂ available for the production of carbohydrates would become limited. The tree would respond to this depletion of a CO₂ reservoir by discriminating against ¹³C to a lesser extent in the second phase of fractionation. The result would be a relative “enrichment” of ¹³C, in which the difference in abundance between ¹³C and ¹²C would be less pronounced. One external influence that has been shown to limit CO₂ intake is large-scale emission of industrial aerosols (Savard et al., 2004). The limited CO₂ intake is attributed to closure of stomata resulting from exposure to aerosol pollution. Sulfur dioxide, the most prominent gas released by smelter operations in the 2004 Savard study, is also a prominent volcanic aerosol (Pearson et al., 2005). Volcanic eruptions that emit large volumes of sulfur dioxide gas should then be

capable of inducing closure of stomata in nearby trees, thereby producing a temporary reduction in discrimination against internal ^{13}C used in photosynthesis. This would generate a relative ^{13}C enrichment that is coincident with the timing of volcanic eruption. If this isotopic enrichment also coincides with shifts in elemental concentrations in an annual growth ring, it may serve as compelling evidence for volcanic eruption.

1.8 Previous Work

Dendrochemistry

Previous work concerning dendrochemistry at Mount Saint Helens is limited. The majority of tree-core studies conducted in the area immediately surrounding the volcano have considered the occurrence of thin annual growth rings on and after eruptive years, but have not conducted chemical analysis of the same rings (Brantley et al., 1986; Sheppard et al., 2008; Sheppard et al., 2009; Yamaguchi, 1983; Yamaguchi 1985; Yamaguchi and Hoblitt, 1986; Yamaguchi et al., 1990; Yamaguchi and Lawrence, 1993). The extensive body of dendrochronological research in the area provides a starting point for the application of analytical chemistry. No standard procedure exists for laser-ablation inductively coupled plasma mass spectrometry (LA-ICP-MS) on natural wood, but the certainty of the historic eruption dates make Mount Saint Helens an ideal location to experiment with the technique. Analysis of tree ring chemistry using LA-ICP-MS at other locations, and solution ICP-MS at Mount Saint Helens suggest that tree-ring chemistry has strong potential to serve as a record of volcanic history.

Old-growth Douglas firs were cored and individual growth rings were analyzed using solution ICP MS in one prior study at Mount Saint Helens (Hall et al., 1990). These

trees were taken from a location 15 km northeast of the AD 1980 crater, and samples were introduced to the ICP by microwave digestion in sealed Teflon capsules (Hall et al., 1990). When rare earth element abundances were plotted against time, this study recorded anomalously high abundances of several REEs at AD 1478 and AD 1490. These dates correspond loosely with the AD 1480 and AD 1482 eruptions of the Kalama period, but are somewhat unsettling. The AD 1480 and AD 1482 eruptions were established using dendrochronology (Yamaguchi, 1985). Ideally, chemical analysis of tree rings dated using the same technique should yield chemical anomalies for the same years that show limited growth. The size of the sample set for this study was very small ($N = 2$) and the ambiguity of results may be due to an insufficient amount of data.

Tree-core studies in other locations have used LA-ICP-MS. Inductively Coupled Plasma Mass Spectrometry (ICP-MS) is a method of trace-element analysis in which samples are decomposed to neutral elements in a high-temperature argon plasma and analyzed based on their mass-to-charge ratio. Solution ICP-MS accomplishes sample decomposition by way of multi-acid digestion techniques while laser ablation ICP-MS (LA-ICP-MS) introduces solid samples into the ICP without acid digestion. The lack of chemical pre-treatment required for laser ablation analysis reduces the risk of contamination and simplifies the process of sample preparation. Also, smaller quantities of sample material are necessary for laser ablation, and the small spot size (as little as 30 μm diameter) can easily isolate wood cellulose from a single annual ring. It is also possible to discriminate between earlywood and latewood of a single growth ring in most cases. Laser ablation is, however, a new technology being applied to dendrochemical

studies, and ablation techniques for natural wood are not well established. Calibration of equipment and creation of solid standards are of particular concern in this type of study.

Initial chemical analyses of trees at Volcán Parícutin in Mexico show that high levels of phosphorus and low levels of both calcium and strontium coincide with the onset of eruption (Sheppard et al., 2008) (figure 1.7).

These chemically distinct growth rings are thinner than growth rings that pre-date the AD 1943 eruption (figure 1.8). The increase in phosphorus may be due either to direct input from volcanic deposition, or to a subsequent change in soil acidity (Sheppard et al., 2008). Rain water that percolates through tephra and into underlying soils may become acidic through interaction with volcanic materials in both the atmosphere and on the surface of the ground. Phosphorus, nearly immobile in most natural conditions, becomes more mobile in soils with acidic pH (Pritchett and Fisher 1981). Phosphorus at Volcán Parícutin may have been transported in solution to the wood of a tree via the root system. An increase in the mobility of phosphorus may also be linked to a decrease in the Si/Al ratio of volcanic ash and tephra (Felitsyn and Kirianov, 2002). Si is more mobile than Al during the weathering of volcanic glass, causing the Si/Al ratio to decrease with palagonization and kaolinization of hyaloclastites. Multiple rhyolitic tephtras have shown an increase in P content that correlates to a decrease in the Si/Al ratio in tephra (Felitsyn and Kirianov, 2002). Weathering of dacitic tephra at Mount Saint Helens may also correspond to a post-emplacment period of increased phosphorus mobilization. High concentrations of Na were found, in addition to P and S, in post-eruption rings from old-growth Jeffery pine trees at Cinder Cone in northeastern California in a similar study

(Sheppard et al. 2008). In this study, a combination of ring-width and ring chemistry helped to constrain an eruption date after AD 1666.

Changes in soil acidity can be directly related to volcanic eruption, and are likely related to the spike in phosphorus observed at Volcán Parícutin. The observed calcium depletion may, however, be the result of a biological response to volcanism. When acidic deposition reduces soil pH, phosphorus is not the only element to experience increased mobilization. Aluminum also becomes highly mobile in solution with increasing acidity. Calcium, which may be displaced by aluminum ions, plays a vital role in many different plant physiological processes that influence growth rates (McLaughlin et al., 1987). When an increased abundance of mobile aluminum in soil displaces significant amounts of calcium, the tree experiences what is known as aluminum toxicity (Smith and Shortle 2001; Shortle et al. 1997; Lawrence et al. 1997). The capacity of plants to resist environmental stresses depends on the maintenance of an uninterrupted flow of Ca from the soil to growing centers within trees (McLaughlin et al., 1987). Interruption of calcium intake due to a volcanic increase of soil acidity may then be responsible for the irregular growth and chemistry of later-produced tree rings in the case of Volcán Parícutin.

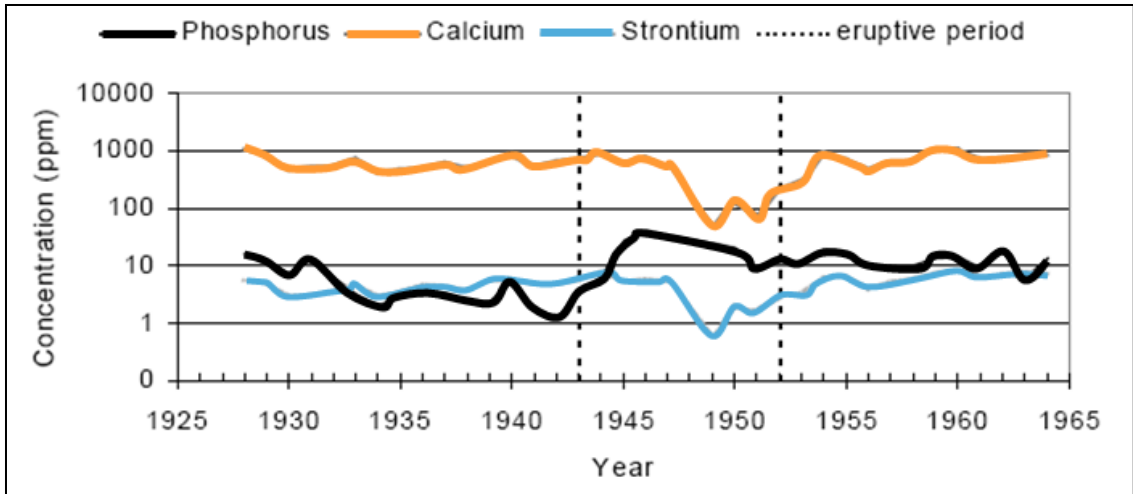


Figure 1.7

Dendrochemical results from one pine tree growing within the ash-fall zone of Volcán Parícutin, Michoacán Mexico. Vertical dashed lines mark the eruptive period from 1943 to 1952.

From Sheppard et al. (2008).



Figure 1.8

Thin annual growth rings were produced during the eruptive period from 1943-1952.

From Sheppard et al. (2008).

Isotopes

As mentioned in section 1.7, studies of anthropogenic pollution have documented a relative enrichment of ^{13}C in growth rings that coincide with the onset of gas emissions. One such study observes the effects of a sulfur-smelter operation on spruce trees located up to 116 km downwind (Savard et al., 2004). Twenty-one spruce trees from seven sample sites located southwest and northeast of the Horne smelter in Rouyn-Noranda, Canada, were studied. This smelter operation has been servicing mining companies in northern Quebec since December of 1927, emitting large amounts of sulfur dioxide gas almost continuously.

Sampled species include black spruce (*picea mariana*) and white spruce (*picea glauca*). These species are abundant throughout the boreal forest, and exhibit qualities that are amenable to dendrochronology. In order to minimize the number of cored trees, an express population signal (EPS) evaluation was used to elect the number of trees needed to accurately represent the entire population (McCarroll and Pawellek, 1998). Control trees were sampled from the northern border of the boreal forest ecozone in an unpopulated coastal region, nearly 800 km north of Rouyn-Noranda. This site is well outside of the zone contaminated by Horne smelter, and considered to be an area of low risk for other sources of anthropogenic pollution (Savard et al., 2004). Analysis of control trees provided a $\delta^{13}\text{C}$ profile representative of normal (unaffected) trees in the region. A test site, located 9 km southwest of the Horne smelter, was elected to test the dendrochemical response of spruce trees to sulfur dioxide emissions. Five other sites, trending SW-NE of the smelter, were chosen to demonstrate the dendrochemical response at varying distance from the point source.

Three trees were selected for isotopic analysis from each field site, and all were assigned calendar dates using conventional methods of dendrochronology. Annual rings were separated into ring pairs, equivalent to two growth years, in the laboratory using ultra-clean blades. Samples were analyzed for $\delta^{13}\text{C}$ using an element analyzer in continuous flow with an isotope ratio mass spectrometer (Savard et al., 2004). Precision on standard analyses was better than 0.3‰, equal to 2 standard deviations.

All three trees analyzed at the test site show a positive shift in $\delta^{13}\text{C}$ values of +4‰ or more coincident with the initiation of sulfur-smelter operations. Trees at the control site did not show any major fluctuations in carbon during the time period of smelter initiation. Of the remaining sample sites, two within 15 km of the smelter showed carbon fluctuation comparable to that at the control site. Two at greater distances showed abrupt enrichments of ^{13}C of a lower magnitude, indicating a decrease in signal strength inversely related to distance from the point source. Only one field site did not show a pronounced enrichment in ^{13}C .

The relative enrichment in ^{13}C observed at five of the six sampled sites (excluding control site 7) is attributed to a decrease in carbon uptake resulting from closure of stomata on trees exposed to the industrial aerosols (Savard et al., 2004). Stomatal closure may also occur in trees that are covered with significant amounts of volcanic ash, or exposed to high levels of sulfur dioxide aerosols. If stomata do close for any amount of time, then a similar enrichment in ^{13}C may be measurable in the core samples from Mount Saint Helens. Because ^{13}C enrichment in this case reflects photosynthetic activity, it would serve as an indication of volcanic eruption that is independent of stunted growth rings or major element dendrochemistry.

Dendrochronology at Mount Saint Helens

Prior to the May 1980 eruption of Mount Saint Helens, a large convex fan of rock debris containing a sparse population of young trees was located downslope of the Goat Rocks dome on the northern flank of the volcano (Crandell, 1987). The downslope reaches of the debris fan interfingered with mature forest. Although the fan was destroyed by a debris avalanche associated with the 1980 eruption (Lipman and Mullineaux, 1981), several lines of evidence were used to constrain the timing of its deposition.

Paleomagnetic data from samples taken on the debris flow prior to 1980 suggest that the fan originated as a hot avalanche associated with the extrusion of the Goat Rocks dome (Crandell, 1987). Such evidence confirms earlier deductions based on cross-cutting relations and other field observations (Verhoogen, 1937). According to the above studies, the debris fan was younger than tephra layer T (CE 1800) and older than the oldest tree observed on the fan prior to its destruction, a tree that began growth before AD 1876 (Crandell, 1987). Prior to 1980, the analysis of trees growing on the debris flow and in the adjacent mature forest could have provided evidence to further constrain the age of fan deposition (Lawrence, 1938). Core samples from trees growing on or near the debris fan were obtained by Lawrence between 1938 and 1940 but resulting data were not published at the time (Yamaguchi, 1992). Unusually narrow tree rings in these, along with more recently sampled old-growth Douglas firs, provide age evidence for the deposition of the debris fan that was destroyed in 1980 (Yamaguchi, 1992). The calendar dates assigned to thin growth rings coincide with eyewitness accounts of eruptions on the north flank of Mount Saint Helens, providing further proof that the stunted ring growth is consequent to volcanism (Holmes, 1955; Majors, 1980; Yamaguchi, 1992).

In the 1992 publication by Yamaguchi, the growth rings of 21 old-growth Douglas firs collected from various locations between 1987 and 1992 are considered along with five core samples (two lodgepole pines, and three Douglas firs) obtained by Lawrence between 1938 and 1940. The 21 trees sampled by Yamaguchi came from sites along the Pine Creek and Muddy River drainages and were either abraded or passively buried by lahars that resulted from the 1980 eruption of Mount Saint Helens. Physical damage to these trees varied significantly. Three of the core samples collected by Lawrence (two lodgepole pines and one Douglas fir) came from younger trees rooted on the debris fan, and two (Douglas firs) came from the mature forest adjacent to the downslope margin of the fan. Control growth patterns were established with ring measurements of 46 cores from 25 old-growth Douglas firs located beyond the fallout zone for Goat Rocks tephra (26 km east of Mount Saint Helens). These trees were cored in 1981, and so include growth rings up to that calendar year. Growth trends in the control set were determined according to standard procedure (Stokes and Smiley, 1968; Fritts, 1976; Graybill, 1982; Sheppard and Jacoby, 1989). Three additional Douglas firs were cored from a location 29 km southeast of the cone to establish control patterns for tree growth after 1981.

The two Douglas firs sampled adjacent to the debris fan show a series of unusually thin growth rings that begin with the AD 1843 ring and persist for ten to eleven years (Yamaguchi, 1992). These trees survived 11-12 cm of fine tephra deposition from the May 18, 1980 eruption of Mount Saint Helens. Lawrence (1938) noted a 13 cm layer of fine ash near the base of the Goat Rocks dome debris fan. Yamaguchi suggests that the thin growth rings are an indication of a single instance of physical injury to the trees that

occurred in late 1842 or early 1843 and affected ring growth for more than a decade thereafter. The trees rooted on the debris fan were too young to record the same event. No such pattern of thin growth rings were present in the set of 25 control trees, suggesting that climatic variations were not responsible for the generation of abnormally thin rings (Yamaguchi, 1992).

Several of the modern analog trees affected by lahars in 1980 showed growth patterns similar to those sampled by Lawrence adjacent to the debris fan. Results among trees injured by lahars varied more, and growth was likely influenced by a lack of competition for light and nutrients associated with the death of nearby trees in addition to the injury sustained by the sampled surviving trees. Thin ring growth similar to that observed in the samples affected by the surge deposits was not observed in control trees. This suggests that climatic variation was also not responsible for the generation of thin rings that began in 1986. Yamaguchi concluded that deposition of 11-12 cm of fine ash from the 1980 eruption did not affect the width of annual growth rings in this study (Yamaguchi, 1992).

Major eruptive events were also identified using dendrochronology of old-growth Douglas firs in a study by the same author (Yamaguchi, 1985). Trees from sample locations at Smith Creek, Smith Creek Butte, Clear Creek and Wright Meadow were examined for effects from the eruption of tephra layers We and Wn, east of the volcano. Douglas firs from Spirit Lake, Bear Meadow, Iron Creek and Jefferson Creek were studied for effects from the eruptions of the set W tephras, and from the eruption of layer T at AD 1800 (Yamaguchi, 1983). Two to seven trees were cored at each site, using 51 cm and 91 cm increment borers at breast height. Trees with anomalously narrow or

missing rings that correlate to dates of AD 1480 and AD 1482 were identified at Smith Creek Butte and Bear Meadow sites. Normal ring patterns at the end of the fifteenth century AD were recorded in trees from sites at Clear Creek, Jefferson Creek, and Wright Meadow. Missing rings in cores from the Spirit Lake site helped to revise the date of eruption marking the onset of the Goat Rocks eruptive period from AD 1802 (Lawrence 1939, 1954) to AD 1800 (Yamaguchi, 1983). Narrow rings correlating to the AD 1800 eruption were also observed at Bear Meadow. Cores from Jefferson Creek and Iron Creek showed the level of restricted growth diminishing with distance from the cone (Yamaguchi, 1983).

1.9 Project Outline

In order to test the hypothesis that a volcanic eruption could cause a measurable chemical alteration of wood cellulose in the growth rings of a tree (section 1.6), I performed chemical analyses of 49 core-segments from 31 old-growth Douglas firs at Mount Saint Helens. Trees were selected for analysis on the basis of age, location, and microclimatic factors that will be discussed in chapter two. The majority of samples were taken from previously studied areas that showed limited growth in eruption years (section 1.8) (Yamaguchi 1983; Yamaguchi, 1985). The locations of field sites are outlined in section 2.2. Douglas firs showed thin growth rings (Lawrence, 1939; Lawrence, 1954; Yamaguchi 1983; Yamaguchi, 1985) and chemical irregularities (Hall et al., 1990) coincident with eruption years, and the same species was selected for chemical analysis in this experiment.

LA-ICP-MS was the primary method of analysis for individual growth rings in this study. Instrumentation is discussed in section 2.5, along with techniques for calibration and data reduction. Solution ICP-MS was performed on a subset of samples, as was carbon isotopic analysis. Solution ICP-MS is better established as a method for chemical analysis of tree cores than LA-ICP-MS. The difference between solution and laser-ablation analysis is the method by which samples are introduced to the ICP (section 2.9). Comparison of chemical data produced from the same samples by two different methods was intended to provide a way of cross-checking data quality. Results of both methods of analysis are presented in chapter 3. Discrepancies between elemental concentrations measured by LA-ICP-MS and solution ICP-MS indicate a large degree of uncertainty regarding the quantitative accuracy of LA-ICP-MS, as used in this experiment.

Interpretations for chemical data are discussed in chapter four. Laser-ablation analyses of individual growth rings corresponding to the eleven-year period centered at AD 1980 and the ten-year period centered at AD 1800 do not conclusively indicate a chemical response to these eruptions. At least five of the analyzed tree cores show similar changes in the concentrations of two or more elements (Al, Ca, Zn, K, Na) that may indicate a response to one or both eruptions. Speculation for the lack of chemically distinct growth rings in the majority of the sample set is also discussed in chapter four along with potentially problematic aspects of instrumentation and sample preparation that were implemented in this study. Maps indicating the slope, aspect, and surface geology of all sample sites are available in appendix 1.0. Surface Geology maps were produced in ArcMap from data available through the Washington State Department of Natural

Resources, 2010. Unit descriptions and the color-coded legend that supplement these maps are available in tables 2.0 and 2.1 (appendix 1.0) of the CD accompanying this book. Several trees exhibit a chemically “complacent” pattern of elemental abundance. This complacency is discussed further in chapters 4 and 5. No link between surface geology, aspect, slope, or chemical composition of annual growth rings (complacent or otherwise) was determined in this study. Summaries of project design, execution, and results are presented in chapter five with suggestions for future work.

As mentioned in section 1.8, there is no procedure currently in place for laser-ablation analysis of tree cores. LA-ICP-MS analysis of tree cores as a means of dating volcanic eruption is a new and uncertain technique (Pearson et al., 2005). If volcanic eruption does cause a change in the chemistry of xylem tissue in trees, the magnitude and character of the chemical alteration as measured by LA-ICP-MS cannot be anticipated due to a lack of conclusive previous work. However, the certainty of the historic eruption dates at Mount Saint Helens provides a point of experimental control. Chemically distinct growth rings occurring on or after AD 1800 or AD 1980 from this sample set may be attributed to the eruption of Mount Saint Helens. As discussed in section 1.1, a goal of this study was to identify a xylem-tissue chemistry that can be attributed exclusively to the occurrence of a volcanic eruption. The development of a procedure for the use of LA-ICP-MS on tree cores is a goal of equal importance that may enhance the progress of future work.

CHAPTER 2: METHODS

2.1 Field Methods

Abnormally thin annual growth rings thought to be consequent of volcanic eruption at Mount Saint Helens have been identified in old-growth Douglas fir trees (Yamaguchi, 1983; 1985; 1993; Yamaguchi et al., 1990; Yamaguchi and Lawrence, 1993). Tree cores from the above studies exhibit thin annual growth rings associated with multiple eruptions of Mount Saint Helens, including that of May 1980, and at least two eruptions each from the Goat Rocks eruptive period (CE 1800), and the Kalama eruptive period (CE 1480) (Yamaguchi, 1983, 1985; Yamaguchi and Lawrence, 1990). If trees in the above-mentioned studies exhibit physical characteristics that are the result of eruption-related phenomena, then chemical influence of the same event may also be present in the wood cellulose of nearby trees. That is, areas in which trees endured physical damage due to volcanic eruption may have also experienced changes in soil and air chemistry that locally affected the cycling of nutrients. Therefore, several locations from previous work by Yamaguchi and others were selected as sample sites for trees of the same species in this study. Permit restrictions prohibited the coring of trees from the area around Spirit Lake.

Forty-two trees were sampled from eight different field sites located northeast, east, and southeast of the volcano (figure 2.0). Additionally, seven trees were cored from two sites located south of the volcano in order to establish control patterns for elemental abundances in the annual growth rings of interest. One of these sites is located east of Salem, Oregon, and is beyond the zone of measurable tephra accumulation (figure 2.1).

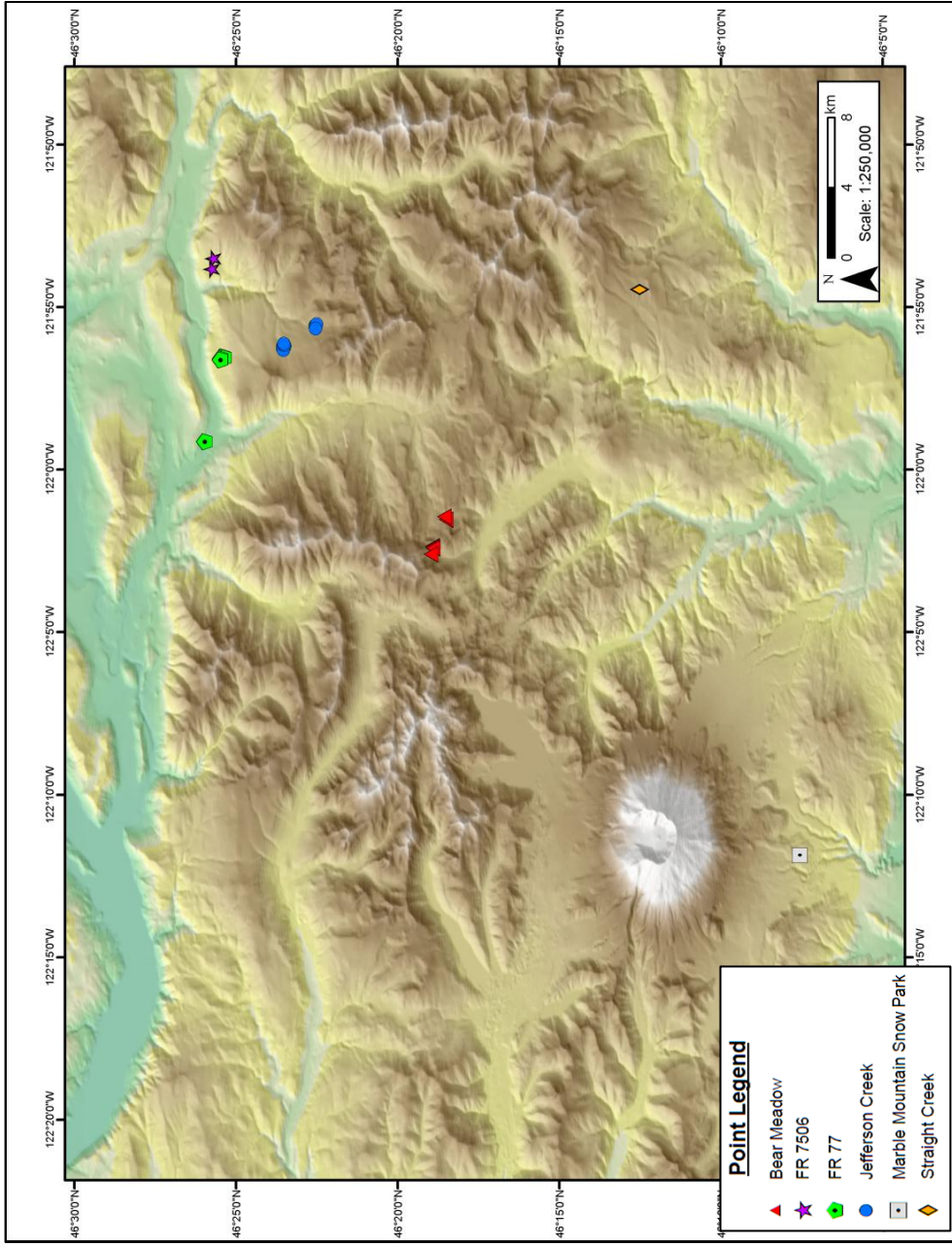


Figure 2.0*
 Hillshade map of the sample sites northeast, east, and south of Mount Saint Helens. Symbols indicate the location of individual trees, or clusters of trees cored for LA-ICP-MS analysis.

*Also available in Appendix 1.0

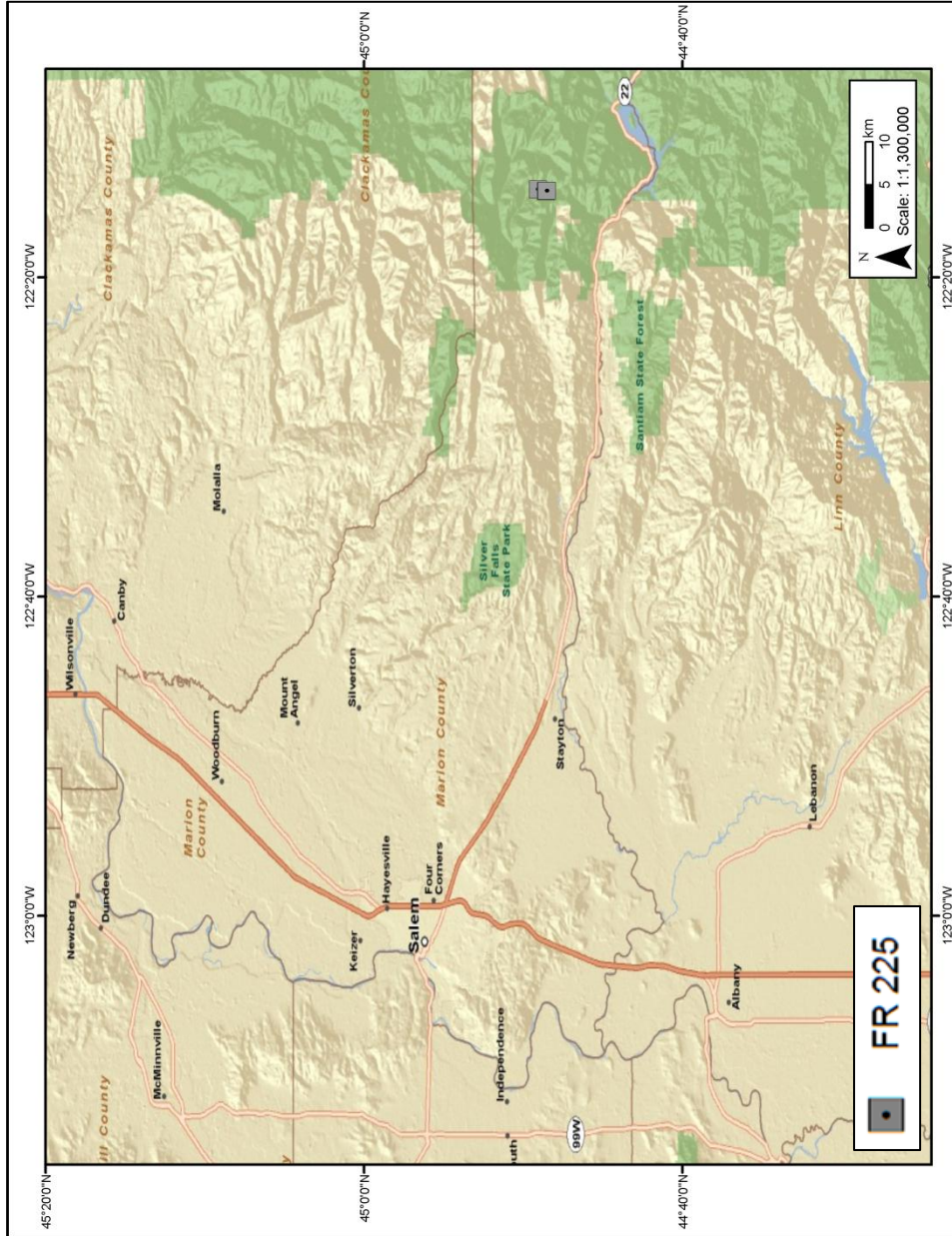


Figure 2.1*
 Map showing the location of control site at FR225 east of Salem, Oregon.
 *Also available in Appendix 1.0

The other control site is located 7 km south of the crater (Marble Mountain Snow Park), where tephra from the 1980 eruption does not exceed three cm depth (Criswell, 1987).

Trees in each of the eight sampled locations were selected from an old-growth stand on the basis of age and species. Hill slope, depth of substrate, canopy position, and proximity to other trees may influence the availability of nutrients and the growth patterns of a tree (Pearson et al., 2005). Factors that influence the growth of an individual tree are referred to as microclimatic and micro-environmental factors. Even trees that are in close proximity to each other, rooted in the same soil and exposed to similar macroclimatic conditions, may respond differently to environmental change due to the conditions of the microclimate of the individual tree (McCarroll and Loader, 2003; Stokes and Smiley, 1968). For this reason, trees at each field site were selected so as to include a range of conditions that might impact the microclimate of a given tree, and in turn, its response to volcanic eruption. Samples were obtained from trees rooted on slopes ranging from flat to near vertical. Several younger trees were sampled in addition to the old-growth Douglas firs in order to test the impact of an eruption on trees of varying maturity. Descriptions of the microclimatic conditions for each sampled tree were systematically recorded in the field prior to core collection (appendix 2.0). Measurements were taken using a tape measure and a Brunton compass to determine circumference, height, and distance to nearby trees. Core samples were obtained using tree borers that are approximately 47 cm long, and produce cores with a 5 mm diameter. Borers were cleaned with isopropyl alcohol between each use to reduce the risk of contamination. Each tree was cored twice at breast height with an angle of separation of approximately 90°. In some instances, extreme hill slope required a wider angle of separation between

cores. Cores were stored and transported in the field in plastic straws with >5 mm diameter, and placed inside of a cardboard map case for protection from the elements.

Permit restrictions limited the sampling of soil and tephra to exposures at natural cut-banks. Four of the eight sample sites had natural cut-banks that were sufficient to record volcanic deposits in stratigraphic section. Stratigraphic descriptions from earlier publications were used to identify deposits from the AD 1980, AD 1800, and AD 1480 eruptions of the volcano, in addition to layer X and unnamed units associated with minor eruptions of the Goat Rocks eruptive period (Crandell, 1987; Criswell, 1987; Mullineaux, 1996). Observation of fallout from the 1980 eruption and tephra layers T (CE 1800), We, and Wn (CE 1480) in stratigraphic sequence was meant to ensure the presence of, and record the unit thickness for, each depositional unit in close proximity to sampled trees (figure 2.3).

2.2 Sample Sites

A total of ten Douglas firs were cored from the area around Jefferson Creek, approximately 23 km northeast of the 1980 crater (figure 2.0). The elevations of trees cored at this site lie between 1000 m and 1100 m above sea level (figure 2.3, appendix 1.0). Natural cut-banks were cleaned and described according to conventional methods in two locations at this field site.

Eight Douglas fir trees were cored at the Bear Meadow sample site, located approximately 12 km northeast of the 1980 crater (figure 2.4). The old-growth trees sampled in this location are rooted along the edge of the blast zone from the 1980 eruption. Several trees west of this site died as a result of the explosion. Trees cored at this site are at an elevation of approximately 1200 m above sea level. One natural

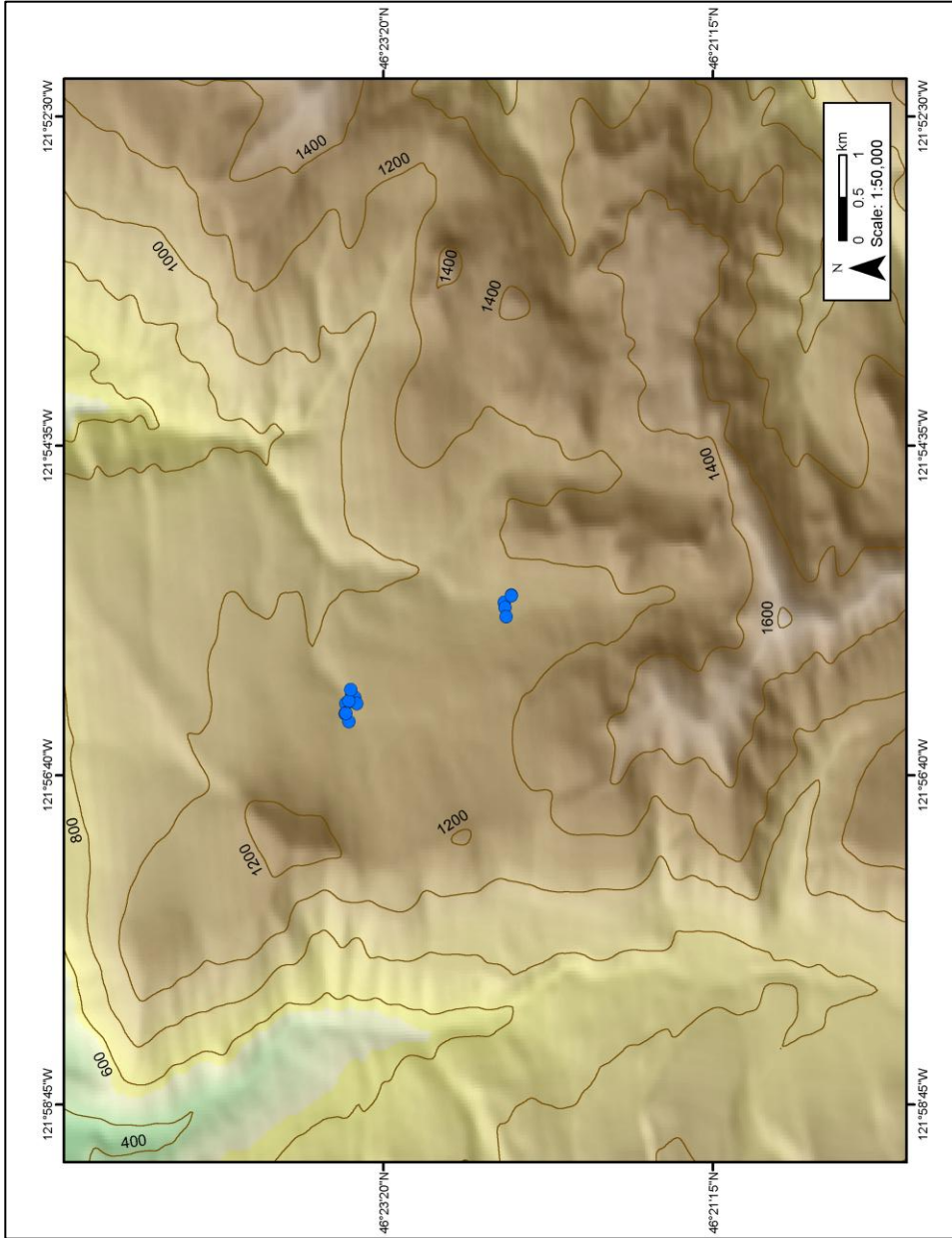


Figure 2.3 *
 Topographic map showing locations and elevations of trees cored at Jefferson Creek, northeast of Mount Saint Helens. Slope and aspect maps are available for this area in appendix 1.0.
 *Also available in Appendix 1.0

cut-bank shows an exposed deposit of (<25 cm) of tephra layer T (CE 1800) extended to the base of the cut-bank. No earlier deposits were visible at this site.

Ten Douglas fir trees were cored northeast of the volcano along forest road 77 (figure 2.5). This sample site extends from approximately 2 km east of the sample site at Jefferson Creek to 2 km southeast of the same site. These trees are rooted at elevations just under 700 m above sea level, on a down-to-the-northwest slope. One natural exposure at the base of sampled tree FR77 5A reveals deposits of 1980 ash and pumice, and tephra layers T, X, We and Wn (appendix 2.0). Several young Douglas firs are included in this sample set.

Seven Douglas fir trees were cored northeast of the volcano along forest road 7506 (figure 2.6). This site is located approximately 4 km directly north of the site along forest road 77 at an elevation of approximately 740 m above sea level. One natural exposure at the base of sampled tree FR7506 1A reveals fallout from multiple eruptive events that is separated by several layers of soil.

One tree was cored from Straight Creek, approximately 18 km east of the 1980 crater at an elevation of 500 m above sea level. A natural cut-bank was not found in this area, and so tephra deposits were not observed in stratigraphic section. An old-growth Douglas fir tree from this location showed evidence of the 1800 eruption of Mount Saint Helens in a previous study (Yamaguchi, 1982). Only one sample was collected from this site due to a failure to locate other old-growth Douglas firs, and to limited time in the field.

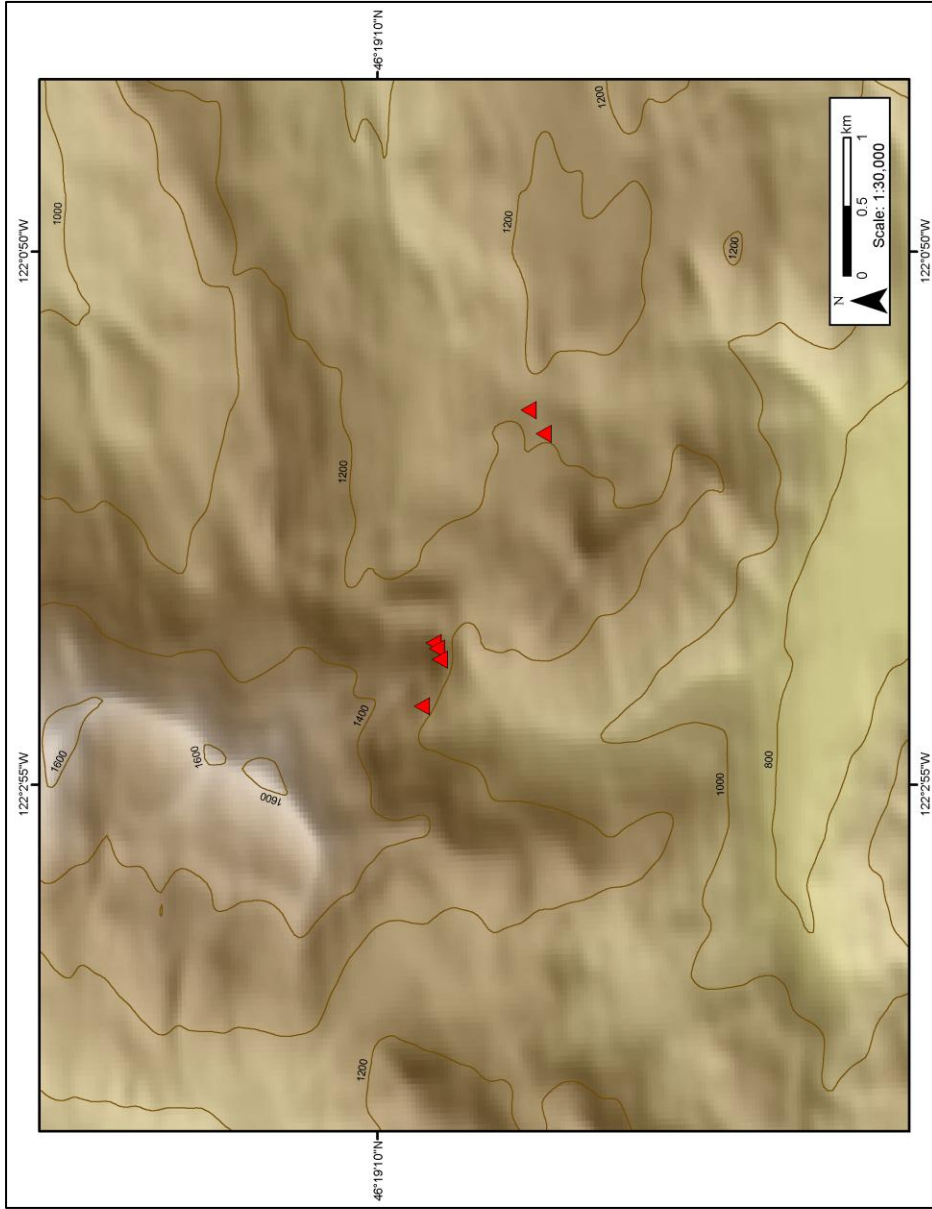


Figure 2.4*

Topographic map showing locations and elevations of trees cored at Bear Meadow, northeast of Mount Saint Helens, and southwest of Jefferson Creek (figure 2.0). Only five GPS points were recorded for the eight sampled trees because the distance between sampled trees was less than the resolution of the GPS unit in some cases. Slope and aspect maps are available for this area in appendix 1.0.

*Also available in Appendix 1.0

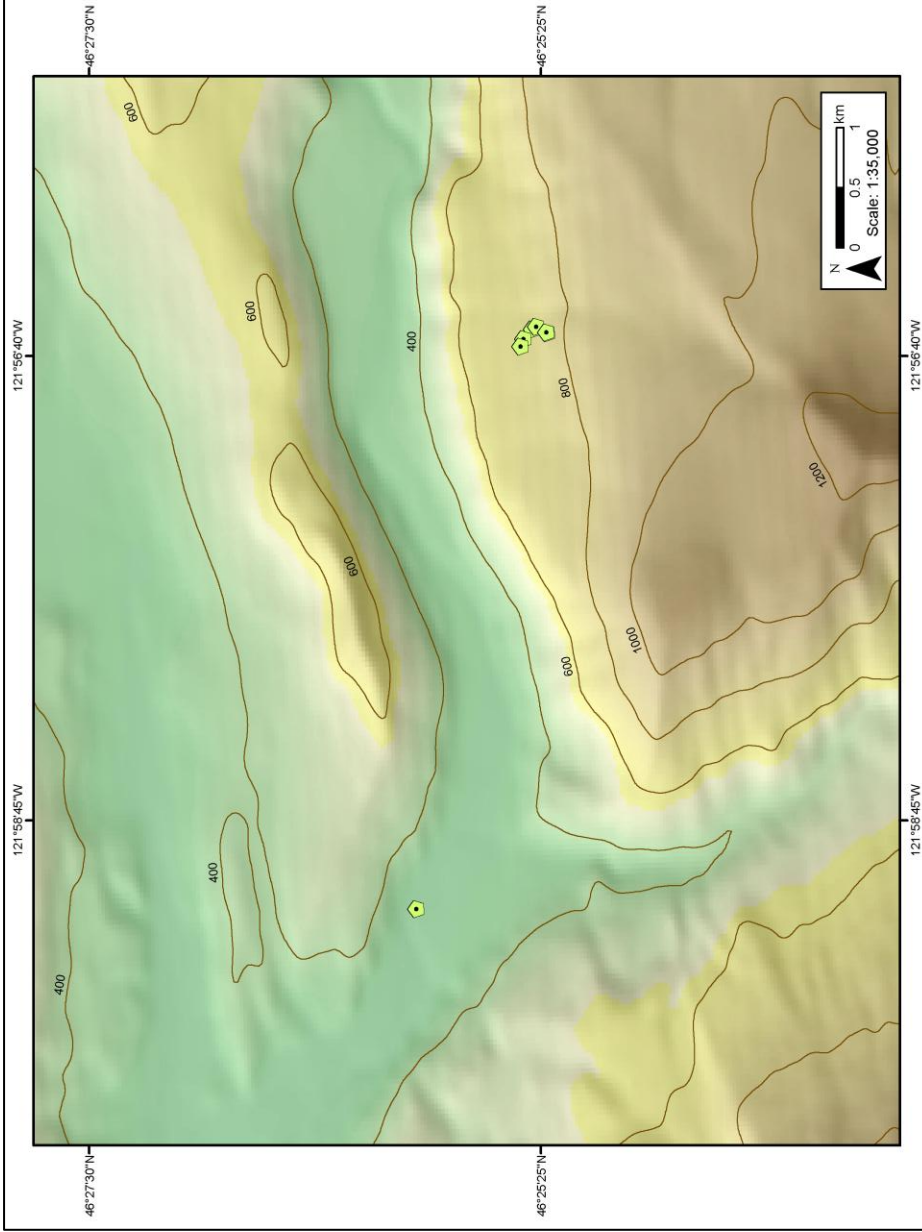


Figure 2.5*

Topographic map showing locations and elevations of trees cored along forest road 77, northeast of Mount Saint Helens, and north of Jefferson Creek (figure 2.0). Only six GPS points were recorded for the ten sampled trees because the distance between sampled trees was less than the resolution of the GPS unit in some cases. Slope and aspect maps are available for this area in appendix 1.0.

*Also available in Appendix 1.0

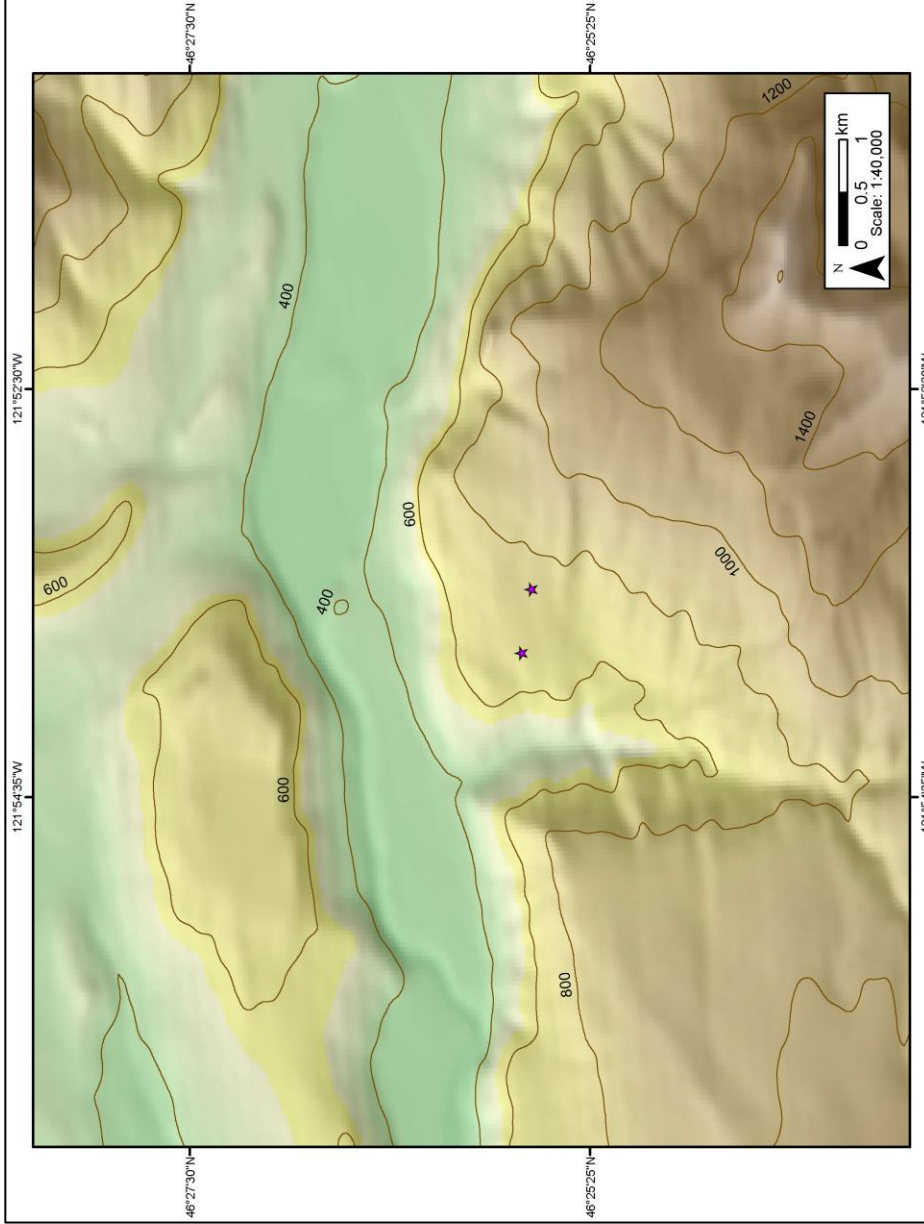


Figure 2.6 *

Topographic map showing locations and elevations of trees cored along forest road 7506, northeast of Mount Saint Helens, and northeast of Jefferson Creek (figure 2.0). Only two GPS points were recorded for the seven sampled trees because the distance between sampled trees was less than the resolution of the GPS unit in some cases. Slope and aspect maps are available for this area in appendix 1.0.

*Also available in Appendix 1.0

Two trees were cored at Marble Mountain Snow Park, approximately 7 km south of the 1980 crater, at an elevation approximately 1200 m above sea level (figure 2.7). One of the sampled trees is a Douglas fir, and the other is a Pacific Silver fir. No natural exposures or cut-banks were available at this site, and inclement weather prevented the sampling of a greater number of trees. This sample site received only light ash fall due to north and east-directed prevailing winds at the time of the 1980 eruption moving north and east from the cone (figure 1.4). These trees were therefore intended to be candidates for control trees.

Three Douglas firs were sampled off of Cispus Road, approximately 41 km northeast of the 1980 crater, roughly 3 km west of Blue Lake (figure 2.0A, appendix 1.0). These trees are located between 400 and 600 m above sea level.

Three trees were sampled 2-3 km south of the sample site at Cispus Road along forest road 23 (figure 2.0A, appendix 1.0). These trees are Douglas firs growing at elevations between 400 m and 700 m above sea level. No natural cut-banks were available at this sample site, nor at the sample site at Cispus road. Inclement weather and heavy snow prevented a thorough search for such exposures at these sites.

Five additional control trees were sampled from an area near Opal Creek, Oregon. Opal Creek is located 137 km due south of the volcanic center at Mount Saint Helens and 90 km east of Salem (figure 2.1). These trees are rooted well outside of the fallout zone for the 1980 eruption of the volcano, and are likely outside of the range of deposition from any of those from the Goat Rocks or Kalama eruptive periods. They are rooted at elevations between 750 and 800 m above sea level, and experience macroclimatic conditions similar to those in and around Gifford Pinchot National Forest.

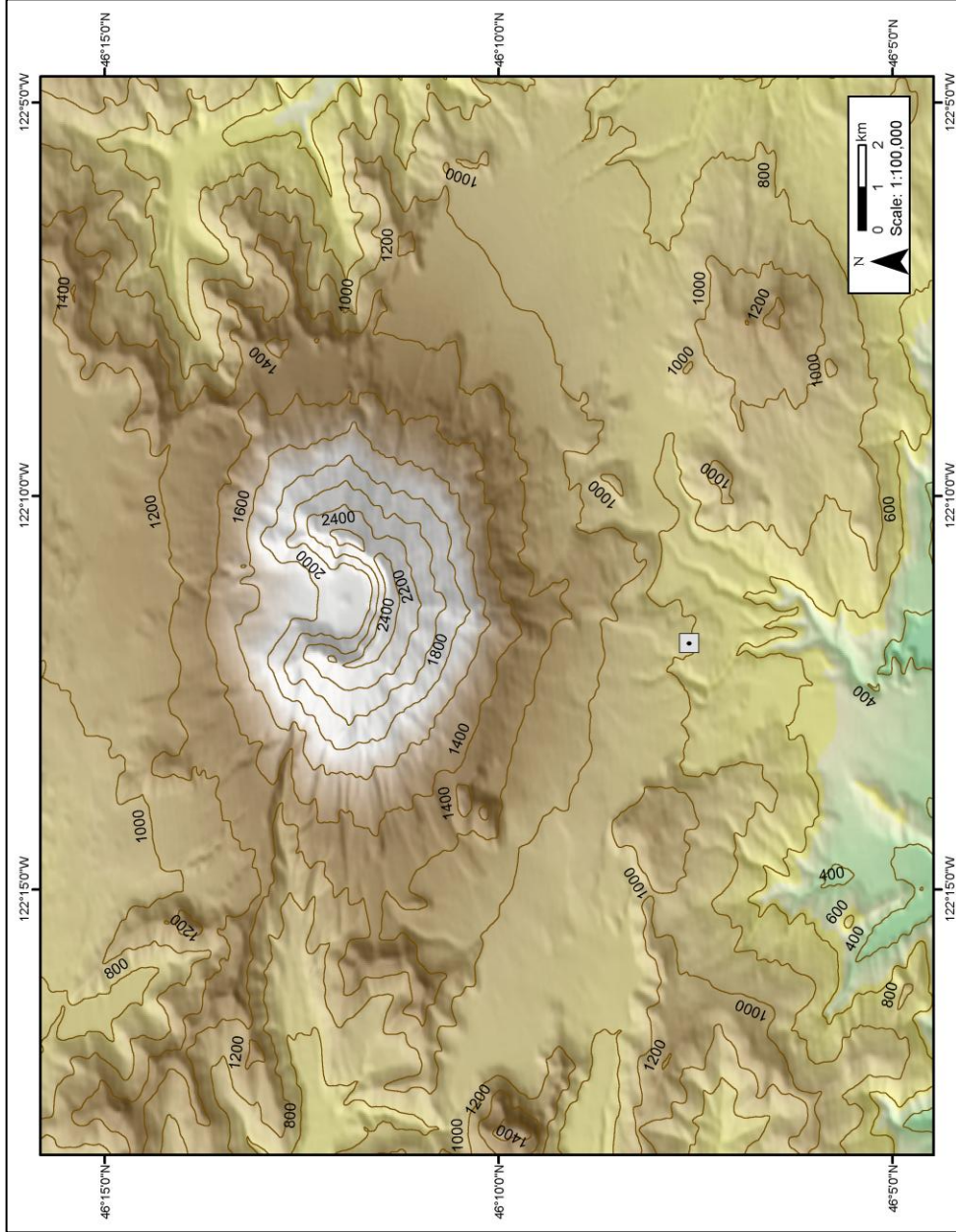


Figure 2.7*

Topographic map showing location and elevation of trees cored at Marble Mountain Snow Park, south of Mount Saint Helens (figure 2.0). One GPS point was recorded for both sampled trees. Slope and aspect maps are available for this area in appendix 1.0.

*Also available in Appendix 1.0

2.3 Lab Methods

Surfacing

Upon return to Northern Arizona University, tree cores were removed from the plastic straws and laid on wax paper to dry in open air. Cores remained untouched for a period of 12 weeks, and dried to ambient humidity prior to the first stage of preparation.

In order to preserve the chemistry of the wood cellulose, tree cores were not mounted according to standard procedure. Traditionally, cores are glued to a slotted mount and wrapped tightly with string until the glue dries, in preparation for surfacing (Stokes and Smiley, 1968). Surfacing is the process of exposing a smooth and level face of a core sample. Because application of glue to porous core samples might alter the chemistry of the wood, samples were prepared without any adhesive product. Instead, custom tracks for a low-angle block plane were used to hold a core sample in place during two stages of surfacing (figure 2.8). Each track was designed to allow a low-angle block plane with a custom-cut blade to pass over the sample and remove a fixed amount of wood from the surface of the core. The blade was cut to a width of 4 mm so that it would contact only the core sample as it moved along the track.

The track used in the first stage of surfacing holds the core sample in a trough that is 4 mm deep. The upper 1 mm of the core sample is exposed above the trough, and can be methodically removed by the blade of the low-angle block plane. A low-angle block plane cuts at an angle of 12 degrees from horizontal. After the first stage of surfacing, the flat face of the core sample was sanded with fine sandpaper until the surface was completely smooth to the touch, and cell walls (tracheids) were clearly visible under a microscope. For this sample set, three grits of sandpaper were used: 40 μm , 30 μm , and

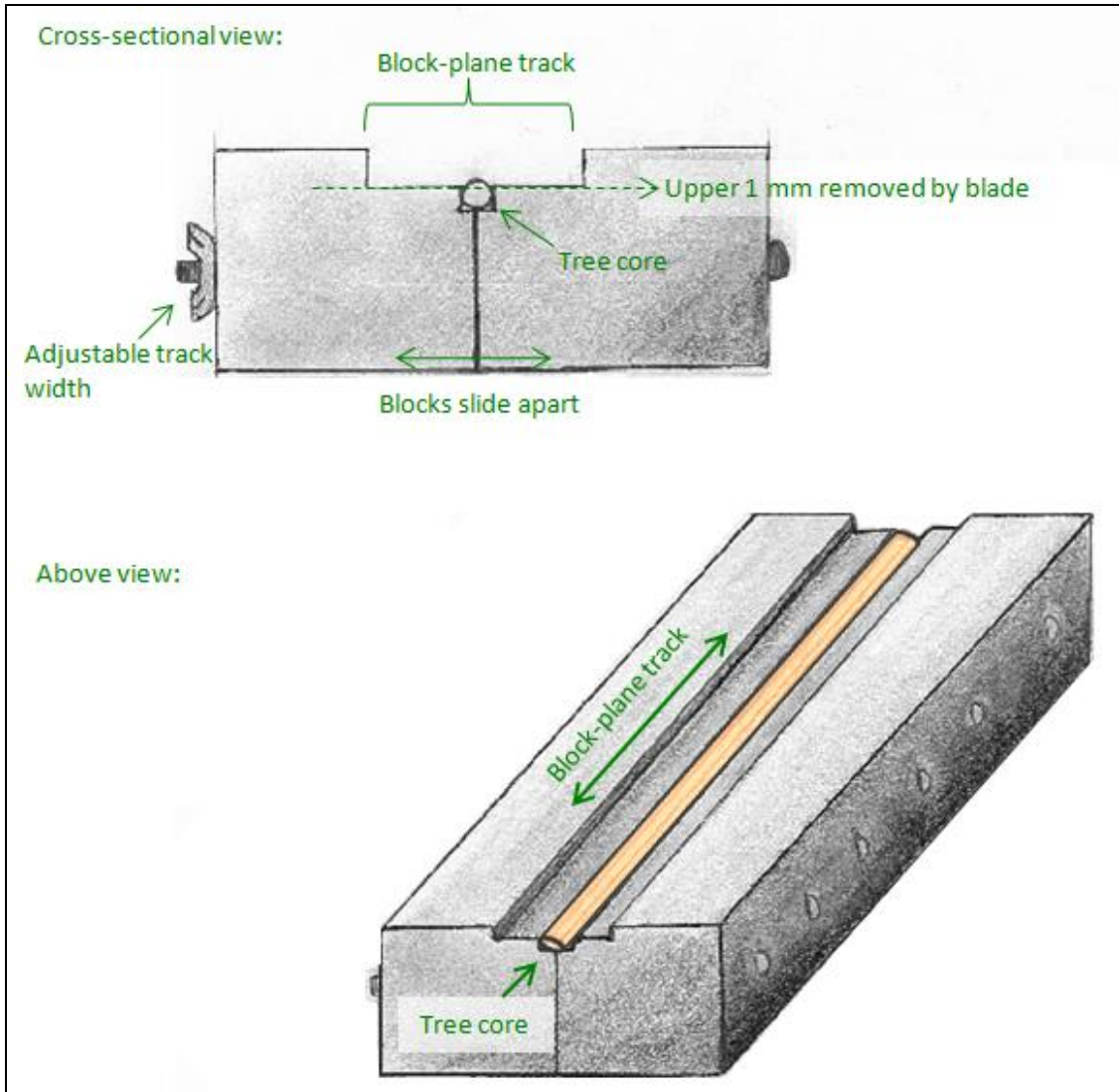


Figure 2.8

Sketch of custom block-plane track used to hold core samples in place during each stage of surfacing. The first stage of surfacing is shown above. In the block-plane track used for stage two, the tree core sits in a shallower trough.

15 μm . The 15 μm grit, too fine to produce sawdust, acted as a polishing tool. Because laser ablation would not be conducted on this surface of the core, contamination of material across rings was not a concern at this phase of sample preparation. Samples were then fastened to a slotted wood mount with rubber bands for ease of handling and storage. Cores were then studied under a microscope and growth rings were assigned years according to the methods discussed in section 2.4. After dendrochronology of each core was established, a second stage of surfacing was completed to expose a clean face parallel to the sanded surface.

The track used in the second stage of surfacing has a trough that is only 3 mm deep. During the second stage, a core was placed into this track with the sanded face down. The upper 1 mm of core sample was then removed in the same fashion as the first stage to expose a clean surface suitable for laser ablation analysis. The second surfacing is among the last items of sample preparation prior to LA-ICP-MS analysis. Before a core sample could be surfaced for a second time, the assignment of calendar years to growth rings had to be completed and double-checked by a second party.

2.4 Dendrochronology

Calendar years were assigned to each of the growth rings in a core sample by a combination of ring counting and cross-dating. Cross-dating is a technique in which patterns of ring width and density are matched between a new sample and those in a chronology, for which widespread growth patterns (often climatically controlled) are established (Yamaguchi, 1983; Fritts and Swetnam, 1989; Stokes and Smiley, 1968). A chronology is a record of ring-width variations, or growth patterns, that are specific to a

field site. Cross-dating reduces the risk of counting errors due to the rare occurrence of false or missing rings (Yamaguchi, 1983).

Control patterns for this sample set were compiled from three chronologies in the International Tree Ring Data Base (ITRDB) (WA 089, Earle, Brubaker and Segura; WA033, Brubaker; WA 081, Briff and Scheingrubber). A list of marker years referenced in an earlier study at Mount Saint Helens was also used as a reference chronology (Yamaguchi, 1985; Appendix 4.1). Two of the chronologies archived at the ITRDB (WA089 and WA033) were based on Douglas fir trees from two field sites in Gifford Pinchot National Forest (figure 2.9). The time spans for these chronologies are AD 1539 to 1987 and AD 1534 to 1976. The time span for the third chronology from the ITRDB (WA081) is AD 1609 to 1993. This chronology is based on Pacific Silver firs, also from Gifford Pinchot National Forest.

Annual ring widths were reduced to a master list of marker years for each species through application of a program called COFECHA (Holmes, 1983). COFECHA is a program designed to check the quality of tree-ring chronologies and the potential for cross dating within a sample set through employment of statistical analyses (National Climatic Data Center (www.ncdc.noaa.gov)). Master bar plots for each of the three chronologies (WA081, WA033, and WA089) demonstrate one method of designating marker years based on variations in ring width (appendix 4.1). This particular COFECHA output file compares ring width of a given year from one tree to the average ring width of a 50-year segment in the entire sample set.

Ring counting is the process of assigning calendar years to annual growth rings by back counting the number of rings from the most recently produced to the oldest

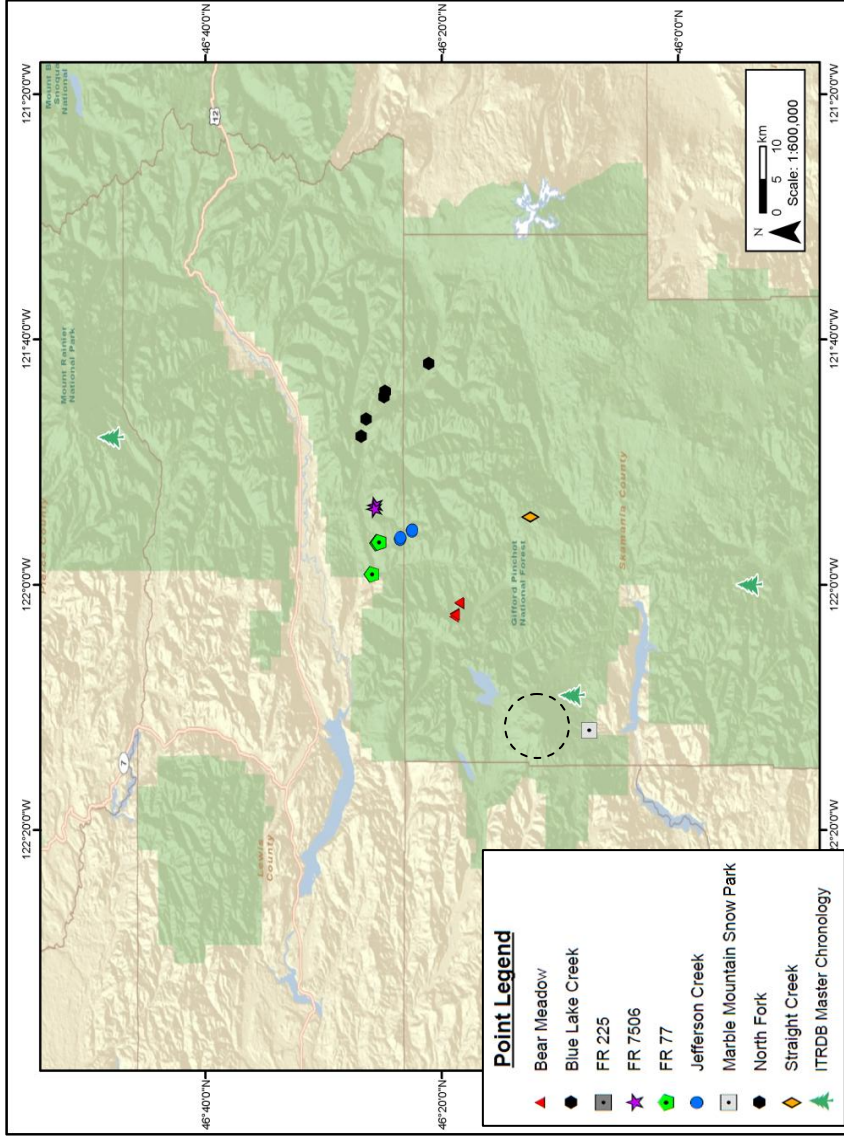


Figure 2.9 *

Hillshade map showing the locations of the ITRDB chronologies relative to cored trees at all sample sites in Washington. ITRDB chronologies are represented by the three tree symbols. WA033 is the southernmost, MSH3 is located south of the cone, and east of Marble Mountain Snow Park, and WA089 is the northernmost point on the map. The black dots represent the trees cored near Cispus Road and forest road 23. These trees did not undergo LA-ICP-MS analysis. Mount Saint Helens is outlined by the dashed line.

*Also available in Appendix 1.0

available ring in a core sample. All of the trees sampled in this study, with the exception of the stump at Jefferson Creek, were alive at the time they were cored. Therefore, the calendar year assigned to the outermost ring of each core sample corresponds to the date on which it was obtained. The calendar year assigned to the outermost ring of the stump at Jefferson Creek field site should correspond to the date of the clear cut for that area, and could be verified by cross dating. All field work was completed between the months of September and November in 2008 and 2009. This ensures that the majority of earlywood seasonal growth for the year had been completed in the living trees (Reukema, 1965; Dobbs, 1966).

An individual growth ring in conifers is composed of a light-colored earlywood belt and a dark-colored latewood belt. Earlywood is produced during the most active part of the growing season whereas latewood is produced during a stage of reduced radial growth (Stokes and Smiley, 1968). The xylem is the woody part of a tree (figure 1.5). In conifers, the xylem is composed mostly of elongate tracheid cells whose long axis is parallel to that of the stem or branch of the tree (Stokes and Smiley, 1968). Differences in color of earlywood and latewood are due primarily to differences in the thickness of tracheid cell walls, where latewood cell walls are thicker than those of earlywood (Kaye, 1997).

The transition from earlywood to latewood appears gradual under a microscope, as the thickness of cell walls incrementally increase and the rate of radial growth incrementally decreases toward the end of a growing season. Rapid radial growth ensues with the onset of the next growing season, and the start of the next earlywood cycle. Consequently, the transition from latewood to earlywood is marked by an abrupt,

prominent boundary between dark, thick-celled tracheids and light, thin-celled tracheids (figure 2.10). This boundary delineates the periphery of an annual growth ring. False or double rings are rare in Douglas firs, but can occur when a dark-colored band appears within the earlywood of a given year (Stokes and Smiley, 1968). The production of false rings is not entirely understood, but may be due to any growth-limiting factor that causes the premature and temporary slowing of radial growth during the growing season. In the southwestern United States, false rings have been attributed to the delay of monsoon rains (Kaye, 1997).

When false rings are not identified as such, the growth ring of a single year may be counted as two individual years. Fortunately, techniques for identifying false rings in Douglas firs are simple and effective. The most distinguishing characteristic of a false ring is the gradual transition of cell-wall thickness on both sides of the apparent latewood belt (figure 2.11) (Stokes and Smiley). This contrasts with the start of an annual growth ring, which is marked by the abrupt boundary that marks the transition from true latewood to true earlywood (figure 1.6). A false ring may also be identified when it is discontinuous around the entire stem of a tree, a test that requires the availability of an entire cross-section. Missing rings, as indicated by the name, occur when severe physiological stress completely inhibits the radial growth of a tree for an entire season (Fritts, 1976). Micro rings are very narrow growth rings that are also caused by physiological stress.

Each core sample was marked using a number-two pencil according to the conventional dating scheme (Stokes and Smiley, 1968; Kaye, 1997) and the time span for each core was noted on the slotted wood mount. This dating scheme prescribes that the

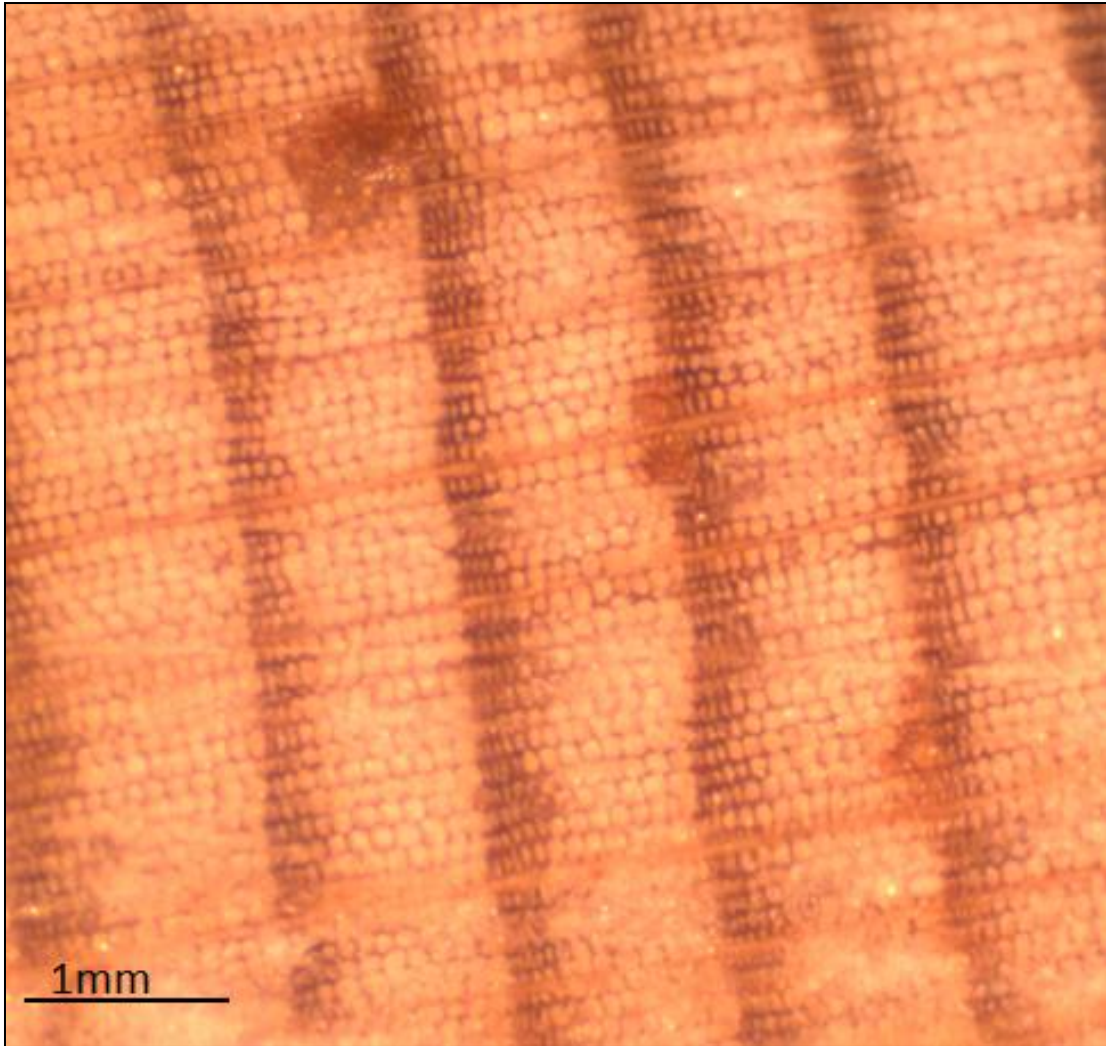


Figure 2.10

Photo-micrograph of sample JFCK 4A, showing the difference in size, density, and color of earlywood and latewood. Earlywood cells are the large, thin-walled cells that form the light-colored bands. Latewood cells are smaller and darker, with thicker cell walls. Bark is to the left of this photo, as indicated by the abrupt transition from latewood (right) to earlywood (left) across growth-ring boundaries.

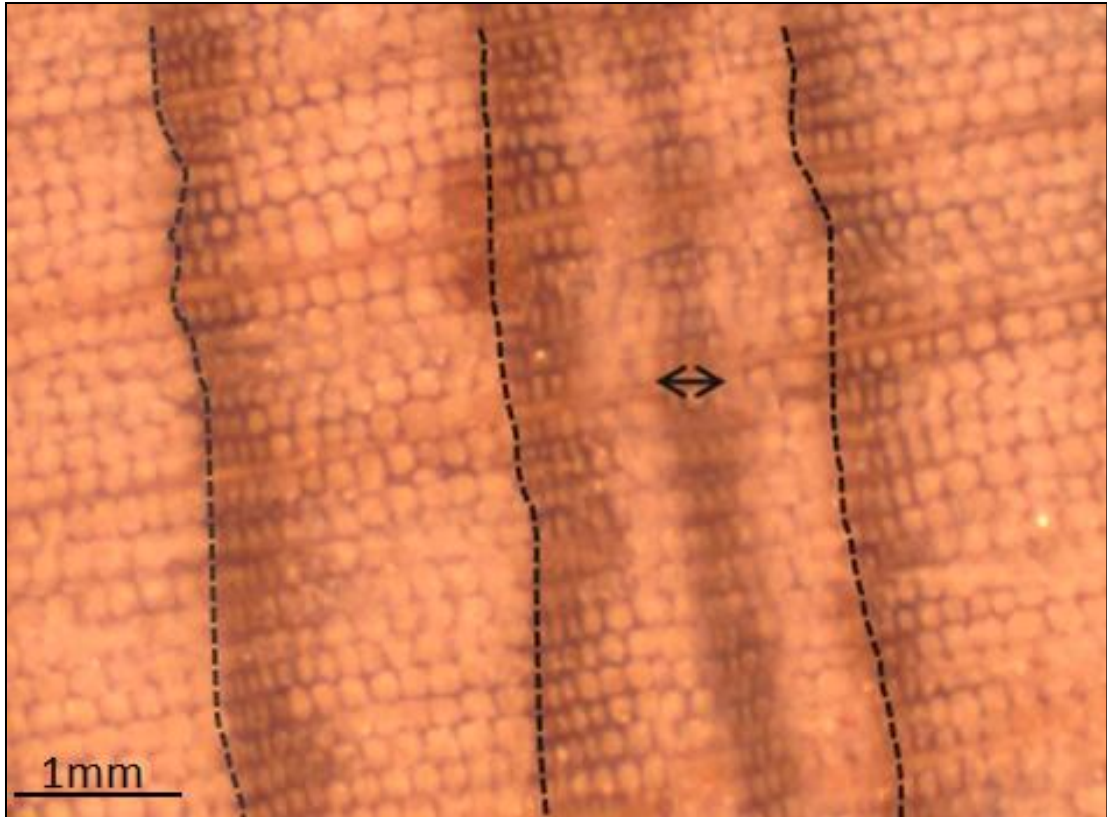


Figure 2.11

Example of a false ring in a Douglas fir. The double arrow indicates the gradual transition of cell-wall thickness on both sides of the false ring. Dotted lines indicate the abrupt boundary that marks the transition from latewood to earlywood in a true growth ring. The bark in this picture is to the left.



Figure 2.12

Photo of samples from MSH that were surfaced and rings were assigned years by counting. The standard dot notation is shown above, with three dots corresponding to the year AD 1800. The uniform width of growth rings makes this a good example of “complacent” growth, discussed in chapters 4 and 5.

ring corresponding to each calendar decade be marked by a single dot at the center of the growth ring. Similarly, each half century is marked by two vertical dots, and each century is marked by three vertical dots (figure 2.12). Two dots aligned on either side of a ring boundary indicate the presence of a micro (very thin) ring, and two offset dots indicate the occurrence of a missing ring. False Rings in this sample set were marked with an A.

Traumatic resin canals are features that commonly appear consequent to instances of physical damage to a tree (Kuroda and Shimaji, 1983). They were present in seven of the 15 sampled Douglas fir trees that were damaged by lahars associated with the 1980 eruption of Mount Saint Helens (Yamaguchi and Lawrence, 1993). They were also common in tree cores in the years following the eruption of Volcán Parícutin (Sheppard et al., 2008). For this reason, the presence of resin canals was noted during this phase of sample preparation.

After cores from each sampled tree were marked, several from each field site were selected for LA-ICP-MS analysis. The number of cores eligible for chemical analysis was limited by available time and funding. Cores that were selected for the next analytical phase were surfaced for a second time, as described in section 2.3, and cut with a razor blade to fit into the sample chamber of the LA-ICP-MS. The sample chamber limits the length of a core section to 6.5 cm. Segments were cut to include no fewer than ten years prior to and ten years after an eruption year while not exceeding 6.5 cm in length. All cores had a segment cut that centered on the 1980 growth ring, and most had a segment cut that centered on the 1800 annual growth ring. Only one core sample from the Jefferson Creek field site had growth rings that included years from the Kalama eruptive

period. This core, JFCK 2A, had a segment cut for each of the 1980, 1800, and 1480 growth rings. A total of 49 core segments were analyzed by LA-ICP-MS in this study.

During and after the second surfacing of a sample, a core was handled only with latex-free gloves. Core segments that were intended for laser ablation analysis were fastened to a smaller core mount with rubber bands. Core segments that came from the same tree were mounted together, and the years corresponding to the growth rings on either end of each segment were noted on the core mount. Samples were then stored prior to LA-ICP-MS analysis.

2.5 Laser Ablation of Natural Wood

The use of laser ablation (LA) in conjunction with ICP-MS is advantageous in that it offers a method for direct solid sampling in analytical chemistry. Laser ablation for dendrochemical analysis allows particles of wood to be introduced to the ICP without acid digestion. Although this method reduces the risk of sample contamination by circumventing chemical pretreatment (Mokgalaka and Gardea-Torresdey, 2006), two major concerns must be addressed when ablating natural wood (Hoffman et al., 1996). The first is a product of the physical heterogeneity of a core sample. As discussed in section 2.4, the xylem of a conifer is composed mainly of tracheid cells. On a microscopic level, the porous structure of these cells causes density variation within and across annual growth rings. Also, when a laser is set to ablate at a fixed depth beyond the surface of a sample, apparent changes in density may result from ablation of an uneven surface. That is, variation in the distance between the focal plane and the sample surface will have an effect on the amount of material that is introduced to the ICP. The ability of

a laser to adapt to an uneven surface during ablation is limited by the speed and accuracy of the autofocus function. In the case of the LA unit at NAU, the autofocus function is inconsistent with regard to speed and accuracy.

To better explain this effect, recall that core segments selected for LA-ICP-MS analysis in this study were not sanded after the second surfacing in order to prevent the transfer of wood particles across annual growth ring boundaries (section 2.4). Hence, the ablated surfaces of all of the core segments in this study were irregular. Previous studies have attempted to resolve the issue of density variation and uneven ablation surface by monitoring the abundance of ^{13}C as an internal standard (Watmough et al., 1998; Prohaska et al., 1998; Hoffman et al., 1996). An isotope is suitable for internal standardization when the signal intensity of this isotope in the mass spectrum has the same order of magnitude as the signal intensity of the elements being quantified in an experiment (Prohaska et al., 1998). In the above studies, the internal standard ^{13}C was used to correct for differences in the amount of material ablated from isolated points on a sample. Changes in ablation mass therefore correlate directly to a fixed point and a finite period of collection time for which wood particles were introduced to the ICP. In this study, core samples were not ablated at isolated points. Instead, the laser ablated material at a depth of 5 μm below the sample surface while moving at a constant speed along a predetermined path within a single annual growth ring. Consequently, the material introduced to the ICP during a collection period is not all coming from a fixed point. Because the position of the laser was constantly changing on the sample, the count analysis for each element also corresponds to a unique position on the ablation path. That is, ^{13}C would be collected from a different part of the ablation path than, say, ^{31}P , and

consequently the surface could be a different distance from the focal plane. The conditions of the experiment then do not allow for accurate application of an internal standard. In addition, the signal intensity of ^{13}C in the mass spectrum does not have the same order of magnitude as all of the 19 elements considered in this study. For these reasons, no internal standard was applied during sample collection or data reduction.

The possibility of chemical heterogeneity in an annual growth ring is also a concern in dendrochemical analysis. Elemental abundances within annual growth rings tend to vary both around the ring and at various heights along the stem or trunk of a tree (Pearson, 2005; Hagemeyer et al., 1993; McLaughlin et al., 1987). Chemical variation is also prominent between earlywood and latewood of a single growing season (Lövestam et al., 1990). Ablation along a raster path provides a more appropriate sample population than ablation on isolated points, but, as the analyzed area is less than 5 mm wide, the chemistry still may not be representative of the entire (apical and radial growth) ring. The same principle applies to acid digestion ICP-MS. Although acid digestion of a tree ring sample requires a greater amount of material than laser ablation, it does not sample the entire growth ring, and so may not be representative of the overall ring chemistry.

The second major concern in laser ablation of natural wood is the lack of availability of matrix-matched standards for LA-ICP-MS (Watmough et al., 1997; Martin et al., 1994). No wood standards for this type of analytical technique are currently available. Ideally, calibration standards should be the chemical and physical counterpart to the sample set. Pressed wafers of cellulose powder doped with a standard solution have served as suitable standards in several previous studies (Hoffman et al., 1996) and similar

in-house standards were produced at NAU to meet the calibration needs of this experiment.

2.6 Calibration Standards

Cellulose has a naturally similar structure to wood, as it is a major constituent of wood. Standard wafers were pressed from cellulose powder doped with four different concentrations of a standard solution to produce a calibration curve for the LA-ICP-MS analysis of tree-core segments. The custom-made standard solution was produced by CPI International and contained 10 µg/ml of La, Rb, Sr, Cd, Ba, B, Cu, Ni, Mn, Ti, Pb, 100 µg/ml of P and S, and 1000 µg/ml of Ca, Na, Fe, K, Al, and Zn (table 2.4, Appendix 3.1). These elements were selected for analysis based on results from previous studies (Pearson, 2005; Sheppard et al., 2008; Hall et al., 1990) and on expected chemical fluctuations associated with changes in soil acidity (McCarroll and Loader, 2003; Felitsyn and Kirianov, 2002).

To create a liquid base to mix with cellulose powder, 2M HNO₃ was diluted with deionized H₂O to duplicate the 2% HNO₃ matrix of the standard solution. This water mixture was then added to various amounts of the liquid solution standard and cellulose powder to produce slurries of known chemical composition. Slurries with four distinct chemical compositions were dried overnight in an oven at 76 °C to dehydrate, leaving behind a cake-like substance that was then ground into a powder using a mortar and pestle. Powder was compressed into wafer form using a hydraulic press and 2,000 psi of pressure. Each wafer was pressed from 2 g of powder, and five wafers of each composition were produced. No additional bonding agent was used. As mentioned

previously, slurries with four different concentrations of standard solution were made to create a calibration curve for the LA-ICP-MS. The four concentrations are outlined below.

0.0 (blank) wafer: 10 g of cellulose powder were mixed with 60 ml of the water base and no standard solution. This wafer represents a control with 0 ppm of every element in the experiment.

0.5 wafer: 10 g of cellulose were mixed with 60 ml of the water base and 5 ml of the solution standard. This wafer represents a control with 5 ppm each of La, Rb, Sr, Cd, Ba, B, Cu, Ni, Mn, Ti, and Pb, 50 ppm each of P and S, and 500 ppm each of Ca, Na, Fe, K, Al, and Zn.

1.0 wafer: 10 g of cellulose were mixed with 60 ml of the water base and 10 ml of the solution standard. This wafer represents a control with 10 ppm each of La, Rb, Sr, Cd, Ba, B, Cu, Ni, Mn, Ti, and Pb, 100 ppm each of P and S, and 1000 ppm each of Ca, Na, Fe, K, Al, and Zn.

2.0 wafer: 10 g of cellulose were mixed with 60 ml of the water base and 20 ml of the solution standard. This wafer represents a control with 20 ppm each of La, Rb, Sr, Cd, Ba, B, Cu, Ni, Mn, Ti, and Pb, 200 ppm each of P and S, and 2000 ppm each of Ca, Na, Fe, K, Al, and Zn.

Wafers were analyzed by LA-ICP-MS using the same procedure and settings as prepared tree-core segments. Wafers were analyzed multiple times on each day of data collection, and core-segment analyses were calibrated according to the control wafer analyses from the same day. Calibration curves and data reduction techniques will be discussed in greater detail in a later section.

2.7 Instrumentation

Laser ablation was conducted in the analytical chemistry laboratory at Northern Arizona University using a New Wave UP 213 laser-ablation unit interfaced with a ThermoScientific X-Series 2 quadrupole mass spectrometer. Helium was used as the sweep gas. Samples were run using one of three similar configurations that were designed to meet the needs of this experiment. Detuning of the instrument sensitivity was required to obtain accurate counts for nineteen elements of varying abundance. The nebulizer was set at 0.5. The laser settings for all samples included a 20 Hz output, a 100 μm spot size, and 40% intensity (2800V). Ablation depth was set to 5 μm . Three sweeps with a dwell time of 27 seconds each were required for the analysis of nineteen elements in each annual growth ring. The ablation path for the laser was set to include only earlywood whenever possible.

2.8 Data Reduction

The configuration used for the majority of the LA-ICP-MS analyses conducted in this study required three sweeps with a dwell time of 27 seconds each for chemical analysis of every annual ring. Plasmalab software reports elemental abundance in counts per sweep. Approximately ten annual growth rings from forty-nine core segments and 30 different trees were analyzed by LA-ICP-MS. This sample set includes 29 core segments spanning the time period from AD 1976 to AD 1986, 19 core segments spanning the time period from AD 1795 to AD 1805, and one core segment spanning two time periods between AD 1475 and AD 1495. LA-ICP-MS data collection for this sample set was

completed over the course of ten nonconsecutive days. Raw data for each collection day are available, as reported by Plasmalab software, in appendix 3.6.

Data were converted from counts per sweep to concentration (ppm) using quantitative calibration curves for individual elements that were produced on each day of LA-ICP-MS data collection (appendix 3.1). As discussed in section 2.6, four wafers of known chemical composition were created as calibration standards. These standard wafers were analyzed at approximately four-hour increments for the duration of each day of data collection and were always analyzed at the beginning and end of every session. Calibration curves were produced by plotting the known chemical concentration (ppm) of each element in a standard wafer on the x-axis against the average value of counts per sweep reported by Plasmalab on the y-axis (figure 2.13). The equation for the slope of a line of best fit was then used to calculate the chemical concentration of each element in a growth ring. In order to account for background abundances, the y-intercept for each line was set according to the lowest average number of counts for a given element provided by analysis of the standard blank. Then the equation used to calculate the concentration (ppm) of an element from counts per sweep is as follows:

$$y = mx + b$$

where y = the average number of counts per sweep (known)

b = the lowest number of counts in the standard blank (known)

m = the slope of the line (known)

x = the concentration (ppm) that corresponds to the known y

Solving for x provides the chemical concentration of a given element in an annual growth ring. Consistent analysis of standard wafers allowed for a method for calculating

elemental abundances that also accounted for drift. Drift is the change in the sensitivity (typically a loss of sensitivity) of the instrument that occurs over time. If drift is not accounted for, then samples that are analyzed toward the end of the day may appear to have deceptively low or high elemental abundances. Elemental concentrations calculated for annual growth rings are available in appendix 3.1.

It is also important to note that the same standard wafers produced calibration curves that were unique on each day of sample collection. Although the same detuned configuration was used for all data collection that occurred between 5/19/2009 and 8/29/2009, variation in instrument sensitivity is apparent.

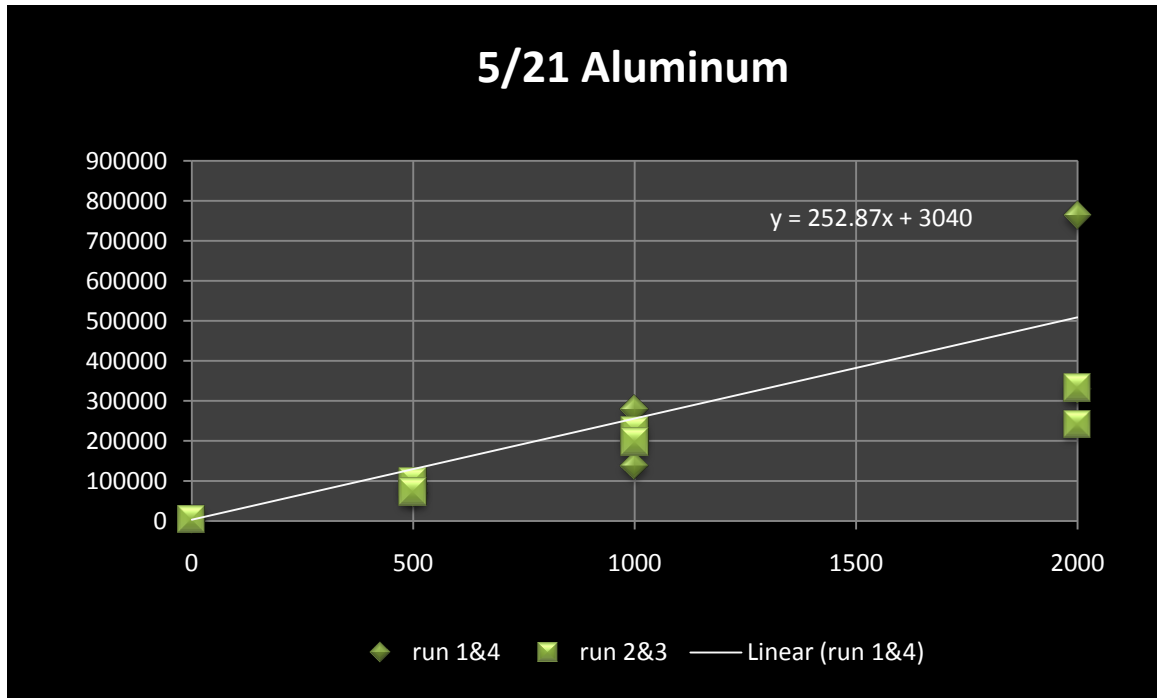


Figure 2.13

Example of a calibration curve. “Run 1&4” and “run 2&3” represent analyses conducted at four different times of day. The title indicates the date on which these data were collected, and the element measured. Y-axis values are in counts per sweep of aluminum and the values on the x-axis indicate the concentrations (ppm) of aluminum in each of the four standard wafers. The equation for the line of best fit is shown in the upper right-hand corner of the plot. This equation was used to convert counts per sweep (y-axis) to concentration of aluminum (x-axis). Values of 0, 500, 1000, and 2000 ppm on the x-axis correspond to the blank, 0.5, 1.0, and 2.0 standard wafers, respectively (pg 61). Calibration curves for all elements are available in figures 3.1-3.6 (appendix 3.1).

2.9 Acid Digestion

The use of laser ablation in conjunction with solution ICP-MS was intended to be a means of cross-checking elemental analyses. Seven of the tree-core segments that were analyzed by LA-ICP-MS were also analyzed by solution ICP-MS (table 2.3, appendix 3.3). Solution ICP-MS accomplishes sample decomposition and dissolution by way of multi-acid digestion techniques, and homogenized sample enters the nebulizer in liquid form. Solution ICP-MS has some advantage over laser ablation ICP-MS in the case of natural wood because it is an established technique for which standardization and calibration are less complicated. Additionally, the dissolution of wood cellulose in acid removes the concern associated with laser ablation of an irregular surface that was discussed in section 2.5. The amount of liquid sample introduced to the ICP is consistent and quantifiable for solution ICP-MS, but not for LA-ICP-MS.

Core segments that were selected for solution ICP-MS showed strong variance in elemental abundance between growth rings by LA-ICP-MS analysis. Growth rings in these core segments were separated with the use of a clean razor. Earlywood and latewood for each annual growth ring were isolated and only the earlywood was analyzed.

Acid digestion was accomplished following standard procedures (appendix 4.2). Prior to the separation of annual growth rings, core segments were dried in an oven at a temperature of 65 °C for a period of approximately four days. Wood separates were weighed on an analytical balance with precision to the tenth of a milligram (table 2.3, appendix 3.3). Each weighed wood separate was placed in a 6 ml Teflon container with 1 ml of doubly two-bottle distilled 7.5 M nitric acid for a period of at least 24 hours at room temperature. Samples were then placed on a hotplate for 24 hours at a constant

temperature of 70 °C. Samples were then removed from the hotplate and allowed to cool to room temperature. Twenty-four hours after samples were removed from heat, they were placed in an ultrasonic bath for approximately 3 hours. Containers were then opened, and the acid solution was transferred to a centrifuge tube for five minutes of spinning at a rate of 3000 rpm. The final step of preparation was to dilute samples for ICP-MS analysis.

Samples were diluted with doubly two-bottle distilled water spiked with scandium and rhodium for internal standardization. To achieve a concentration of 0.5 ppm Sc and Rh, 0.75 ml of elemental standard was diluted with 150 ml of doubly distilled water. After 5 minutes in the centrifuge, 0.75 ml of acid solution was removed from the centrifuge tube and added to 4.25 ml of the spiked doubly distilled water. Samples were diluted immediately prior to ICP-MS analysis. Fifty-two annual growth rings from seven tree-core segments were analyzed by solution ICP-MS over the course of two nonconsecutive days.

Calibration standards were made using the standard solution produced by CPI International (table 2.4, appendix 3.1). This is the same standard solution that was used to create the cellulose wafers for laser-ablation analyses. Four concentrations of standard solution were mixed with doubly two-bottle distilled water spiked with rhodium and scandium for internal standardization as outlined below. These standard solutions were mixed to lower concentrations than the standard wafers used in laser ablation analyses. The lower concentrations in the standard solution were meant to bracket the low concentrations measured in samples by LA-ICP-MS.

0.0 Standard (blank): 10 ml of spiked doubly two-bottle distilled water was not mixed with any standard solution. This solution represents a control with 0 ppm of every element in the experiment.

0.5 Standard: 10 ml of spiked doubly two-bottle distilled water was mixed with 5 μ l of standard solution. This solution represents a control with 0.005 ppm each of La, Rb, Sr, Cd, Ba, B, Cu, Ni, Mn, Ti, and Pb, 0.05 ppm each of P and S, and 0.5 ppm each of Ca, Na, Fe, K, Al, and Zn.

1.0 Standard: 10 ml of spiked doubly two-bottle distilled water was mixed with 10 μ l of standard solution. This solution represents a control with 0.01 ppm each of La, Rb, Sr, Cd, Ba, B, Cu, Ni, Mn, Ti, and Pb, 0.1 ppm each of P and S, and 1.0 ppm each of Ca, Na, Fe, K, Al, and Zn.

2.0 Standard: 10 ml of spiked doubly two-bottle distilled water was mixed with 20 μ l of standard solution. This solution represents a control with 0.002 ppm each of La, Rb, Sr, Cd, Ba, B, Cu, Ni, Mn, Ti, and Pb, 0.2 ppm each of P and S, and 2.0 ppm each of Ca, Na, Fe, K, Al, and Zn.

Quantitative calibration curves for individual elements were produced by the same method discussed in section 2.8 for laser ablation analyses (appendix 3.3). Standard solutions were analyzed by solution ICP-MS before and after the analysis of dissolved annual growth rings. Solution ICP-MS is less time consuming than LA-ICP-MS in the case of tree cores, and analyses of standard solutions were performed every 12 to 15 samples rather than every four hours. A detuned configuration, similar to those used for laser-ablation analyses, was put in place to scan for 18 elemental abundances. ^{13}C , present in the configuration for LA-ICP-MS analyses, was omitted in solution ICP-MS

analyses. Three sweeps, each with a dwell time of 27 seconds, were required for analysis of each sample solution. Data are available, as reported by Plasmalab software, in appendix 3.6. Counts per sweep were converted to elemental concentrations using the same equation discussed in section 2.8. The average number of counts for three sweeps was used in all calculations (appendix 3.3).

2.10 Carbon Isotope Analysis

Carbon isotopic ratios were measured for annual growth rings from five of the seven tree-core segments that were analyzed for elemental abundances using solution ICP-MS (table 2.5, appendix 3.5). Analyses were completed using gas isotope-ratio mass spectrometry at the Colorado Plateau Stable Isotope Laboratory at Northern Arizona University. Prior to submission, samples were weighed, dried, and placed into tin capsules for analysis. Annual growth rings from the analyzed cores were separated using a clean razor blade. During the preparation of samples for acid digestion, the earlywood from annual growth rings that had sufficient mass for both solution ICP-MS analysis and carbon isotope analysis were cut into two pieces. Recall that prior to the separation of annual growth rings, core segments were dried to ensure that all excess moisture had been expelled. Between 0.9 and 1.1 mg of material was required for carbon isotopic analysis. Samples were weighed into tin capsules using a micro-analytical balance with precision to 1 μg (table 2.5). Samples were not homogenized due to the small mass of each wood separate.

Analyses of 33 annual growth rings were completed using a Thermo-Finnigan Delta^{plus} Advantage gas isotope-ratio mass spectrometer interfaced with a Costech

Analytical ECS4010 elemental analyzer in continuous-flow mode. Data were normalized using the internationally accepted isotope standard known as Vienna Pee Dee Belemnite (VPDB). The main standards used in analysis of these samples were peach leaves (NIST 1547). External precision on this standard is $\pm 0.10\%$ or better for $\delta^{13}\text{C}$.

As discussed in section 1.7, carbon isotope abundances are expressed as the ratio of ^{13}C to ^{12}C in a sample as compared to the same ratio in the standard (VDPB) and are expressed in delta (δ) notation. Values reported in delta notation are in parts per thousand (‰).

$$\delta^{13}\text{C}_{\text{sample}} = \left\{ \left(\frac{^{13}\text{C}/^{12}\text{C}_{\text{sample}}}{^{13}\text{C}/^{12}\text{C}_{\text{standard}}} \right) - 1 \right\} \times 1000$$

The generally accepted absolute ratio of $^{13}\text{C}/^{12}\text{C}$ is 0.0112372 (<http://www.mpcer.nau.edu/isotopelab>). A positive delta value will be reported for samples that have a $^{13}\text{C}/^{12}\text{C}$ ratio that is greater than 0.0112372 and a negative delta value will be reported for samples that have a $^{13}\text{C}/^{12}\text{C}$ ratio less than 0.0112372. Carbon isotope data for the 33 annual growth rings selected from Mount Saint Helens are listed in appendix 3.5.

2.11 Statistical Analyses

In order to test the statistical significance of short-lived increases or decreases in elemental abundances of annual growth rings, minimum and maximum values of statistical outliers within a population of data were determined (appendix 3.4). Statistical outliers are defined as values that are more than 1.5 iqr away from the nearest quartile. That is, values that are greater than $q_3 + (1.5 \text{ iqr})$ or values that are less than $q_1 - (1.5 \text{ iqr})$ where q_1 is equal to the median value of the lower two quartiles and q_3 is equal to the

median value of the upper two quartiles. The “iqr” is the inter-quartile range, and is defined as $q_3 - q_1$. The inter-quartile range is a measure of variability that is less sensitive to the presence of outliers than the standard deviation. The median of the entire population separates the lower and upper quartiles. In the case of an odd-numbered population, the median is excluded from both quartiles two and three.

Because micro-environmental conditions can affect the background levels of elements available for uptake in individual trees (Pearson, 2005), each core segment was considered to be a separate population. The variation in elemental abundances between annual growth rings is then only compared among growth rings of the same tree-core segment. Calculations for statistical outliers of each element in each analyzed tree-core segment were completed as outlined below.

The concentrations for each annual growth ring in a population were sorted from lowest to highest, and divided into quartiles. In most cases, the number of annual growth rings in a population (n) was equal to 11. Once the iqr and the values for q_1 and q_3 were determined, statistical outliers were identified (appendix 3.3).

It is important to note that recognition of statistical outliers is only one way of evaluating the statistical significance of a change in elemental abundance that occurs between annual growth rings of a tree. It does not require that these variations in chemical concentration are related to a volcanic eruption. It also does not provide any means of quantifying the significance of a change in elemental abundance that is sustained for many years. Long-lived changes in the chemistry of growth rings must be evaluated qualitatively.

CHAPTER 3: RESULTS

Chapter Summary

Data from LA-ICP-MS, solution ICP-MS, and carbon isotopic analyses are presented in this chapter. LA-ICP-MS was conducted on 49 core segments from thirty-one trees in seven field locations. Elemental concentrations were determined with the aid of calibration curves (section 3.1) produced by analyses of standard cellulose wafer standards (appendix 3.1, figures 3.1-3.19, tables 3.1-3.19). Measured concentrations of each element are plotted against the year of the analyzed annual growth ring (appendix 3.2, figures 3.2-3.6). Changes in elemental concentration based on an eighteen-element LA-ICP-MS configuration are qualitatively discussed based on patterns observed in these plots (section 3.2). A five-element LA-ICP-MS configuration was used to re-analyze 14 of 49 core segments (appendix 3.2, figure 3.27). Qualitative changes in elemental abundance for these data are pointed out in this chapter (section 3.3), but causes for the change are discussed in chapter 4. Quantitative statistical data for spikes in elemental concentration are discussed for individual core-segments and for groups of tree cores based on field location (section 3.4).

Solution ICP-MS was conducted on 52 annual growth rings from seven core segments and six trees (section 3.5, appendix 3.4). Elemental concentrations for core segments that were analyzed by solution and LA-ICP-MS are compared (section 3.6). Carbon isotope analysis for 31 annual growth rings from five core segments and four trees are also presented (section 3.7, appendix 3.5)

3.1 LA-ICP-MS Calibration

Calibration Curves

Data collection for the 49 analyzed core-segments was completed over the course of ten nonconsecutive days (section 2.8). Calibration standards (section 2.6) were analyzed at the beginning and end of each day of LA-ICP-MS work, and every four to five hours throughout the course of most days. These data were used to develop calibration curves to relate counts to elemental concentrations (appendix 3.1).

Nineteen elements were selected for analysis (table 3.7, appendix 3.1) but only 15 to 16 produced adequate calibration curves on a given day. Carbon is excluded from consideration on all days for reasons that will be discussed in chapter 4. Phosphorus and sulfur standard analyses from all ten days of LA-ICP-MS analysis produce a flat standardization curve despite the increasing concentration of each element in the standard wafers (appendix 3.1, figures 3.25 and 3.26). Because there is no apparent correlation of counts per sweep with the known increase in elemental concentration, the concentration of phosphorus and sulfur in annual growth rings cannot be calculated for any day of LA-ICP-MS work.

Counts per sweep of both phosphorus and sulfur in annual growth rings are also consistently lower than the counts per sweep of the standard wafers (appendix 3.1, figures 3.25 and 3.26, tables 3.25 and 3.26). That is, the counts per sweep recorded for core samples are much lower than the counts per sweep measured on the 0.5 standard wafer, and are often lower than counts per sweep measured on the blank standard wafer. One full day of analysis for each of the two elements yielded average counts per sweep in

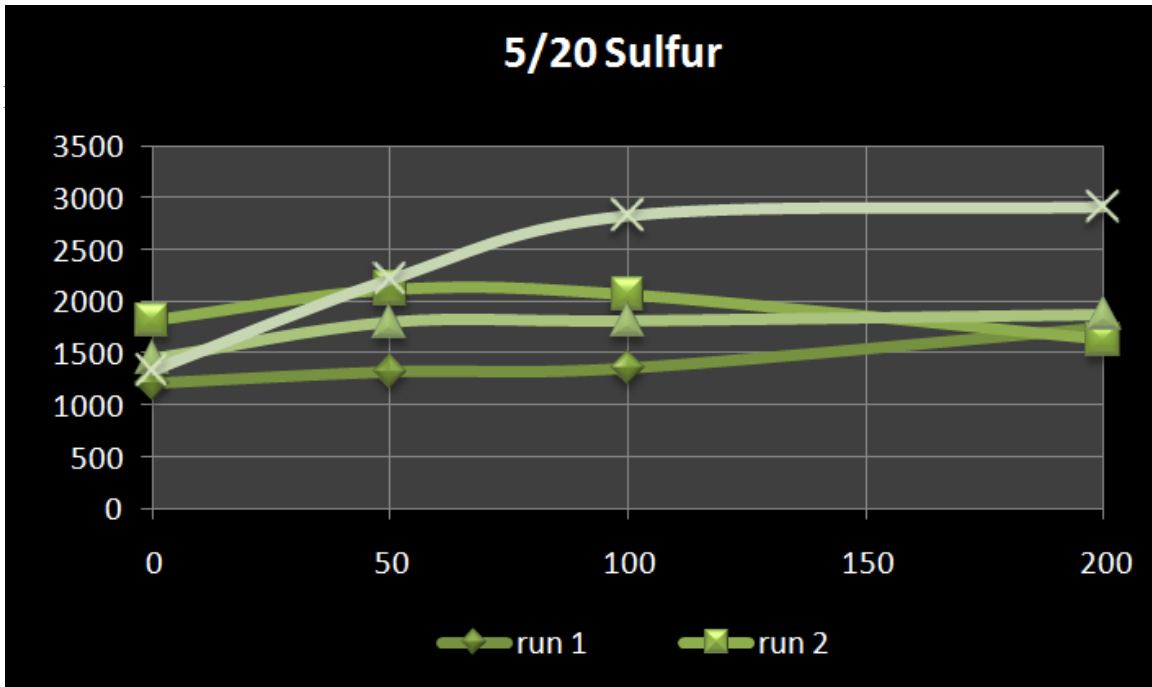


Figure 3.25T

Example of an inadequate calibration curve. “Run 1” and “run 2” represent analyses conducted at two different times of day. The title indicates the date on which these data were collected, and the element measured. Y-axis values are in counts per sweep of sulfur and the values on the x-axis indicate the concentrations (ppm) of sulfur in each of the four standard wafers. Values of 0, 50, 100, and 200 ppm on the x-axis correspond to the blank, 0.5, 1.0, and 2.0 standard wafers, respectively (pg 61). In this case, the increasing sulfur concentration in standard wafers does not coincide with an increase in counts per sweep, indicating an inadequate calibration of sulfur. Calibration curves for all elements are available in figure 3.1-3.26 (appendix 3.1).

annual growth rings that are higher than those for the blank standard wafer. For phosphorus, this is true on December 14th, and for sulfur, it is true on December 10th.

An adequate calibration curve could also not be produced for boron on four of the ten data collection days (appendix 3.1, figure 3.8). Elemental concentrations of boron can therefore not be calculated from counts per sweep on these days. The average number of counts per sweep in annual growth rings analyzed on these four days is consistently near or below counts per sweep recorded on the blank standard wafer (appendix 3.1, figure 3.8, table 3.8.)

A suitable calibration curve for titanium was produced on nine of the ten days of LA-ICP-MS analysis (appendix 3.1, figure 3.13). On May 21st, the calibration curve is flat and counts per sweep of annual growth rings average slightly higher than counts per sweep on the blank standard wafer (figure 3.13, table 3.13). Concentration data therefore cannot be calculated for titanium on this day.

Instrument drift is apparent for several elements on every day of LA-ICP-MS analysis (figures 3.1-3.6). In all cases, instrument drift is not great enough to require more than one line of best fit for an entire day of data collection. That is, elemental concentrations in all of the annual growth rings analyzed in a given day can be calculated using the same slope and y-intercept values. In cases where calibration curves diverge at the highest concentrations, the divergence occurs beyond the range of count values obtained for samples on that day. Therefore, no recalibration was needed.

Boron, potassium, calcium, titanium, nickel, zinc, rubidium, strontium and barium have calibration curves that seem to display a measurable amount of instrument drift on one or more dates (appendix 3.1, figure 3.27). Calibration curves display the LA-ICP-MS

analysis of standard wafers at different times throughout the day (figure 3.7). Analyses are listed in chronological order as “run 1” “run 2” “run 3” and “run 4”. Each day of data collection includes at least two and no more than four LA-ICP-MS analyses of each standard wafer.

As mentioned in section 2.8, the term “drift” refers to the change in instrument sensitivity that occurs over time. However, in figure 3.27, it is apparent that drift was not consistent over the ten nonconsecutive days of LA-ICP-MS analysis conducted at NAU. Calibration curves produced for manganese, strontium, and barium on May 19th and manganese only on December 10th show a pattern of instrument drift in which each consecutive analysis of the same standardized wafer has a lower number of counts per sweep than the previous analysis. In these instances, instrument sensitivity is clearly decreasing over time. A different pattern of instrument drift occurs more commonly among the data in figure 3.27. Calibration curves for boron (May 19th, June 13th, December 10th) and manganese, strontium, and zinc, (May 23rd) all show a reverse drift in which instrument sensitivity seems to increase with time. Several other elements, including calcium on May 20th, have calibration curves that drift in more than one direction. That is, instrument sensitivity decreases and then increases within a single day of LA-ICP-MS analysis.

Despite the problems with phosphorus, sulfur, and occasionally boron, calibration curves for most elements were produced successfully. LA-ICP-MS analysis of standard wafers produced data that were representative of material with known concentrations of at least 15 elements ranging from 5 ppm to 2000 ppm consistently at a given time. However, analysis of annual growth rings revealed that the concentrations of many

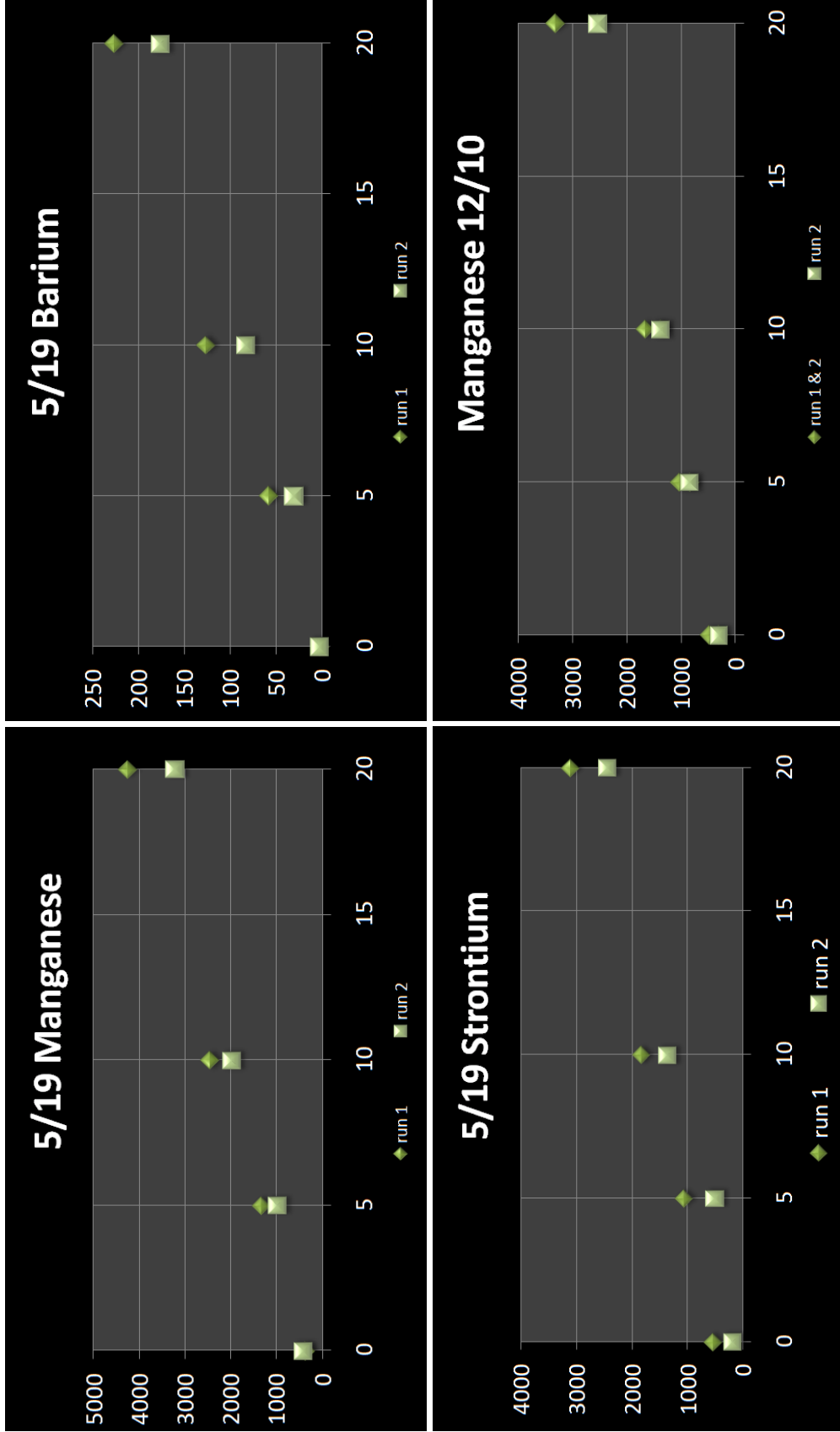


Figure 3.27T (Data for all elements is available in figure 3.27 of appendix 3.1 on the accompanying compact disc) The title of each graph indicates the element analyzed and the date of analysis. X-axis values represent concentration (ppm) in the standard wafer. Y-axis values represent counts per sweep measured by LA-ICP-MS. “Run 1” and “run 2” represent analyses conducted at two different times of day, with run 1 being before run 2. In all cases, run 1 indicates higher instrument sensitivity.

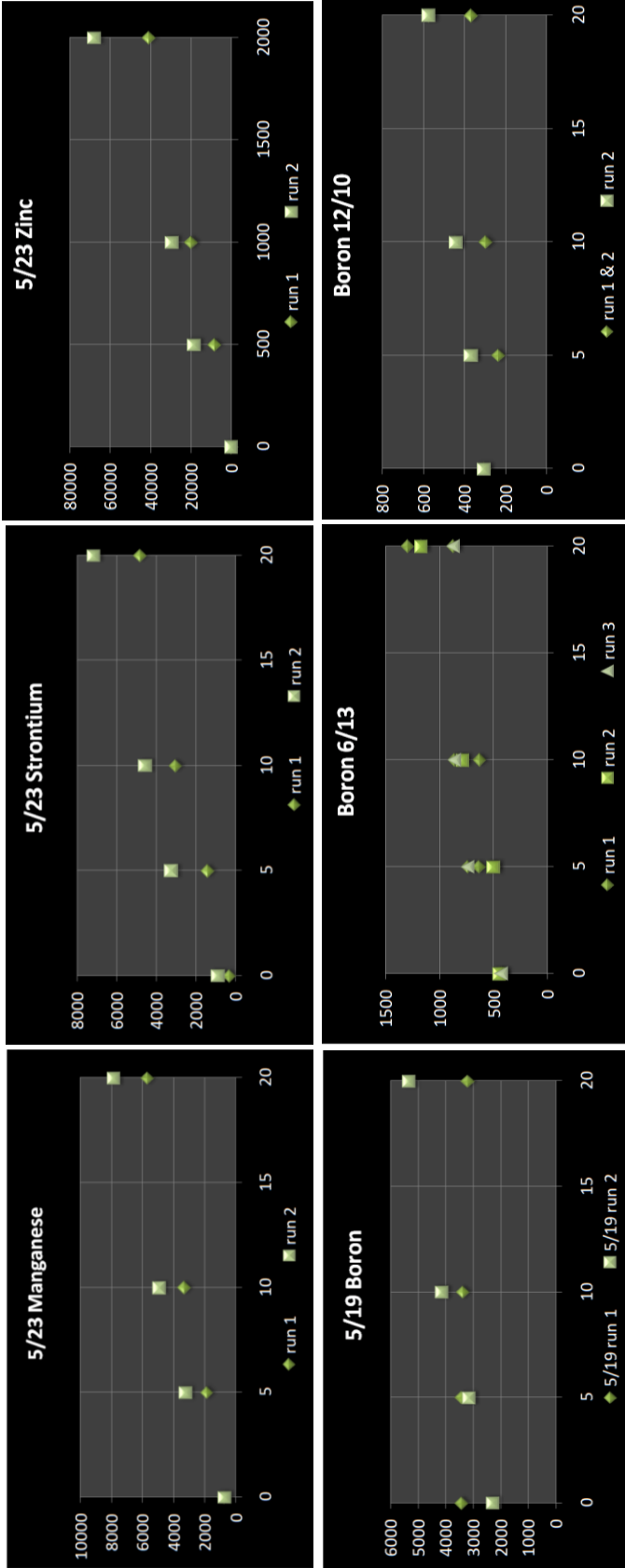


Figure 3.27T_2

The title of each graph indicates the element analyzed and the date of analysis. X-axis values represent concentration (ppm) in the standard wafer. Y-axis values represent counts per sweep measured by LA-ICP-MS. Runs 1, 2, and 3 represent analyses conducted at different times of day, with run 1 being before run 2. In all cases, Runs 2 and 3 indicate higher sensitivity than run 1. Data for all elements are available in appendix 3.1 (compact disc).

elements in the standard wafers were much higher than concentrations in the analyzed wood. Cadmium, lanthanum, and lead in annual growth rings average concentrations that are much less than the concentration measured in the 0.5 standard wafer (figures 3.21, 3.23, 3.24 and tables 3.21, 3.23, 3.24) on all days of LA-ICP-MS analysis. On many occasions, the average concentration of these elements in annual growth rings is less than that of the blank standard wafer. This is the case for aluminum and iron on nine of ten days of LA-ICP-MS analysis, for copper on eight of ten days, nickel on seven of ten days, rubidium on six of ten days, and zinc on three of ten days. Although LA-ICP-MS analysis of these elements provided generally good representations of concentrations in standard wafers, analytical accuracy may not be as reliable for the much lower concentrations in samples. This, and other factors that are discussed in chapter four, may affect the quality of LA-ICP-MS data for some elements on a given day.

3.2 Elemental Abundances

Concentrations for all collection days are shown by location and by date (appendix 3.2, figures 3.28-3.33). Forty-nine core-segments were analyzed from seven locations by LA-ICP-MS and results are described below by sample-site location. The prefix (JFCK, FR77, FR7506, BM, STRCK) denotes the sample site in which the tree is located. The number (1-9) that follows the prefix indicates the specific tree within the field site from which the core was taken. To avoid confusion in the cases of FR77 and FR7506, a space is placed between the prefix and the tree number. The letter (A, B, or C) that follows the tree number indicates from which core the core-segment was taken. For example, FR77 2A and FR77 2C describe two core segments from the second tree

sampled along forest road 77. As mentioned in chapter two, at least two cores were taken from every tree.

Jefferson Creek

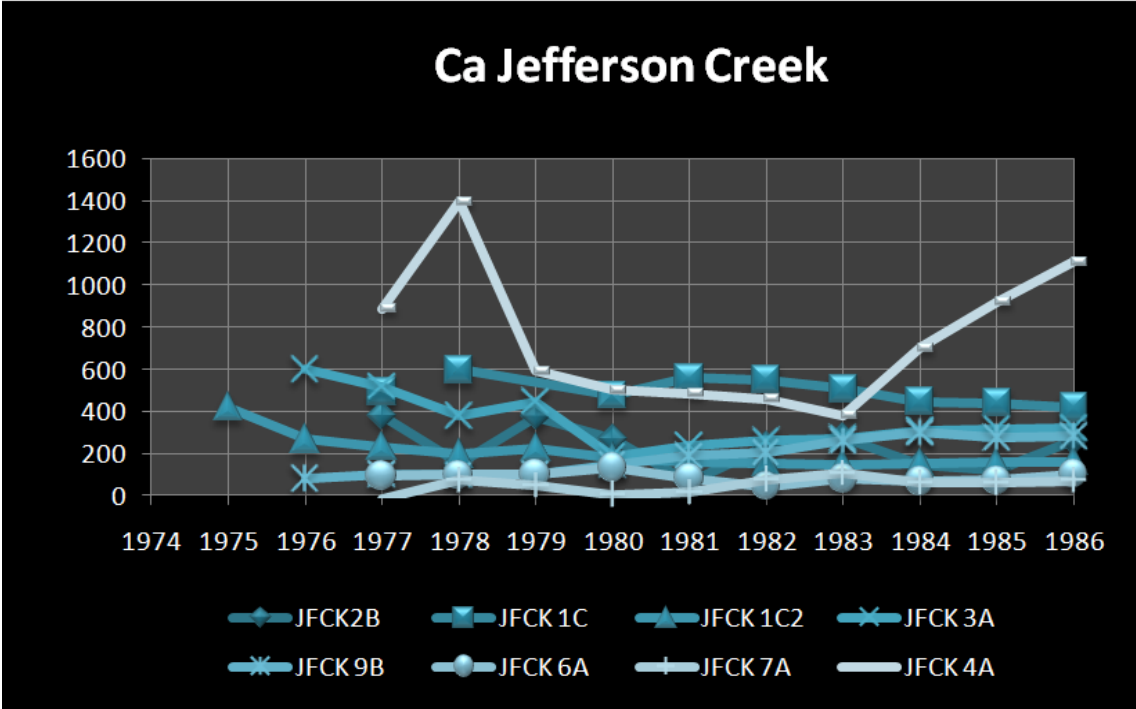
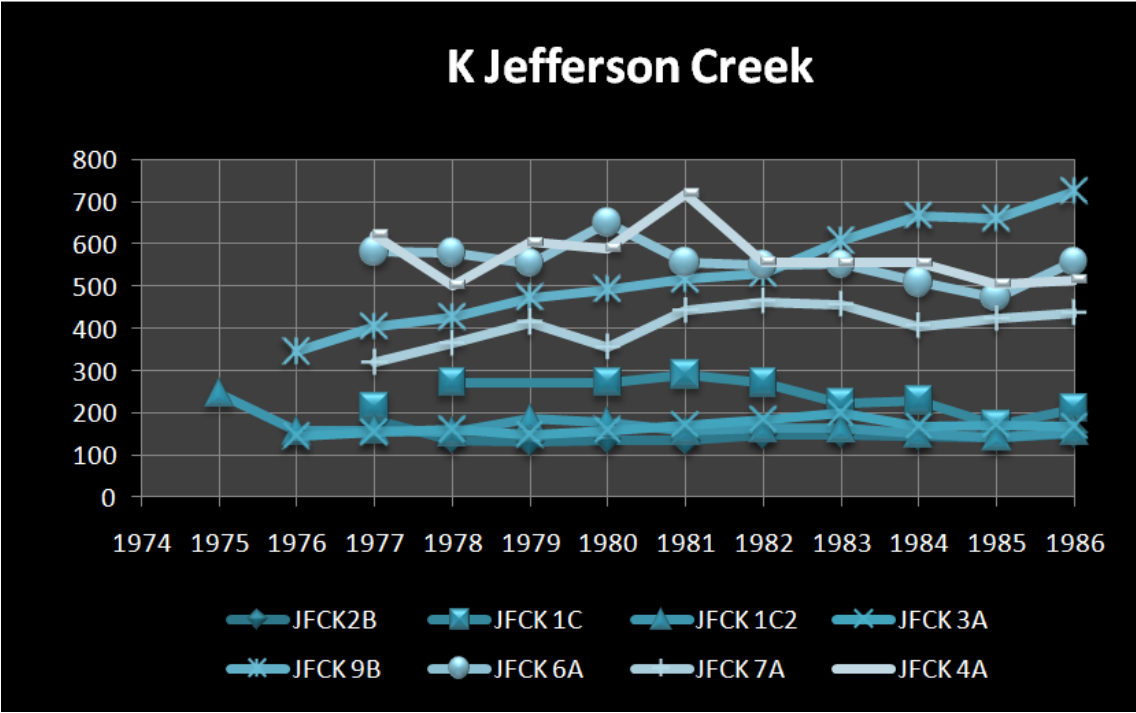
Fifteen core segments from seven trees in the Jefferson Creek field site were analyzed by LA-ICP-MS on seven different days (appendix 3.2, figure 3.28). Seven of these core segments include annual growth rings between AD 1976 and AD 1986. JFCK 1C includes AD 1974 and AD 1975 in addition to the other years. This sample was analyzed twice on May 21st, and JFCK 2B was analyzed on two different dates. The configuration used on December 14th (appendix 3.1, table 3.7) was different from those used on all earlier dates (section 3.3). Six core segments from Jefferson Creek include annual growth rings from AD 1795 to AD 1805. These six core segments are from six of the same trees analyzed for the AD 1976-1986 period. JFCK 4A is the only sample in the entire data set to include core segments dating to the end of the fifteenth century.

Phosphorus and sulfur were not successfully calibrated for any of the core segments from this field site (appendix 3.2, table 3.28). Boron was not successfully calibrated on two of the dates pertaining to this field site. No concentration data are available for boron in JFCK 1C, JFCK 2B, or JFCK 3A. The concentrations of titanium in annual growth rings could also not be calculated for JFCK 1C or JFCK 2B. Detection levels for ICP-MS analysis are in the parts per billion range for the least abundant elements quantified in this study.

Four of the eleven core-segment analyses show concentrations that are below detection for boron (appendix 3.2, table 3.28). Of the samples that show detectable

amounts of boron, no notable variation in the elemental concentration occurs between annual growth rings. JFCK 9B shows a steady increase in boron from AD 1978 to AD 1986 and AD 1797 to AD 1805 (figure 3.38). Aluminum is below detection limits for ten of the sixteen core-segment analyses while iron and cadmium are below detection for nearly all of the annual growth rings analyzed (table 3.28). Copper, strontium and lanthanum are also below detection for a large number of samples analyzed in this field site. Concentrations of lanthanum and lead rarely exceed a value of 1 ppm (table 3.28).

Most core segments from Jefferson Creek show a notable change in elemental abundance of at least one element between AD 1795-1805 and AD 1976-1986. JFCK 1C and JFCK 9B do not show notable chemical variation for the time period between AD 1795 and AD 1805. Some core segments show notable increases or decreases in abundance of aluminum, potassium, calcium, titanium, copper, zinc, rubidium, strontium, or barium between the years of AD 1976 and AD 1986 (appendix 3.2, figure 3.38). In four of the core segments from this time period, potassium varies in concentration. Potassium is also constant in four core segments (figure 3.38). “Constant” in this case refers to a lack of variation in elemental abundance. Three core segments each from AD 1976 to AD 1986 vary in calcium, rubidium and barium. Changes in the abundance of aluminum, copper, zinc, and strontium are noted in two cores each, and a change in the abundance of titanium is noted in only one core in the twentieth century. All of the core segments that show changes in calcium concentration also show a change in the concentration of potassium (figure 3.38). The concentrations of calcium and potassium have positive correlation in some cases, and negative correlation in others. The character of co-variation for these elements is inconsistent.



From figure 3.38T
 Four of the core segments from Jefferson Creek show chemical complacency, or a lack of variation in elemental abundance, of potassium. Elements that show variable K concentrations also show variation in the concentration of Ca. All of figure 3.38 is available in appendix 3.2 (compact disc).

For the time period between AD 1795 and AD 1805, only five elements show significant variation between annual growth rings compared to nine for the twentieth-century core-segments. Zinc, manganese and strontium are each noted for affecting two of six core segments while aluminum and titanium show a change in concentration for one of six core segments each. None of these elements show consistent co-variance among this group of samples. Some elemental concentrations change on or after eruption years, and some beforehand (appendix 3.2, figure 3.28, figure 3.38).

JFCK 9B shows a drop in the concentration of aluminum from 10 ppm in AD 1796 to less than 3 ppm in AD 1797 (appendix 3.2, figure 3.38, table 3.28). Concentrations immediately increase again the following year and continue to increase until AD 1803. JFCK 4A shows a more subtle increase in the same element between AD 1799 and AD 1800. The concentration of aluminum in this core segment jumps from 1.17 ppm to 3.52 ppm, and immediately falls the following year.

In AD 1980, two samples show a short-lived change in the abundance of potassium (figure 3.38, table 3.28). JFCK 6A jumps from 554 to 650 ppm, the highest concentration for the eleven years analyzed. JFCK 7A drops from 413 ppm to 355 ppm, the second lowest concentration for the eleven-year period. JFCK 1C shows a slight increase in potassium in AD 1979 and JFCK 3A shows a slight decrease in the same year, followed by a steady, sustained increase.

Calcium concentrations vary greatly between years in four of the fifteen core segments analyzed from Jefferson Creek (figure 3.38, table 3.28). JFCK 3A and JFCK 6A show sudden, short-lived increases in calcium followed by an immediate decrease and sustained low elemental abundances for several years. The spike occurs in AD 1979 for

JFCK 3A and in AD 1980 for JFCK 6A. In AD 1980, calcium decreases in JFCK 1C.

The fifth core segment to show a change in the concentration of calcium is JFCK 2B and this change is only apparent in the analysis conducted on December 14th. The analysis of the same core segment conducted on May 19th does not exhibit a similar pattern. This will be discussed further in section 3.3.

A decrease in the concentration of zinc occurs in JFCK 4A between AD 1800 and AD 1801 and remains low through AD 1805 (figure 3.38, table 3.28). JFCK 9B shows a small spike in zinc in 1981 and again in AD 1985. A pronounced spike in copper occurs in AD 1981 for JFCK 3A and JFCK 4B. The concentration of copper in JFCK 4B more than quadruples between AD 1980 and AD 1981 (figure 3.38).

Changes in elemental concentrations on and after eruption years occur among JFCK 4A, JFCK 6, JFCK 7A, and JFCK 9B for titanium, manganese, rubidium, or strontium (figure 3.38). Concentrations of barium become more variable in JFCK 1C and JFCK 9B after AD 1980.

Sodium, potassium, calcium, and barium are characterized by complacency, or a lack of variation in concentration, in several core segments (figure 3.28, appendix 3.2).

FR77

Ten core segments were analyzed from forest road 77 by LA-ICP-MS (appendix 3.2, figure 3.29, table 3.29). This includes seven core segments containing growth rings from AD 1976 through AD 1986 and three core segments with growth rings from AD 1795 through AD 1805. The ten core segments come from a total of six trees. FR77 2C and FR77 6B were analyzed prior to December 14th, and on December 14th (section 3.3).

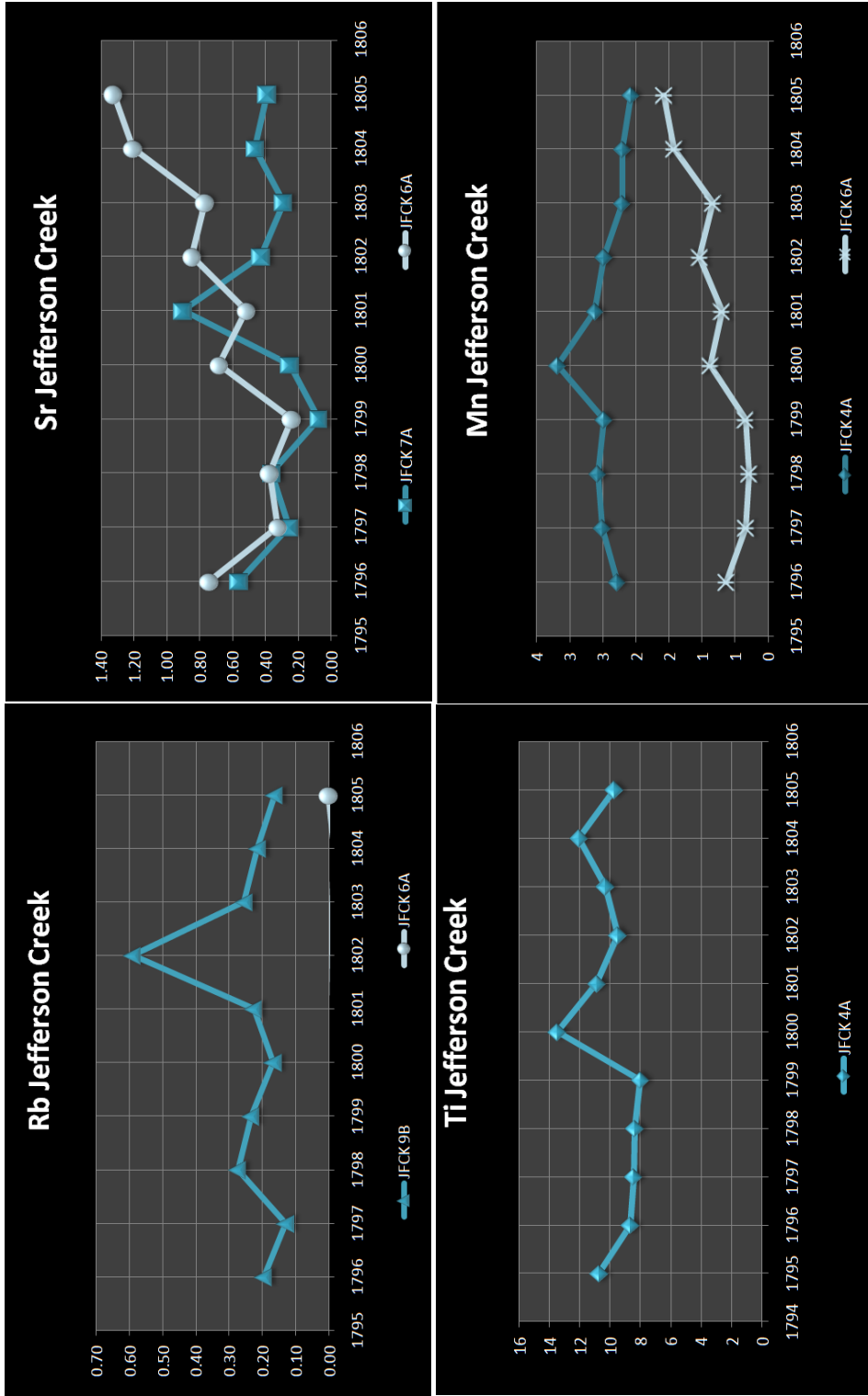


Figure 3.38T_2
 The title of each graph indicates the element analyzed. The x-axis shows the year corresponding to a growth ring. Y-axis values represent concentration (ppm) of the element indicated by the title. These are examples of spikes in elemental concentration that occur on or after an eruption year (CE 1800). All of figure 3.38 is available in appendix 3.2 (compact disc).

Aluminum is below detection limits for all or most of the growth rings in seven of the ten cores analyzed (table 3.29). Iron, cadmium, and lead are also present in abundances that are below detection in the majority of growth rings from this location. When elements are present in measurable abundance for cadmium or lead, they rarely exceed 1 ppm (table 3.29). Nine of the ten core segments show some notable change in elemental abundance for the growth rings analyzed. Only FR77 3B maintains consistent concentrations of all elements between the years of AD 1976 and AD 1986 (figure 3.29).

Core segments that contain the growth rings from AD 1976 to AD 1986 show variations in the concentrations of aluminum, potassium, calcium, titanium, nickel, copper, zinc, rubidium and strontium occur between annual growth rings. Three of these core segments show significant variation in the concentrations of four or more elements while two core segments, FR77 5A and FR77 8B, only show significant variation in the concentration of one element each. FR77 2A shows variation in the concentrations of potassium and strontium while FR77 2C, a core segment from the same tree, shows variation in the concentrations of aluminum, potassium, calcium, zinc and rubidium (figure 3.39). Eight of the nine elements mentioned above show similar patterns of changing concentration in all of the noted core segments. Strontium is the exception, showing a steady and sustained increase beginning in AD 1980 of FR77 2A, and a short-lived decrease in the same year for FR77 6B.

FR77 6B shows a steady and moderate increase in calcium that begins in AD 1980. The concentration of calcium in this sample climbs from 269 ppm in AD 1980 to 453 ppm by AD 1986 (figure 3.39, table 3.29). In FR77 2C, the increase in calcium is large and short-lived, jumping from 365 ppm to 859 ppm between AD 1979 and AD

1980. The next year, calcium drops to pre-1980 levels and remains low through 1986. Zinc increases similarly in the same year for the same sample, nearly doubling in AD 1980, and immediately dropping again the following year (figure 3.39). In FR77 6B, the increase in the concentration of zinc is, like calcium in the same sample, sustained over many years. The increase in zinc is large, from 5 ppm in AD 1980 to 17 ppm the following year, and reaches 44 ppm by AD 1986. This increase is steady, dropping drastically and then recovering between AD 1984 and AD 1986.

An increase in the concentration of potassium is present in AD 1980 of FR77 2A and FR77 2C. In both cases, potassium increases from approximately 60 ppm to more than 150 ppm, and remains high through AD 1986. FR77 2C is the only core segment to also show an increase in rubidium that begins in AD 1980. Although the concentration of rubidium is consistently low (< 1 ppm), it nearly triples between 1979 and 1980 and then remains high through 1986 (figure 3.39, table 3.29).

The significant increase in zinc that occurs in FR77 7A and FR77 8B occurs prior to an eruption year. FR77 7A spikes in AD 1977 while FR77 8B spikes in AD 1976. FR77 7A shows an increase in titanium, nickel, and copper in AD 1981. All three elements exhibit a similar pattern in this sample, drastically increasing for only one year, and then dropping back to low abundances. The same pattern occurs in the same year for FR77 5A with copper only (figure 3.39).

Core segments that contain annual growth rings from AD 1795 to AD 1805 are much more erratic in character (figure 3.29, table 3.29). Apparent changes in the concentration of several elements occur between growth rings of this time period and location, but there is typically no discernable pattern. FR77 6B shows decreases in boron

and titanium that begin at AD 1799 (figure 3.39). Concentrations of titanium are lower in 1799 and 1800 than all other years for this sample. The same is true for boron in AD 1799 only (figure 3.39).

Potassium in FR77 8B decreases slightly in 1801. Barium in the same sample decreases at AD 1799 and continues to do so until AD 1800.

Rubidium and lanthanum both increase drastically for one year in FR77 7A. Rubidium increases at AD 1798, while lanthanum increases at AD 1800.

Sodium, potassium, barium, and titanium show chemical complacency in several core segments from FR77 (figure 3.29). Calcium is more variable here than at Jefferson Creek.

FR7506

Eight core segments from five trees were analyzed by LA-ICP-MS from forest road 7506 (appendix 3.2, figure 3.30, table 3.30). Five of these core segments include growth rings from AD 1975 through AD 1986, and three include growth rings from AD 1795 through AD 1805 (table 3.30). Barium is below detection or unavailable for six of the eight core segments. Aluminum and iron are below detection for nearly every growth ring in this sample set. Cadmium and lead are present in detectable concentrations for one and a half of the eight core segments. Measured concentrations that are above detection do not exceed 1 ppm for cadmium, or 4 ppm for lead (table 3.30). FR7506 5B was also analyzed by LA-ICP-MS with a five-element configuration on December 14th, (section 3.3).

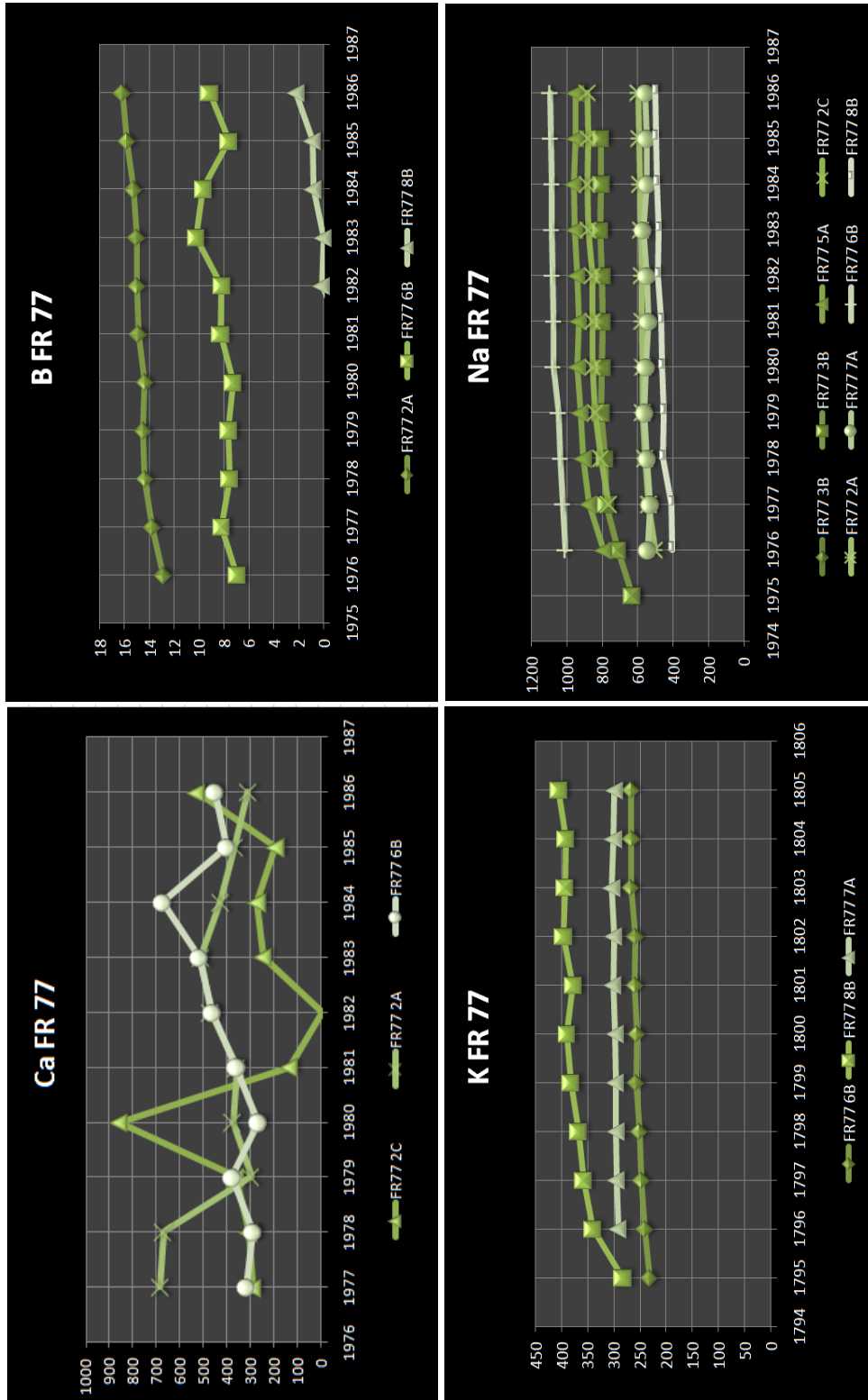


Figure 3.29T

The title of each graph indicates the element analyzed. The x-axis shows the year corresponding to a growth ring. Y-axis values represent concentration (ppm) of the element indicated by the title. B, K, and Na are complotent over ten years of growth. Calcium concentration here varies, and in FR77 2A, spikes in concentration at AD 1980. All of figure 3.29 is available in appendix 3.2 (compact disc).

Three of five cores show changes in elemental abundance during the time period between AD 1975 and AD 1986. Many of the identified changes in elemental concentrations from these samples are based upon patterns in their plots (figure 3.30, 3.40). In many cases, the character of the line on a graph changes from erratic to consistent at some point in time. In FR7506 5B, this pattern is true of titanium and nickel. Both elements are present in consistent concentrations beginning at AD 1980. Zinc and cadmium in this sample both decrease considerably in abundance between AD 1979 and AD 1980 (figure 3.40). Zinc decreases by more than 70 ppm while cadmium decreases by more than 30 ppm. In both cases, the decrease is sustained for several years.

Copper decreases in FR7506 5B and FR7506 6B in AD 1977 and AD 1978, respectively. Both decreases in elemental abundance follow a prior spike in concentration. FR7506 6B increases in potassium, nickel and rubidium at AD 1980 (table 3.30). The increase in potassium and rubidium are slight and short-lived, while that of nickel is sustained for many years (figure 3.40). Potassium and barium decrease slightly at AD 1980 in FR7506 7B.

FR7506 4A increases steadily in the concentration of barium beginning at AD 1800 (table 3.30, figure 3.40). Calcium in the same sample decreases at AD 1798 and again at AD 1800 and 1804 (figure 3.40). FR7506 1A exhibits an increase in the concentration of zinc at AD 1799 that remains high through AD 1800 (figure 3.40).

Sodium and potassium are complacent in core segments from this sample site (figure 330). Calcium is highly variable at FR7506, and spikes do not correlate to any particular growth year.

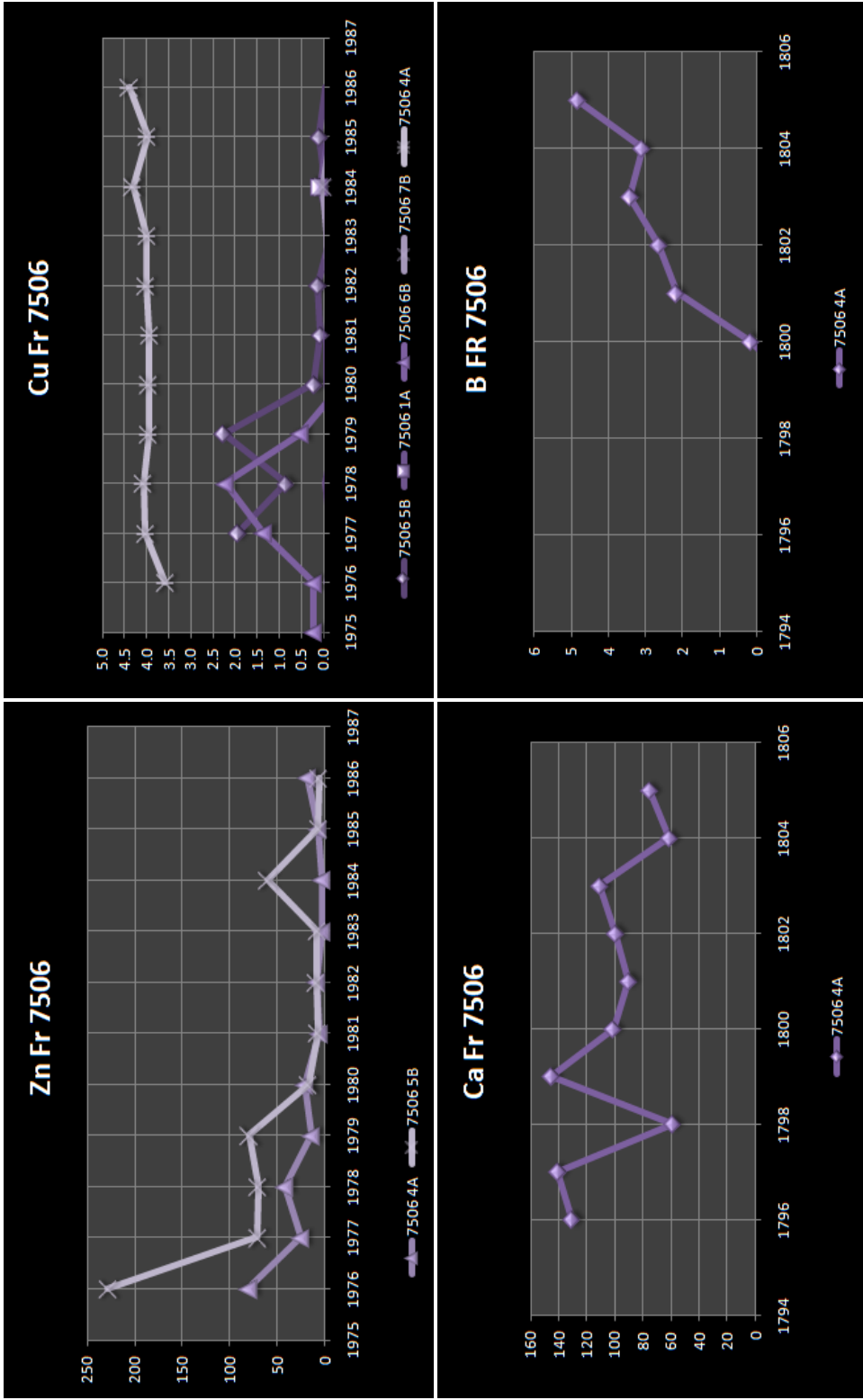


Figure 3.40T

The title of each graph indicates the element analyzed. The x-axis shows the year corresponding to a growth ring. Y-axis values represent concentration (ppm) of the element indicated by the title. Elemental concentration varies in all elements in growth rings corresponding to different years. There is no consistent pattern of variation among most samples from all sample sites. All of figure 3.40 is available in appendix 3.2 (compact disc).

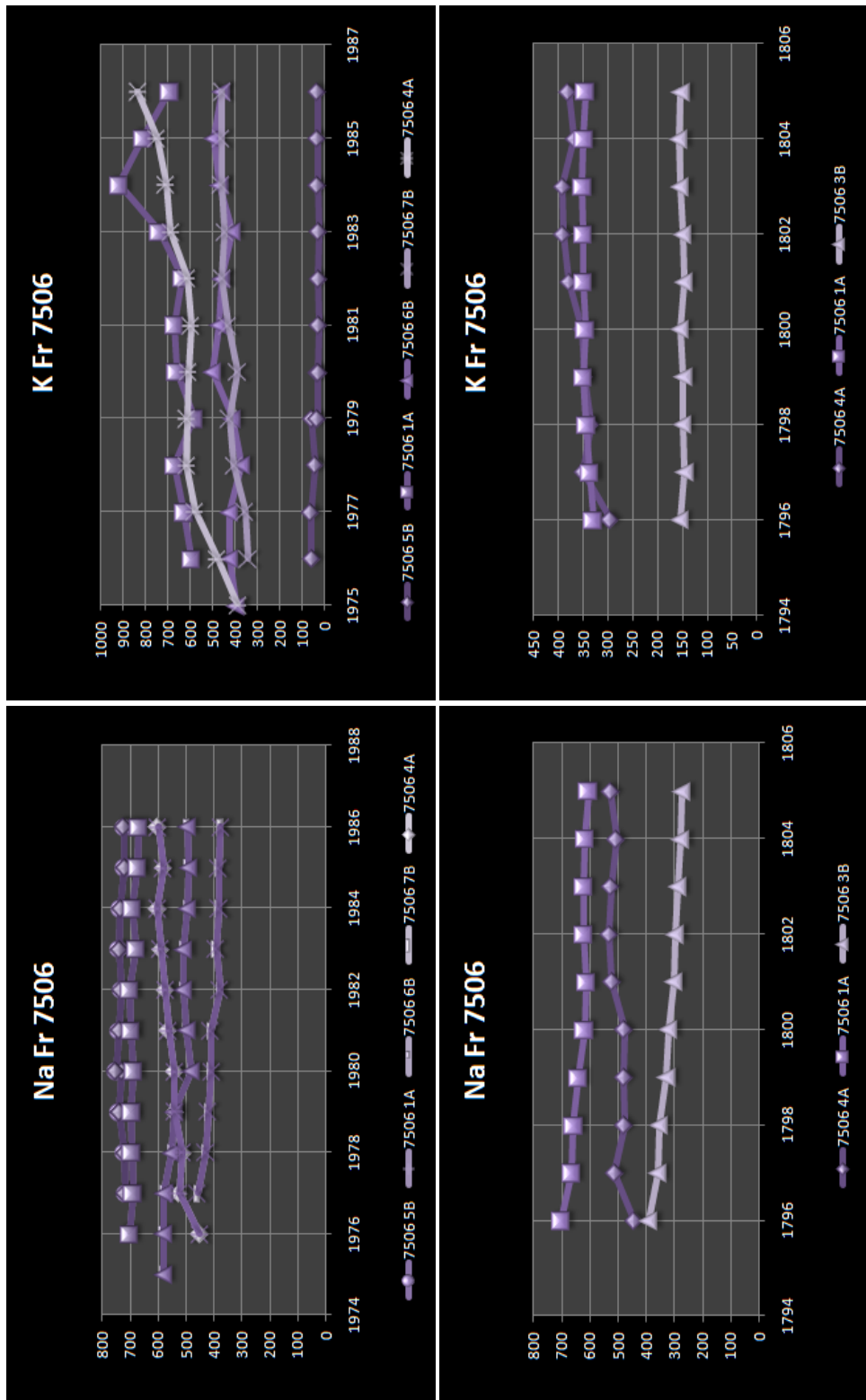


Figure 3.30T
 The title of each graph indicates the element analyzed. The x-axis shows the year corresponding to a growth ring. Y-axis values represent concentration (ppm) of the element indicated by the title. K, and Na do not vary in concentration in most of the core samples from this sample site. All of figure 3.30 is available in appendix 3.2 (compact disc).

Bear Meadow

Nine core segments from six trees at Bear Meadow were analyzed by LA-ICP-MS. These include four core segments including growth rings from AD 1976-1986 and six core segments including growth rings from AD 1795-1805 (appendix 3.2, figure 3.31, table 3.31). Concentration data for boron and aluminum are only available for two of nine core segments. Iron is present in detectable concentrations for one core segment of the nine, and not all growth rings in this core segment are above detection limits. Cadmium was detectable in four of the nine core segments and lead was detectable in two of the nine. Neither element exceeds a concentration of 1 ppm for any annual growth ring in this sample set (table 3.31).

Eight of the nine core segments from Bear Meadow show some variation in elemental concentration. BM 1A shows a decrease in sodium and titanium and an increase in potassium, calcium, and manganese at AD 1979 (figure 3.41). In all cases, the change in elemental concentration is limited to a single growth year. In BM 2B, a decrease in sodium and an increase in potassium occur in AD 1977 and again in AD 1982. These changes in concentration are also short-lived. A decrease in titanium and an increase in manganese both occur in BM 2B at AD 1977. A decrease in potassium occurs along with an increase in calcium, copper, zinc, barium, and strontium in BM 5B (figure 3.41, table 3.31). The change in potassium, strontium, and barium are all short-lived, occurring in only one annual growth ring. The increase in calcium concentration is sustained for two growth rings before dropping at AD 1982 and remaining low. The increase in the concentration of copper in BM 5B is sustained through AD 1986. BM 8B exhibits a slight decrease in the abundance of titanium at AD 1981.

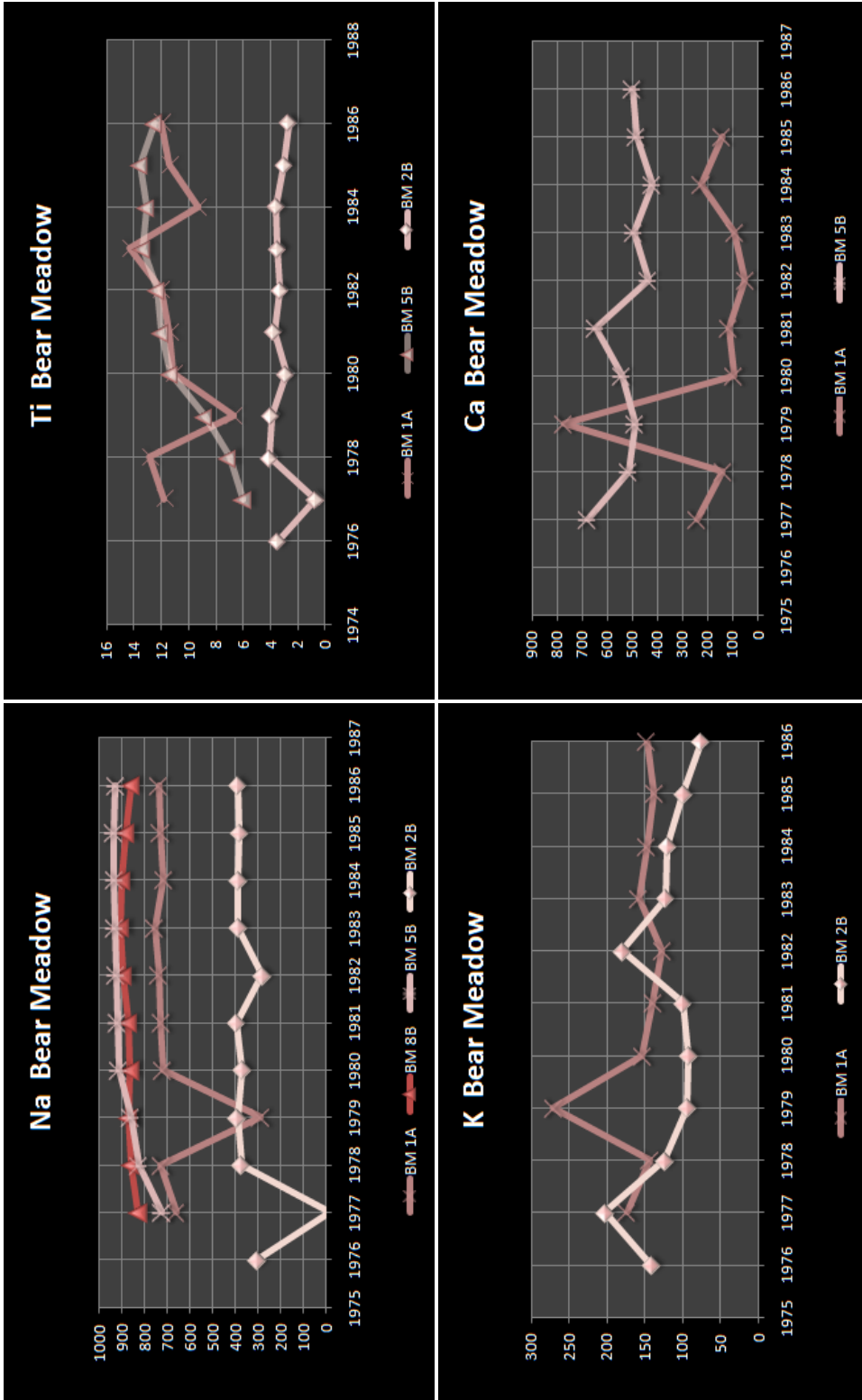


Figure 3.41T

The title of each graph indicates the element analyzed. The x-axis shows the year corresponding to a growth ring. Y-axis values represent concentration (ppm) of the element indicated by the title. Na and Ti decrease in concentration at AD 1979 for BM1A. K and Ca increase in the same year of the same sample. All of figure 3.41 is available in appendix 3.2 (compact disc).

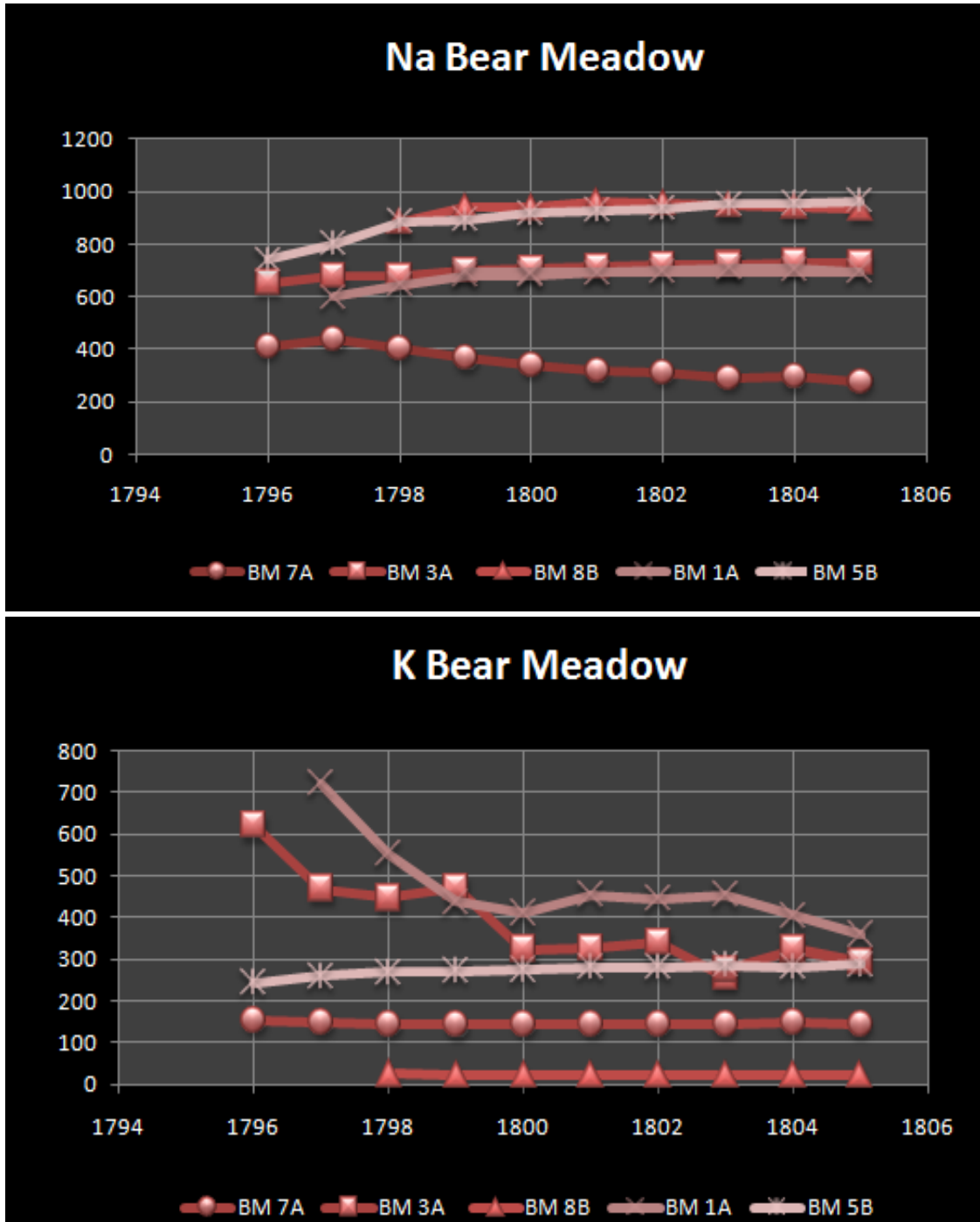


Figure 3.31T

The title of each graph indicates the element analyzed. The x-axis shows the year corresponding to a growth ring. Y-axis values represent concentration (ppm) of the element indicated by the title. K and Na in most samples from Bear Meadow show a low variability in concentration. This trend in K and Na is similar among samples from other sites. All of figure 3.31 is available in appendix 3.2 (compact disc).

Barium increases in concentration in BM 7A, BM 8B, and BM 5B at AD 1798, AD 1800, and AD 1801, respectively (figure 3.41). Nickel in BM 8B spikes at AD 1802. In BM 7A, nickel stops climbing at AD 1800 and remains consistent through AD 1805 (table 3.41). Zinc in the same sample becomes detectable at AD 1800, and remains above detection but erratic until AD 1805 (figure 3.41). Rubidium in BM 3A decreases in concentration at AD 1800 and remains low through AD 1805.

Potassium and sodium are complacent in nearly all core segments from Bear Meadow for AD 1795- AD 1805. Two core segments (BM 1A and BM 2B) from AD 1977-CE1986 have spikes in each of these elements at different years. BM 8B and BM 5B have similar complacency to the AD 1975-CE 1805 sample set (figure 3.31, appendix 3.2).

Straight Creek

Two core segments from the same tree were analyzed from Straight Creek by LA-ICP-MS. One core segment contains annual growth rings from AD 1975 through AD 1986 and the other contains annual growth rings from AD 1795 through AD 1805 (appendix 3.2, figure 3.32, table 3.32). Boron is below detectable concentrations for the first four annual growth rings of each core segment. Aluminum is present in concentrations that are detectable for fewer than half of the growth rings analyzed. Cadmium and iron concentrations are below detection limits in all samples, and lead is detectable for AD 1795 to AD 1805 only (table 3.32).

Boron in both core segments becomes detectable and continues to increase steadily in concentration until the last growth ring in the core segment. Boron becomes

detectable at AD 1980 and AD 1799 (figure 3.42). Calcium decreases at AD 1800 in STRCK 1A, and changes from a decreasing to an increasing trend at AD 1980 in the same tree. Copper increases in concentration abruptly at AD 1799 (figure 3.40). Barium, rubidium, strontium, and potassium have similar trends from CE1975- CE1986. Calcium and manganese have nearly identical trends from AD 1795- AD 1805 and AD 1975- CEE 1986.

Control Trees

Seven core segments from five trees were analyzed from two locations south of Mount Saint Helens (appendix 3.2, figure 3.33, table 3.33). Two of these were cored at Marble Mountain Snow Park (1980 tephra < 3cm) located on the southern flanks of Mount Saint Helens, off-axis of the path of the ash cloud produced by the 1980 eruption (figure 1.4). These trees are located within 19 km of the trees sampled at Bear Meadow and are at a similar altitude (figures 2.0). For this reason, they have experienced climatic conditions that are similar to those at Jefferson Creek, FR77, FR7506, Bear Meadow and Straight Creek. Five more trees were sampled from a location east of Salem, Oregon, near Opal Lake (figures 2.1 and 2.15, appendix 1.0). These trees are located approximately 115 km south of the 1980 crater, far beyond the zone of deposition from the AD 1980 eruption of Mount Saint Helens. All of the trees cored from this site in Oregon are Douglas firs. The type of forest in this area is similar to that at Gifford Pinchot National Forest, and the climate and elevation of the sample site are comparable to those of the sample sites north and east of Mount Saint Helens.

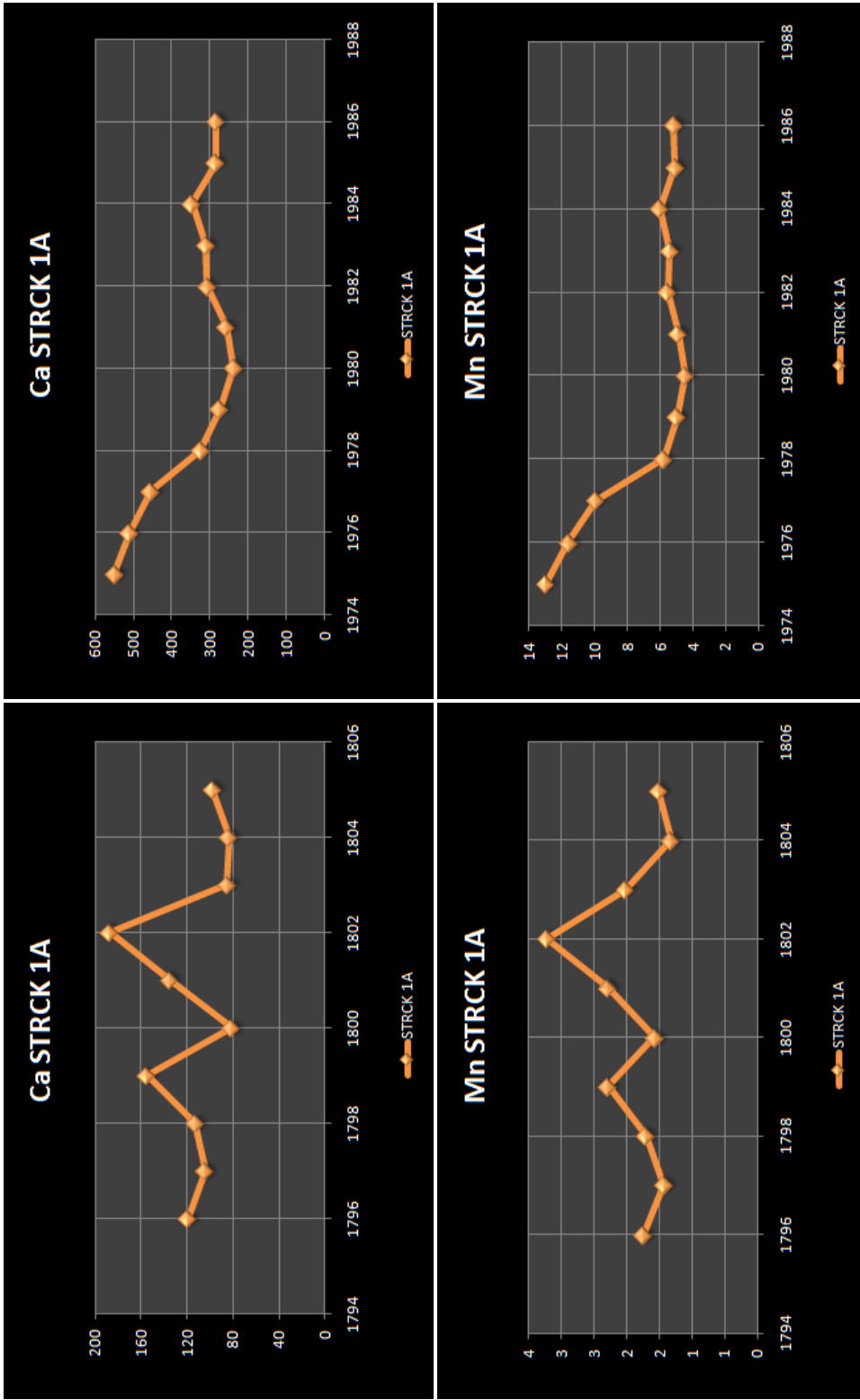


Figure 3.32T

The title of each graph indicates the element analyzed. The x-axis shows the year corresponding to a growth ring. Y-axis values represent concentration (ppm) of the element indicated by the title. Ca and Mn have nearly identical trends in STRCK 1A from AD 1795- 1805 and AD 1976- 1986. All of figure 3.32 is available in appendix 3.2 (compact disc).

One of the tree-core segments from Marble Mountain Snow Park is PSF MMSP 1B. This tree, a Pacific silver fir, is unique in that it is of a different species than the others in the sample set. Several of the changes in elemental concentration that were observed among trees from Jefferson Creek, forest road 77, forest road 7506, Bear Meadow, and Straight Creek were also apparent in this core segment. Decreases in sodium, aluminum, potassium, and calcium all occur at AD 1980 (figure 3.43). In all cases, the decrease is abrupt, and limited to one growth ring. Increases in the concentrations of rubidium, cadmium, zinc, and nickel all occur at AD 1981 in the same sample. In all cases, the initial increase is dramatic. In the following year, concentrations in these four elements decrease again, but never return to the levels seen prior to 1981. A change in trend occurs in PSF MMSP 1B at AD 1980 for the concentrations of titanium and iron. Both elements change from a decreasing trend to an increasing trend (figure 3.43, table 3.33). The Douglas fir from the same site (DF MMSP 1B) does not show the same changes.

FR225 1B, from the site at Opal Creek, east of Salem, Oregon, shows slight increases in potassium and calcium at AD 1980 (table 3.43). A pronounced spike occurs in nickel at AD 1980 for the same sample (figure 3.43). Also in FR225 1B, aluminum doubles in concentration at AD 1980 and remains elevated through AD 1986.

FR225 3A exhibits a notable spike in calcium at AD 1982, and in lanthanum at AD 1979. Also in FR 225 3A, a dramatic spike occurs in the concentration of every element except for boron at AD 1800 (figure 3.43).

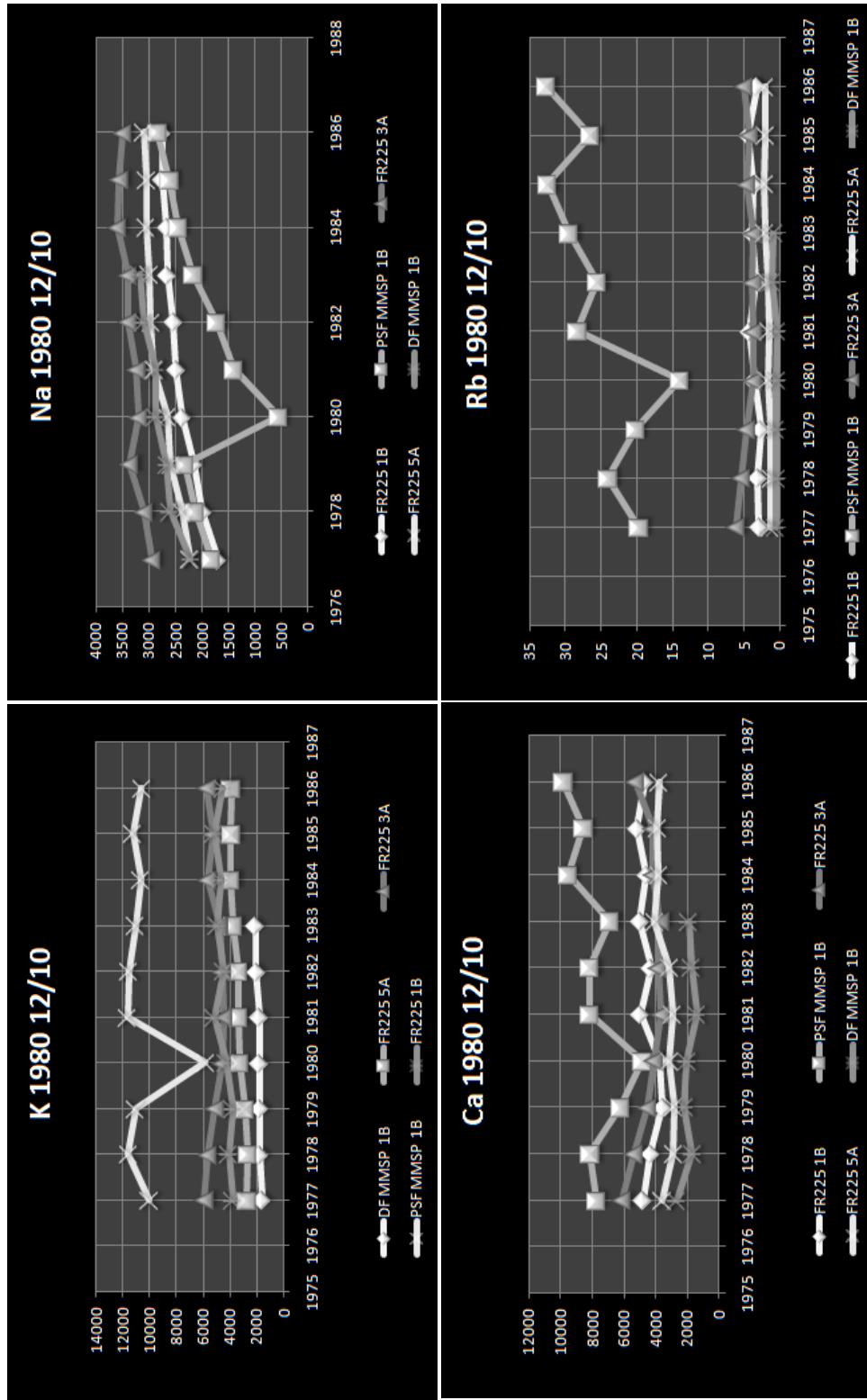


Figure 3.33T

The title of each graph indicates the element analyzed. The x-axis shows the year corresponding to a growth ring. Y-axis values represent concentration (ppm) of the element indicated by the title. PSF MMSP 1B has an evident change in concentration of all elements shown above at AD 1980. All of figure 3.33 is available in appendix 3.2 (compact disc).

3.3 Elemental Concentrations Measured on 12/14

As discussed in section 2.6, LA-ICP-MS analysis for the range of elements considered in this study required a large degree of detuning. Detuning refers to the reduction of sensitivity of selected elements. In a sample that contains both high and low concentrations of elements being analyzed, detuning of the high-concentration elements prevents saturation in the detector. In order to test the consequence of such low sensitivity, a second experiment was set up on the ICP-MS for one day of data collection. This experiment included the analysis of only five elements: aluminum, calcium, zinc, phosphorus, and sulfur (appendix 3.1, table 3.7). Phosphorus and sulfur were chosen because previous studies observed a change in the concentration of these two elements in annual growth rings that coincided with the eruption of Volcán Parícutin and Cinder Cone (Sheppard et al., 2008; Sheppard et al., 2009). These elements were considered for the five-element configuration despite problems with calibration on earlier dates in order to test the idea that a simpler experiment might allow for accurate counting of phosphorus and sulfur. Aluminum and calcium were chosen because of the potential for the increase of aluminum in soil due to weathering of volcanic material (Felitsyn and Kirianov, 1981). Large amounts of aluminum in a root system can displace calcium, causing the condition known as aluminum toxicity (McCarrol and Loader, 2005). If weathering of tephra were to lead to aluminum toxicity in the trees analyzed in this study, I would expect a decrease in the concentration of calcium to accompany an increase in the concentration of aluminum in an annual growth ring. Zinc was chosen as the fifth element in the configuration because it was shown to co-vary with calcium in a previous laser-ablation study of dendrochemical changes related to volcanic eruptions (Pearson et al., 2005).

Calibration curves for phosphorus and sulfur could not be produced on any day of the eighteen-element experiment (appendix 3.1, figure 3.6). The five-element configuration did not resolve this issue with either of the two elements. Aluminum, calcium and zinc are therefore the only elements for which data will be presented in tree cores that were analyzed on December 14th.

Fourteen core segments from ten trees and several field sites were analyzed by LA-ICP-MS on December 14th (appendix 3.2, figure 3.46, table 3.44). All of these core segments had been analyzed at an earlier date using the eighteen-element LA-ICP-MS configuration. Six core segments from five trees were from control trees that were analyzed on December 10th. The remaining eight core segments came from five trees that were cored at Jefferson Creek, forest road 7506, forest road 77, and Straight Creek. Results from the analyses completed on the five-element configuration will be compared to those completed on the eighteen-element configuration at the end of this section (appendix 3.2, figure 3.45).

PSF MMSP 1B shows a decrease in the concentration of calcium from 6662 ppm at AD 1980 to 2843 ppm the following year (appendix 3.2, figure 3.46). The same sample exhibits a small spike in zinc at AD 1980, and a larger spike (from 2000 ppm to approximately 14,000 ppm) in zinc at AD 1984.

FR225 1B shows a small spike in calcium, aluminum and zinc at AD 1981 (figure 3.46). A larger spike in zinc occurs in the same sample at AD 1978. FR225 5A exhibits an increase in calcium from 3,000 to 4,000 ppm at AD 1801. The higher calcium concentration is sustained until AD 1805. The same sample shows a small spike in zinc at AD 1803 and a decrease in aluminum at AD 1798.

JFCK 2B shows a drop in aluminum concentration from 36 ppm in AD 1979 to 16 ppm in AD 1980. This decrease is sustained, as aluminum concentrations do not exceed 20 ppm from AD 1980 through AD 1986. The same sample shows a spike in calcium and zinc at AD 1979. In both cases, elemental concentrations decrease the following year and stay low through AD 1986. JFCK 2B also shows a decrease in calcium and zinc at AD 1800 (figure 3.46).

Aluminum increases in AD 1980 and 1981 in FR77 6B and FR77 2C, respectively. In both cases, aluminum increases in a step-like manner that is sustained through AD 1986. FR77 6B increases in aluminum from 1047 ppm in 1979 to 1078 ppm in 1980, reaching a concentration of 1095 ppm by AD 1986 (figure 3.46, table 3.44). Similarly, FR77 2C shows an increase in the concentration of aluminum from 809 ppm in AD 1980 to 839 ppm the following year, and 854 ppm by AD 1986. FR77 6B shows a steady and moderate increase in calcium that begins at AD 1980 and AD 1800 and is sustained for several years. Zinc in the same sample increases in concentration steadily between AD 1980 and AD 1984 before a drastic increase at AD 1985. A spike in zinc also occurs in FR77 6B at AD 1800. The concentration of zinc decreases steadily over the next four years before climbing again.

FR7506 5B shows erratic behavior in all three elements analyzed with the five-element configuration. Dramatic increases and decreases occur in calcium, zinc and aluminum, but a discernable pattern is not apparent over the eleven-year interval analyzed.

STRCK 1A changes from a decreasing trend to an increasing trend in the concentration of aluminum at AD 1801 (figure 3.46). Aluminum increases in same

sample at AD 1982. Higher aluminum concentrations are sustained through AD 1986. Calcium in STRCK 1A increases in concentration at AD 1802, and remains elevated through AD 1805. The same sample shows a steady climb in calcium concentration between AD 1980 and AD 1983. Zinc concentrations decrease in STRCK 1A at AD 1800 and remain low for two years before rising again at AD 1803. A small spike in zinc occurs in the same sample at AD 1982.

Comparison of two configurations

The fourteen cores that were analyzed by the five-element configuration were also analyzed on earlier dates using the eighteen-element experiment (appendix 3.2, table 3.45). Ten of these core segments include annual growth rings from AD 1976-1986. DF MMSP 1B shows fair correlation between aluminum and calcium measured by each LA-ICP-MS configuration. Elemental concentrations are similar, with the exception of AD 1979. Data for the first growth ring analyzed shows opposite signals between the two configurations (appendix 3.2, figure 3.45). Zinc concentrations in DF MMSP 1B showed considerably different results as measured by each LA-ICP-MS configuration. The average concentration measured by the five-element experiment is much greater than that measured by the eighteen element experiment. In AD 1983, the concentration difference is more than 5,000 ppm (table 3.45).

PSF MMSP 1B has similar average concentrations of aluminum, calcium, and zinc measured by both configurations, but plot patterns are not so similar (figure 3.45). The five-element configuration measured lower concentrations of aluminum than the eighteen-element experiment from AD 1981-1983. The same is true of calcium between

AD 1981 and AD 1982. The large spike in aluminum recorded by the eighteen-element experiment is not as pronounced in the five-element experiment. A large spike in the concentration of zinc is detected only by the five-element experiment for the same sample (figure 3.45).

The two configurations for aluminum and calcium correlate well in FR225 1B (figure 3.45). Concentrations from the five-element and eighteen-element configurations are not as similar for zinc in this sample. The five-element experiment shows generally higher and more variable concentrations than the eighteen-element experiment (table 3.45). The plot patterns are, however, similar (figure 3.45). The eighteen-element configuration shows spikes in concentration at AD 1978, AD 1980, and AD 1985 while the five-element configuration shows spikes in concentration at AD 1978, AD 1981 and AD 1985.

FR225 3A shows very strong correlation between the five and eighteen-element LA-ICP-MS configurations for aluminum, in AD 1980-1986. Calcium and zinc for the same sample are more variable. Discrepancies in the concentration of either element for a given year reach quantities of several thousand ppm, and plot patterns are not similar. In FR77 6B, aluminum and calcium vary greatly, but zinc shows strong correlation between AD 1976 and AD 1984 (appendix 3.2, figure 3.45).

Analysis of FR7506 5B by the eighteen-element LA-ICP-MS configuration showed aluminum and calcium to be below detection limits (table 3.45). Concentrations of zinc measured by the same configuration are much lower than the highly variable concentrations measured by the five-element configuration. The same is true for calcium and zinc in FR77 2C, JFCK 2B, and STRCK 1A. Aluminum was below detection limits

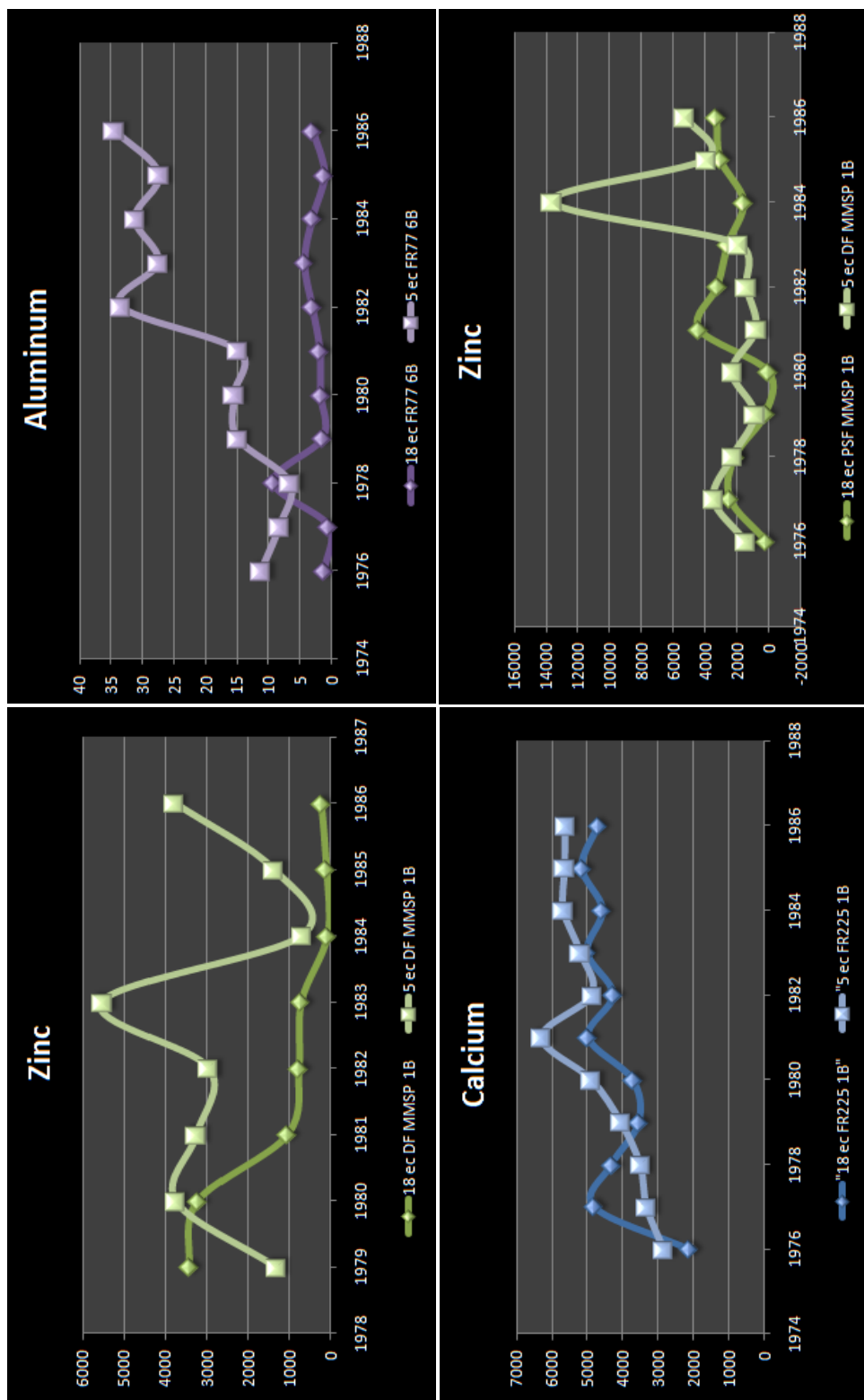


Figure 3.45T

The title of each graph indicates the element analyzed. The x-axis shows the year corresponding to a growth ring. Y-axis values represent concentration (ppm) of the element indicated by the title. Each graph shows chemical concentrations measured from the same sample by two different L.A.-ICP-MS configurations. All of figure 3.45 is available in appendix 3.2 (compact disc).

in all of these samples for analysis by the eighteen-element configuration (table 3.45).

Zinc in STRCK 1A showed more comparable concentrations than the other two samples.

Four core segments containing growth rings from AD 1795-1805 were analyzed by both LA-ICP-MS experiments (figure 3.45, sheet 3). FR225 5A is the only core segment of the four that shows fair correlation between the five and eighteen-element experiments. Zinc shows good correlation only after AD 1979. The remaining three core segments show higher elemental concentrations as measured by the five-element experiment.

Summary

A total of 49 core segments from 29 trees were analyzed using LA-ICP-MS. Of these, 29 core segments include annual growth rings for AD 1976- 1986 and 21 include annual growth rings for AD 1795-1805. Seven of the 49 core segments were sampled from one of two control sites located south of Mount Saint Helens (figure 1.0). Five of these core segments include annual growth rings from the twentieth century, and two include annual growth rings from AD 1795-1805. Of the 49 core segments analyzed by LA-ICP-MS analysis, seventeen show a change in the abundance of one or more elements that begins at AD 1980. Six additional cores show a change in the abundance of one or more elements that begins between AD 1981 and AD 1982. Ten of the core segments show a change in the abundance of one or more elements at AD 1800. Three core segments show a change in the abundance of one or more elements that begins between AD 1801 and AD 1802.

Thirteen core segments, including one from the control site east of Salem, Oregon, show changes in the abundance of potassium that begin on or after AD 1980. A total of eleven core-segments show a change in the abundance of calcium, six of which co-vary similarly to potassium. Eight core segments show a change in the concentration of rubidium, while seven show similar changes in the concentration of strontium on or after the same date. Seven core segments show a change in the abundance of zinc, and five core segments each show a change on or after the same date for titanium, copper, nickel and barium. Four core segments show an increase in the concentration of barium on or after AD 1800, and three show an increase in zinc on or after the same year. Aluminum, calcium, and zinc were analyzed in fourteen samples by more than one LA-ICP-MS configuration. There is a large discrepancy in concentration and the pattern of concentration variation in the majority of these samples. Only four of the fourteen core segments show similar quantities and patterns of elemental variation for both LA-ICP-MS configurations. Where discrepancies occur, the five-element experiment generally shows higher concentrations than the eighteen-element experiment. Quantitative statistics for core segments that were analyzed using the five-element configuration on December 14th, as well as those analyzed with the eighteen-element configuration, are discussed in the next section.

3.4 Statistical Analysis of LA-ICP-MS Data

The statistical significance of short-lived increases or decreases in elemental abundances of annual growth rings was evaluated by identification of mild or extreme outliers (appendix 3.3, tables 4.1- 4.38). Mild outliers are defined as more than 1.5 (iqr)

from the nearest quartile and extreme outliers are identified as more than 3 (iqr) from the nearest quartile. Recall from section 2.11 that “iqr” refers to the inter-quartile range of a population of data. For reasons discussed in section 2.11, each core segment was considered as an individual population for statistical analysis. In this case, the elemental concentrations of a single growth ring are compared only to the other growth ring from the same core segment. These data are presented by element in this section. Core segments including annual growth rings for AD 1976-1986 will be discussed first. Some of the core segments in this group also include data from AD 1974 and AD 1975. For aluminum, calcium and zinc, data from the five-element LA-ICP-MS configuration are displayed below data from the eighteen-element configuration on the same figure.

Aluminum

Aluminum (CE 1976-1986) was above detection limits for ten core segments on the eighteen-element configuration, and for ten core segments on the five-element configuration (appendix 3.3, table 4.1). FR77 6B and FR225 1B are the only two samples that had aluminum in concentrations above the detection limit for both LA-ICP-MS configurations. Of the 20 total analyses, seven core segments contain statistical outliers. All of these outliers are high outliers, greater than 1.5 (iqr) of the Al concentration in annual growth rings of the core segment.

BM 5B and FR225 5A (control) have high concentrations of aluminum in AD 1977. The value of the outlier for BM 5B is 10.6 ppm in AD 1977. The concentration of aluminum nearly doubles from 3 ppm in AD 1979 to 6 ppm in AD 1980 and 1981 (table 4.1). Because the concentration of aluminum is so high in AD 1977, the concentration in

AD 1980 is not considered an outlier. However, it should be noted that the increase in elemental concentration does coincide with an eruption year. The outlier value in FR225 5A is 21 ppm, which is approximately double the average concentration for a growth ring in the core segment. The only abrupt increase in concentration of aluminum occurs in the year of the outlier.

JFCK 4A and FR77 6B both have outlier concentrations of aluminum in AD 1978. The values of the outlier in these cores are 11 ppm and 9 ppm, respectively and both are much higher than the average for the core segment (<3 ppm in both cases). JFCK 4A jumps from 1 ppm Al in AD 1980 to 3.7 ppm Al in AD 1981 (appendix 3.3, table 4.1).

FR225 1B shows an increase in the concentration of aluminum from 27 ppm in AD 1980 to 63 ppm in AD 1981 (table 4.1). The concentration of aluminum in AD 1981 is a statistical outlier for the core segment. It should be noted that, although this abrupt increase in aluminum coincides with an eruption year, the tree that provided this core segment is located more than 200 km south of Mount Saint Helens, at the control site east of Salem, Oregon (figure 2.1).

FR77 2C and STRCK 1A show aluminum concentrations that are statistical outliers in AD 1985 and AD 1986, respectively. Although the concentrations of aluminum in earlier years are not considered to be statistical outliers, an abrupt change occurs in each of these samples (table 4.1). In FR77 2C, the concentration of aluminum more than doubles from AD 1980 to AD 1981. In STRCK 1A, a similar increase in aluminum occurs one year later. In both cases, the aluminum concentrations remain high after these abrupt increases, so the abrupt changes do not form statistical outliers.

Ten core segments analyzed by LA-ICP-MS had concentrations of aluminum that were above detection limits for AD 1795-1805 (appendix 3.3, table 4.2). Four of these core segments were analyzed using the five-element configuration. Two core segments, both of which were analyzed using the eighteen-element configuration, had aluminum present in concentrations that are statistical outliers (table 4.2). In both cases, the high outliers occur in AD 1800. In JFCK 4A, the second highest concentration of aluminum occurs in AD 1801.

Barium

Twenty-nine core segments containing annual growth rings from AD 1976-1986 have detectable concentrations of barium (appendix 3.3, table 4.3). Twelve of these core segments contain statistical outliers, eleven of which are high outliers, and two of which are low outliers. BM 5B has both a high and a low outlier. All of the core segments containing outliers have outliers that occur between AD 1977 and AD 1979. Two core segments also have a later outlier, one in AD 1980, and one in AD 1984. The concentration of barium in all samples tends to be highest in the years prior to AD 1980. On and after AD 1980, concentrations of barium generally do not fluctuate to a large extent.

Twenty core segments containing annual growth rings from AD 1795-1805 have detectable concentrations of barium (appendix 3.3, table 4.4). Eight of these core segments had annual growth rings with concentrations of barium that are considered statistical outliers. The outliers in this group occur in seven of the ten years included in each core segment. Outliers most commonly occur in AD 1798, as five of the eight cores

have a high statistical outlier that occurs in this year. Most of the eight cores have multiple outliers in any combination of years including AD 1796, 1798, 1799, 1800, 1801, 1803, and 1805.

Boron

Fourteen core segments including annual growth rings from AD 1976-1986 contain boron in detectable concentrations (appendix 3.3, table 4.5). No core segments from this group have concentrations of boron that are statistical outliers. The concentration of this element does not vary greatly between annual growth rings in any sample. The same is true of nine core segments including annual growth rings from AD 1795-1805 (appendix 3.3, table 4.6).

Cadmium

Cadmium was below detection for the majority of annual growth rings analyzed. No core segment has cadmium concentrations that are above detection limits in more than six annual growth rings (appendix 3.3, tables 4.7 and 4.8). Therefore, no statistical data are available for this element.

Calcium

Thirty-eight core-segment analyses show detectable concentrations of calcium for annual growth rings from AD 1976-1986 (appendix 3.3, table 4.9). Twenty-eight of these analyses were performed using the eighteen-element LA-ICP-MS configuration, and ten of these analyses were performed using the five-element configuration. Ten core

segments have concentrations of calcium in one or more annual growth rings that are high statistical outliers (table 4.9). Two of these core segments were analyzed using the five-element configuration, and eight were analyzed using the eighteen-element configuration. No samples have outliers that were measured by both configurations.

Outliers for this group occur in several different years, including AD 1975, AD 1977, AD 1979, and AD 1980-1984. Although they are not statistically significant, the lowest concentrations of calcium in six of these ten cores occur between AD 1980 and AD 1981. The same is true of eight of the cores that do not have statistical outliers. In the case of FR77 2C, in which the highest concentration of calcium occurs as an outlier in AD 1980, the lowest concentrations occur in the following two years, with calcium dropping to below detection limits in AD 1982. IN BM 1A, the statistical outlier occurs in AD 1979.

Seventeen core segment analyses have detectable calcium concentrations for annual growth rings from AD 1795-1805 (appendix 3.3, table 4.10). Four core segments in this group were analyzed by both the five-element and eighteen-element LA-ICP-MS configurations. Only one core segment contains a high statistical outlier (table 4.10).

Copper

Seventeen core segments containing annual growth rings from AD 1976-1986 contain detectable concentrations of copper (appendix 3.3, table 4.11). Nine of these core segments contain copper in concentrations that are considered to be statistical outliers (table 4.11). For three core segments, the high statistical outlier occurs in AD 1981, and for three core segments it occurs in AD 1986. A significant increase in the concentration of copper occurs in AD 1980 or AD 1981 for six of the core segments that do not have

statistical outliers in this group. With the exception of PSF MMSP, the increase in copper concentration during this time period is more commonly present in core segments from Jefferson Creek and forest road 77. Statistical outliers also occur in AD 1976-1977, AD 1979 and AD 1984.

One of five core segments containing detectable copper concentrations from AD 1795-1805 contains statistical outliers. These outliers occur in AD 1800 and AD 1801 (appendix 3.3, table 4.12.) The concentration of copper in FR2253A jumps from 13 ppm in 1799 to 176 ppm in AD 1800. This core segment was taken from a tree nearly 200 km south of Mount Saint Helens at the control site east of Salem, Oregon.

Iron

No statistical data are available for iron due to a lack of detectable concentrations in samples from AD 1976-1986 (appendix 3.3, table 4.13). BM 5B, including annual growth rings from AD 1795-1805, has detectable concentrations of iron, but no statistical outliers (appendix 3.3, table 4.14).

Lanthanum

Although lanthanum is present in detectable concentrations for several annual growth rings that were analyzed from AD 1976-1986, the spread is so limited that outliers of statistical significance are not likely to be identified (appendix 3.3, table 4.15). Two core segments from AD 1795-1805 have high statistical outliers in AD 1800 and AD 1801 (appendix 3.3, table 4.16).

Lead

Thirteen core segments from AD 1976-1986 have lead in detectable concentrations for at least some of the annual growth rings analyzed. None of the growth rings in this group contain lead in concentrations that are considered to be statistical outliers (appendix 3.3, table 4.17). One of five core segments containing growth rings from AD 1795-1805 has a high statistical outlier that occurs in AD 1800 (appendix 3.3, table 4.18). FR225 3A is the same core segment that has high concentrations of lanthanum, copper, calcium, and barium in the same year.

Manganese

Twenty-eight core segments including annual growth rings from AD 1976-1986 have detectable quantities of manganese (appendix 3.3, table 4.19). Eight of these core segments have concentrations that are statistical outliers, seven of which occur between AD 1976 and AD 1979 (table 4.19). PSF MMSP 1B has an outlier in AD 1984, and high concentrations of manganese in AD 1981-1982 and AD 1984-1986. In BM 1A, the statistical outlier occurs in AD 1979. Core segments that have outliers typically do not have a large spread among the nine other years in the population.

Two of eighteen core segments including annual growth rings from AD 1795-CE 1805 have concentrations of manganese that are statistically high outliers (appendix 3.3, table 4.20). An outlier occurs in AD 1797 in BM 1A and in AD 1800 in JFCK 4A. No pattern of concentration variation in manganese occurs for the core segments in this group.

Nickel

Twenty-seven core segments containing annual growth rings for AD 1976-1986 have detectable concentrations of nickel (appendix 3.3, table 4.21). Ten of these core segments contain concentrations of nickel that are statistical outliers (table 4.21). In four core segments, the outlier occurs between AD 1976 and AD 1979. In five core segments, the outlier occurs between AD 1980 and AD 1983. Two core segments have outliers in AD 1985 or AD 1986. These core segments have the lowest average concentration of nickel in the group, and the outlier years have concentrations of nickel that are < 1 ppm greater than the previous year. No statistical outliers occur in the sixteen core segments containing annual growth rings from AD 1795-1805 (appendix 3.3, table 4.22).

Phosphorus

Forty core-segment analyses recorded counts per sweep data for samples containing annual growth rings from AD 1976-1986 (appendix 3.3, table 4.23). This includes data for both the five-element configuration and the eighteen-element configuration. Although a calibration curve for phosphorus could not be produced on any day of LA-ICP-MS analysis, and counts recorded for samples were typically at or near background levels, the data collected may be of some use. In some cases, in which background levels of an element are higher than in the sample, a high enough flow rate from the nebulizer may move material through the cones fast enough to negate the high background. Fifteen of the 40 core-segment analyses show counts for phosphorus that are statistical outliers (table 4.23). In seven of these cores, the outlier occurs on or after AD 1980, and in BM 1A, the outlier occurs in AD 1979. In chapter 4, an error in the raster

path will be discussed for BM 1A. In this sample, the data collection that was labeled AD 1979 was actually taken from a raster path on the AD 1980 annual growth ring.

Considering this error, more than half of the statistical outliers identified for phosphorus occur on or after AD 1980.

Counts per sweep for phosphorus were recorded for 25 core-segment analyses that include annual growth rings from AD 1795-1805 (appendix 3.3, table 4.24). Only four core segments from this group contain phosphorus in concentrations in annual growth rings that are statistical outliers. In all cases, the outlier occurs in either AD 1796 or AD 1797.

Potassium

Thirty core segments including annual growth rings from AD 1976-1986 have detectable concentrations of potassium (appendix 3.3, table 4.25). Seven of these core segments have concentrations of potassium in one or more annual growth rings that are statistical outliers. In BM 1A and BM 5B, an outlier occurs at AD 1979 and AD 1980, respectively. In BM 5B, the outlier in AD 1980 is a statistical low. In JFCK 6A and FR7506 1A, high outliers occur in AD 1985 and AD 1984, respectively. Three of the seven cores have outliers in AD 1977 and one has the outlier in AD 1975. A large spread in potassium concentration occurs between trees within individual sites. For example, the average concentration in FR7506 5B is more than an order of magnitude less than that for FR7506 1A.

Twenty core segments containing annual growth rings from AD 1795-1805 have detectable concentrations of potassium (appendix 3.3, table 4.26). Eight of these core

segments have concentrations in one or more growth rings that are statistical outliers. Six of the eight core segments have outliers in AD 1796, and two have an outlier in AD 1797 or AD 1798. BM 8B has a low statistical outlier that occurs in AD 1803, in addition to a high outlier in AD 1798. Potassium concentrations do not typically vary by a large amount on or around eruption years in this group. FR225 3A is the exception, jumping from 2022 ppm in AD 1799 to 7098 ppm in AD 1800. The concentration in AD 1800 is not a statistical outlier in this core segment.

Rubidium

Twenty-nine core segments including annual growth rings from AD 1976-1986 have detectable concentrations of rubidium (appendix 3.3, table 4.27). Ten of these core segments contain concentrations of rubidium that are statistical outliers. In half of the core segments that have statistical outliers, the outlier occurs in AD 1976 or AD 1977. In JFCK 4A, the outlier occurs in AD 1981, and the outlier occurs between AD 1984 and AD 1986 in four other core segments. Rubidium concentrations are typically low in this group, on the order of <1 ppm. PSF MMSP 1B and three trees from FR 225 are the exceptions, averaging 25 ppm and 3 ppm per annual growth ring, respectively.

Sixteen core segments from AD 1795-CE1805 have detectable concentrations of rubidium (appendix 3.3, table 4.28). Concentrations of rubidium are also low for this group, typically averaging <1 ppm in an annual growth ring. FR225 3A is the exception, containing two growth rings with concentrations >4 ppm rubidium. Five cores have concentrations of rubidium in one or more annual growth rings that are statistical outliers

(table 4.28). Three of the five cores have high statistical outliers that occur between AD 1800 and AD 1802. In the other two cores, the outlier occurs in AD 1796 or AD 1798.

Sodium

Thirty core segments from AD 1976-1986 have sodium in detectable concentrations (appendix 3.3, table 4.29). Concentrations of sodium are typically high in this group, ranging from several hundred to several thousand ppm in an annual growth ring. Fourteen of these core segments contain concentrations of sodium that are statistical outliers. The majority of these outliers are low, and only two of the fourteen core segments, both from Jefferson Creek, contain high outliers. FR77 7A contains both high and low statistical outliers, occurring in AD 1983 and AD 1977, respectively. BM 2B has a low statistical outlier in AD 1982. BM 1A has a low statistical outlier that occurs in AD 1979. All other cores have outliers that occur between AD 1975 and AD 1978.

Only three of 20 core segments from AD 1795-1805 have concentrations of sodium that are statistical outliers (appendix 3.3, table 4.30). All are low statistical outliers, and all occur in AD 1796 or AD 1797 (appendix, table).

Strontium

Twenty-three core segments from AD 1976-1986 contain detectable concentrations of strontium (appendix 3.3, table 4.31). Concentration within this group range from an average of <1 ppm to tens of ppm per annual growth ring in a core segment. Concentrations in growth rings from a single core segment typically vary by large amounts, and no statistical outliers were identified for this group.

Fourteen core segments from AD 1795-1805 contain detectable concentrations of strontium. Two cores, BM 5B and STRCK 1A, contain statistically high concentrations of strontium in AD 1801 and AD 1802, respectively (appendix 3.3, table 4.32).

Sulfur

Counts per sweep data were recorded for forty core-segment analyses, ten of which were collected with the five-element LA-ICP-MS configuration (appendix 3.3, table 4.33). Nineteen core-segment analyses show counts in one or more annual growth rings that are statistical outliers. Eighteen of the nineteen core-segment analyses have a statistical outlier that occurs between AD 1975 and AD 1978. Only PSF MMSP 1B has statistically high counts for sulfur that occur in AD 1980 (table 4.33).

Eleven of 25 core segments from AD 1795-1805 contain counts for sulfur that are statistical outliers (appendix 3.3, table 4.34). In this group, ten core segments have high statistical outliers that occur between AD 1795 and AD 1797. Only FR225 3A has an outlier that occurs in AD 1800. This tree is from the control site east of Salem, Oregon, and commonly has high statistical outliers for several elements in the same year.

Titanium

Twenty-nine core segments including annual growth rings from AD 1976-1986 have detectable concentrations of titanium (appendix 3.3, table 4.35). Concentrations for this group typically average <20 ppm titanium for trees located east and northeast of Mount Saint Helens. Core segments from trees that were taken from the two locations south of Mount Saint Helens average on the order of several hundred ppm titanium. All

analyses for this group were completed using the eighteen-element LA-ICP-MS configuration. Nine core segments contain concentrations of titanium in one or more annual growth rings that are statistical outliers (table 4.35). The majority of the core segments have outliers that occur between AD 1976 and AD 1978. BM 1A has three statistical outliers, in AD 1979, AD 1983 and AD 1984. The outlier that occurs in AD 1983 is a high statistical outlier, and the other two are low. DF MMSP 1B also has a high statistical outlier that occurs in AD 1983.

Seven of eighteen core segments containing growth rings from AD 1795-1805 have titanium in concentrations that are statistical outliers (appendix 3.3, table 4.36). Concentrations for the group of 18 core segments typically average >20 ppm titanium. Similar to core segments from AD 1976-1986, those taken from trees located south of the cone average concentrations in the range of several hundreds of ppm titanium. FR225 3A has a high statistical outlier in AD 1800, and two of the three core segments from Bear Meadow have a high statistical outlier in AD 1805. JFCK 2B also has a high statistical outlier in AD 1805. Outliers in the remaining three core segments occur between AD 1796 and AD 1799.

Zinc

Thirty-eight core segment analyses show concentrations of zinc that are above detection limits (appendix 3.3, table 4.37). Analyses for ten core segments were completed using the five-element LA-ICP-MS configuration, and 28 analyses were conducted on core segments using the eighteen-element LA-ICP-MS configuration. Eighteen core segment analyses have concentrations of zinc that are statistical outliers.

Of these, seven were completed using the five-element configuration. FR77 6B recorded concentrations of zinc that are statistical outliers on both the five and the eighteen-element LA-ICP-MS configurations. The five-element configuration recorded a high statistical outlier for FR77 6B in AD 1986, with the second highest concentration occurring in AD 1984. The eighteen-element configuration recorded the high statistical outlier in AD 1984, with the second highest concentration occurring in AD 1986. The patterns are similar for these two analyses, but the quantitative values for concentration of zinc differ by an order of magnitude (appendix 3.3, table 4.37). BM 5B has high statistical outliers in AD 1985 and AD 1986, while FR77 2C has a high statistical outlier in AD 1980. FR7506 5B has a high statistical outlier in AD 1979 and AD 1981. JFCK 7A and STRCK 1A have high statistical outliers in AD 1984 and AD 1986, respectively. In half of the core segments that have statistical outliers for zinc, the outlier occurs between AD 1976 and AD 1978.

Twenty core-segment analyses including annual growth rings from AD 1795-1805 show detectable concentrations of zinc (appendix 3.3, table 4.38). Of these, eleven have concentrations of zinc that are statistical outliers (table 4.38). FR77 6B records a high statistical outlier in AD 1805 as measured with the five-element LA-ICP-MS configuration. No core segments in this group show outliers recorded by both configurations. JFCK 1C also shows a high statistical outlier in AD 1805, and BM 7A has outliers occurring in AD 1802 and AD 1804. FR7506 1A shows a high statistical outlier in AD 1800. FR225 5A and FR225 3A show high concentrations of zinc in AD 1800-1802.

Statistics by location

Statistical outliers were also determined using samples from each field site as a population, rather than samples from each core segment. In this case, the elemental concentrations of annual growth rings are compared to those of all of the core segments taken from a particular field site. All samples discussed below were analyzed by the eighteen-element LA-ICP-MS configuration.

Jefferson Creek

Eight core segments including annual growth rings from AD 1976-1986 and six including annual growth rings from AD 1795-1805 were analyzed by LA-ICP-MS from Jefferson Creek (figures 2.0 and 2.3). Comparing all annual growth rings in the area allows for the identification of statistical outliers in a larger population. In some cases, an entire core segment is identified as having elemental concentrations that are high or low statistical outliers. An advantage to this type of comparison is that trees in localized areas that may have experienced similar environmental change due to eruption can be observed as a group. However, biological differences in individual trees may lead them to vary in how they react to the same macro-environmental change.

No statistical outliers for boron, sodium, or potassium occur and no statistical data for aluminum, iron, or cadmium are available at this field site (appendix 3.3, table 5.1). The lack of statistical data is due to a majority of growth rings showing elemental concentrations that are below the limits of detection.

Of the core segments containing annual growth rings from AD 1976-1986, JFCK 1C and JFCK 9B show statistical outliers in the concentration of manganese and nickel,

respectively, for all years (table 5.1). JFCK 3A has high concentrations of nickel for three years between AD 1983 and AD 1986. JFCK 9B had manganese in concentrations that are high statistical outliers for six of the ten years in the core segment. JFCK 9B also has elemental concentrations that are statistical outliers on or after AD 1980 for barium and titanium. JFCK 4A has concentrations of calcium and zinc that are statistical outliers on or after AD 1980. In AD 1980, JFCK 6A has a high statistical outlier for the concentration of rubidium. Statistical outliers for concentrations of a total of nine elements are identified before AD 1980 for several core segments from this area.

Of the core segments including annual growth rings from AD 1795-1805, JFCK 9B has the highest number of statistical outliers (table 5.1). The entire core segment has high concentrations of zinc, nickel, and titanium that are statistical outliers within the population of growth rings from Jefferson Creek. JFCK 9B also has outliers that occur in AD 1795 and AD 1802 for copper. No correlation of a high density of outliers with either AD 1980 or AD 1800 is found for any element.

Forest Road 77

Eight core segments including annual growth rings from AD 1976-1986 and three core segments including annual growth rings from AD 1795-1805 were analyzed by LA-ICP-MS from the field site along forest road 77 (figures 2.0 and 2.5). No statistical outliers for boron, sodium, or potassium are apparent in this group, and no statistical data are available for iron, cadmium, or lead (appendix 3.3, table 5.2).

FR77 8B has statistically high concentrations of aluminum at AD 1976 and AD 1978, and high concentrations of titanium from AD 1976-1978 and AD 1984. The entire

core segment from AD 1976-1986 contains statistical outliers for concentrations of nickel and copper, and most of the core segment has statistically high concentrations of rubidium. The same sample has statistical outliers for nickel concentrations from AD 1795-1805.

FR77 2C is the only core segment that has statistical outliers for calcium concentrations (table 5.2). These outliers are high, and occur in AD 1976 and AD 1980. FR77 2C also has a high statistical concentration of zinc at AD 1976, and although not an outlier, the second highest concentration of zinc occurs in AD 1980.

FR77 6B has statistically high concentrations of manganese in AD 1983-84, and a high concentration of lanthanum in AD 1985. FR77 7A has concentrations of rubidium that are statistical outliers for AD 1976-1985 and for strontium in AD 1980-1982. The same sample has a statistically high concentration of zinc at AD 1801. A large number of statistical outliers that are identified for this group occur before AD 1980 or AD 1800 (table 5.2).

Forest Road 7506

Five core segments containing growth rings from AD 1976-1986 and three core segments containing growth rings from AD 1795-1805 were analyzed by LA-ICP-MS from the field site along forest road 7506 (figures 2.0 and 2.6). No statistical outliers for potassium, titanium, or manganese occur in this group and only one statistical outlier for sodium is apparent (appendix 3.3, table 5.3). No statistical data are available for boron, aluminum, iron, cadmium, or lead from this field site. The majority of outliers identified occur before AD 1980 or AD 1800. Only FR7506 4A and FR7506 1A have outliers

occurring on or after eruption years. FR7506 4A has statistically high concentrations of copper in AD 1797, AD 1799, and AD 1801-1802. FR7506 1A has statistically high concentrations of rubidium and strontium that occur in AD 1984.

Bear Meadow

Four core segments containing annual growth rings from AD 1976-1986 and five core segments containing growth rings from AD 1795-1805 were analyzed by LA-ICP-MS from Bear Meadow (figures 2.0 and 2.4). No statistical outlier for sodium, titanium, or copper occurs from this group and no statistical data are available for iron, cadmium, lanthanum, or lead (appendix 3.3, table 5.4).

BM 5B shows statistical outliers for boron, aluminum, potassium, calcium, rubidium, strontium, and barium concentrations that occur between AD 1976 and AD 1977 (table 5.4). The same sample has statistically high concentrations of zinc from AD 1795-1801. BM 7A has high concentrations of zinc that occur in AD 1802 and AD 1804. High concentrations of manganese occur in AD 1979 for BM 1A. The majority of outliers identified from this field site occur in the first four annual growth rings of each core segment analyzed, prior to AD 1980 or AD 1800.

Straight Creek

Only two core segments were analyzed from Straight Creek (figure 2.0). One includes growth rings from AD 1976-1986, and the other includes growth rings from AD 1795-1805. These core segments come from the same tree, STRCK 1A. No statistical data are available for boron, aluminum, iron, cadmium, lanthanum, or lead from this field

site (appendix 3.3, table 5.5). Statistical outliers are identified for only three elements; sodium, manganese, and copper. The outliers for sodium occur in the first year analyzed for each core segment, in AD 1975 and AD 1795. The concentration of manganese is statistically high in AD 1975 and AD 1976. The concentration of copper is high in AD 1975, and AD 1803-1805.

Control Trees

Five core segments including annual growth rings from AD 1976-1986 and two core segments including annual growth rings from AD 1795-1805 were analyzed by LA-ICP-MS from one of two control sites; forest road 225 or Marble Mountain Snow Park (figures 2.0, 2.1, and 2.7). All measured elements were above detection limits in this group, and at least one statistical outlier was identified for all but strontium and boron (appendix 3.3, table 5.6). Most outliers occur in the first four growth rings analyzed, prior to AD 1980. Only PSF MMSP 1B has high concentrations of manganese, copper, zinc, rubidium, and lanthanum that occur on or after AD 1980 in this sample. FR225 3A is the other core segment that has several outliers. This sample shows a spike in most elements in AD 1800, or shortly thereafter. This spike in concentration is commonly large enough to be a statistical outlier.

3.5 Solution ICP-MS

Fifty-two annual growth rings from seven of the core segments that were analyzed by LA-ICP-MS were also analyzed by solution ICP-MS in order to test the reproducibility of the laser-ablation analyses (section 2.9). These core segments come

from six different sample locations. An eighteen-element configuration similar to that used for the majority of LA-ICP-MS analyses was used for solution ICP-MS analyses. In addition to the seven core segments, a piece of each of the standard wafers used for calibration of LA-ICP-MS data was also analyzed by solution ICP-MS (figure 5.3). Concentrations were obtained from counts per sweep in the same manner as for LA-ICP-MS (section 2.8). Because fewer annual growth rings were analyzed per core segment, statistical data are not available for four of the individual core segments in this group.

Calibration Curves

Data collection for fifty-two growth rings was completed over the course of two nonconsecutive days. Twenty-two samples were analyzed on April 27, 2010 (appendix 3.4, table 5.1) and thirty samples were analyzed on May 4, 2010, along with standard wafers A, C, E, and G (table 5.2). Suitable calibration curves were produced for all elements except boron and sulfur on both days of data collection (appendix 3.4, figures 5.1 and 5.2). Calibration of phosphorus did not present a problem using solution standards. Instrument drift was more consistent for solution ICP-MS than for LA-ICP-MS on both days of data collection. On both days of data collection, instrument drift was normal, with sensitivity decreasing over time (figures 5.1 and 5.2). In order to account for instrument drift, multiple lines of best fit were assigned to each calibration curve. The line of best fit corresponding to the analysis of standard solutions that was performed closest in time to a given sample was used to calculate concentration data (section 2.9 and figure 5.1, 5.2 and table 5.1, 5.2).

Statistical Outliers

As mentioned earlier, the smaller number of annual growth rings analyzed by solution ICP-MS per core segment restricts the availability of statistical data that consider the core segment to be a population. Statistical data are available for three of the seven core segments: PSF MMSP 1B, FR77 2C and FR7506 5B (appendix 3.4, table 5.3). The calculation of elemental concentration in each wood sample, as opposed to the measured elemental concentration of the sample solution, is discussed later in this section. Statistical data presented here are for the elemental concentration calculated for the wood separate.

FR7506 5B has statistically high concentrations of sodium in AD 1980 and a high concentration of aluminum in AD 1983 (table 5.3). A high statistical outlier for potassium in AD 1980 occurs in the same sample. Although there is no statistical outlier, FR77 2C shows an abrupt increase in potassium concentration in AD 1980 that is sustained through AD 1986. The same is true of calcium and zinc in FR77 2C.

The highest Al concentrations measured by solution ICP-MS occur in AD 1980 and AD 1982-1983 in PSF MMSP 1B, but they are not statistical outliers. The highest concentrations measured by LA-ICP-MS in this sample occurred in the first two annual growth rings analyzed. Solution ICP-MS shows little variation in the concentration of aluminum in the years prior to AD 1980 in this sample. There is a high statistical outlier for phosphorus in the first collection year for PSF MMSP 1B. Copper in this sample has a high statistical outlier in AD 1980 that is sudden and short-lived. A similar increase in copper occurs in AD 1980 for FR77 2C and FR7506 5B, but the high concentrations in these years are not statistical outliers.

Sample solutions versus sample solids

Solution ICP-MS analysis measures the concentration of selected elements in the sample solution. Recall from section 2.9 that wood separates composed of the earlywood of annual growth rings were dissolved in acid and diluted prior to ICP-MS analysis. The elemental concentrations measured by this type of analysis are the concentrations of elements in the diluted sample solution. In order to calculate the concentrations of elements in the actual wood separates, we must mathematically reverse sample dilution (appendix 3.4, tables 5.4 and 5.5). This can be achieved through application of the following formula:

$$x = (5c / .75) / W$$

where x = elemental concentration (measured) in wood separate (ppm)

c = diluted elemental concentration (ppm)

W = weight of the wood separate (g)

The number (5) in this formula represents the volume of the total sample solution, in this case, 5 ml. Wood separates were digested in 1 ml of HNO_3 (section 2.9). After several stages of preparation, 0.75 ml of the solution containing the dissolved wood separate was added to 4.25 ml of spiked, doubly distilled water (section 2.9). The value of 0.75 in the above equation represents the fraction of dissolved wood separate that was diluted and analyzed.

Although samples were diluted with doubly distilled water, analysis of blank solution standards showed a significant background concentration of sodium and potassium (figure 5.1, 5.2). These elements were typically more abundant in samples than in standard blanks (figure 5.1, 5.2, and table 5.1, 5.2), so the measured concentrations of

these elements are therefore sufficient for the determination of variation in elemental concentration between growth rings. However, the quantities measured for Na and K are inaccurately high due to the concentration of these elements in the water used to dilute the samples. The same water was used to create the standard solutions, producing high background levels of K and Na, but the background could not be factored out because variation in Na and K did not exceed the margin of error associated with these counts.

3.6 Isotopes

Isotope data for the five trees analyzed are available in appendix 3.5 (figure 4.0, table 2.5). Five consecutive growth rings were analyzed in JFCK 2B, FR7506 5B, FR77 2C, and BM 1A. Two core segments, including growth rings from AD 1798- AD 1803 and AD 1978-CE 1983 from JFCK 2B were analyzed. In figure 4.0 (appendix 3.5), $\delta^{13}\text{C}$ values are shown on the x-axis, and the growth-ring year is shown on the y-axis. Increasingly negative $\delta^{13}\text{C}$ values correspond to a depletion of ^{13}C relative to ^{12}C . As discussed in section 1.7, if stomatal closure were to temporarily reduce photosynthesis in a tree, we would expect to see a short-lived enrichment of ^{13}C , or a less-negative $\delta^{13}\text{C}$ value in figure 4.0. A relative enrichment of ^{13}C can be seen in JFCK 2B at AD 1982, and a relative depletion of ^{13}C can be seen in BM 1A at AD 1980. Results for the other three core segments are highly variable. The number of isotopic analyses conducted was limited by funding. The span of five years represented by these data is not enough to establish a “normal” isotopic ratio. Consequently, the variation shown in figure 4.0 (appendix 3.5) cannot be attributed to a cause. More data are required before any conclusion can be drawn regarding carbon isotopic ratios in these trees.

CHAPTER 4: DISCUSSION

Chapter Summary

Data regarding the chemistry of 52 tree cores obtained through LA-ICP-MS, acid digestion ICP-MS, and carbon isotopic analyses were presented in the previous chapter. These data were obtained with the intention of observing chemical evidence of volcanic eruption in the xylem tissues produced in the years spanning the two largest volcanic eruptions of Mount Saint Helens of the previous two centuries. Recognition of a chemical response to volcanic eruption in tree rings requires that some measurable change in the chemical composition of wood cellulose, initiated by the volcanic eruption, be isolated and preserved. Simply, a chemical signal must exist in a limited number of growth rings and it must be measurable. In section 4.1, the limitations of LA-ICP-MS as applied to natural wood are considered in order to evaluate the likelihood that the data accurately represent the chemistry of the core segments analyzed. There were anticipated complications regarding the variable density of xylem tissue in trees, as discussed in section 2.5. These concerns are revisited and the possible effects of density variation on perceived elemental concentrations are discussed along with methods for sample preparation and ICP-MS instrument parameters that may improve data quality (section 4.1). The shortcomings of calibration methods used in this study are discussed in the last part of this section along with a likely explanation for the inability to calibrate for sulfur.

In section 4.2, chemical concentrations of aluminum, calcium, and zinc measured by the eighteen-element ICP-MS configuration are compared to concentrations of the same three elements obtained using the five-element ICP-MS configuration in the same core segments. This comparison is discussed as a means of determining the reliability of

LA-ICP-MS analysis of the tree cores considered in this study. The discrepancies in elemental concentration measured with each of the two experiments suggest that concentrations are not quantitatively accurate. However, similar trends produced by both data sets suggest that the relative concentration of elements indicated by LA-ICP-MS analysis may reflect true changes in concentration between growth rings.

Data presented in chapter 3 demonstrated a lack of strong chemical correlation between the eruption of Mount Saint Helens and the composition of xylem tissue produced in the decade spanning the time of the eruption. This lack of chemical correlation is either the result of inaccurate analysis, or a true representation of trees that were chemically unaltered by the volcanic eruption. Possible reasons for the lack of chemical response to the eruption are discussed in section 4.3 with regard to sample site and species selection.

Similar changes in the abundances of calcium, zinc and sodium occur at AD 1980 in four core segments, one of which was taken from the Pacific Silver fir. In section 4.4, these changes in elemental abundance are discussed as possible responses to volcanic eruption.

Suggestions to improve the quality of data or the process by which samples are prepared are discussed throughout chapter four. Additional suggestions to improve the overall experimental design and considerations for future studies are made in chapter five.

4.1 LA-ICP-MS Analysis- Limitations

Elemental concentrations have been shown to vary throughout a growth ring, both vertically and laterally (Pearson et al., 2005; Hagemeyer et al., 1993; McLaughlin et al., 1987). Consequently, a larger sample volume should be more representative of tree-ring chemistry and there may be some benefit to considering core segments that are taken from various heights along the stem. However, unless an entire growth ring is subject to chemical analysis, the issue of chemical heterogeneity cannot be resolved. It is also unlikely that any significant increase in sample volume could be accomplished with the use of an increment borer. It should be emphasized that this chemical heterogeneity is one that is inherent to a tree ring. It does not refer to a perceived variation in chemical composition that is the result of inconsistent analytical techniques. Another type of apparent variation is, however, a concern regarding the interpretation of data collected in this study, and will be a topic of discussion for the remainder of section 4.1.

Calibration Standards

Accurate calibration techniques for analysis of natural wood by ICP-MS are not established when laser ablation is the method of sample introduction to the ICP. As discussed in section 2.5, the physical heterogeneity of tree cores can be problematic for laser ablation, and should be considered in the design of protocol for sample preparation and instrument settings. The calibration technique used in this study involved the manufacture and periodic analysis of cellulose standard wafers (section 2.6). Standard wafers were an appropriate choice for calibration of the LA-ICP-MS given that

commercial standards are not currently available for xylem tissue. The manufacture of standard wafers allowed for all of the eighteen elements of interest to be included in the calibration process, in quantities that were expected to be comparable to those measured in sampled tree cores. Analysis of core segments revealed that the anticipated concentration of most of the elements considered was much higher than the actual measured concentrations. As a result, the calibration curves that were produced were accurate reflections of the various concentrations in the standard wafers, but were not necessarily a suitable reference for the lesser elemental concentrations of the core segments. More precise calibration curves could be made with standard wafers of more dilute chemical concentration and should be used in future studies and future interpretation of data from this study.

The physical homogeneity of the standard wafers also presents a problem for calibration (section 2.6). The pressing of doped cellulose powder produced perfectly flat, chemically and physically homogenous wafers. Although the chemistry of these wafers is controlled and ideally similar to that of the tree-core segments, the physical character is dissimilar. The consistent density of the wafers allows for a similar volume of ablated material to be collected into the ICP at every point along the ablation path. The lack of pore space in the standard wafers compared to the extremely porous nature of xylem tissue suggests that even if chemical concentrations are similar between the two, the apparent concentrations for a given ablation depth, intensity, and sweep time will be greater for the standard wafer. This is due to the fact that more material will be introduced to the ICP, resulting in a higher number of counts per sweep for any given

element. Until another method for calibration of xylem tissue becomes available, this discrepancy in apparent concentration should be noted.

Solution ICP-MS analysis of the standard wafers produced in this study produced accurately measured concentrations for Ti, Mn, Ni, Cu, Rb, Sr, Cd, Ba, La, Pb, P, and Al (figure 4.1, appendix 3.4). Na, K, Ca, Fe, and Zn were not accurately quantified. These elements likely overwhelmed the multiplier, causing the false report of 0 ppm concentration. Sulfur was also not accurately measured. This was likely the result of contamination within the instrument and will be discussed later in this section.

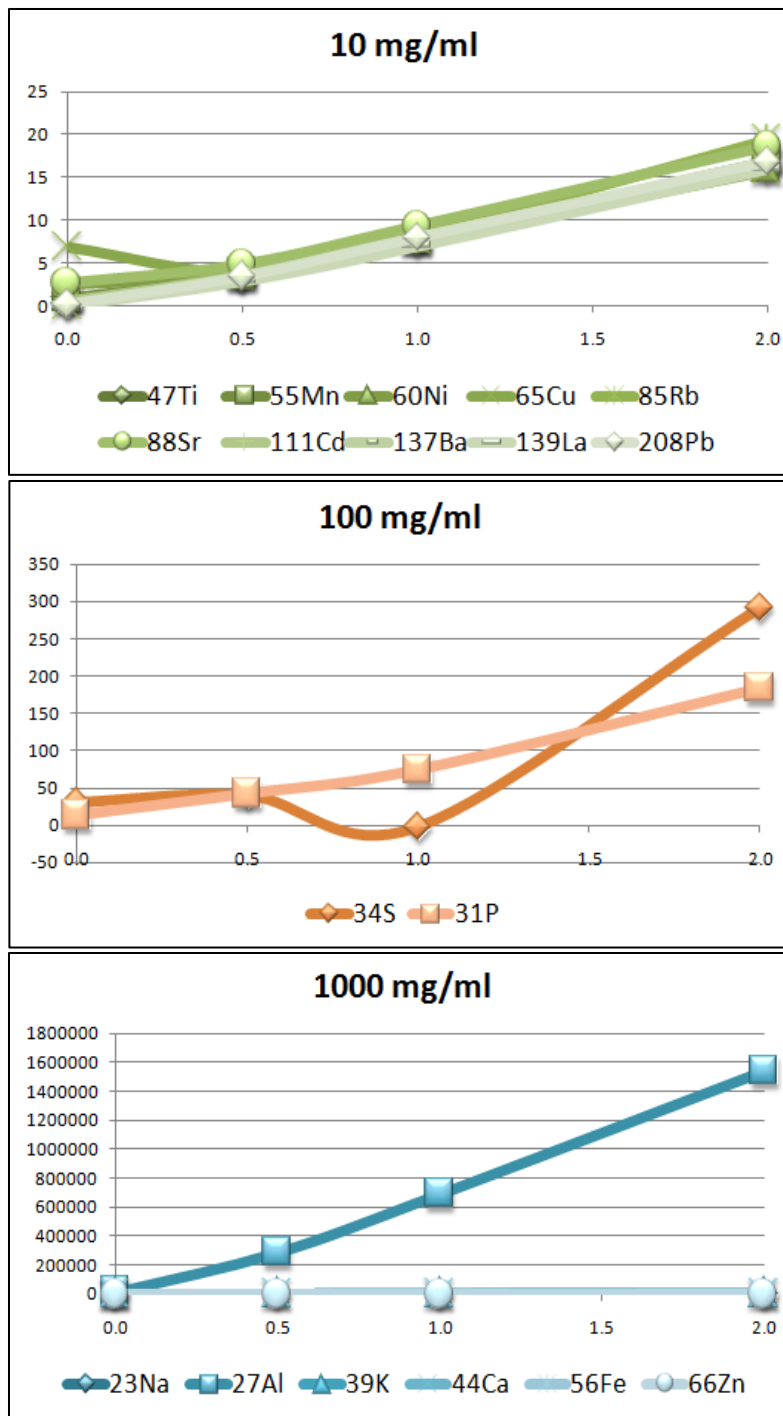


Figure 4.1**
 Elemental concentrations in standard wafers as measured by solution ICP-MS. The flat line shown for Na, K, Ca, Fe, and Zn in the bottom plot is the result of counts for these elements overwhelming the multiplier in the quadrupole. These elements are not actually present in such a low concentration.
 **Also available in appendix 3.4 (compact disc).

Effects of Density Variation on Data Quality

Physical heterogeneity of annual growth rings results from the porous nature of the xylem tissue, composed of tracheid cells in conifers (see section 2.5) (Stokes and Smiley, 1968). In this experiment, the laser was set to ablate at a fixed depth of 5 μm while traversing the width of an individual growth ring. The fixed ablation depth was intended to provide a control on the volume of ablated material entering the ICP. However, the movement of the laser across the uneven surface of the core segments made ablation volume impossible to quantify (section 2.5). Ablation along a set path (line ablation), as opposed to a single spot location, also inhibited the quantification of sample volume by monitoring an internal standard (section 2.5).

Despite the problems with volume quantification and internal standardization, line ablation may be a superior technique to spot analysis. The effect of density variation within an annual growth ring is something that may be unavoidable in LA-ICP-MS analysis of tree cores. Denser segments of xylem tissue will provide higher counts per sweep of a given element than less dense segments of the same chemical composition. However, the issue of density variation in this study is really the result of two separate factors: cell geometry and uneven ablation surface. Certain improvements to sample preparation may minimize the influence of an uneven ablation surface. Complications related to the structure of xylem tissue are largely unavoidable, and if discrepancies in ablated material due to uneven sample surface could be avoided, then application of a travelling laser could be more advantageous than spot analysis for reasons that will be discussed below.

The geometry of tracheid cells contributes greatly to the density variation within a growth ring. Tracheid cells are shaped like soda straws that are tapered on either end. The pore space to cell wall ratio varies at the tapered ends. Density also varies between earlywood and latewood in a given growth year. The ablation paths set for growth rings in this study were originally a product of the large amount of time required to perform three sweeps for an eighteen-element configuration (section 2.5). Coincidentally, the long ablation path that moved back and forth from earlywood to latewood incorporated the tissue of a large number of tracheid cells, and may have had an averaging effect on the density of the sampled xylem tissue. This “averaging” effect may render density variation negligible in a relative sense. That is, although the counts recorded by the ICP-MS likely reflect lower concentrations than would be recorded for a non-porous sample of the same chemical composition, these concentrations are consistent among growth rings. Similar patterns in the varying concentrations of Na, Ca, Zn and B, for example, support this idea. If variations in measured concentrations due to density differences were great enough to render data unreliable, then we should expect to see less uniformity in chemical trends.

Boron in FR77 8B, JFCK 9B, STRCK 1A, and FR7506 4A show the same trend from the first annual growth ring with concentrations above detection to the end of the sampled core segment. Most samples show a complacency (or lack of sharp variation between any two growth rings) across the entire sampled interval. Recall that complacency in tree-ring width reflects the lack of a growth-limiting factor over some period of time (section 1.5). Chemical “complacency” in this case refers to a lack of significant change in the concentration of an element over the ten-year period that was

analyzed. Calcium and zinc show a covariance that is similar in trend in BM 1A, FR77 2C, JFCK 2B, FR 7506 5B, and PSF MMSP 1B (figures 6.1-6.3, appendix 3.4).

Given the chemical heterogeneity of xylem tissue, a larger sample volume that traverses the width of a growth ring may be more representative of a growth ring than a sample volume taken from a single ablation point, or a collection of ablation points. Employment of a travelling laser to ablate material along a line is better than averaging the results of several spot analyses along the same line because the temperature and intensity of the travelling laser will be more consistent. The time that it takes a laser to warm up prior to ablation of sample may vary slightly and if ablation rates were affected, associated errors would be likely to compound, given multiple ablation points on the same growth ring. Additionally, a travelling laser allows for a longer period of ablation time while limiting the exposure of the wood to the laser. As discussed in chapter 2, beam intensity was reduced to prevent sample burning. If spot analysis had been elected in place of line analysis, sample burning may have been more difficult to avoid.

Suggestions

Although the size, shape, and density of tracheid cells cannot be controlled, the physical homogeneity of the ablation surface can be. Core segments were prepared for LA-ICP-MS analysis as discussed in section 2.3. The final stage of preparation involved the use of a razor blade for exposure of a clean, flat ablation surface. A razor blade was elected instead of sand paper in order to minimize the scatter of material across growth-ring boundaries. Pearson et al. (2005) also used a razor blade to surface cores. Although a block plane and track were used to ensure that the razor was applied with even pressure at a fixed angle to the core segment, tearing of xylem tissue prevented the manufacture of a

truly flat face. Variation in the surface topography of core segments was on the order of several micrometers. With the ablation depth set at 5 μm , the potential for the uneven surface to skew measured elemental concentrations over a given line segment is great, especially given the limitations of the autofocus function (see section 2.5). Ablation of the standard wafers did not require the use of the autofocus function because the flat surface of the wafers allowed for the distance between the focal plane and the ablation surface to remain constant along the ablation path. If this were the case for core segments, then apparent discrepancies in elemental concentrations due to the use of the autofocus function could be eliminated and concentrations perceived by the ICP-MS could be consistent for each sample.

In future studies, ablation surfaces of core segments should be prepared in a similar manner to the first and second stages of surfacing discussed in section 2.4. Once the dendrochronological analysis is complete, the sample should be pressed in a vise with enough force to flatten the sample surface. The sample should be covered to prevent contamination during pressing. This procedure, once established through trial and error, may help to reduce the effects of an uneven ablation surface, and may also help to close pore space, making the ablation surface similar to that of the standard wafers.

Calibration of Sulfur

Sulfur calibration was unsuccessful for twelve of twelve attempts with the ICP-MS in this experiment. This includes ten days of sample analysis using LA-ICP-MS, and two days of solution ICP-MS. The likely cause for this problem is a contamination of sulfur internal to the ICP-MS. During an attempted acid digestion analysis, the nebulizer stopped collecting fluid. Counts for seventeen elements dropped to zero, but those for

sulfur remained on the order of 7,500 counts per sweep for each of the standard wafers (figure 5.2, appendix 3.4). Figure 5.2a, seen below, shows the graph for sulfur. This suggests that the presence of sulfur somewhere in the machine is preventing an accurate analysis for this element. Sulfur is known to present problems in ICP-MS analysis when regular cleaning of the cones is not carried out (Perkinelmer.com). The ICP-MS unit at NAU that was used for tree-core analysis in this study was also being used for a biology experiment involving the uranium content of mouse tissue over a period of several months. Sulfur was not monitored for mouse-tissue samples, but it is reasonable to suspect that sulfur from the tissue may have clogged the cones of the ICP-MS. In future studies, all experimentation on the ICP-MS unit employed should be considered. Cleaning of the cones should be performed as necessary based on this knowledge.

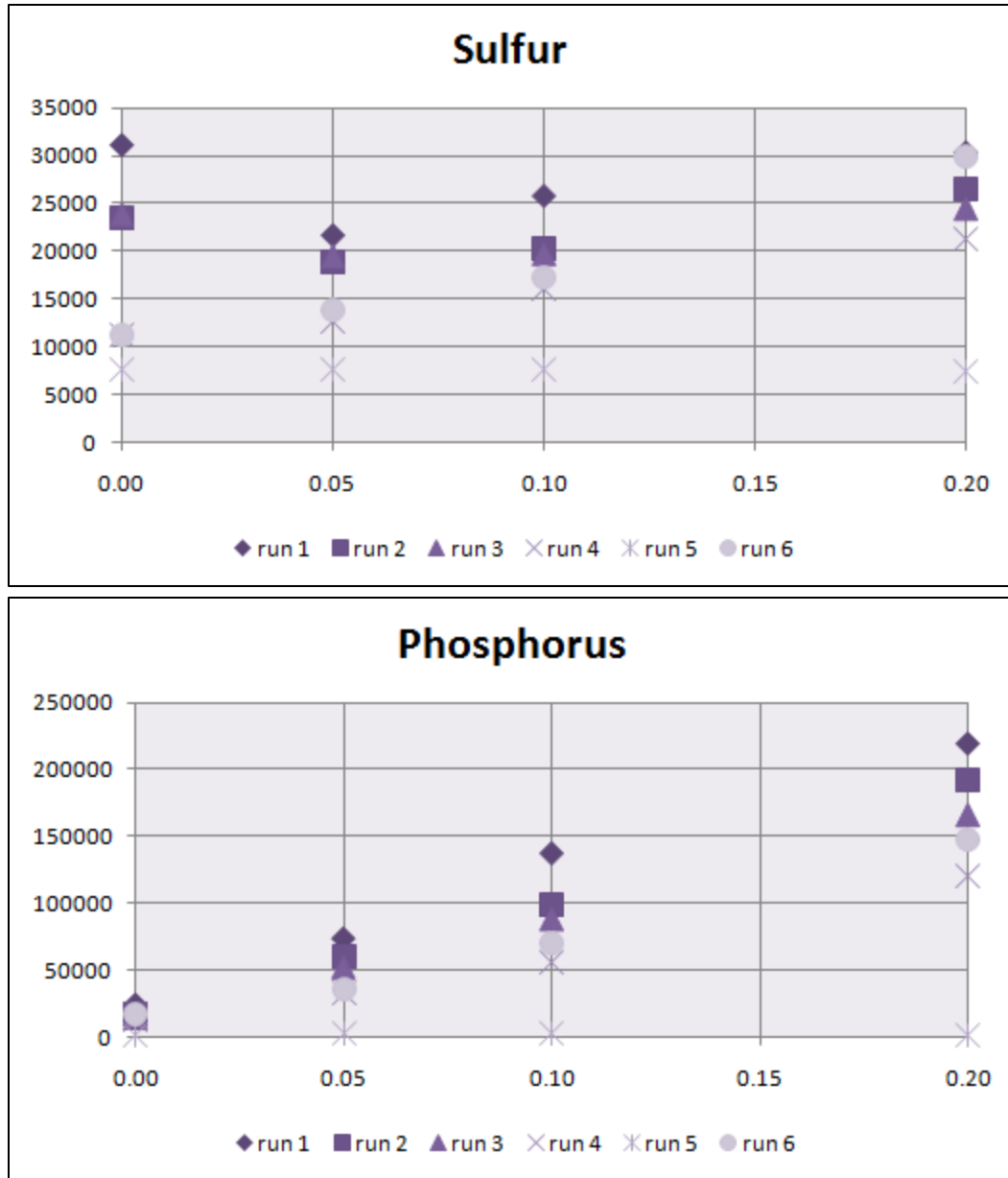


Figure 5.2a

The title of each graph indicates the element analyzed. X-axis values correspond to the relative concentrations of this element in each of four standard wafers. The nebulizer was not functioning properly during run 4. The top graph shows a concentration of sulfur holding at 7,500 counts per sweep. All other elements drop to zero counts per sweep during run 4, consistent with the dysfunction of the nebulizer. Data for all elements are available in figure 5.2 of appendix 3.4 (compact disc).

4.2 Comparison of Two Configurations- Data Reliability

Tree-core segments that were analyzed by both the eighteen-element and five-element configurations may provide the most insight as to the reliability of LA-ICP-MS data in this study (section 3.3). Because LA-ICP-MS analysis was run on the same sample with the same machinery and identical laser settings, elemental concentrations measured by the eighteen-element and five-element configurations should be very close. As discussed in section 3.3, correlation between the two experiments is weak. Of the nine core segments analyzed by both configurations, only three (DF MMSP 1B, FR225 5A, and FR 225 1B) show moderate or strong correlations of elemental concentration for calcium and aluminum between the five-element and eighteen-element configurations (figure 3.45). Zinc in these three samples was measured in higher concentrations by the five-element configuration than by the eighteen-element configuration. The pattern of concentration variability between growth rings was also inconsistent. Phosphorus and sulfur did not calibrate properly for any of the LA-ICP-MS analyses. The remaining six core-segments that were analyzed by both elemental configurations showed high variability in concentrations of calcium and aluminum between the two configurations. Zinc in PSF MMSP 1B showed moderate correlation between the two analyses. In five of the core segments, calcium and aluminum seem to co-vary. That is, the concentration of calcium increases and decreases across growth rings in a similar manner to that of aluminum (figures 3.45 and 6.1-6.3).

The lack of strong correlation between elemental concentrations of zinc, calcium, and aluminum measured by each of the two configurations suggests that LA-ICP-MS data from this study do not accurately quantify the chemical composition of the trees

cored from Mount Saint Helens. Whether the largest factor contributing to the ambiguity of data in this study is instrument calibration, appropriateness of methodology, human error, or otherwise is unclear. Although the data obtained by LA-ICP-MS analysis in this study are not consistent in terms of quantitative elemental abundance, the covariance of aluminum and calcium in five of the nine core segments suggests that measured concentrations may be accurate in terms of relative increase or decrease across growth rings.

Of the nine core segments analyzed by both configurations, six show large discrepancies in the concentrations of calcium, zinc, and (when measurable) aluminum. In most cases, the five-element configuration measured a higher elemental concentration than the eighteen-element configuration. The similarity in trends in elemental concentrations across the ten-year period suggests that the skewing is systematic, and is not a reflection of non-representative or “bad” data. Rather, the higher counts associated with the five-element configuration may be a side effect of instrument detuning. As discussed in chapter 2.7, detuning of the instrument sensitivity was required to obtain accurate counts for nineteen elements of varying abundance. Detuning refers to the reduction in sensitivity of the nebulizer. Sodium and calcium had counts that were orders of magnitude above others (B, Ni, Cu, Rb, Sr, Ba, La, Pb) in analytical trials. Sensitivity was reduced in order to prevent the multiplier from becoming overwhelmed during analysis of these elements in standard wafers. The reduced sensitivity was maintained for all core-segment analyses completed with the eighteen-element configuration. Sodium was generally the element with the greatest measured concentration in both the standard wafers and the tree-core samples. Ni, Cu, Rb, Sr, La, and Pb were generally present in

concentrations that did not exceed 1 ppm. Consequently, the level of detuning was dictated by the discrepancy between counts per sweep recorded for sodium and least abundant elements. The five-element configuration did not include Na, Ni, Cu, Rb, Sr, La, or Pb, and therefore required a lesser extent of detuning in order to measure the concentration of all five elements in a single ablation pass.

Ideally, standard wafers would regulate the effect of detuning on measured elemental concentration. That is, the conversion of counts per sweep to concentration in ppm that is discussed in section 2.8 should be unaffected by a given number of counts per sweep associated with some known chemical concentration in a standard wafer. This is true if all other variables are held constant. However, discrepancies associated with detuning may compound when combined with the chemical and physical heterogeneities of xylem tissue. Just as the apparent concentration in a given sample might drop as porosity increases (section 4.3), apparent concentration may decrease along with instrument sensitivity. In the five-element experiment, in which sodium and low-abundance elements were not considered, instrument sensitivity to calcium was less detuned, resulting in relatively higher nebulizer sensitivity. Higher counts per sweep of these elements may have contributed to higher apparent elemental concentrations.

Suggestions to Reduce the Effects of Detuning

The need for detuning can be controlled by the element configuration that is elected for analysis. Tree-core segments in this study were analyzed for eighteen elements, present in a wide range of concentrations. If a configuration consisted only of elements expected to be present in similar concentrations, then nebulizer sensitivity

would not have to be altered in order to detect elements of interest. The anticipated relative abundance of elements for this study is reflected by the composition of the standard solution. The elements expected to be more abundant in core samples have higher concentrations in the standard solution. In future studies, the group of elements analyzed by a single ICP-MS configuration should be limited by the relative concentrations of each element that are anticipated to be present in the sample in order to reduce the influence that nebulizer detuning has on apparent chemical concentrations.

4.3 Evaluation of Site and Species Selection

Data shown in chapter three reveal a range of elemental concentrations and patterns of concentration variation across the annual growth rings produced from AD 1795-1805 and AD 1976-1986 as measured by LA and solution ICP-MS analysis with multiple elemental configurations. No distinct change in the relative abundance of any element consistently coincides with the timing of either the AD 1980 or AD 1800 eruptions of Mount Saint Helens in the majority of samples. Carbon isotopic analysis of the five-year sequence of growth rings spanning AD 1980 was also inconclusive. Sections 4.2 and 4.3 discuss potential shortcomings of the techniques used to obtain chemical analyses of tree cores in this study. Whether the results of ICP-MS analyses reflect the true composition of annual growth rings is unclear, and scrutiny of data interpretation and validity is necessary in any experimental evaluation. However, for the sake of discussion in chapter 4.4, we will consider the data obtained for the 49 tree-cores from Mount Saint Helens to be a reasonably accurate representation of the actual xylem tissue chemistry. Data support the notion that LA-ICP-MS analyses performed in this

study are relative indicators of xylem-tissue chemistry. Even in the absence of a volcanic indicator, if these data are considered reasonable, then we must consider the significance of a lack of evidence for volcanic eruption.

Because no dendrochemical analysis had been attempted at Mount Saint Helens using LA-ICP-MS prior to the design and completion of this project, the criteria used to select trees for coring were made with no prior knowledge of trees bearing evidence of a chemical response to the eruption of this volcano. It is therefore reasonable to suspect that the sample set used for this study may not be representative of all trees in the area. Suggestions are made to improve the process of sample and site selection in order to maximize potential for the detection of a chemical indicator of volcanic eruption (sections 4.3, 5.1).

Mount Saint Helens was chosen as an ideal location for this study because timing of recent eruptions is well constrained, and a majority of trees in the vicinity produce annual growth rings. This project involved the design and execution of an experimental chemical analysis, the goal of which was to derive a procedure for the application of a particular instrument (LA-ICP-MS). In future studies, when parameters for sample preparation and instrument calibration have been empirically derived from a larger body of work including studies such as this, the goal might be to constrain the timing of an unknown eruption or to monitor the biological response of one. In the case of this experiment, in which eruptive history has been meticulously documented and extensive studies continue to be carried out on the ecological effects of the eruption of AD 1980, the critical unknowns have more to do with the experimental procedure than the eruptive event. In order to recognize a chemical response to the eruption of Mount Saint Helens by

the analysis of growth rings, some measurable change in the chemical composition of wood cellulose that was initiated by the volcanic eruption must be isolated and preserved in a tree. Simply, a chemical signal must exist in a limited number of growth rings and it must be measurable.

In the case of elements that exhibit high variability in concentration within a single growth ring, trends between years are generally considered immeasurable. Data produced in this study and data produced by the USGS at the abandoned Waldorf Mine in Colorado have found cadmium to be an example of an element for which trends are not measurable on the timescale of decades using LA-ICP-MS (Witte et al., 2004). Increasing the number of years that are chemically analyzed may or may not help to reveal long-term trends in elemental variability, but this is not likely to be an economically viable solution.

Just as high variability may mask long-term trends in elemental abundances, concentrations in elements that are consistently high may also mask long-term trends. Certain plants are known to reduce the risk of toxicity by transporting metals from the roots to the leaves if they are present in potentially dangerous quantities. The plant can then shed these excess elements by shedding leaves (Witte et al., 2004). Such behavior suggests that certain elements are not bound to the tissue of an individual growth ring, but mobile within the plant body. If this is also true of trees at Mount Saint Helens, we must consider the possibility that a sudden influx of elements associated with an eruption may not be recorded as such in the xylem tissue of an individual growth ring.

At Mount Saint Helens, the periodic deposition of dacitic tephra over thick substrate is coupled with a high volume of annual precipitation. As discussed in chapter

1, element mobilization may be enhanced by the acidification of rainwater, and is a common byproduct of volcanic eruption (Pritchett and Fischer, 1981). If elements are, in fact, mobile in the xylem tissue of trees at Mount Saint Helens, then a large amount of many elements (whether they are helpful or harmful to growth) added to the system may be inconsequential. This surplus of available nutrients may result in the regular shedding of excess elements through shedding of leaves and needles. In this case, a tree could maintain the preferred abundance of each element and simply discard the excess, thus destroying the potential for any long-term chemical signal. This ability of a tree to discard elements that are excessively available effectively creates a biological buffer. At Mount Saint Helens, continuous weathering of volcanic tephra and consistent precipitation may inspire a soil condition in which a surplus of nutrients is always available to trees.

Tree cores that were sampled in this study did not show a large degree of variation in ring width. As discussed in section 2.4, calendar years were assigned to growth rings through application of ring-counting and cross-dating techniques. A master chronology for Douglas firs was compiled from the ITRDB and a previous study in this location (section 2.4). Although this chronology did indicate the presence of marker years (defined by relatively thin growth rings), the majority of cores analyzed in this study indicated complacent annual growth, and absolute dates were assigned mostly on the basis of ring counting. The complacent growth observed reflects the lack of stress felt by Douglas firs at Mount Saint Helens, and supports the idea that nutrients are available to trees in quantities that exceed necessity. This condition would reflect the chemical complacency seen for several elements in analyzed trees.

As discussed in section 2.4, widespread growth patterns that are used in dendrochronology depend on the effectiveness of a growth-limiting factor in any given year for any given group of trees. In most cases, the dominant growth-limiting factor for trees of a given region is either availability of water or the length of a growing season, as determined by temperature (Fritts and Swetnam, 1989). Douglas fir trees in the Pacific Northwest are a dominant species of spruce tree whose growth is more commonly limited by water availability than temperature (Littell et al., 2008). In Gifford Pinchot National Forest, and in the vicinity of Mount Saint Helens, precipitation is rarely scarce. Additionally, Douglas firs are capable of hydraulic redistribution (Domec and Gartner, 2002; Meinzer et al., 2007). Hydraulic redistribution refers to the ability of a tree to draw water from deep soil layers, and release it into shallower soil layers in order to minimize the response of the tree to a dry soil horizon. This species has adapted a defense to short-term periods of drought, making it more resistant to environmental stress (Littell et al., 2008). Because of a lack of growth-limiting factors, Douglas firs at Mount Saint Helens may therefore be a poor choice of species and location for this experiment.

PSF MMSP 1B is the only non-Douglas fir sample that was analyzed in this study. Data obtained by LA-ICP-MS analysis suggest that subordinate species, such as Pacific silver fir, may be better candidates for preservation of a chemical response to environmental change. This tree exhibits significant changes in elemental concentrations of sodium, potassium, calcium, zinc, and rubidium that begin on or after AD 1980 (figure 3.33). Many elements are present in higher or more variable concentrations in the Pacific silver fir than any of the Douglas firs analyzed on the same day (figure 3.33). A subordinate species may be more susceptible to environmental influence than a dominant

species due to a higher level of stress associated with growth. The changes in elemental abundance that occur on and after the AD 1980 growth ring may be a response to the volcanic eruption, or the largest influence on the growing season that year. These changes in elemental concentration similarly occur at or around AD 1980 in four other trees from four different sample sites, and will be discussed in the next section.

4.4 Dendrochemical Evidence for Volcanic Eruption of Mount Saint Helens

As a whole, chemical data from the Douglas-fir tree cores taken from Mount Saint Helens do not show consistent and conclusive evidence for a shift in elemental concentration that coincides with the AD 1980 or AD 1800 eruptions. Several spikes in elemental concentrations, such as the copper spikes in STRCK 1A at AD 1799 and FR77 7A at AD 1981, occur in some core segments, but are not consistent enough in character or timing to clearly suggest a response to volcanic eruption. However, at least five of the tree cores analyzed (approximately 10% of the sample set) show similar changes in the concentrations of two or more elements that may indicate a response to the AD 1980 eruption. FR 7506 5b, JFCK 2B, FR77 2C, BM 1A, and PSF MMSP 1B show similar variation in some combination of aluminum, calcium, zinc, potassium, or sodium that begins on or around AD 1980. JFCK 2B shows a uniform decrease in calcium and zinc at AD 1800 as well.

As discussed in section 1.8 and 1.6, the mobility of aluminum is expected to increase as weathering of volcanic tephra occurs (Felitsyn and Kirianov, 2002). The availability of calcium plays a significant role in stem growth and may be displaced by aluminum in the root system of a tree (McLaughlin et al., 1987). In the event that

aluminum is abundant and mobile enough to overwhelm the system of nutrient uptake in a tree, a condition known as aluminum toxicity may temporarily stunt the growth of the stem (Smith and Shortle, 2001; Shortle et al., 1997). The potential for displacement of calcium by aluminum suggests that these elements might have a negative correlation on or after an event that could influence the abundance or mobility of either element. If a volcanic eruption deposited aluminum-rich material that resulted in an increase in available aluminum as it weathered, then one might expect to see an increase in aluminum coincident with a decrease in calcium in the period of time subsequent to the eruption. In FR 7506 5b, JFCK 2B, and PSF MMSP 1B, aluminum and calcium do not exhibit a negative correlation in elemental concentration. Rather, these two elements tend to vary in a similar manner across growth rings. In FR7506 5B, aluminum and calcium demonstrate nearly identical relative concentrations between AD 1977 and AD 1986 (figure 3.46). Calcium is much more abundant than aluminum in this and other samples (thousands of ppm Ca compared to tens of ppm Al), but relative increases and decreases of both elements occur simultaneously. JFCK 2B (figure 3.46) and PSF MMSP 1B (figure 3.33) show a similar covariance of calcium and aluminum. In all three cores, both elements decrease significantly in concentration at AD 1980 and in JFCK 2B, concentrations remain low through AD 1986. In FR7506 5B, concentrations recover at AD 1984, and in PSF MMSP 1B, Ca and Al recover immediately to concentrations that are comparable to pre-eruption years. JFCK 2B shows the same immediate recovery for calcium and aluminum in years subsequent to AD 1800 (figure 3.46). A spike in the concentration of calcium occurs at AD 1980 and AD 1979 for FR77 2C and BM 1A,

respectively (figures 3.29 and 3.31). In both of these samples, concentrations of aluminum were below detection.

The positive correlation between aluminum and calcium in JFCK 2B, PSF MMSP 1B, and FR7506 5B does not reflect a condition of aluminum toxicity or calcium displacement. There is effectively no change in the relative abundance of these two elements in xylem tissue in the four years prior to and the six years following the volcanic eruption. Presuming that the data obtained by ICP-MS analysis of these cores is a reasonable representation of the xylem chemistry, several possibilities may explain the lack of influence the eruption seems to have had on the sampled trees. As discussed earlier in this chapter, a tree is not likely to record instances of environmental change if the change is not sufficient enough to impart a great deal of stress to the growth needs of that tree. Douglas firs in this region are not under a great deal of stress, and so are not necessarily sensitive to the change in soil chemistry brought on by the eruption. Hydraulic redistribution, as discussed by Littell (2008), is a defense against drought, the most common growth-limiting factor observed for Douglas firs in the region. If hydraulic redistribution is a defense mechanism that is employed to encourage stem growth in conditions that are less than optimal, then drought should not be the only trigger for its employment. It seems reasonable to suspect that in the event that aluminum begins to overwhelm the root system, a capable tree would pull nutrients from a deeper, more nourishing source, thus eliminating stress and the likelihood of a change in xylem chemistry.

Another possible explanation for the lack of change in relative abundance of aluminum and calcium is that the buffering capacity of the deep, fertile substrate at

Mount Saint Helens is sufficient to preserve soil conditions that are ecologically beneficial. This region has seen more Holocene volcanic activity than any other in the United States and does not struggle to support lush vegetation. Many of the trees in Gifford Pinchot National Forest exceed 700 years of age (section 1.3) and appear to be in excellent health. The complacent growth observed in the 52 tree cores prepared for ICP-MS analysis in this study is evidence that supports a long-standing condition of uninterrupted growth. It is therefore likely to conclude that eruptions at Mount Saint Helens do not greatly affect Douglas firs that do not sustain physical injuries from the blast or associated mass-wasting events. Another possibility is that levels of mobile Al are not high enough to illicit aluminum toxicity.

Calcium and zinc show similar patterns of variation across growth rings in JFCK 2B, PSF MMSP 1B, FR77 2C, FR7506 5B, and several other samples. This common variation in concentration is more easily observed in data obtained by the five-element configuration. In BM 1A, however, calcium spikes one year later than zinc at AD 1979. Recall that in this sample, AD 1979 was incorrectly labeled and the growth ring marked 1979 actually corresponds to AD 1980. Nevertheless, zinc spikes in the growth ring that corresponds to AD 1980, and so the spike does not occur in the same year as it does for calcium in this sample. Padilla and Anderson (2002) observed spikes in copper and barium that coincide with the eruption of Laki (CE 1783) and Krakatau (CE 1883) in the same species. Spikes in copper concentration occur in FR77 7A and 5A, PSF MMSP 1B, and JFCK 3A at AD 1981, and in STRCK 1A at AD 1799.

A sharp decrease in the concentration of potassium and sodium in PSF MMSP 1B occurs at AD 1980 (figure 3.33). BM 1A exhibits an almost identical decrease in sodium

at the growth ring corresponding to AD 1980 that is marked 1979 (figure 3.31). The same sample from Bear Meadow (BM 1A) records a sharp increase in potassium corresponding to AD 1980. The signal here is opposite to that in the Pacific silver fir, but of a similar magnitude and character. Given that sodium and potassium are of similar ionic size to calcium, it may be possible that these elements, which are not as crucial to stem growth, are being replaced by aluminum in the root systems immediately following the volcanic eruption. Aluminum in FR77 2C, as measured with the five-element configuration, increases and remains high from AD 1981 through AD 1985 (figure 3.46). The same is true of aluminum in PSF MMSP 1B, though the relative increase is less pronounced (3.33).

Although the observations discussed in this section are not explicit or clear-cut indications of a biological response to the eruption of Mount Saint Helens, they should be considered *possible* signals associated with it. Tree cores that are analyzed for similar motivation in future studies should include calcium, zinc, aluminum, copper, sodium and potassium in the analytical configuration. If any element is abundant enough to require large amounts of detuning, one should consider leaving it out of the configuration. Similar changes in relative abundance may be more pronounced in trees that are subject to growth-limiting stresses. In environments that provide ample precipitation and long growing seasons, subordinate species should be considered as a sample population.

CHAPTER 5: SUMMARY

Dendrochemical analysis of tree-cores using LA-ICP-MS, as discussed in section 1.9, is highly experimental. No standard protocol is currently in place for the generation of reliable data for this type of chemical analysis. This master's thesis was designed with the intention of working toward the development of a protocol for LA-ICP-MS analysis of annual growth rings. To extract meaningful chemical data from tree cores is to decipher a history of interaction between that tree and its surrounding environment. Such information has enormous potential to increase our understanding of the environmental implications of a wide range of events, natural or anthropogenic, that have occurred in the past thousand years. A summary of project inception, design and execution is presented in this chapter, along with suggestions to improve the quality of data in future studies and move toward the development of a standard procedure for LA-ICP-MS analysis of annual growth rings.

The summary is divided into three parts that discuss the success and limitation of methods used in sample collection, sample preparation, and sample analysis. The fourth and final part of this summary includes a brief discussion on carbon isotopic analysis. Although results obtained in this study were inconclusive, the potential for success in future studies is great. A simple flow chart for future work involving LA-ICP-MS analysis of tree rings is available in appendix 3.6 of the compact disc that accompanies this book.

5.1 Sample Collection

Trees cored for LA-ICP-MS analysis in this study were selected on the basis of location, species, age, and microclimatic conditions (section 2.1). Jefferson Creek, Bear Meadow, and Straight Creek sample sites were chosen based on the presence of thin eruption-related annual-growth rings that were documented in previous studies (Brantley et al., 1986; Sheppard et al., 2008; Sheppard et al., 2009; Yamaguchi, 1983; Yamaguchi 1985; Yamaguchi and Hoblitt, 1986; Yamaguchi et al., 1990; Yamaguchi and Lawrence, 1993). As discussed in section 4.3, thin growth rings were not present in the cores obtained for this study. The 31-tree sample set is instead characterized by complacent growth, indicating a lack of stress (Stokes and Smiley, 1968) that corresponds to the apparent chemical complacency shown by LA-ICP-MS analysis (section 4.3). Several possible explanations for the chemical complacency are offered in section 4.3, including the potential for hydraulic redistribution in Douglas firs (Littell, 2008), and mobilization of elements within a tree leading to shedding of excess constituents (Witte et al., 2004).

Trees that exhibited chemical changes coincident with volcanic eruption at Volcán Parícutin (Sheppard et al., 2008) also had abnormally thin annual growth rings coincident with the eruption (figure 1.8). Here, and in many locations in the southwestern United States, chronologies include robust marker years associated with occurrence of lower levels of annual rainfall (Stokes and Smiley, 1968; Kaye, 1997). The trees analyzed in this study at Mount Saint Helens did not exhibit thin growth rings. Marker years from the ITRDB chronologies (appendix 4.1) were not identified as such in the collected cores. As discussed in section 4.3, the abundant precipitation and thick substrate in Gifford Pinchot National Forest create ideal growing conditions for Douglas firs. These trees

thrive as the dominant species at Mount Saint Helens. Trees that survive under high-stress conditions, and those that contain abnormally thin rings, may have a greater potential to record a chemical response volcanic eruption. Tree-ring studies that aim to refine the use of LA-ICP-MS may have more success if samples have thin growth rings.

In future studies at Mount Saint Helens, subordinate species should constitute some portion of cored trees. Other factors that may contribute to greater stress-levels should also be considered. Trees rooted on steep slopes, or in areas that did not receive excessive amounts of tephra deposition may be more susceptible to environmental change. Trees rooted in thinner substrate or in areas that only endured fallout from one, rather than several, volcanic eruptions may exhibit some evidence of consequent temporary stress.

Recall from chapter 1 that Mount Saint Helens was chosen for this study because the rich eruptive history and presence of old-growth forest seemed like an ideal combination for a dendrochemical experiment. In practice however, some of the characteristics that added to the appeal of Mount Saint Helens may have contributed to the unexpected chemical complacency shown in these trees. If the data produced in this study are accurate representations of xylem tissue chemistry, then we may conclude that repeated eruptions in an environment with vegetation as lush as that at Gifford Pinchot National Forest may result in an adaptation of a species to acidic soil conditions. The accuracy of this conclusion can only be tested with continued research.

5.2 Sample Preparation

Tree-core samples were prepared for dendrochronological analysis in accordance with the standard procedures outlined by Stokes and Smiley (1968) (section 2.1-2.3). Because the trees sampled in this study showed complacent growth, dating of growth rings was accomplished by counting. With more time and resources, additional trees could have been cored in an effort to find indicators of stress, such as thin rings or traumatic resin canals (Kuroda and Shimaji, 1983). A sample set including trees that grew under stressful conditions could have helped to determine whether stress increases the likelihood of a chemical response to volcanic eruption.

The final step in preparation for LA-ICP-MS analysis included the exposure of a clean ablation surface on a core-segment cut to fit the sample chamber (sections 2.3 and 2.4). In order to preserve the chemistry of individual growth rings, sandpaper was not used to create a smooth surface. Instead, a blade attached to a low-angle block plane was used together with a custom-made track that held the tree cores in place. The blade was intended to reduce contamination of wood particles across growth-ring boundaries so that any chemically distinct xylem tissue could be traced to a single growing season. Although cross-ring contamination was likely reduced by application of the block-plane method, tearing of xylem tissue resulted in the creation of an uneven ablation surface. Ablation of an uneven surface makes it difficult to quantify the amount of material that is introduced into the ICP, and leads to further complications related to data reduction. These complications are discussed at length in sections 2.5 and 4.1. As discussed in section 4.1, sanding of sample surfaces should be considered as an alternative method. Some measure must also be taken to reduce the effects of cross-ring contamination. One

possible solution would be to anticipate a depth of contaminated wood based on the grit size of the sandpaper used to level the surface. If an ablation depth could be set to exceed that of the anticipated contamination, then the effects of sanding might be reduced. Alternatively, core segments could be pressed in order to produce a flat ablation surface. Pressing samples might also reduce the pore space in xylem tissue that contributes to variable density and perceived elemental concentrations.

5.3 Data Analysis

Forty-nine tree-core segments were analyzed by an eighteen-element LA-ICP-MS configuration (sections 2.5, 2.6, 2.7). Cellulose powder doped with standard solution was used as an in-house calibration standard (section 2.6) and data were converted from counts per sweep to parts per million by the method outlined in section 2.8. For each core, growth rings for a ten to eleven-year period spanning an eruption were analyzed. AD 1796-1805 growth rings were considered for the AD 1800 eruption of Mount Saint Helens, and AD 1975-1986 growth rings were considered for the AD 1980 eruption of Mount Saint Helens. As discussed in section 4.1, analyses do not indicate a chemical response to these eruptions that is consistent among the sample set. Possible explanations for this lack of chemical response are discussed in sections 4.1, 4.3, and 5.1. These explanations consider biological processes that may help a tree to maintain regular growth potential despite the occurrence of some growth-limiting factor. Additional explanations may be related to the size of the time span analyzed. It is possible that long-term responses to volcanic eruption are not measurable on the scale of a ten-year interval. If any combination of processes were to result in the delayed reaction of a tree to volcanic

eruption, the five-year to six-year period of time that was monitored in this study might simply not be enough to capture it. Especially in the case of Douglas firs at Mount Saint Helens, which are rooted in deep, fertile substrate, and capable of compartmentalizing their root systems to avoid the effects of drought (Littell, 2008), a delayed response to environmental change seems reasonable. In future studies, the number of consecutive years analyzed should be extended to test the possibility of a delayed response.

Solution ICP-MS analyses were also conducted on a subset of samples in order to test the accuracy of data produced by the less-established method of LA-ICP-MS (section 3.5). In this study, 52 annual growth rings from seven trees were analyzed by solution ICP-MS. Solution ICP-MS is a destructive method of chemical analysis in which the xylem tissue of a growing season is dissolved by way of multi-acid digestion, and introduced as a liquid to the ICP. This technique eliminates many of the difficulties associated with laser ablation, including those associated with an uneven ablation surface. Calibration is easily achieved by creation of standard liquids. Laser ablation is a method that gained attention because of the potential to reduce contamination risk associated with the lengthy process of acid digestion. Also, the small spot size that is available with laser ablation suggests that greater resolution is possible by LA-ICP-MS than solution ICP-MS. Growth rings that were separated for acid digestion were large enough to achieve one-year resolution in this study. In many instances, it was more difficult to achieve this resolution with laser ablation. This was due to the large amount of time required for a travelling beam to perform sweeps on eighteen elements. A configuration with fewer elements might resolve this issue. The subset of samples that were analyzed by both LA and solution ICP-MS did not yield consistent results. That is, the elemental

concentrations measured by each technique varied significantly (section 3.5). The issues with density variation that are discussed in section 4.1 may be a major factor in the reason for these results. Solution ICP-MS may provide a means of cross checking the data quality of LA-ICP-MS on tree cores, and should be used in future studies whenever possible.

As discussed in section 4.2, the five-element configuration and eighteen-element configurations of the LA-ICP-MS also produced inconsistent results. Possible explanations are discussed at length in section 4.2. In future studies, a simpler configuration should be used, and elements of a similar ionic radius should be included to reduce the need for excessive detuning of the instrument. Realistically, several configurations should be tested. Laboratory fees, including helium and argon required to run the LA-ICP-MS are expensive, and make it difficult to perform the trials required to instill confidence in this technique.

5.4 Carbon Isotope Analysis

The results of the carbon isotopic analyses are briefly mentioned in section 3.7. Although results were inconclusive in this study, the idea that carbon isotopes might serve as an indicator of stomatal closure, and an indirect indicator of volcanic eruption is conceptually sound (section 1.7). Carbon isotopic analyses in this study were poorly executed. Samples were selected according to the elemental variation measured by LA-ICP-MS. Unfortunately, a lack of funding for carbon isotopic analysis limited the number of growth rings submitted. Five consecutive growth rings from five trees were analyzed. This represents a period of two years prior-to and two years after the AD 1980 eruption

of Mount Saint Helens. Pronounced changes in the relative abundances of ^{12}C and ^{13}C are shown in each of the five trees. These changes are not uniform among the group, and the limited number of consecutive years analyzed does not establish a “normal” isotopic ratio that can be compared to the post-eruptive ratio. In future studies, carbon isotopic analysis should be performed on a larger number of consecutive growth rings in a greater number of trees.

5.5 Evidence for Volcanic Eruption of Mount Saint Helens

As discussed in section 4.4, five tree cores of the 49 analyzed by LA-ICP-MS show changes in elemental abundances of Al, Ca, Zn, K, or Na that occur on or after one of two eruptions of Mount Saint Helens. Given that 44 of 49 core segments do not show similar variation in elemental concentration, it is difficult to attribute these changes to volcanic eruption. However, the potential to improve the quality of, and confidence in, data obtained by LA-ICP-MS is great. Several changes to the experiment must be implemented before the potential for dendrochemistry can be concluded. As discussed in section 1.9, a goal of this study was to identify a xylem-tissue chemistry that can be attributed exclusively to the occurrence of a volcanic eruption. Of equal importance is a progression toward the development of a procedure for the use of LA-ICP-MS on tree cores that may enhance the progress of future work. Although a change in xylem tissue chemistry attributed exclusively to volcanic eruption was not identified, progress toward the development of a procedure for LA-ICP-MS on tree cores was made. The factors that contributed to a lack of confidence in data quality in this study may strengthen the design of future studies.

REFERENCES

- Barbour, M. M., Walcroft, A. S., Farquhar, G. D., 2002, Seasonal variation in $\delta^{13}\text{C}$ and $\delta^{18}\text{O}$ of cellulose from growth rings of *Pinus radiata*, *Plant Cell Environment*, v. 25, p. 1483-1499.
- Brantley, S., Yamaguchi, D., Cameron, K., Pringle, P., 1986, Tree-ring dating of volcanic Deposits, *Earthquakes and Volcanoes*, v. 18, no. 5, p. 184-194.
- Cameron, K.A., Pringle, P.T., 1986, Post-glacial lahars of the Sandy River basin, Mount Hood, Oregon, *Northwest Science*, v. 60, no. 4, p. 225-237.
- Cameron, K.A., Pringle, P.T., 1987, A detailed chronology of the most recent major eruptive period at Mount Hood, Oregon, *Geological Society of America Bulletin*, v. 99, p. 845-851.
- Coplen, T., 1995, Discontinuance of SMOW and PDB, *Nature*, v. 375, p. 285.
- Crandell, D.R., 1987, Deposits of pre-1980, pyroclastic flows and lahars from Mount St. Helens Volcano, Washington, U.S. Geological Survey Professional Paper 1444, p. 91.
- Criswell, W., 1987, Chronology and pyroclastic stratigraphy of the May 18, 1980 eruption of Mount Saint Helens, Washington, *Journal of Geophysical Research*, v. 92, no. 10, p. 237- 266.
- Dobbs, R.C., 1966, The intraseasonal development of longitudinal growth patterns in Douglas-fir *Pseudotsuga Menziesii*, Mirb., Franc, unpublished Ph D dissertation, University of Washington, Seattle, p.157.
- Domec, J.C., Gartner, B.L., 2002. Age and position-related in hydraulic vs. mechanical dysfunction of xylem: inferring the design criteria for Douglas-fir wood structure, *Tree Physiology*, v. 22, p. 91–104.
- Doukas, M.P., 1990, Road guide to volcanic deposits of Mount St. Helens and vicinity, Washington, U.S. Geological Survey Bulletin, v. 1859, p. 53
- Driscoll, C. T., Lawrence, G.B., 2001, Acidic deposition in the northeastern United States: sources and inputs, ecosystem effects, and management strategies, *BioScience*, v. 51, no. 3, p. 180-198.
- Felitsyn, S. B., Kirianov, V.,Y., 2002, Mobility of phosphorus during the weathering of volcanic ashes, *Lithology and Mineral Resources*, v. 37, p. 275–278.
- Fritts, H.C., 1976, *Tree rings and climate*, Academic Press, London, p. 173-174.

- Fritts, H.C., Lofgren, G.R., Gordon, G.A., 1979, Variations in climate since 1602 as reconstructed from tree rings, *Quaternary Research*, v. 12, p. 18-46.
- Fritts, H.C., Swetnam, T.W., 1989, Dendroecology, a tool for evaluating variations in past and present forest environments, *advances in ecological research*, v. 19, p. 111-188.
- Graybill, D.A., 1982, Chronology development and analysis, In *climate from Tree Rings*, edited by Hughes, M.K., Kelly, P.M., Pilcher, J.R., LaMarche Jr, V.C., Cambridge University Press, Cambridge, p. 21-28.
- Hagemeyer, J., 1993, Monitoring trace metal pollution with tree rings, a critical reassessment /n Markert, B., (editor), *Plants as biomonitors, indicators for heavy metals in the terrestrial environment*, VCH, Weinheim, p. 541-563.
- Hall, G.S., Yamaguchi, D.K., Rettberg, T.M., 1990, Multielemental analyses of tree rings by inductively coupled plasma mass spectrometry, *Journal of Radioanalytical Nuclear Chemistry Letters*, v. 146, p. 255-265.
- Hoblitt, R.P., Crandell, D.R., Mullineaux, D.R., 1980, Mount St. Helens eruptive behavior during the past 1,500 years, *geology*, v. 8, no. 11, p. 555-559.
- Hoffer, J.M., Hoffer, R.L., 1986, Chemical composition of the May 18, 1980 Mount St. Helens tephra and the underlying soil, changes from July 1980 to May 1981, /n Keller, S.A.C., (editor), *Mount St. Helens, five years later*, Eastern Washington University Press, Cheney, p. 108-111.
- Hoffmann, E., Stephanowitz, H., Skole, J., 1996, Investigations of the migration of elements in tree rings by Laser-ICP-MS, *Journal of Analytical Chemistry*, v. 355, p. 690-693.
- Holmes, K.L., 1955, Mount St. Helens, recent eruptions, *Oregon Historical Quarterly*, v. 56, p. 196-210.
- Holmes, R. L., 1983, Computer-assisted quality control in tree-ring dating and measurement, *Tree-Ring Bulletin*, v. 43, p. 69-78.
- Hupp, C.R., 1984, Dendrogeomorphic evidence of debris flow frequency and magnitude at Mount Shasta, California, *Environmental Geology and Water Science*, v. 6, no. 2, p. 121-128.
- International Tree-Ring Data Bank (ITRDB), 2010, <http://www.ncdc.noaa.gov/paleo/treering.html>.
- Iverson and Martinson, 1986, Mount St Helens, American Geomorphological Field Group, field trip guidebook and abstracts.

- Kaye, M.W., 1997, Guide to crossdating, Ecology Lab, College of Ecosystem Management, Northern Arizona University, p.1-18.
- Krug, E. C., Frink, C .R., (1983). Acid Rain on Acid Soil: A New Perspective, *Science*, v. 221, no. 4610, p. 520-525.
- Kuroda, K, Shimaji, K., 1983, Traumatic resin canal formation as a marker of xylem growth, *Science*, v. 29, p. 653-659.
- Kuroda, K., Shirnaji, K., 1984, Wound effects on xylem cell differentiation in a conifer, *AWA Bull*, v. 5, p. 295-305.
- Lawrence, D. B., 1938, Trees on the march, *Mazama*, v. 20, no. 12, p. 49-54.
- Lawrence, D. B., 1939, Continuing research on the flora of Mt. St. Helens, a progress report, *Mazama*, v. 21, no. 12, p. 49-54.
- Lawrence, D. B., 1954, Diagrammatic history of the northeast slope of Mt. St. Helens, *Washington, Mazama*, v. 36, no. 13, p. 41-44.
- Lawrence, G.W., David, M.B., Bailey, S.W., Shortle, W.C., 1997, Assessment of calcium status in soils of red spruce forests in the northeastern United States, *Biogeochemistry*, v. 38, p. 19-39.
- Lipman, P.W., Mullineaux, D.R., 1981, The 1980 eruptions of Mount St. Helens, *Washington, U.S. Geological Survey Professional Paper*, v. 1250, p. 844.
- Littell, J. S., Peterson, D. L., Tjoelker, M., 2008, Douglas-fir growth in mountain ecosystems, water effects tree growth from stand to region, *Ecological Monographs*, v. 78, p. 349–368.
- Loader, N.J., Hemming, D.L., 2004, The stable isotope analysis of pollen as an indicator of terrestrial palaeoenvironmental change, a review of progress and recent developments, *Quaternary Science Reviews*, v. 23, p. 893-900.
- Loader, N.J., Robertson, I., McCarroll, D., 2003, Comparison of stable carbon isotope ratios in the wholewood, cellulose and lignin of oak tree-rings, *Palaeogeography, Palaeoclimatology, Palaeoecology*, v. 196, p. 395-407.
- Lövestam, G., Johansson, E., Johansson, S., Pallon, J., 1990, Elemental micro patterns in tree rings, a feasibility study using scanning proton microprobe analysis, *Ambio*, v. 19, p. 87–93.
- Majors, H.M., 1980, Three newly discovered accounts of activity on Mount Saint Helens, 1898, 1903, and 1921, *Northwest Discovery*, v.1, no. 1, p. 36-41.

- McCarroll, D., Loader, N.J., 2004, Stable isotopes in tree rings, *Quarterly Science Review*, v. 23, p. 771–801.
- McCarroll, D., Loader, N.J., 2005, Isotopes in tree rings, *in* Leng, M. J., (editor), *Isotopes in paleoenvironmental research*, The Netherlands, p. 67-116.
- McCarroll, D., Pawellek, F., 1998, Stable carbon isotope ratios of latewood cellulose in *Pinus sylvestris* from northern Finland, variability and signal strength, *The Holocene*, v. 8, p. 675-684.
- McCarroll, D., Pawellek, F., 2001, Stable carbon isotope ratios of *pinus sylvestris* from northern Finland, and the potential for extracting a climate signal from long Fennoscandian chronologies, *The Holocene*, v. 11, p. 517-526.
- McLaughlin, S.B., Downing, D.J., Blasin, T.J., Cook, E.R., Johnson, A.H., Adams, H.S., 1987, An analysis of climate and competition as contributors to decline of red spruce in high elevation Appalachian forests of the eastern United States, *Oecologia*, v. 72, p. 487-501.
- Meinzer, F.C., Grantz, D.A., 1990, Stomatal and hydraulic conductance in growing sugarcane, stomatal adjustment to water transport capacity, *Plant Cell and Environment*, v. 13, p. 383–388.
- Meinzer, F.C., Brooks, J.R., Bucci, S.J., Goldstein, G., Scholz, F.G., Warren, J.M., 2004, Converging patterns of uptake and hydraulic redistribution of soil water in contrasting woody vegetation types, *Tree Physiology*, v. 24, p. 919–928.
- Mokgalaka, N.S., Gardea-Torresdey, J.L., 2006, Laser ablation inductively coupled plasma mass spectrometry, principles and applications, *Applied Spectroscopy Reviews*, v. 41, no. 2, p. 131-150.
- Moore, J. G., Sisson, T. W., 1981, Deposits and effects of the May 18 pyroclastic surge, *in* The 1980 eruptions of Mount Saint Helens, Washington, Lipman, P.W., Mullineaux, D.R., U.S. Geological Survey Professional Paper, v. 1250, p. 421-433.
- Mullineaux, D.R., 1996, Pre-1980 tephra-fall deposits erupted from Mount St. Helens, Washington, U.S. Geological Survey Professional Paper, v. 1563.
- Mullineaux, D.R., Crandell, D.R., 1981, The eruptive history of Mount St. Helens, *in* The 1980 eruptions of Mount St. Helens, Washington, Lipman, P.W., Mullineaux, D.R., 1981, U.S. Geological Survey Professional Paper, v. 1250, p. 844.
- Okazaki, R., Smith, H.W., Gilkeson, R.A., Franklin, J., 1972, Correlation of West Blacktail Ash with pyroclastic layer T from the 1800 A.D. eruption of Mount Saint Helens, *Northwest Science*, v. 46, p. 77-89.

- Padilla, K. L., Anderson, K.A., 2002, Trace element concentration in tree-rings, biomonitoring centuries of environmental change, *Chemosphere*, v. 49, p. 575–585.
- Pearson, C., Manning, S.W., Coleman, M., Jarvis, K., 2005, Can tree-ring chemistry reveal absolute dates for past volcanic eruptions, *Journal of Archaeological Science* v. 32, p. 1265–1274.
- Pringle, 1993, Roadside geology of Mount St. Helens National Volcanic Monument and vicinity, Washington State Department of Natural Resources, division of geology and earth resources information circular, p. 88.
- Pritchett, W.L., Fisher, R.F., 1981, *Properties and Management of Forest Soils*, Wiley and Sons, New York.
- Prohaska, T., Stadbauer, C., Wimmer, R., Stinger, G., Latkoczy, C., Hoffmann, E., and Stephanowitz, H., 1998, Investigation of element variability in tree rings of young Norway spruce by laser-ablation-ICPMS, *The Science of the Total Environment*, v. 219, p. 29-39.
- Reukema, D.L., 1965, Seasonal progress of radial growth of Douglas-fir, western red cedar and red alder, U.S. Forest Science Research Paper PNW, p. 26.
- Savard, Martine M., Begin, C., Parent, M., Smirnoff, A., Marion, J., 2004, Effects of smelter sulfur dioxide emissions, a spatiotemporal perspective using carbon isotopes in tree rings, *Journal of Environmental Quality*, v. 33, p. 13-26.
- Sheppard, P.R., Jacoby, G.C., 1989, Application of tree-ring analysis to paleoseismology, two case studies, *Geology*, v. 17, p. 226-229.
- Sheppard, P.R., Ort, M.H., Anderson, K.C., Elson, M.D., Vázquez-Selem, L., Clemens, A.W., Little, N.C., and Speakman, R.J. 2008, Multiple dendrochronological signals indicate the eruption of Parícutin Volcano, Michoacán, Mexico, *Tree-ring Research* v. 64, no. 2, p. 97-108.
- Sheppard, P.R., Ort, M.H., Anderson, K.C., Clynne, M.A., May, E.M., 2009, Multiple dendrochronological responses to the eruption of Cinder Cone, Lassen Volcanic National Park, California, *Dendrochronologia*, v. 27, p. 213-221.
- Sherrod, D.R., Scott, W.E., Stauffer, P.H. (editors), 2008, *A volcano rekindled: the renewed eruption of Mount St. Helens, 2004-2006*, U.S. Geological Survey Professional Paper 1750.
- Shortle, W.C. and Smith, K.T., 1988, Aluminum-induced calcium deficiency syndrome in declining red spruce trees, *Science*, v. 240, p. 1017-1018.

Shortle, W.C., Smith, K.T., Minocha, R., Lawrence, G.B, and David, M.B., 1997, Acidic deposition, cation mobilization and biochemical indicators of stress in healthy red spruce, *Journal of Environmental Quality*, v. 26, p. 871-876.

Smith, H.W., Okazaki, R., and Knowles, C.E., 1977, Electron microprobe analysis of glass shards from tephra assigned to set W, Mount St. Helens, Washington, *Quaternary Research*, v. 7, no. 2, p. 207-217.

Smith, K.T. and Shortle, W.C., 2001, Conservation of element concentration in xylem sap of red spruce. *Tree Physiology*, v. 20, p. 73-85.

Stokes, M.A., Smiley, T.L., 1968. *An Introduction to Tree-Ring Dating*. University of Arizona Press, Tucson.

Swanson, D.A., Cameron, K.A., Evarts, R.C., Pringle, P.T., and Vance, J.A., 1989, Cenozoic volcanism in the Cascade Range and Columbia Plateau, southern Washington and northernmost Oregon: AGU field trip guidebook T106, July 3-8.

Verhoogen, Jean, 1937, Mount St. Helens, a recent Cascade volcano, California University, Department of Geological Sciences Bulletin, v. 24, no. 9, p. 263-302.

Virtual ChemBook, Elmhurst College: [Acid Rain – Soil Interactions](http://www.elmhurst.edu/~chm/vchembook/index.html), 2010, <http://www.elmhurst.edu/~chm/vchembook/index.html>.

Voight, B., Glicken, H., Janda, R.J., Douglas, P.M., 1981. Catastrophic rockslide avalanche of May 18. *In* P. W. Lipman and D. R. Mullineaux, eds. *The 1980 Eruptions of Mount St. Helens, Washington*. U.S. Geological Survey Professional Paper 1250, p. 347-377.

Voight, B., Janda, R.J., Glicken, H., and Douglas, P.M., 1983, Nature and mechanics of the Mount Saint Helens rockslide-avalanche of 18 May 1980, *Geotechnique*, v. 33, p. 243-273.

Washington State Department of Natural Resources, 2010, http://www.dnr.wa.gov/ResearchScience/Topics/GeoscienceData/Pages/gis_data.aspx, layer name: Surface Geology 1:100,000.

Watmough, S. A. 1997. An evaluation of the use of dendrochemical analyses in environmental monitoring, *Environmental Review*, v. 5, p. 181–201.

Watmough, S.A. & T.C. Hutchinson, 1996, Analysis of tree rings using inductively coupled plasma mass spectrometry to record fluctuations in a metal pollution episode, *Environmental Pollution*, v. 93, p. 93–102.

Watmough, S.A., Hutchinson, T.C., 1999, Change in the dendrochemistry of sacred fir close to Mexico City over the past 100 years, *Environmental Pollution*, v. 104, p. 79–88.

Watmough, S.A., T.C. Hutchinson & R.D. Evans, 1998. Development of solid calibration standards for trace elemental analyses of tree rings by laser ablation inductively coupled plasma– mass spectrometry, *Environmental Science and Technology*, v. 32, p. 2185–2190.

Witte, C.P., Laurent, D.N., Gielbert, J., Parker, J.E., Romeis, T., 2004, Rapid one-step protein purification from plant material using the eight-amino acid StrepII epitope, *Plant Molecular Biology*, v. 55, p. 135-147.

Wolfe, Edward W., and Pierson, Thomas C., 1995, Volcanic-hazard zonation for Mount St. Helens, Washington, 1995: U.S. Geological Survey Open-File Report 95-497.

Woodruff, D. R., Mcculloh, K. A., Waren, J. M., Meinzer, F. C. and Lachenbruch, B., 2007, Impacts of tree height on leaf hydraulic architecture and stomatal control in Douglas-fir, *Plant Cell & Environment*, v. 30, p. 559–569.

Yamaguchi, D.K., 1983, New tree-ring dates for recent eruptions of Mount St. Helens. *Quaternary Research*, v. 20, p. 246-250.

Yamaguchi, D.K., 1985, Tree-ring evidence for a two-year interval between recent prehistoric explosive eruptions of Mount St. Helens, *Geology* v. 13, no. 8, p. 554-557.

Yamaguchi, D.K., 1993, Forest history, Mount St. Helens, *National Geographic Research and Exploration*, v. 9, p. 294-325.

Yamaguchi, D.K., and Hoblitt, R.P., 1986, Tree-ring dating of Mount St. Helens flowage deposits emplaced in the valley of the South Fork Toutle River, Washington, during the past 350 years [abs.], // Keller, S.A.C., Cheney, (editors), *Mount St. Helens, Five years later*, Eastern Washington University Press, p. 441.

Yamaguchi, D.K., Hoblitt, R.P., and Lawrence, D.B., 1990, A new tree-ring date for the "floating island" lava flow, Mount St. Helens, Washington, *Bulletin of Volcanology*, v. 52, p. 545-550.

Yamaguchi, D.K., Lawrence, D.B. 1993, Tree-ring evidence for 1842-1843 eruptive activity at the Goat Rocks dome, Mount St. Helens, Washington, *Bulletin of Volcanology*, v. 55, p. 264-272.

Zobel, D.B., Antos, J.A., 1986, Survival of prolonged burial by subalpine forest understory plants, *American Midland Naturalist*, v.115, p. 282-287.

Zobel, D.B., and Antos, J.A., 1991, 1980 tephra from Mount St. Helens: spatial and temporal variation beneath forest canopies, *Biology and Fertility of Soils*, v. 12, p. 60-66.

APPENDIX 1.0: MAPS OF SAMPLED LOCALITIES

Figure captions

Figure 1.0

Location Map of all sample sites discussed in the text. Mount Saint Helens is located in the dashed circle and the locations of cored trees are indicated by symbols pertaining to each sample site. This map includes points for all of the trees cored for this study, including some that were not analyzed by LA-ICP-MS.

Figure 2.0

Hillshade map of study area around Mount Saint Helens. Symbols indicate the location of trees cored at each sample site.

Figure 2.0A

Map of the study area around Mount Saint Helens. Symbols indicate the locations of trees cored at each sample site and shading indicates slope.

Figure 2.0B

Map of the study area around Mount Saint Helens. Symbols indicate the locations of trees cored at each sample site and shading indicates aspect.

Figure 2.0C

Map of the study area around Mount Saint Helens. Symbols indicate the locations of trees cored at each sample site and shading indicates the surface geology. The same map is available in appendix 1.0 on the compact disc accompanying this book with labeled units (figure 2.0D). Unit descriptions are available in Table 2.0 of the same appendix and a color-coded legend is available in table 2.1. This figure was produced in ArcMap with data from the Washington State Department of Natural Resources, 2010.

Figure 2.1

Location map of trees cored east of Salem, Oregon on forest road 225. Grey boxes indicate the locations of cored trees.

Figure 2.2

Topographic map of sample site at Opal Creek, east of Salem, Oregon. Grey boxes indicate the locations of trees cored on forest road 225.

Figure 2.2A

Map of the sample site at Opal Creek, east of Salem, Oregon. Grey boxes indicate the locations of trees cored on forest road 225. Shading indicates slope.

Figure 2.2B

Map of the sample site at Opal Creek, east of Salem, Oregon. Grey boxes indicate the locations of trees cored on forest road 225. Shading indicates aspect.

Figure 2.3

Topographic map of the sample site at Jefferson Creek, northeast of Mount Saint Helens. Blue circles indicate the locations of cored trees.

Figure 2.3A

Map of the sample site at Jefferson Creek, northeast of Mount Saint Helens. Blue circles indicate the locations of cored trees and shading indicates slope.

Figure 2.3B

Map of the sample site at Jefferson Creek, northeast of Mount Saint Helens. Blue circles indicate the locations of cored trees and shading indicates aspect.

Figure 2.3C

Map of the sample site at Jefferson Creek, northeast of Mount Saint Helens. Blue circles indicate the locations of cored trees and shading indicates surface geology. Unit descriptions are available in table 2.0 (appendix 1.0) on the CD accompanying this book. A color-coded legend is available in table 2.1. This figure was produced in ArcMap with data from the Washington State Department of Natural Resources, 2010.

Figure 2.4

Topographic map of the sample site at Bear Meadow, northeast of Mount Saint Helens. Red triangles indicate the locations of cored trees.

Figure 2.4A

Map of the sample site at Bear Meadow, northeast of Mount Saint Helens. Red triangles indicate the locations of cored trees and shading indicates slope.

Figure 2.4B

Map of the sample site at Bear Meadow, northeast of Mount Saint Helens. Red triangles indicate the locations of cored trees and shading indicates aspect.

Figure 2.4C

Map of the sample site at Bear Meadow, northeast of Mount Saint Helens. Red triangles indicate the locations of cored trees and shading indicates surface geology. Unit descriptions are available in table 2.0 (appendix 1.0) on the CD accompanying this book. A color-coded legend is available in table 2.1. This figure was produced in ArcMap with data from the Washington State Department of Natural Resources, 2010.

Figure 2.5

Topographic map of the sample site at forest road 77, northeast of Mount Saint Helens. Green pentagons indicate the locations of cored trees.

Figure 2.5A

Map of the sample site at forest road 77, northeast of Mount Saint Helens. Green pentagons indicate the locations of cored trees and shading indicates slope.

Figure 2.5B

Map of the sample site at forest road 77, northeast of Mount Saint Helens. Green pentagons indicate the locations of cored trees and shading indicates aspect.

Figure 2.5C

Map of the sample site at forest road 77, northeast of Mount Saint Helens. Green pentagons indicate the locations of cored trees and shading indicates surface geology. Unit descriptions are available in table 2.0 (appendix 1.0) on the CD accompanying this book. A color-coded legend is available in table 2.1. This figure was produced in ArcMap with data from the Washington State Department of Natural Resources, 2010.

Figure 2.6

Topographic map of the sample site at forest road 7506, northeast of Mount Saint Helens. Purple stars indicate the locations of cored trees.

Figure 2.6A

Map of the sample site at forest road 7506, northeast of Mount Saint Helens. Purple stars indicate the locations of cored trees and shading indicates slope.

Figure 2.6B

Map of the sample site at forest road 7506, northeast of Mount Saint Helens. Purple stars indicate the locations of cored trees and shading indicates aspect.

Figure 2.6C

Map of the sample site at forest road 7506, northeast of Mount Saint Helens. Purple stars indicate the locations of cored trees and shading indicates surface geology. Unit descriptions are available in table 2.0 (appendix 1.0) on the CD accompanying this book. A color-coded legend is available in table 2.1. This figure was produced in ArcMap with data from the Washington State Department of Natural Resources, 2010.

Figure 2.7

Topographic map of the sample site at Marble Mountain Snow Park, south of Mount Saint Helens. The white square indicate the location of cored trees.

Figure 2.7A

Map of the sample site at Marble Mountain Snow Park, south of Mount Saint Helens. The white square indicate the location of cored trees and shading indicates slope.

Figure 2.7B

Map of the sample site at Marble Mountain Snow Park, south of Mount Saint Helens. The white square indicate the location of cored trees and shading indicates aspect.

Figure 2.7C

Map of the sample site at Marble Mountain Snow Park, south of Mount Saint Helens. The white square indicate the location of cored trees and shading indicates surface geology. Unit descriptions are available in table 2.0 (appendix 1.0) on the CD accompanying this book. A color-coded legend is available in table 2.1. This figure was produced in ArcMap with data from the Washington State Department of Natural Resources, 2010.

Figure 2.9

Location map of the study area around Mount Saint Helens. The locations of cored trees are indicated for all sample sites. Central locations for the trees cored for master chronologies produced by the International Tree Ring Data Bank are also indicated and labeled.

Figure 2.14

Topographic map of the sample site at Straight Creek, east of Mount Saint Helens. The orange diamond indicates the location of the cored tree.

Figure 2.14A

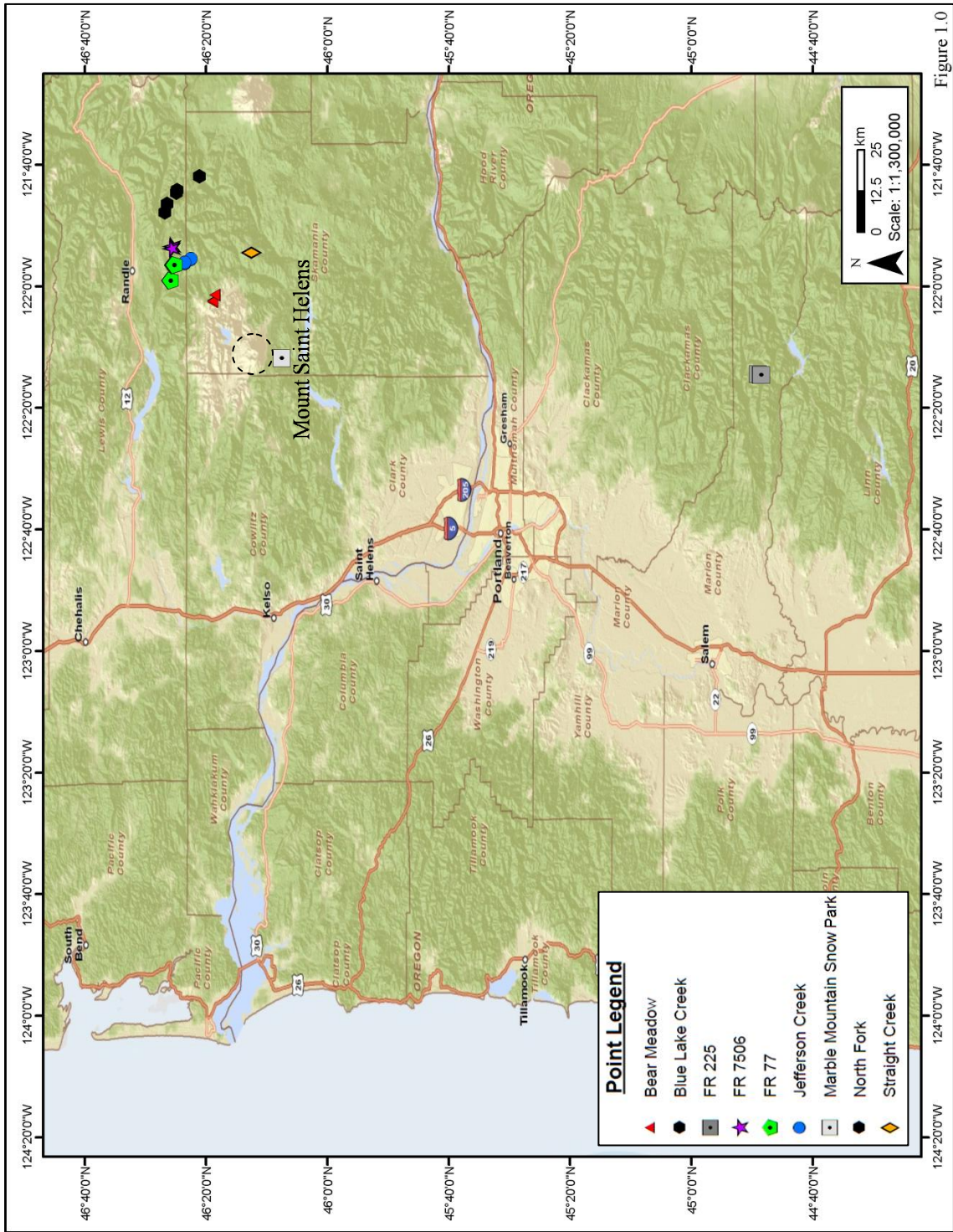
Map of the sample site at Straight Creek, east of Mount Saint Helens. The orange diamond indicates the location of the cored tree and shading indicates slope.

Figure 2.14B

Map of the sample site at Straight Creek, east of Mount Saint Helens. The orange diamond indicates the location of the cored tree and shading indicates aspect.

Figure 2.14C

Map of the sample site at Straight Creek, east of Mount Saint Helens. The orange diamond indicates the location of the cored tree and shading indicates surface geology. Unit descriptions are available in table 2.0 (appendix 1.0) on the CD accompanying this book. A color-coded legend is available in table 2.1. This figure was produced in ArcMap with data from the Washington State Department of Natural Resources, 2010.



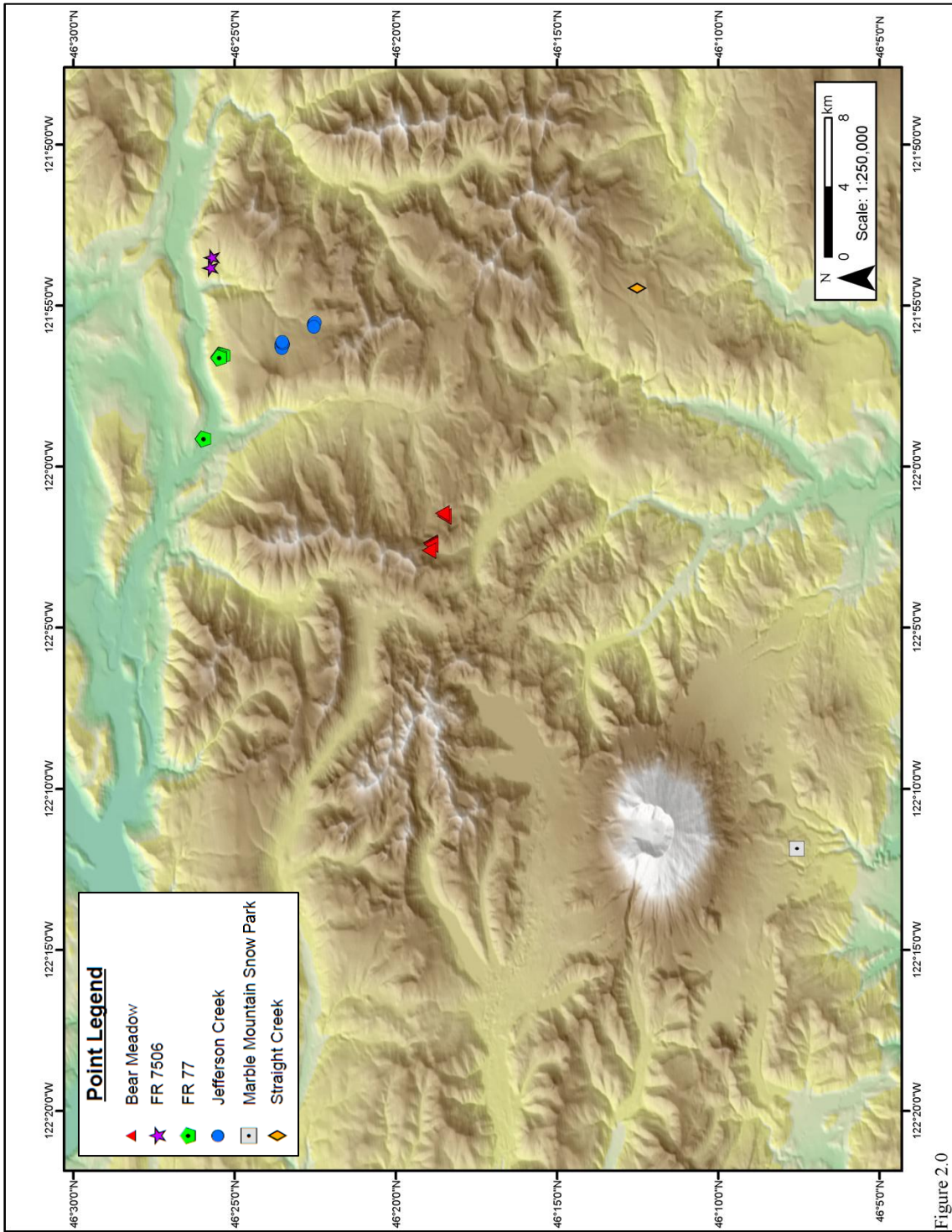
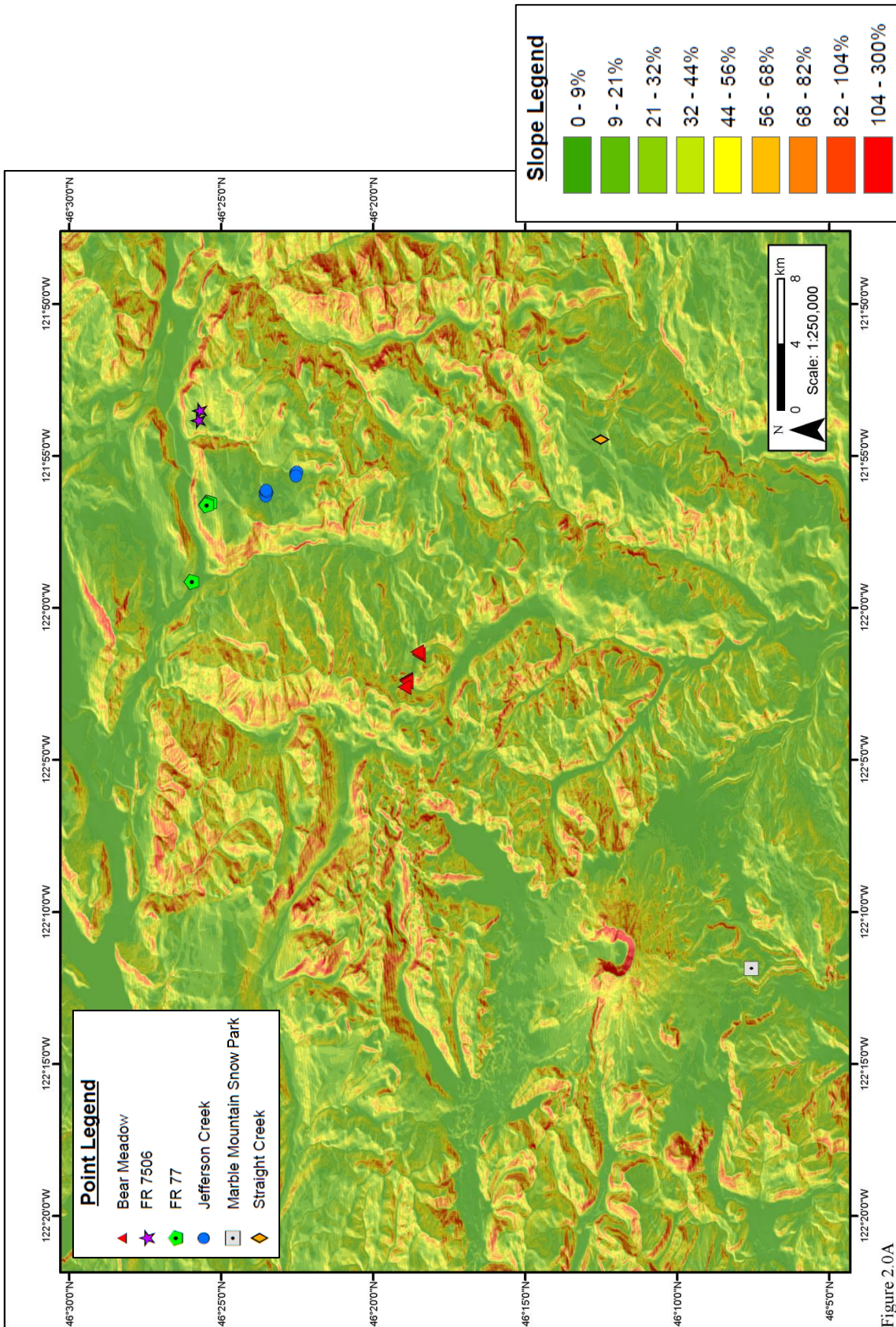


Figure 2.0



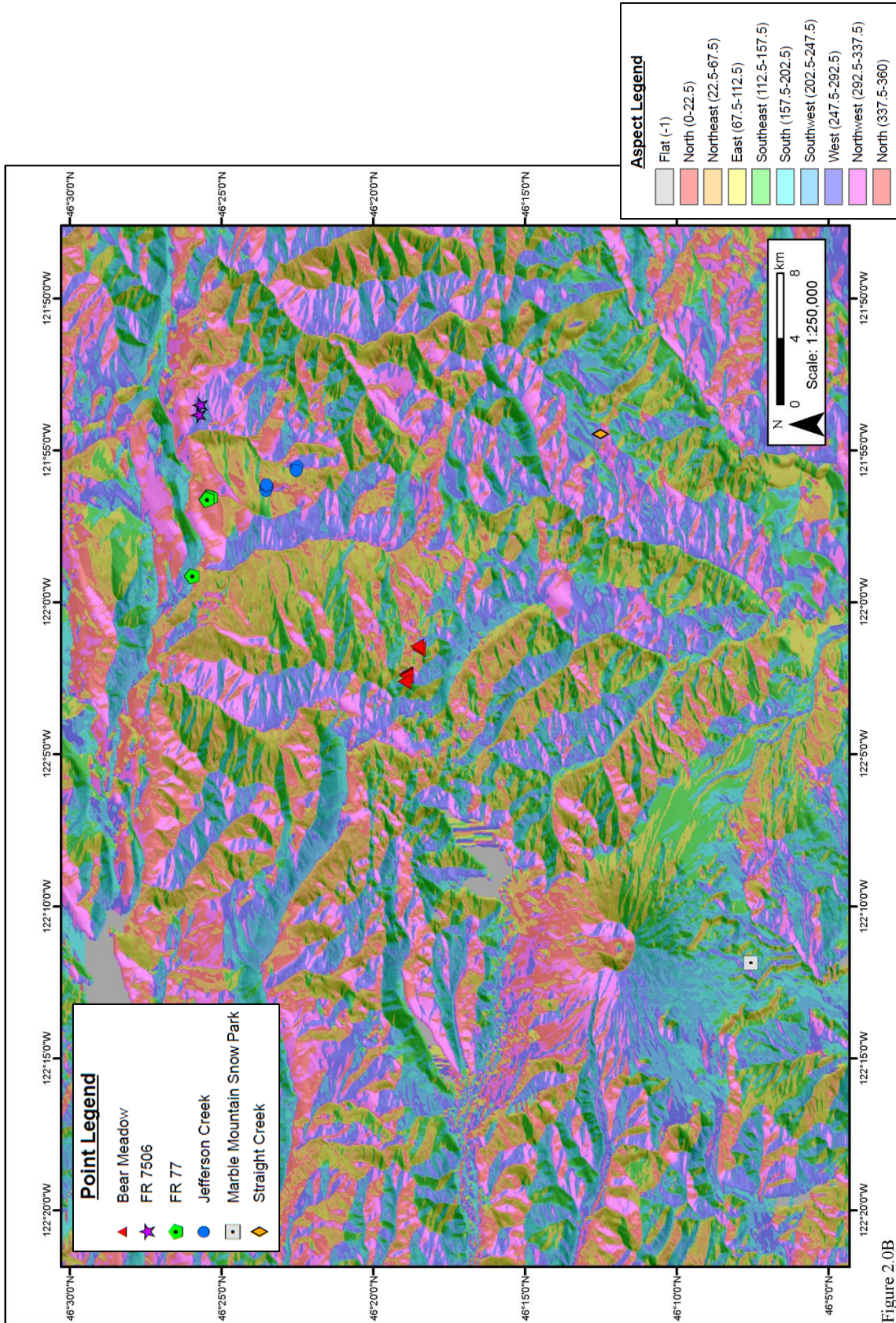


Figure 2.0B

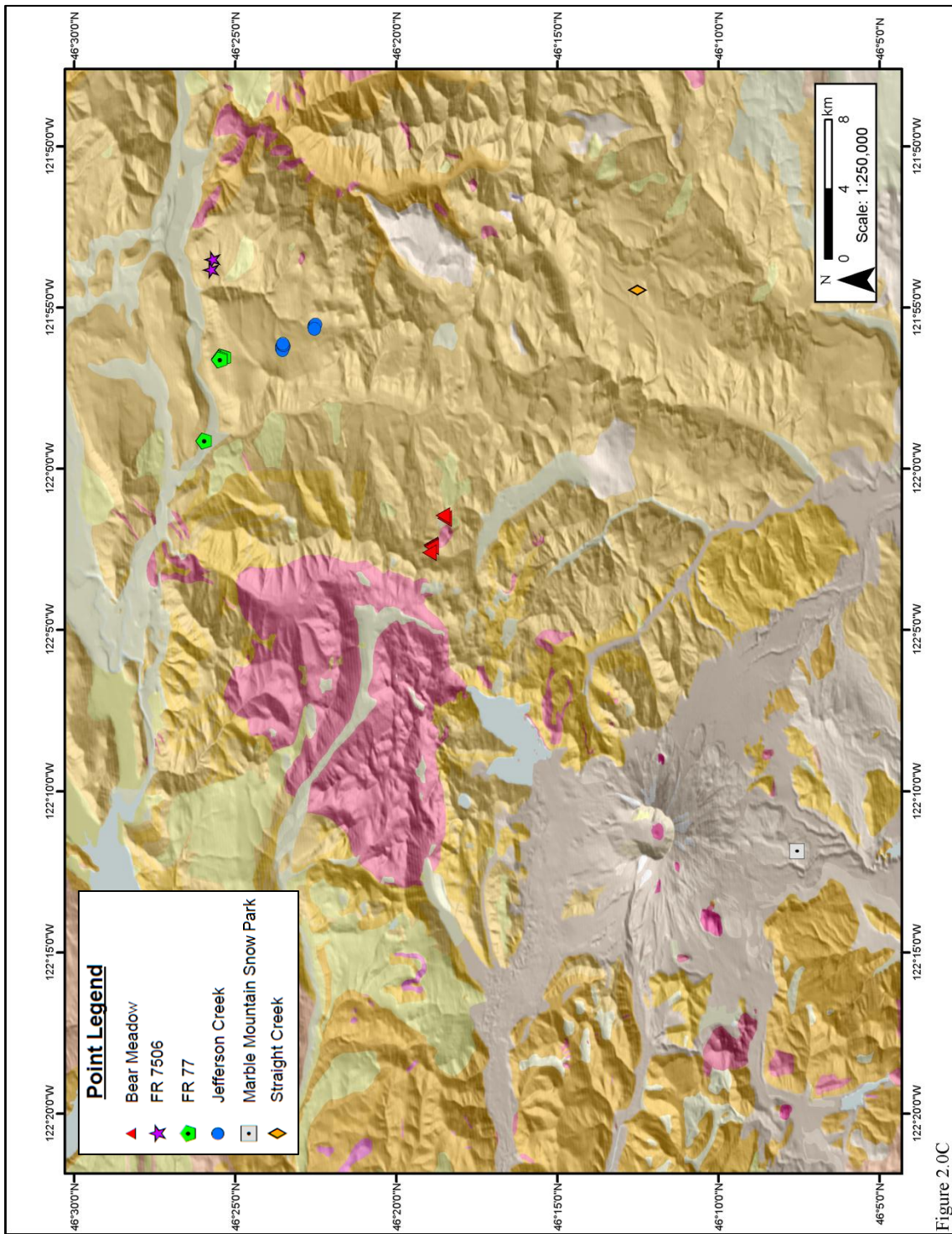


Figure 2.0C

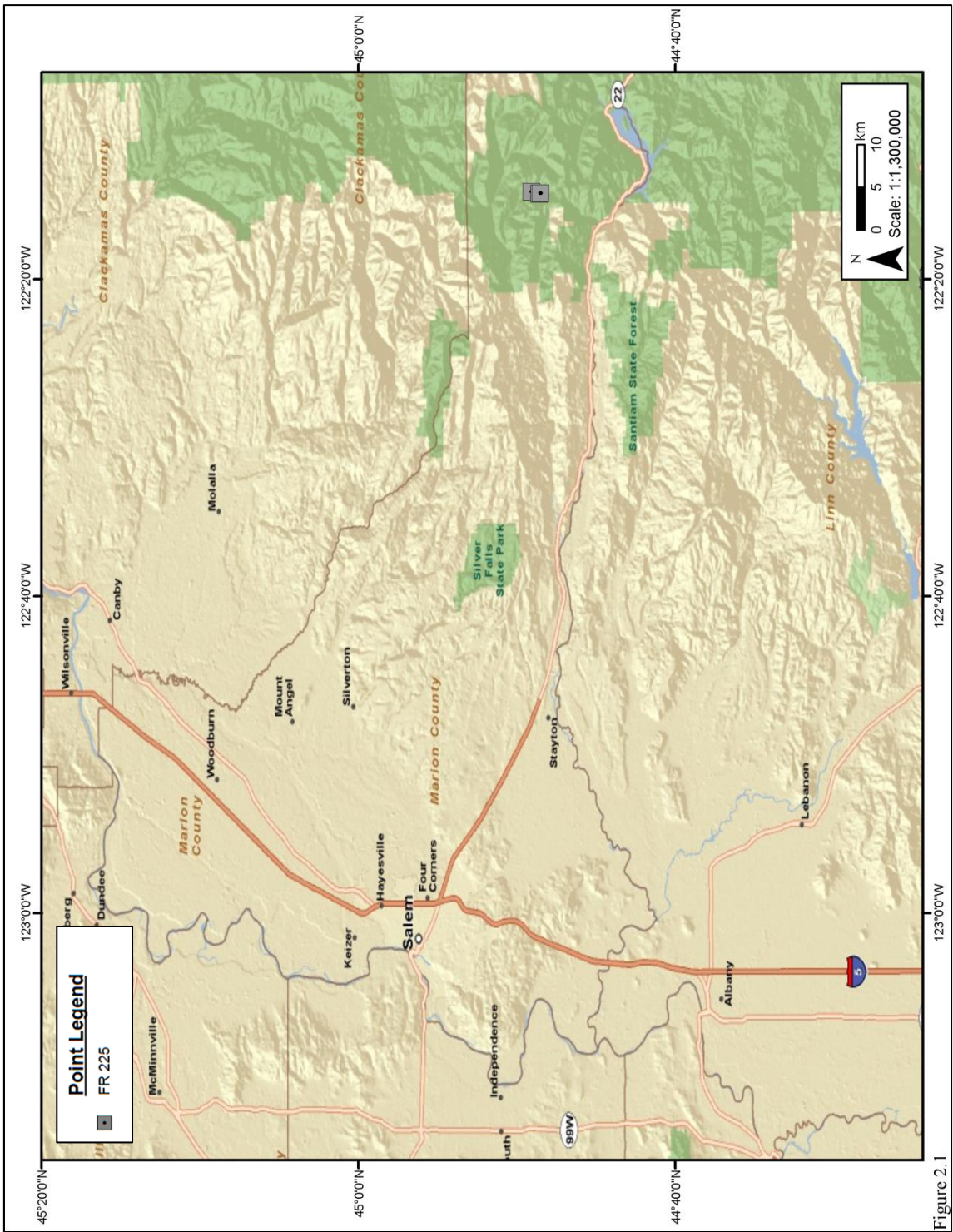


Figure 2.1

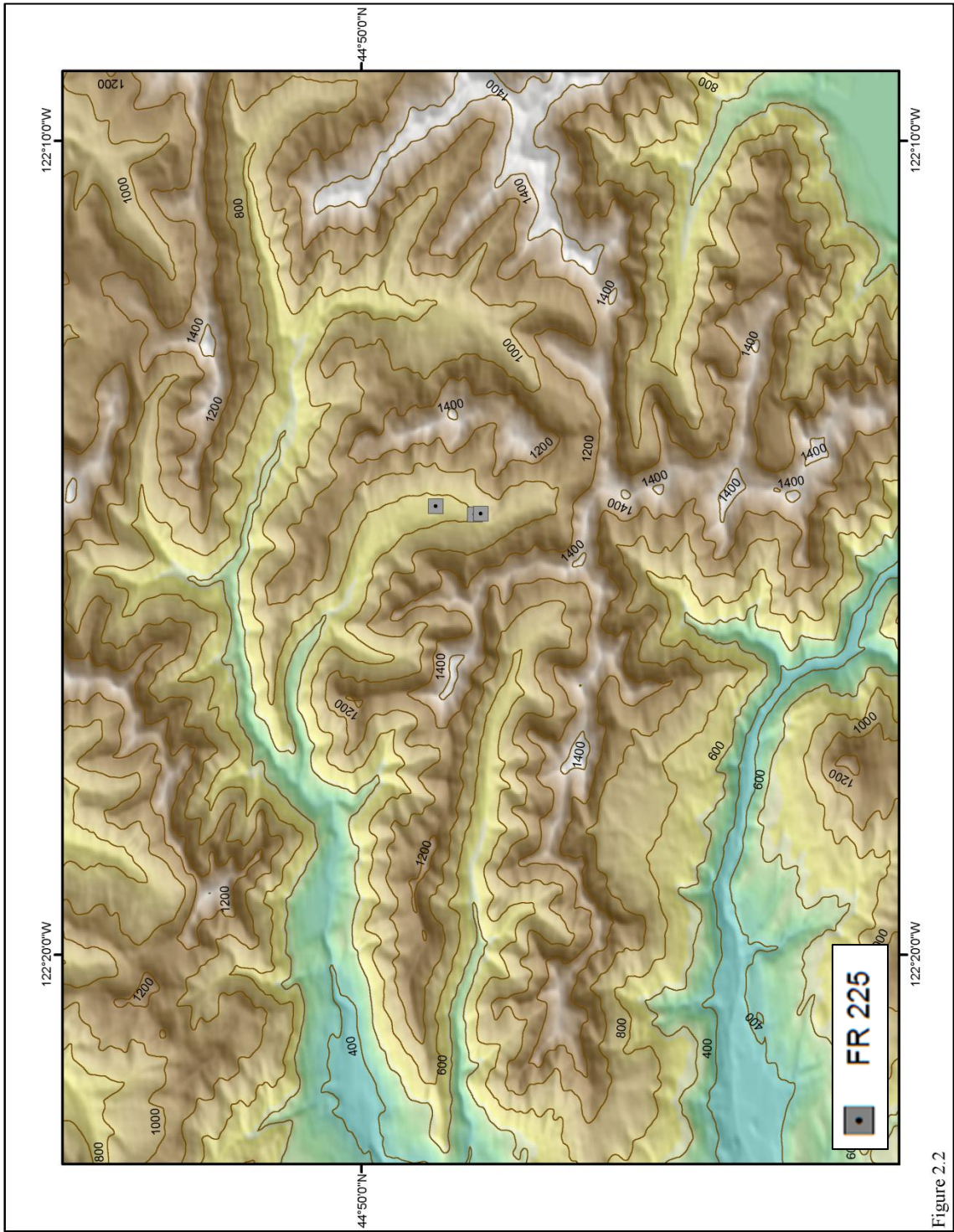


Figure 2.2

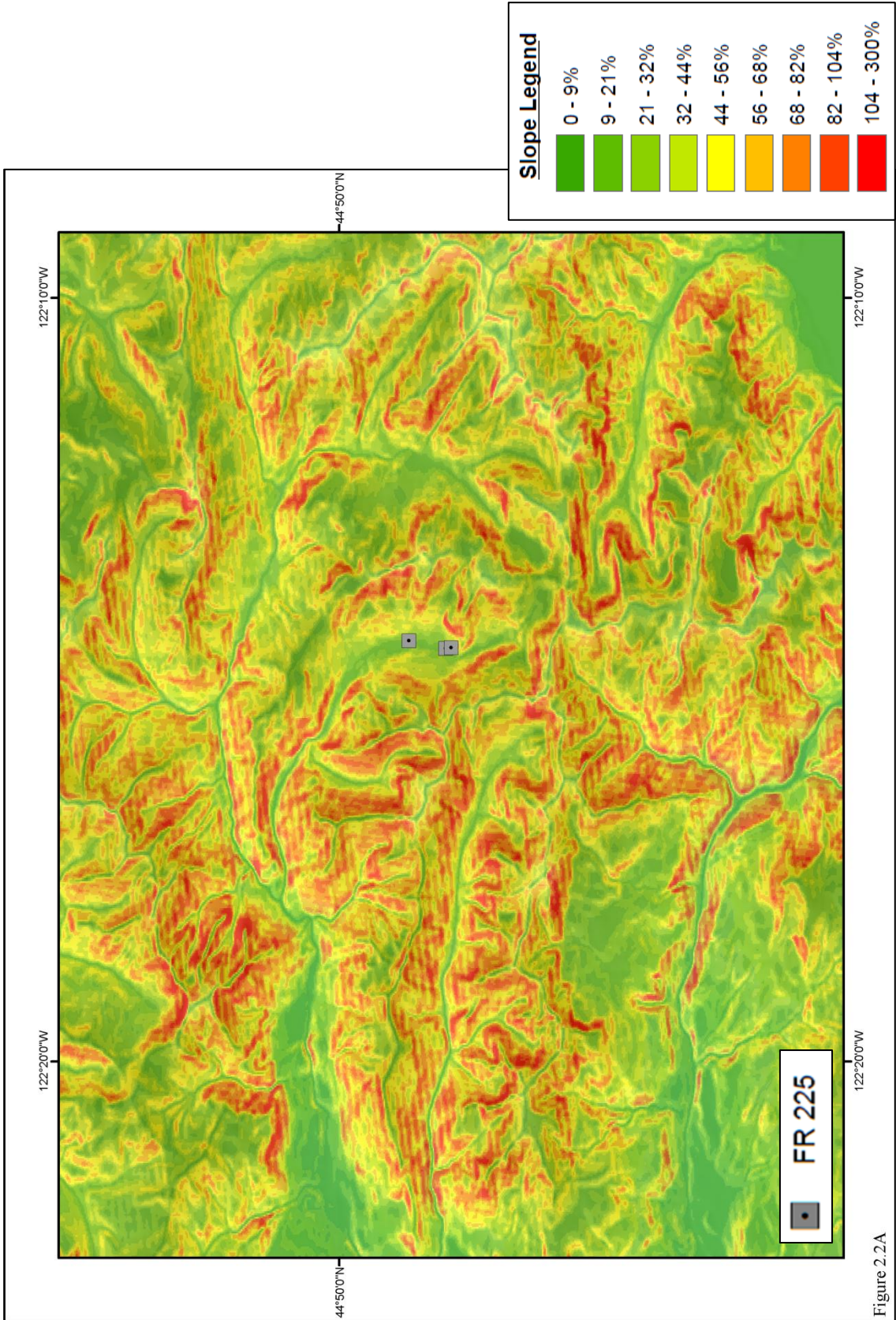


Figure 2.2A

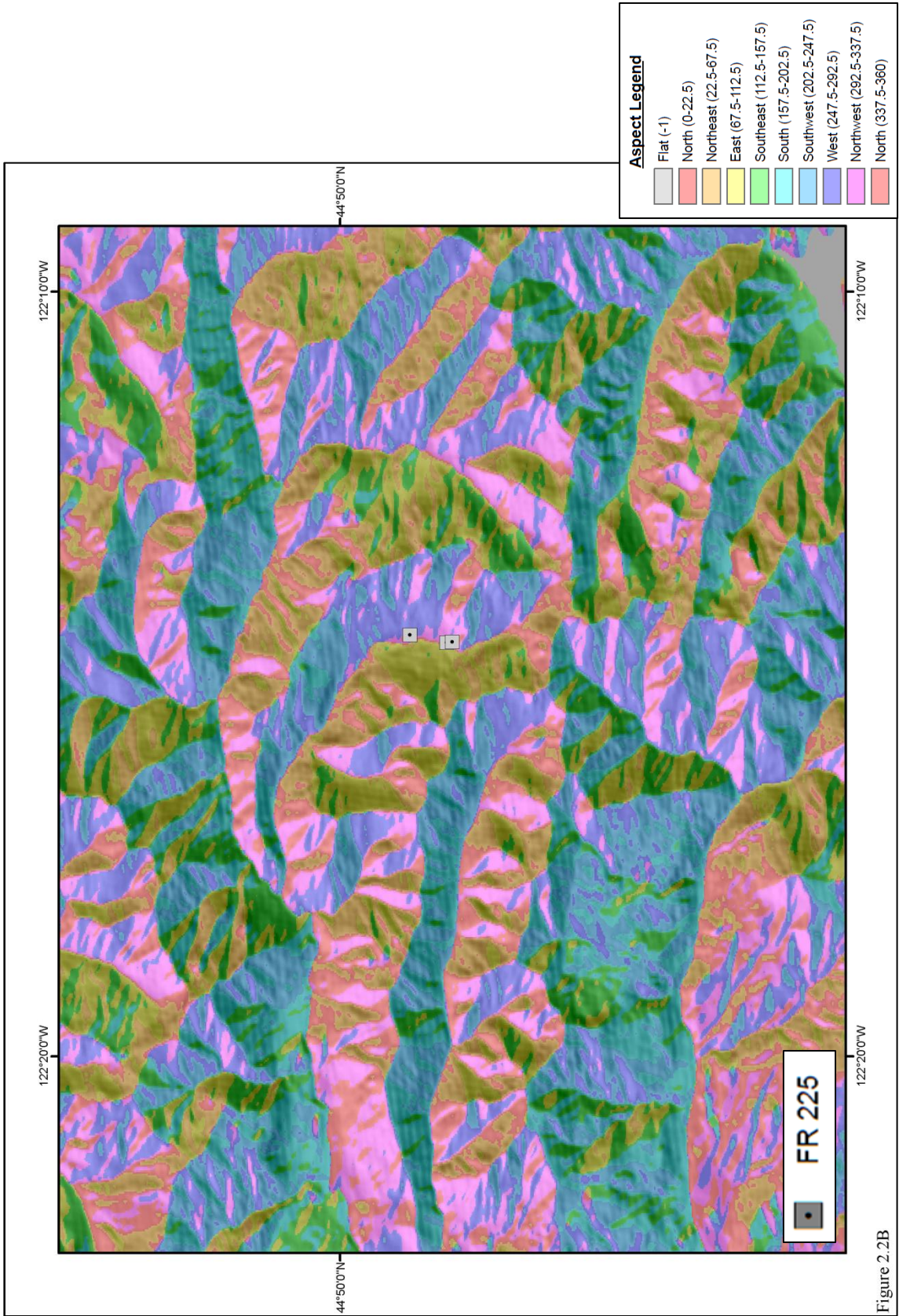


Figure 2.2B

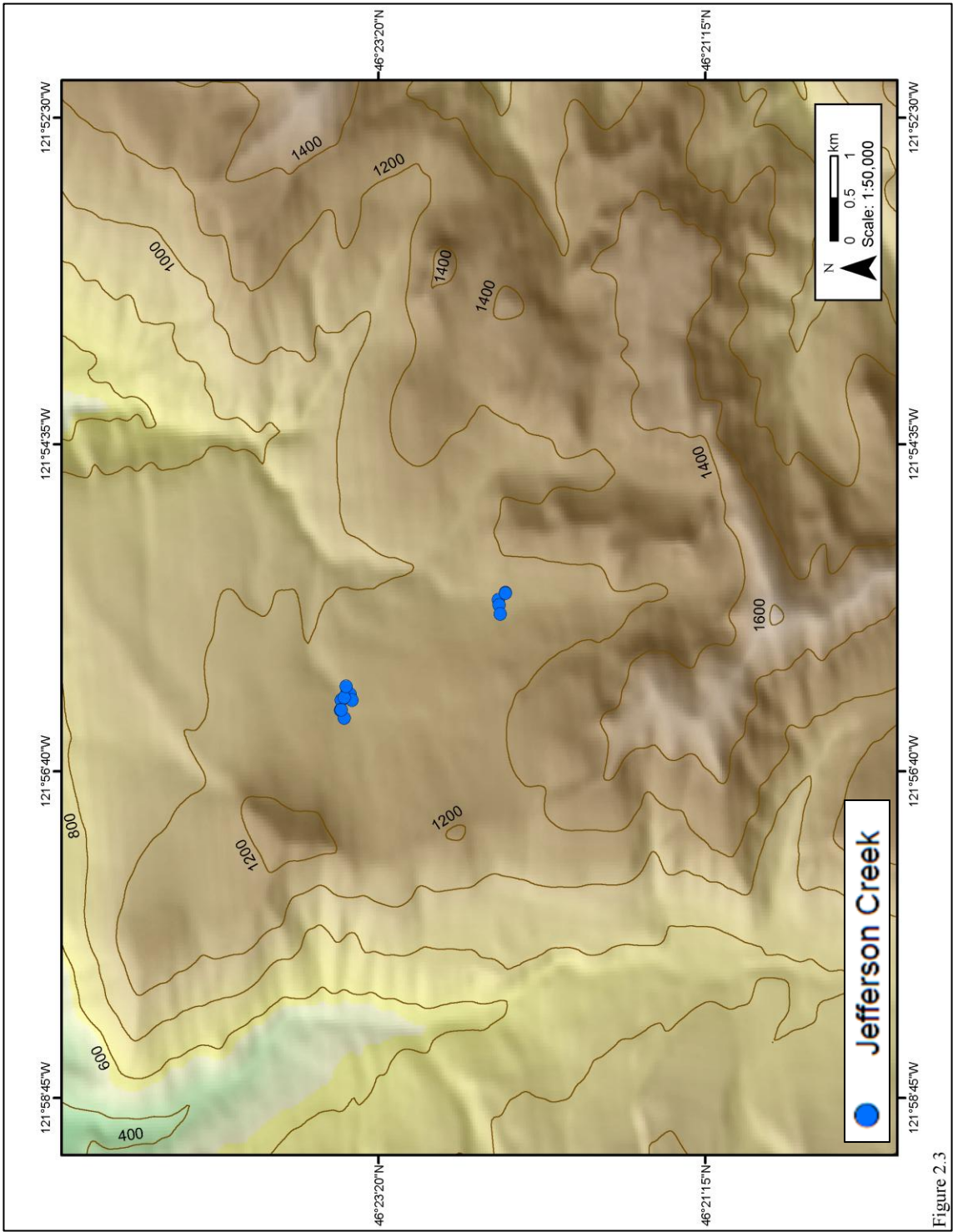


Figure 2.3

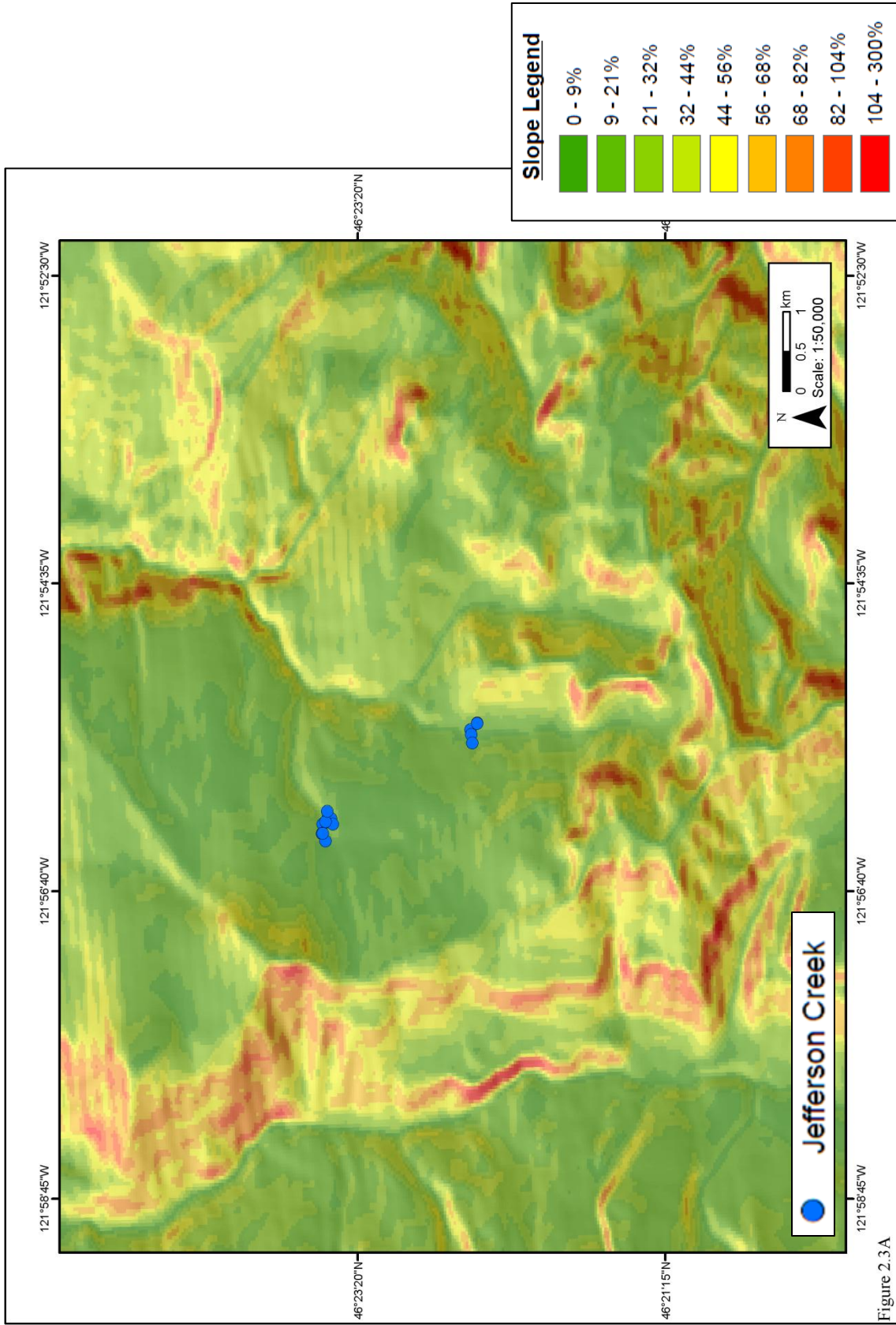
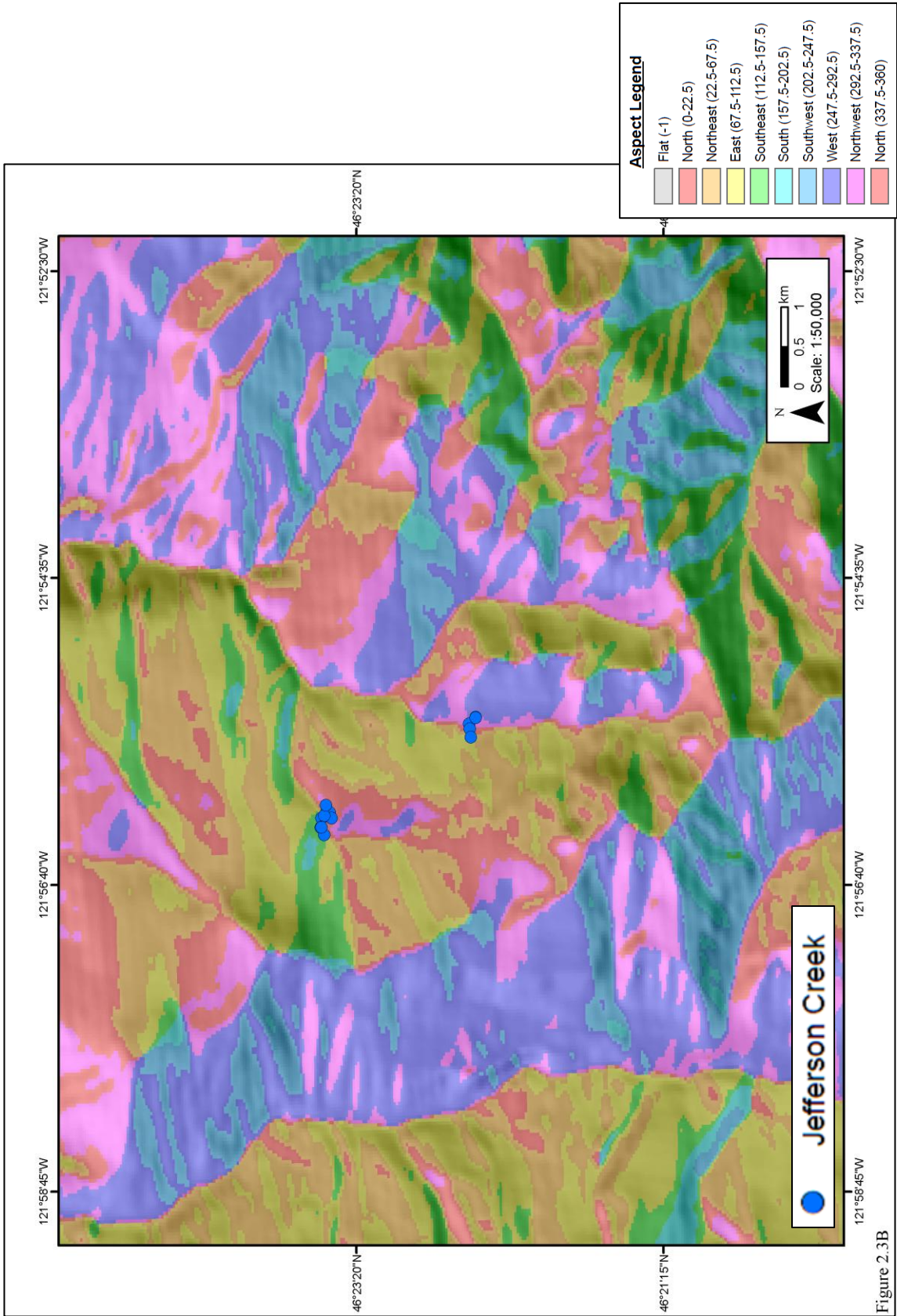


Figure 2.3A



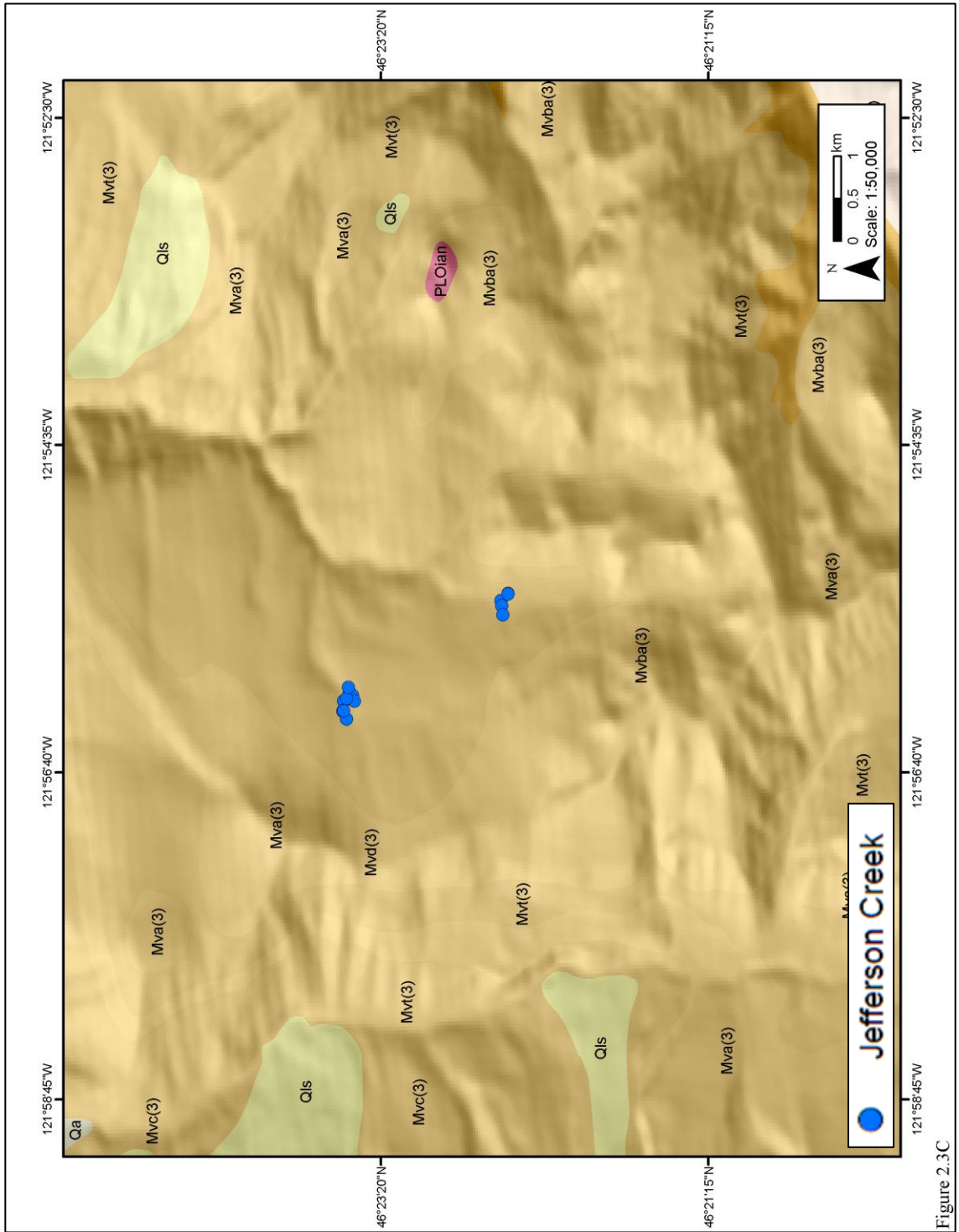


Figure 2.3C

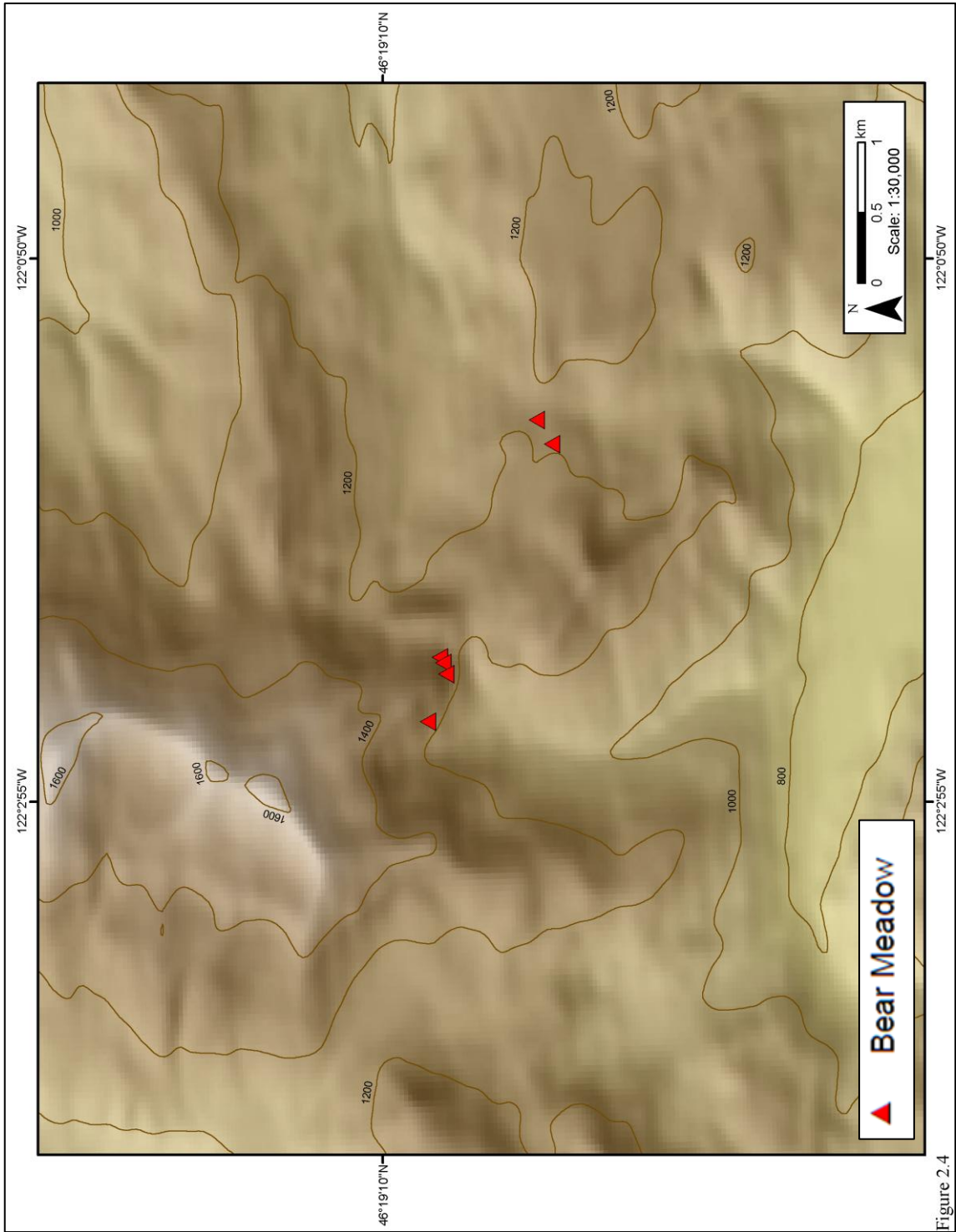


Figure 2.4

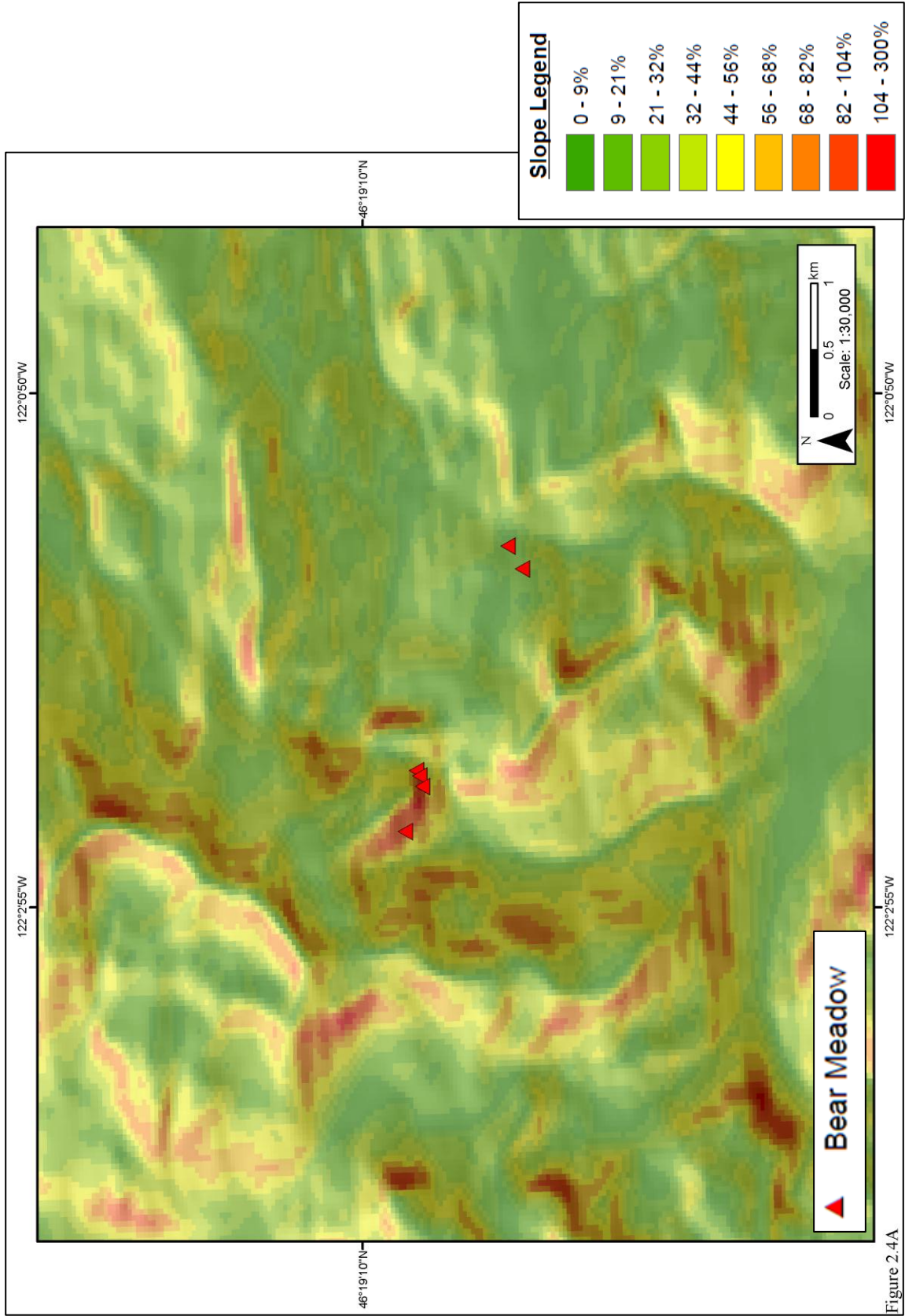
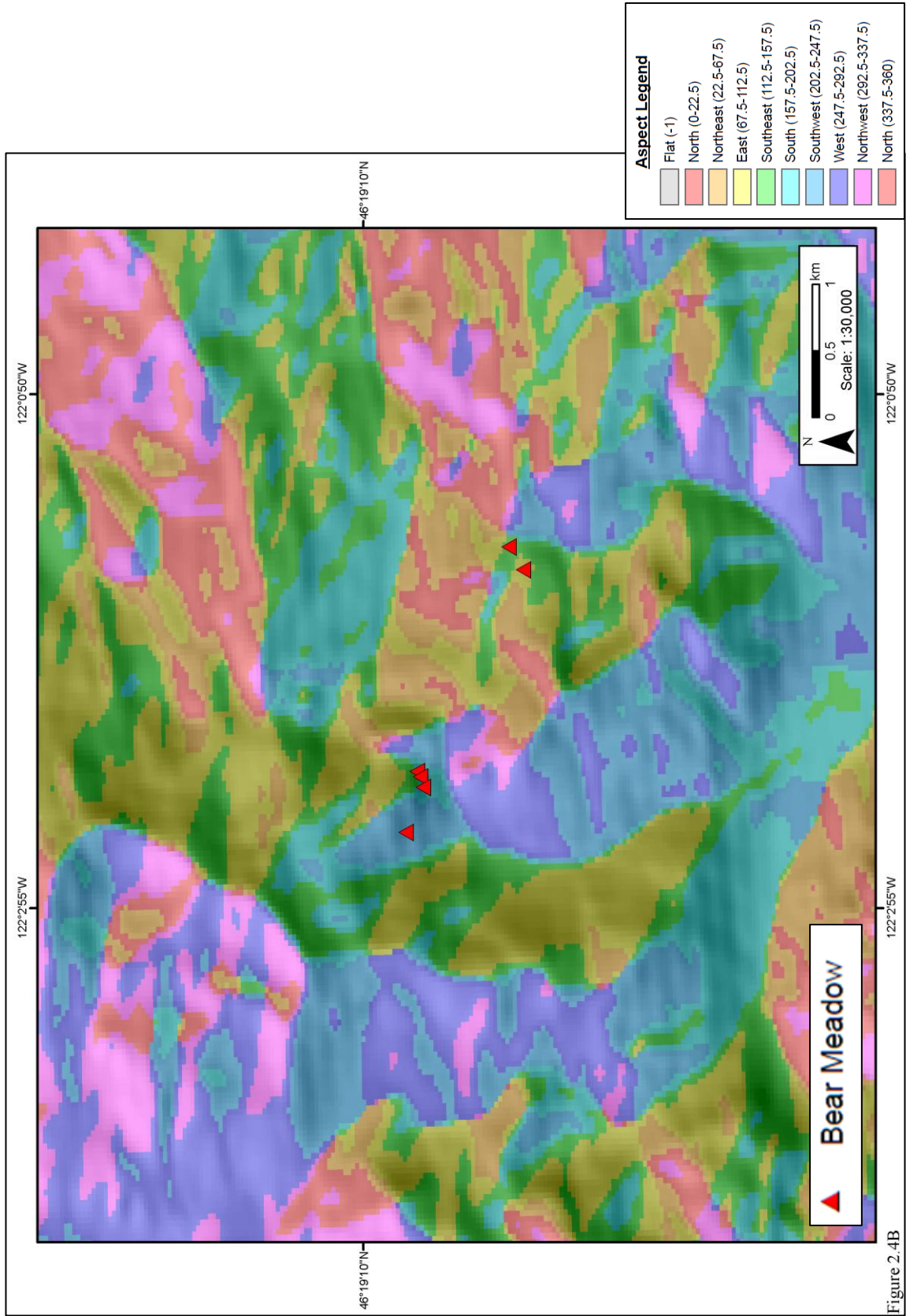


Figure 2.4A



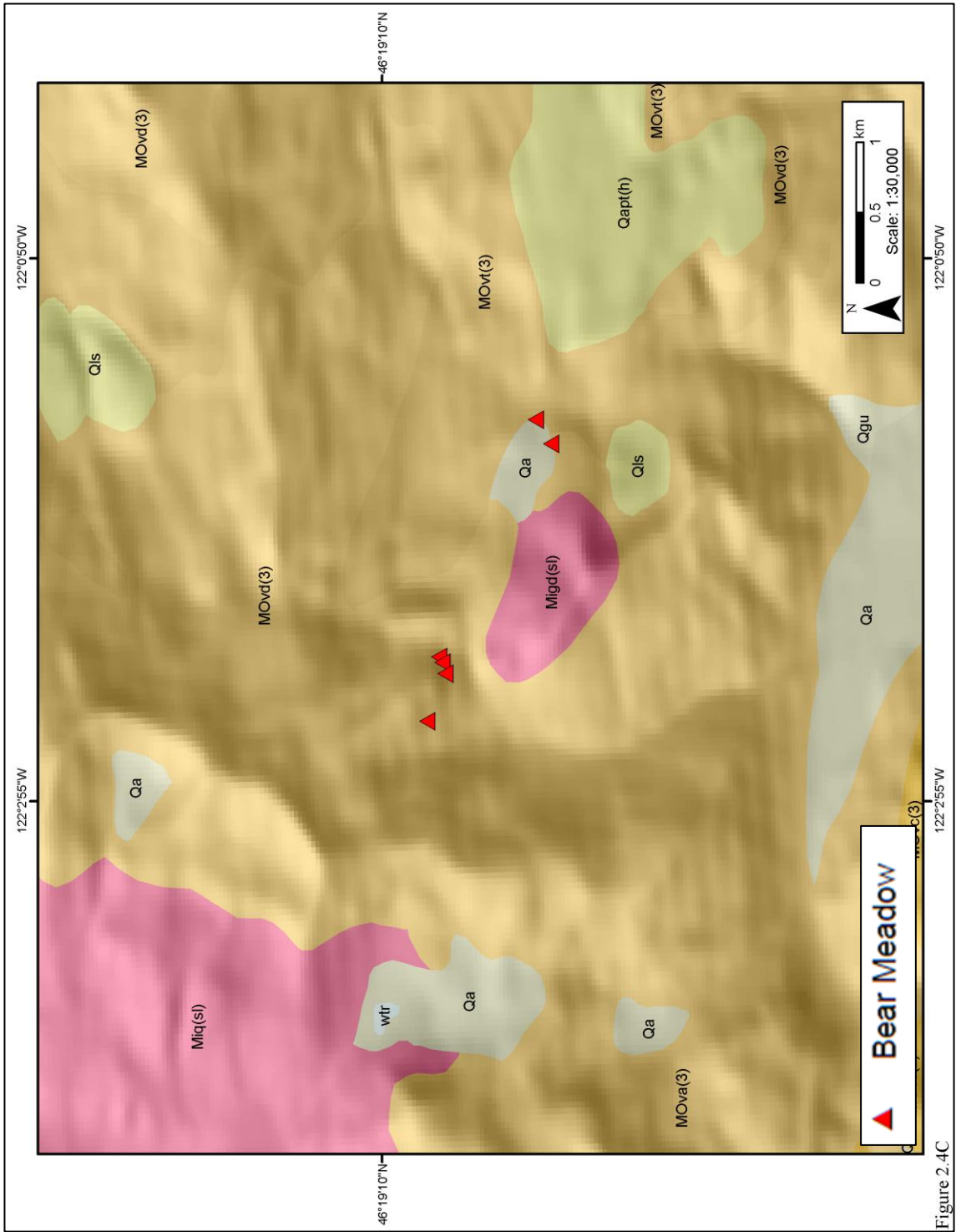


Figure 2.4C

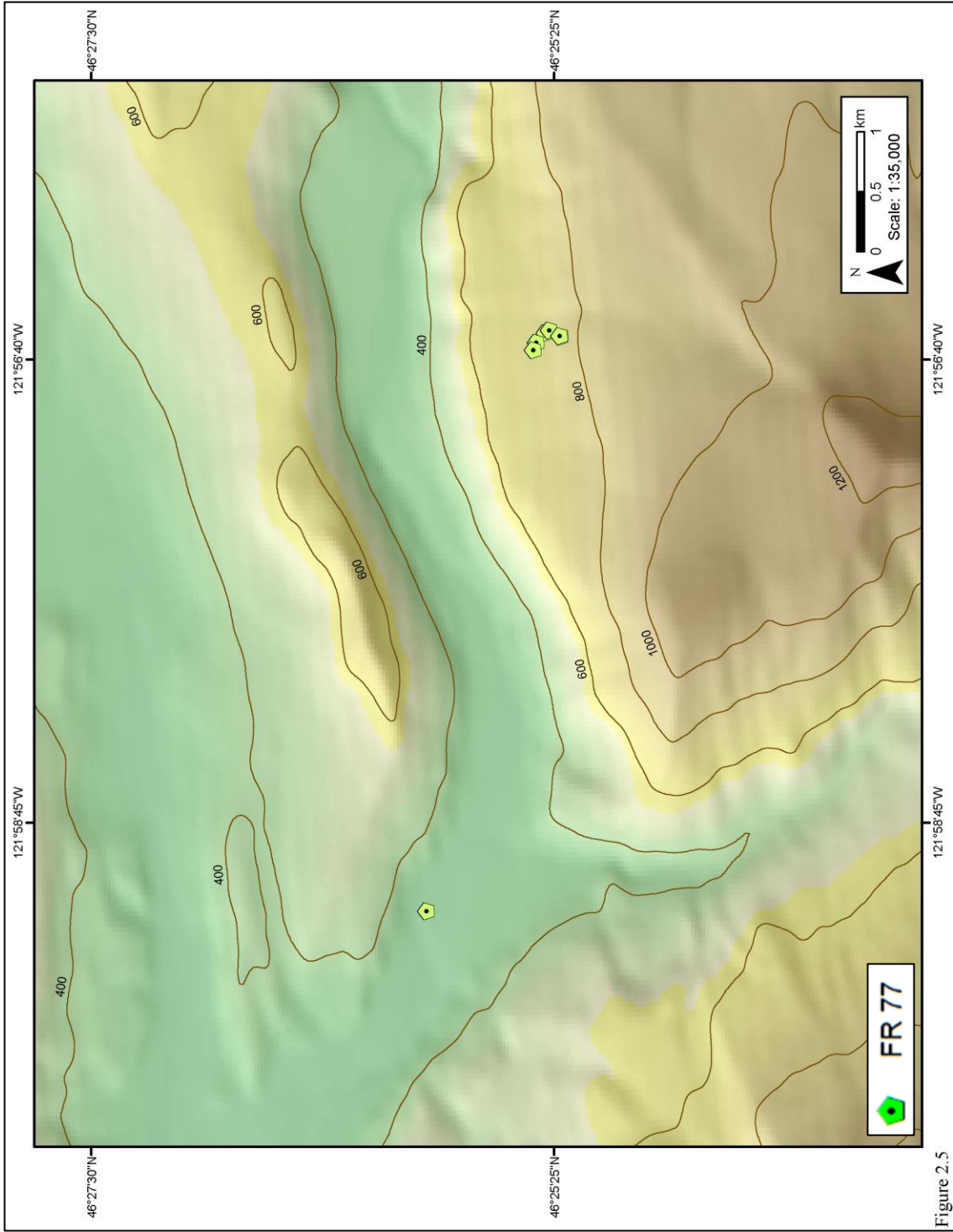


Figure 2.5

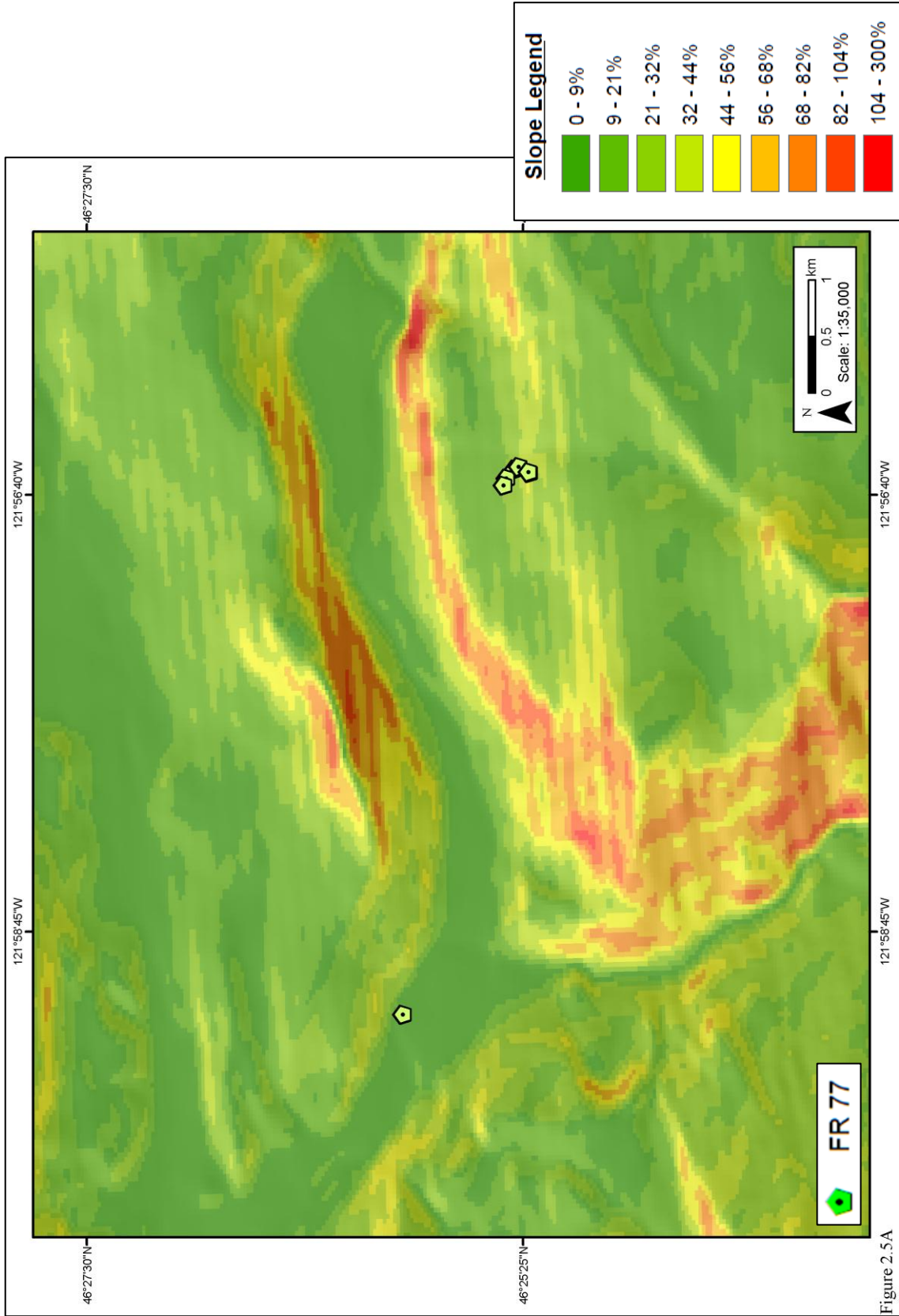


Figure 2.5A

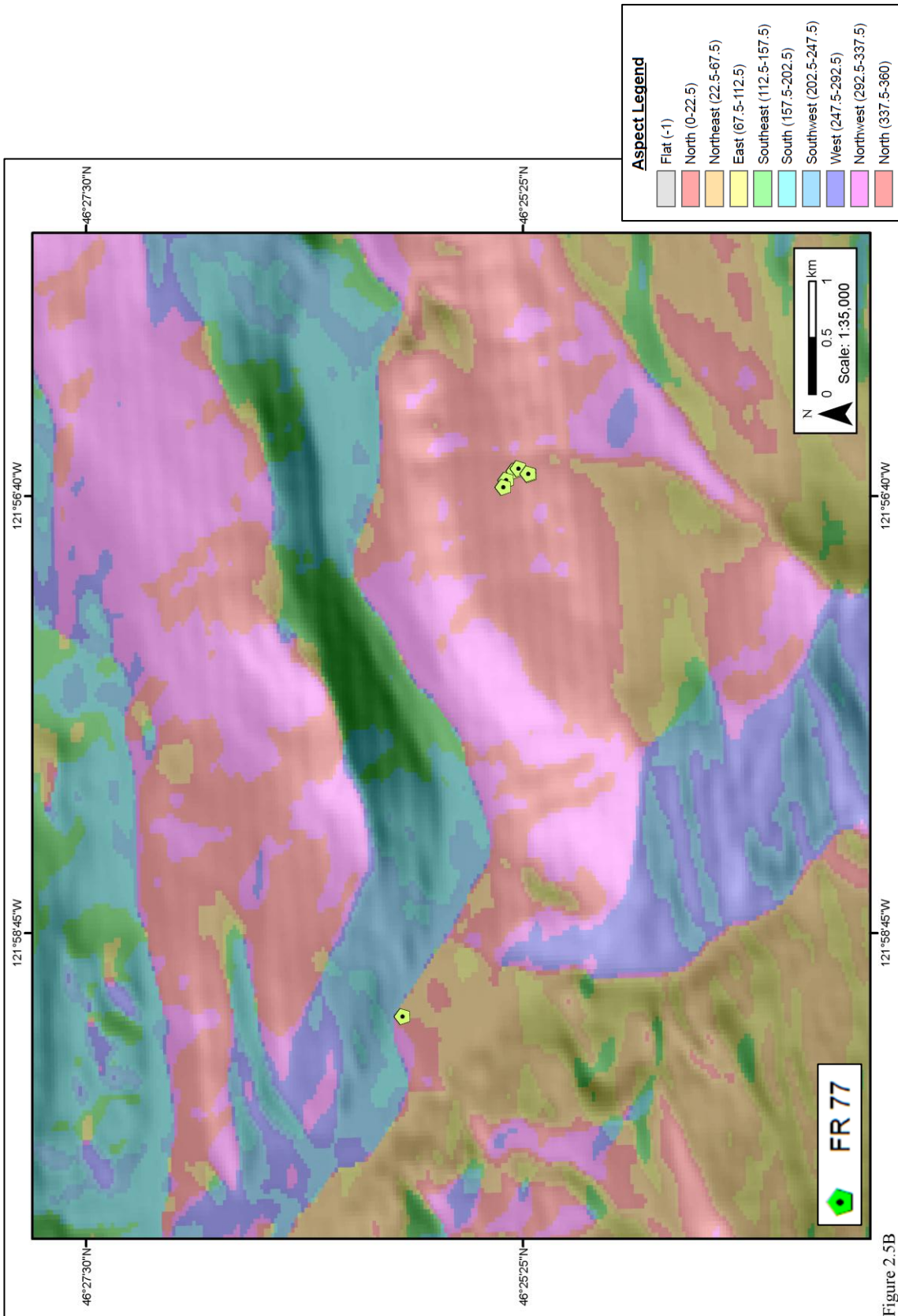


Figure 2.5B

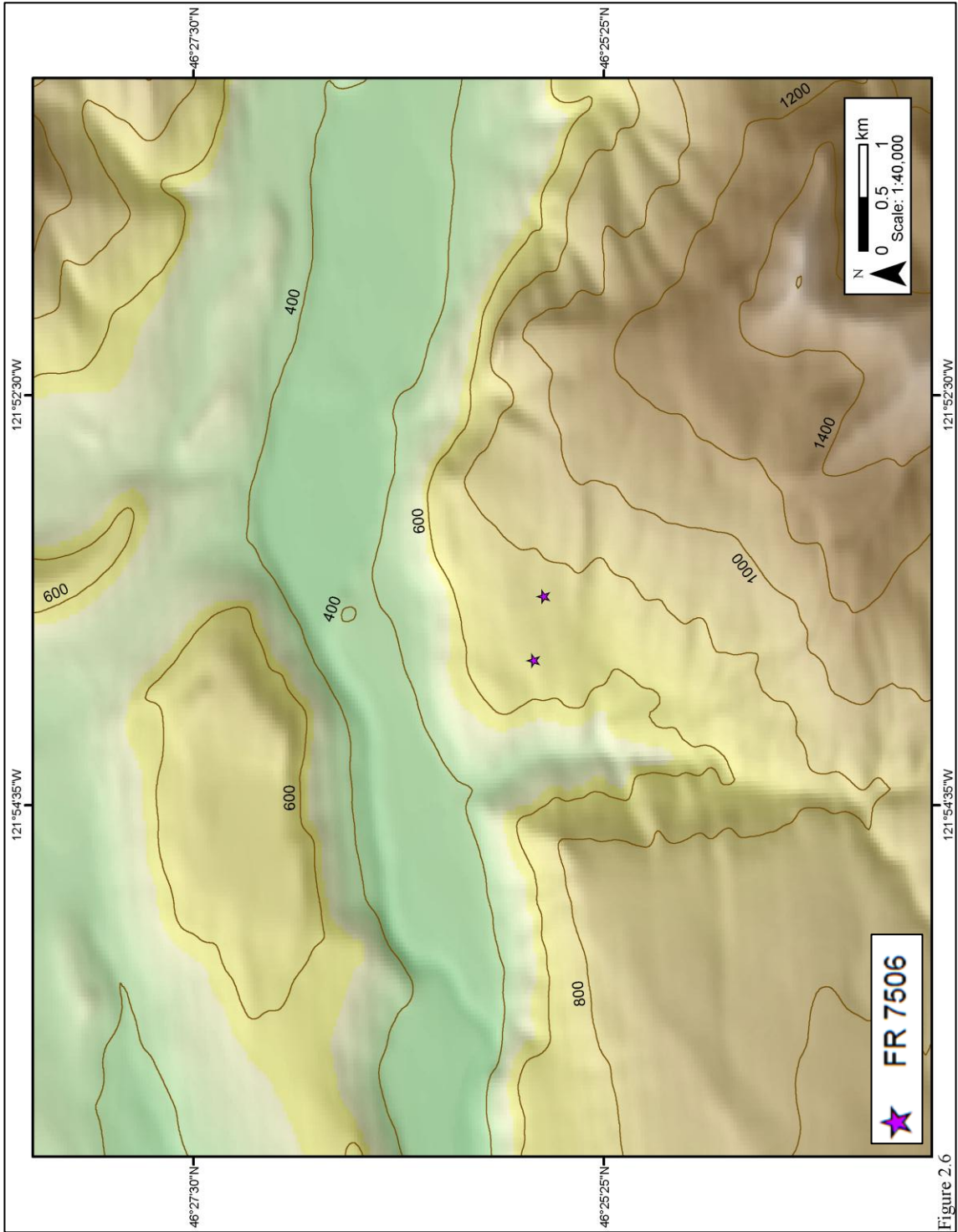
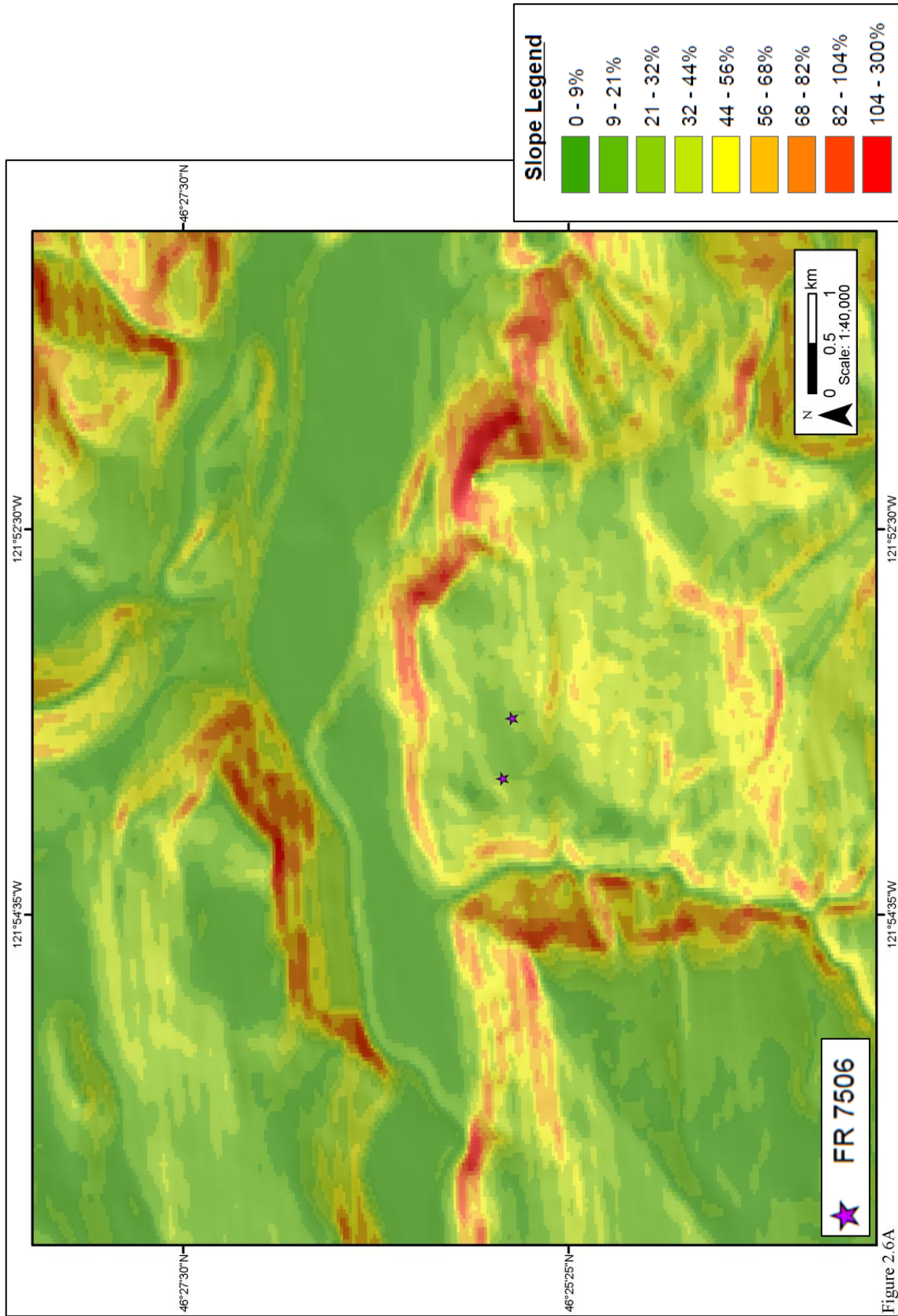


Figure 2.6



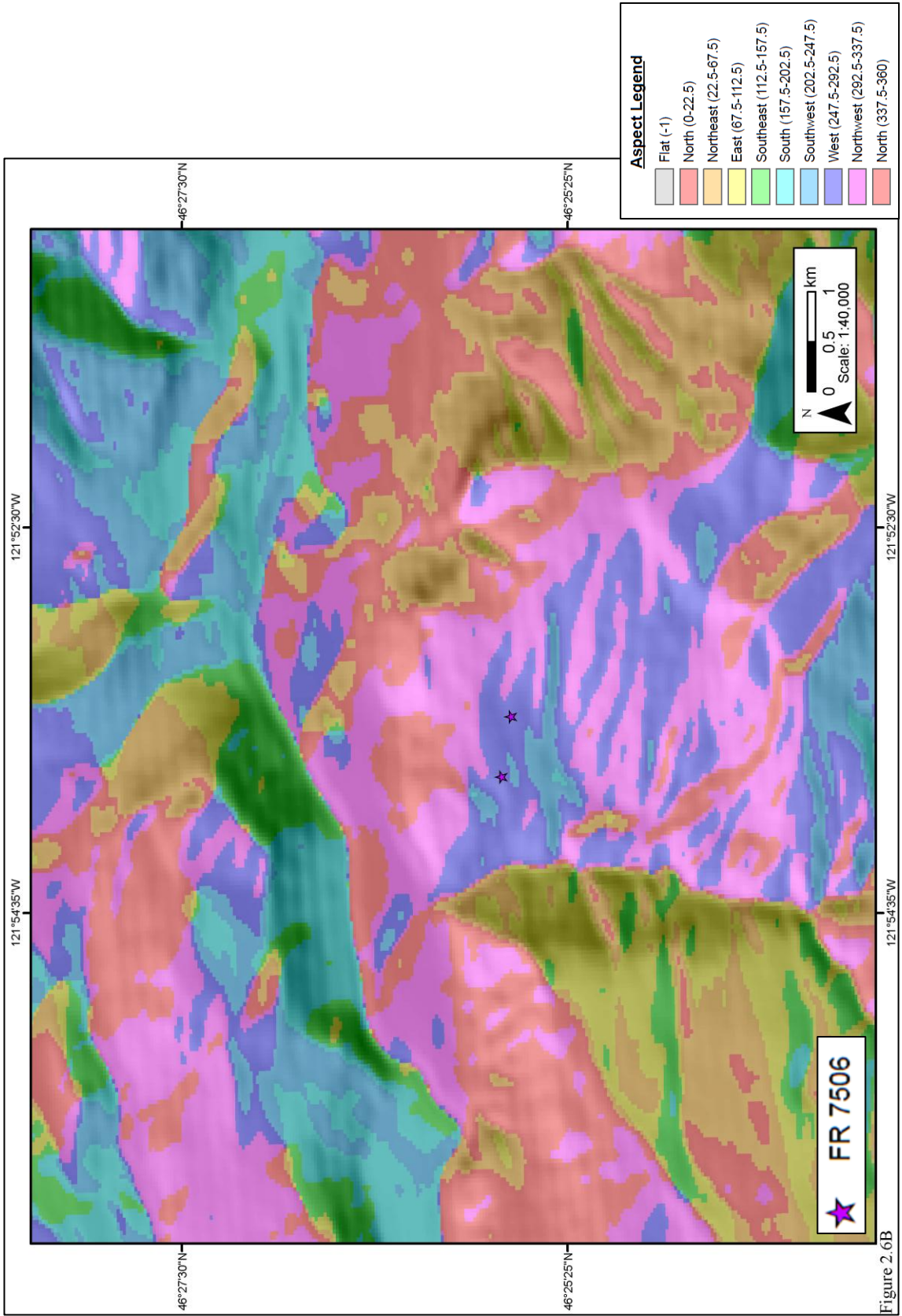


Figure 2.6B

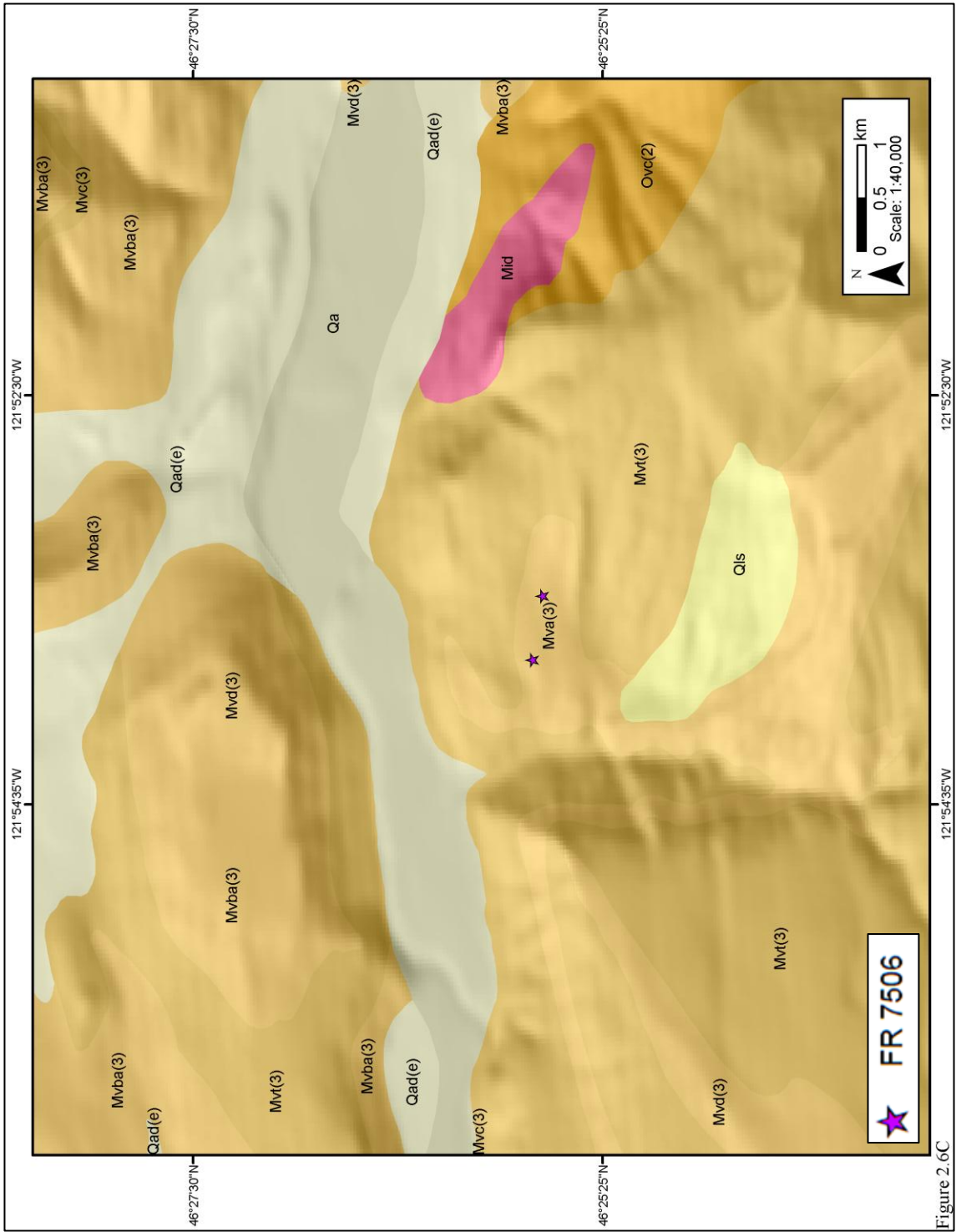


Figure 2.6C

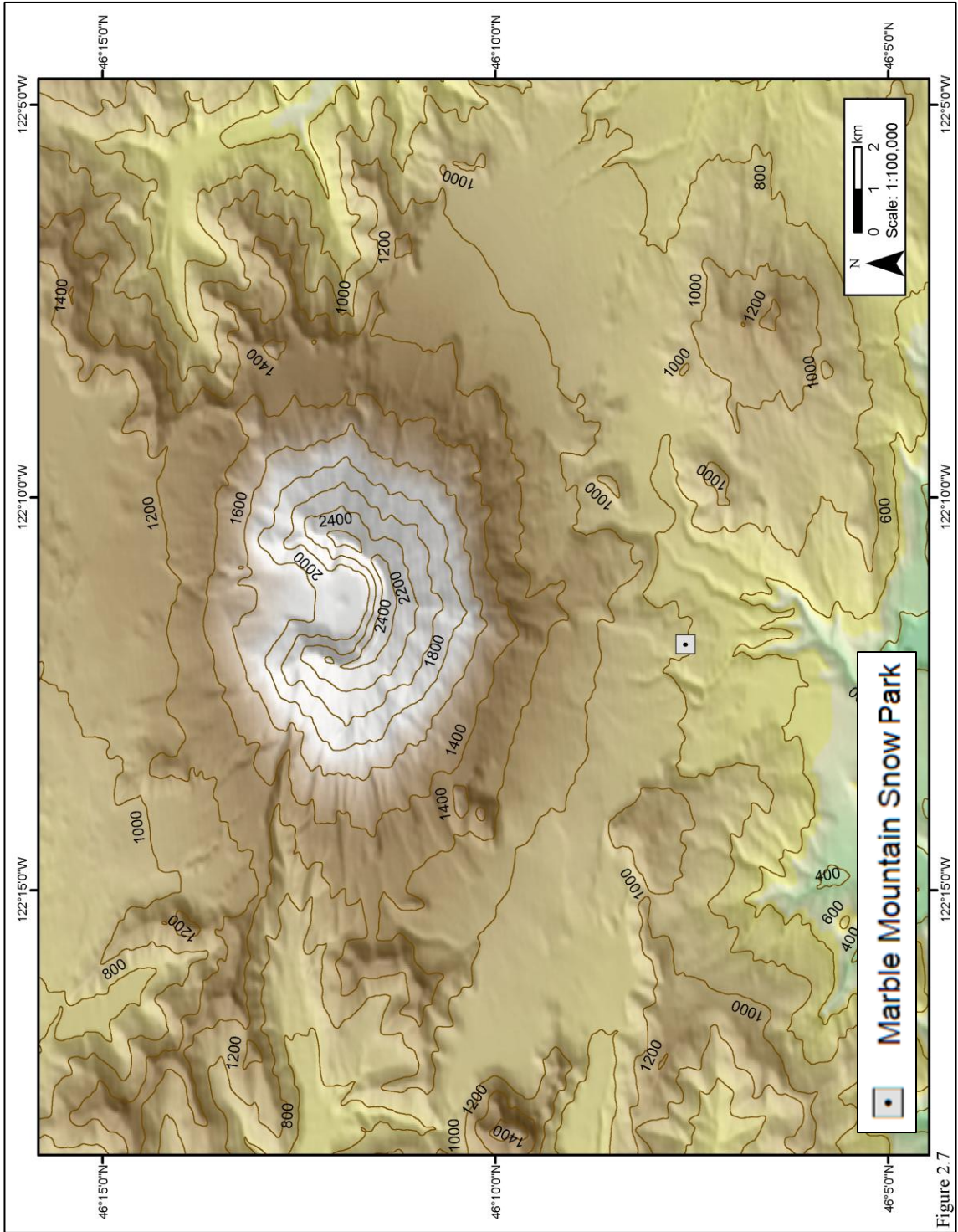
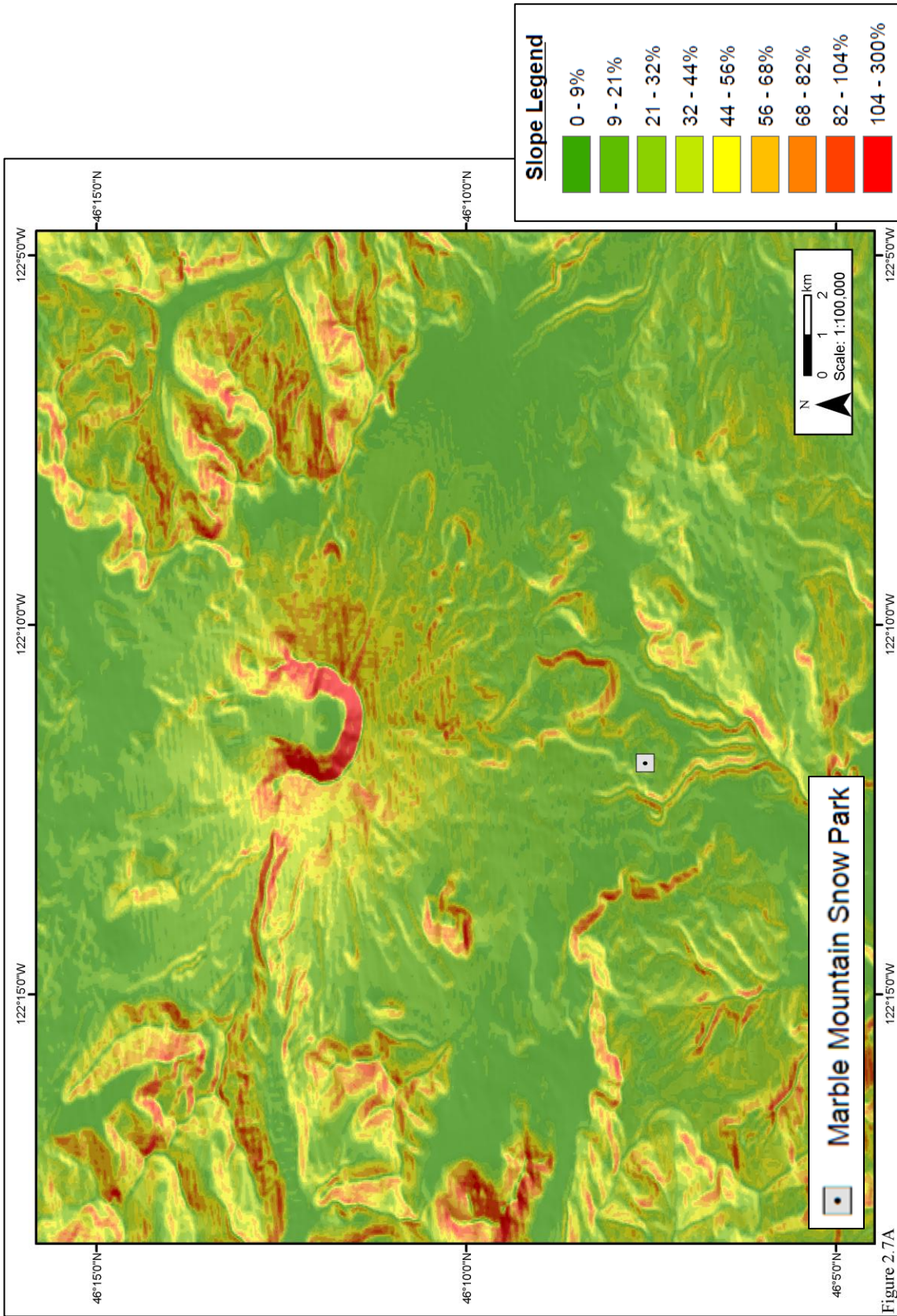
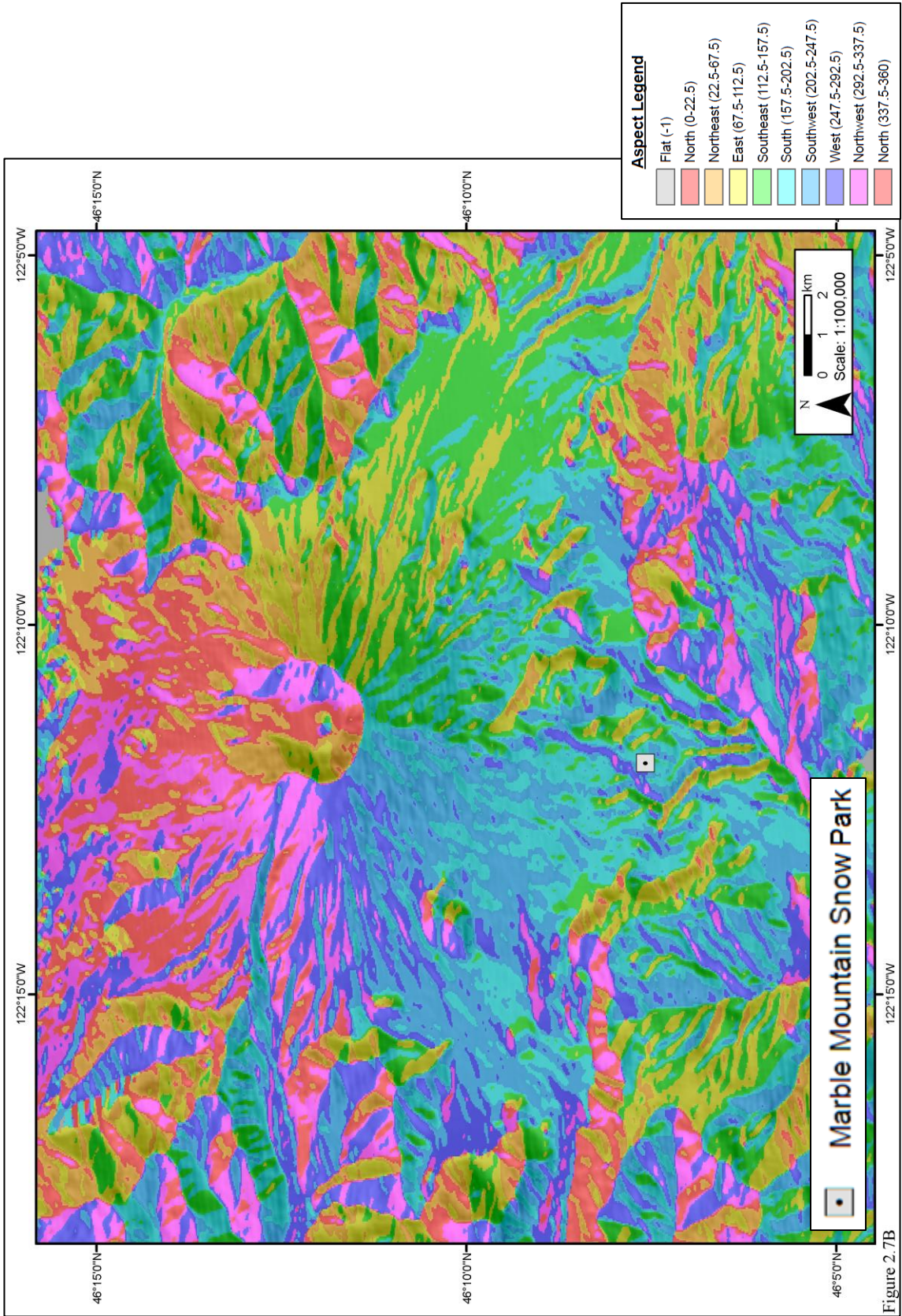


Figure 2.7





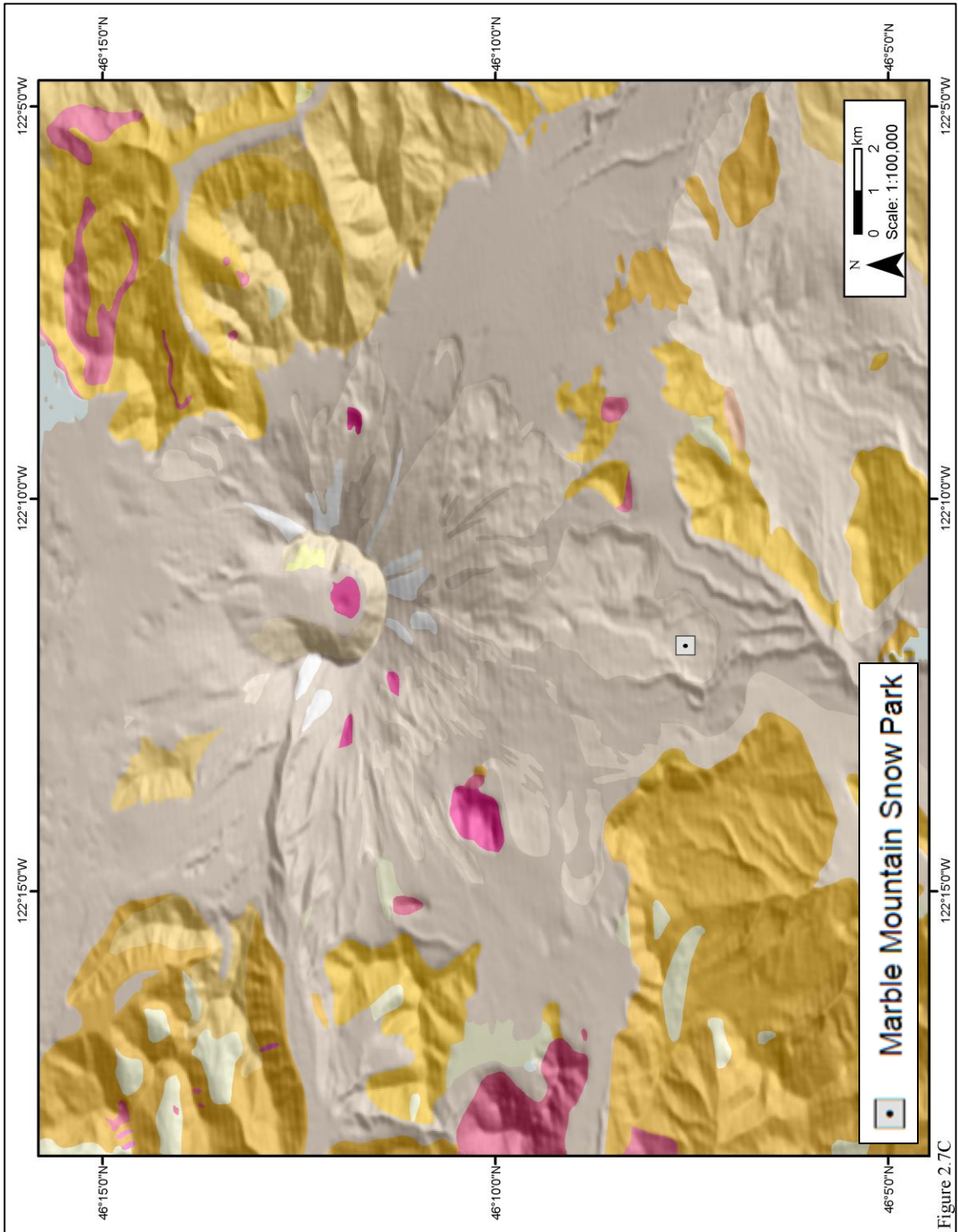


Figure 2.7C

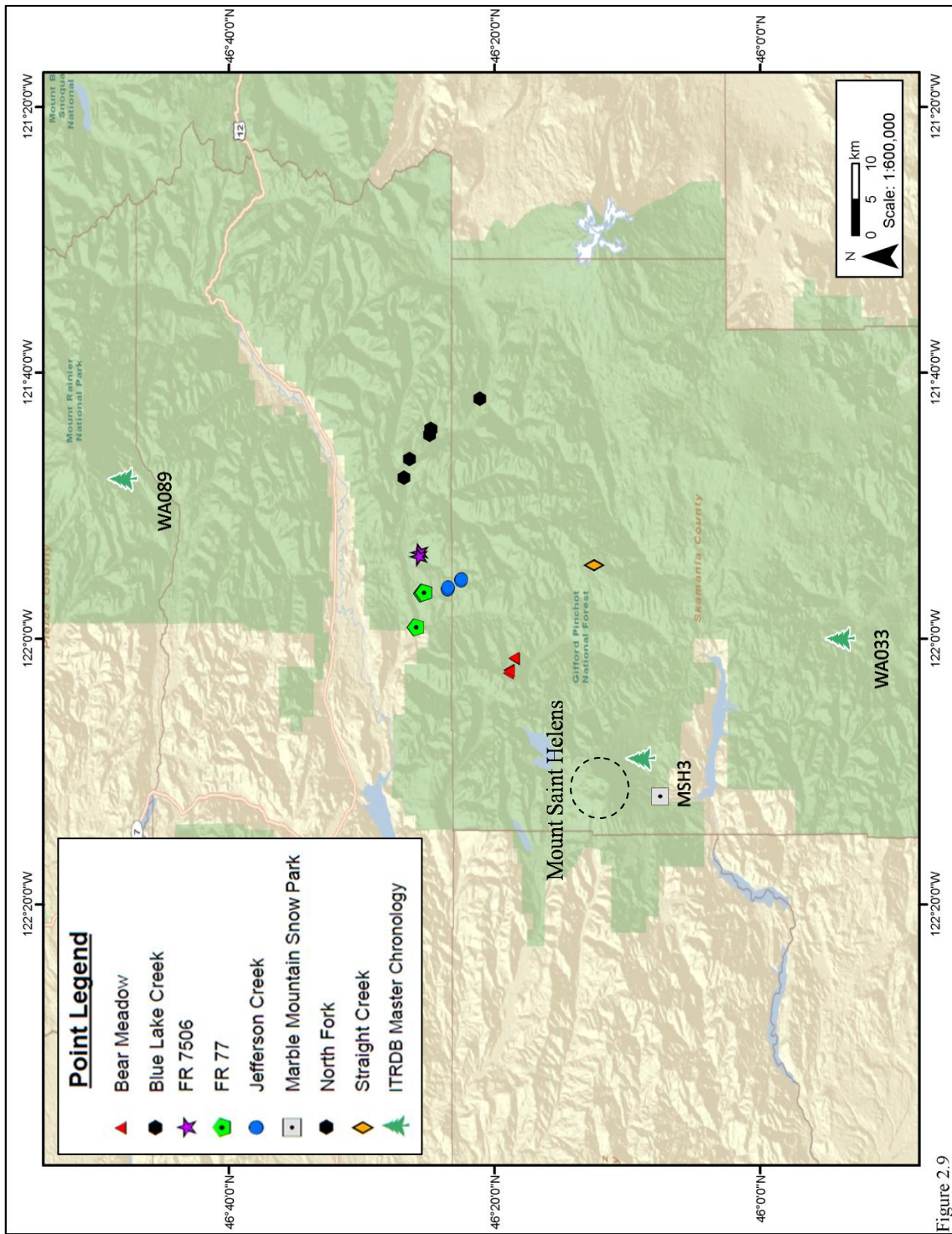


Figure 2.9

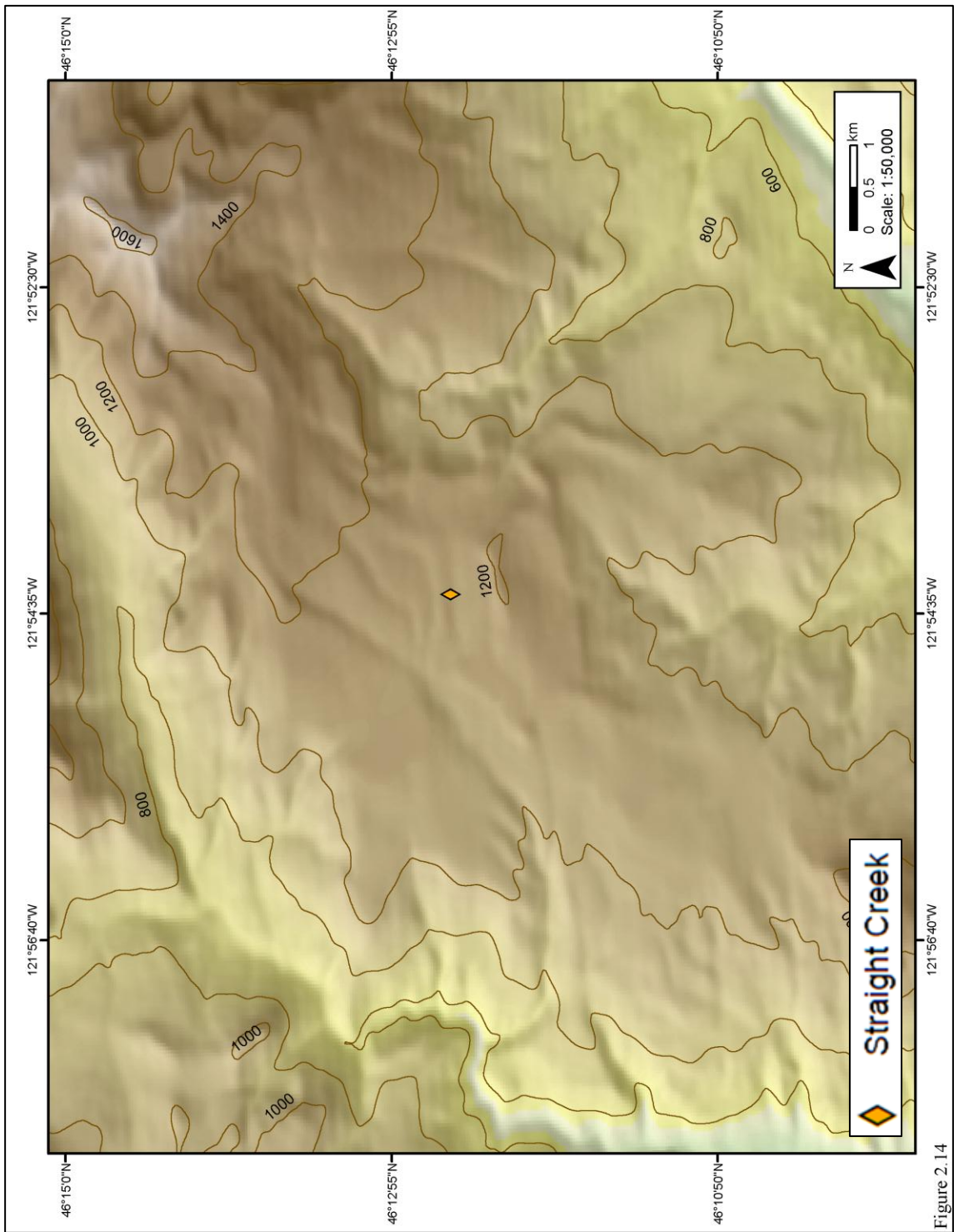
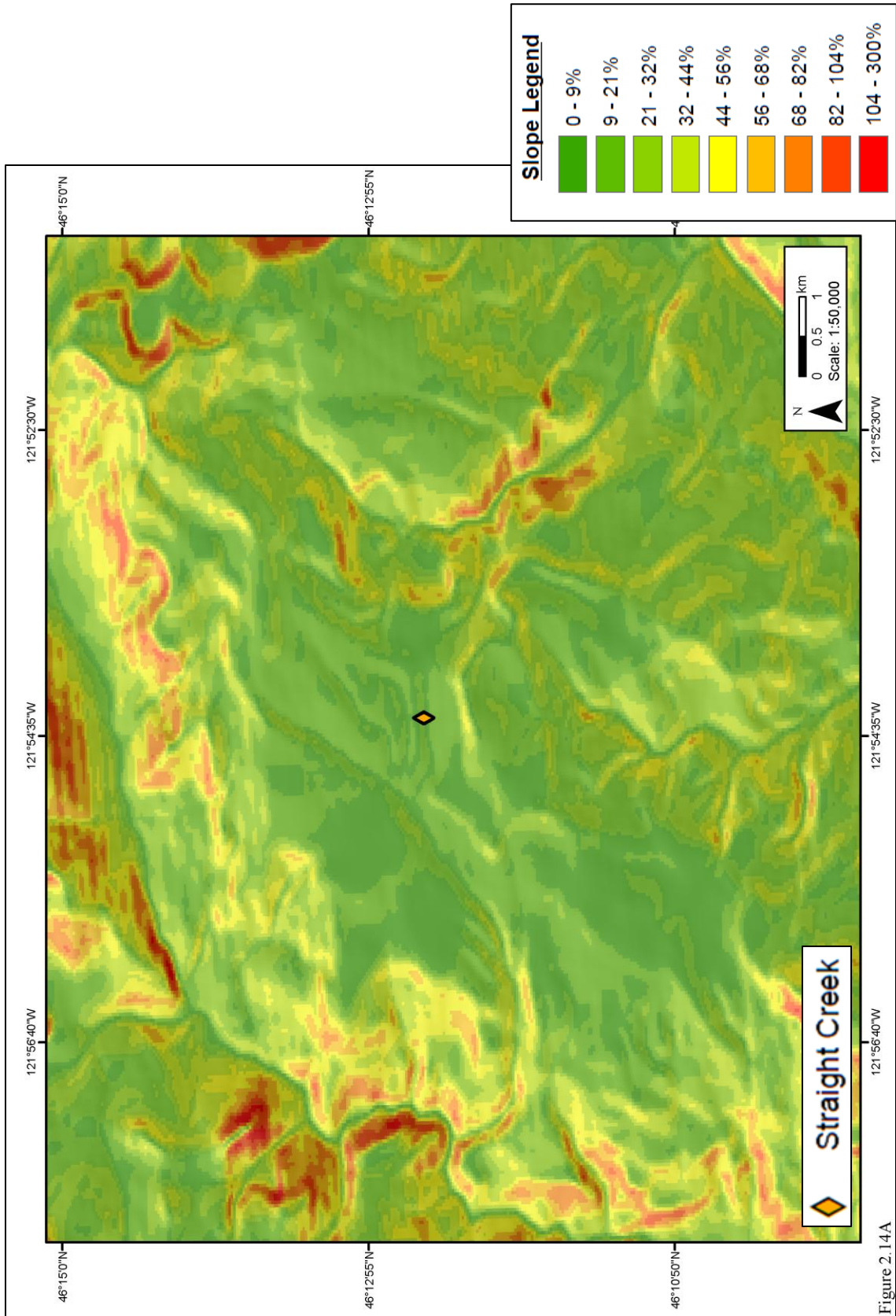
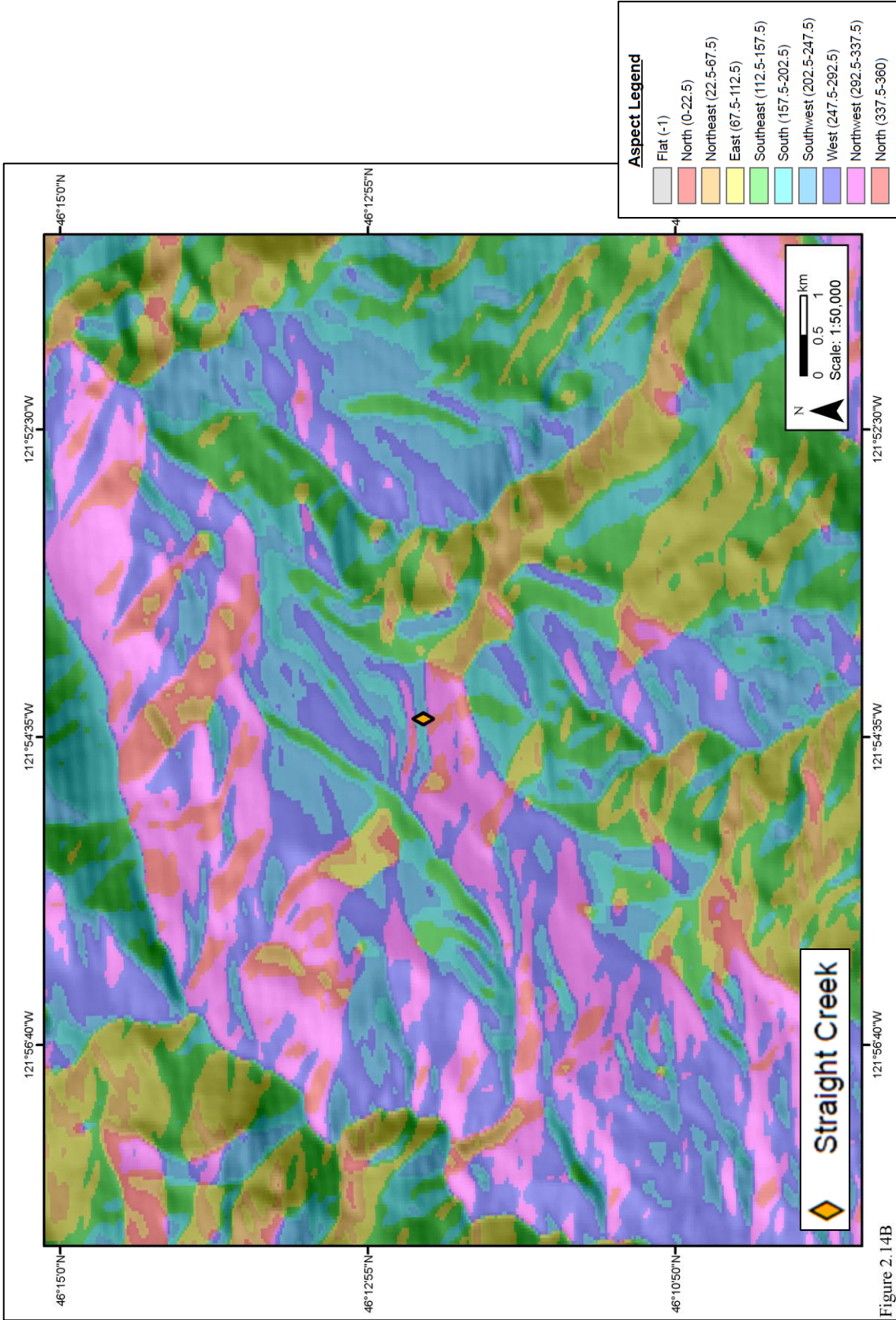


Figure 2.14





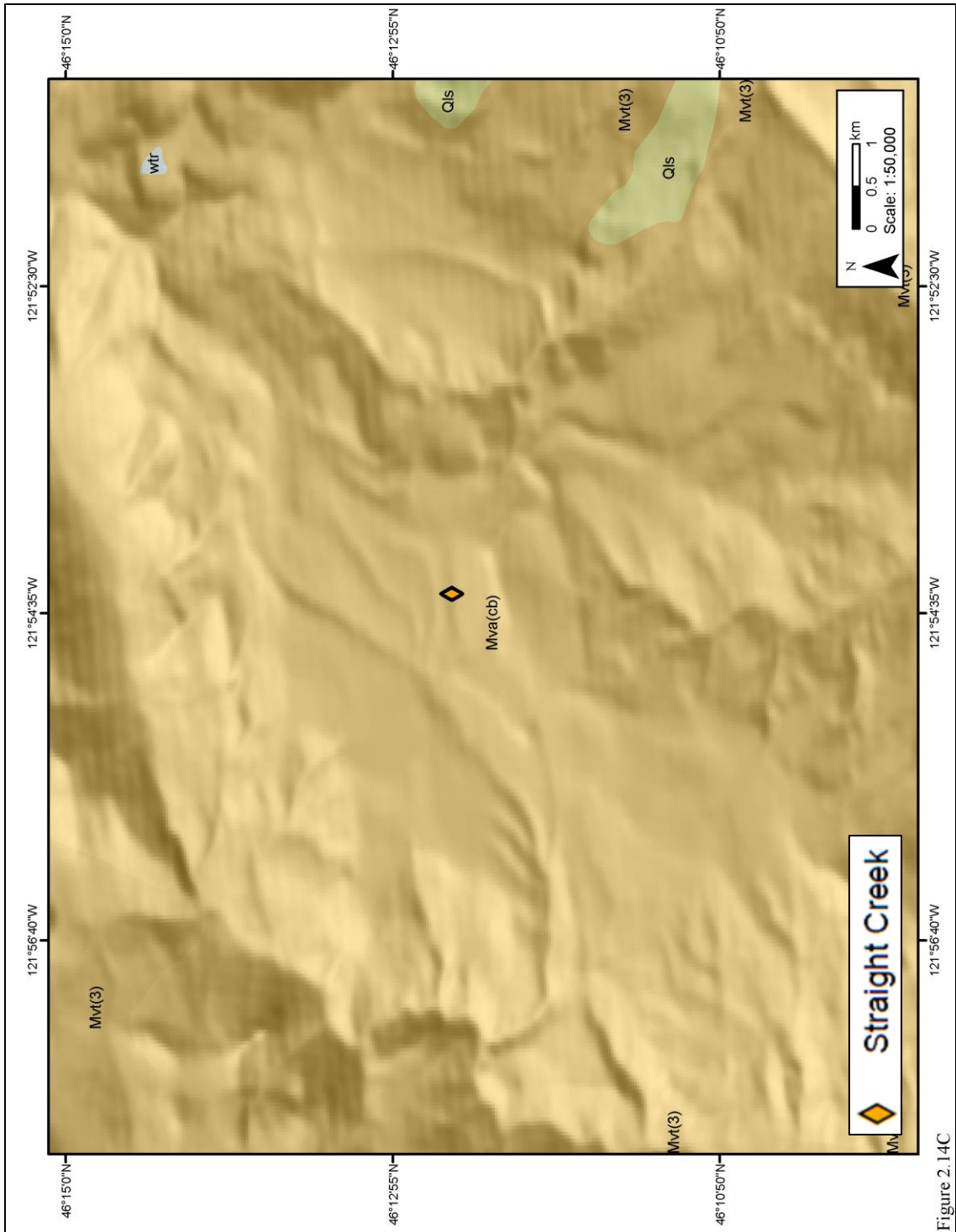


Figure 2.14C